Investigation of the molecular mechanisms downstream of T cell receptor signalling during thymic T cell development

A thesis submitted to the Department of Life Scences,

Faculty of Sciences, Imperial College London

By

Alina Dana Paduraru

For the degree of Doctor of Philosophy

Immunology

August 2020

Statement of Originality

I declare that the contents of this thesis represent my own work and that anything derived from external sources has been appropriately referenced.

Copyright Declaration

Acknowledgements

I would like to thank my incredible supervisor, Dr. Masahiro Ono, for giving me the opportunity to join his lab. He is not just a brilliant scientist, but an inspiring person overall. Due to his wonderful support, I was very fortunate to live the most enjoyable, satisfying and transformational years of my life. The only regret I am left with is that I will never be able to thank him enough for everything he did for me. It has been a privilege.

A lot of gratitude goes to several members of the Ono group who helped me with both practical and theoretical work and who enhanced my experience as a PhD student. In the order I met them, I would like to thank Dr. David Bending, Catherine Mo Ducker, Jehanne Hassan, Dr. Bahire Kalfaoglu and Dr. Jose Santos. I would also like to thank my personal advisors, Prof. Tessa Crompton and Dr. Kenji Okuse, for their advice and support.

A lot of appreciation goes to several people who kindly helped me throughout my journey. I would like to mention Dr. Kleoniki Gounaris, Mr. James Ferguson, Dr. Jessica Rowley, Dr. Jane Sirvastava, Dr. Taku Okazaki, Dr. Tatsuya Takemoto, Mr. Dennis Harnett, Mr. George Zimmerman, Mr. Reece Williams, Ms. Bonnie Glenn, Ms. Roxanne Wood, Mr. Lukas Bukowski, Ms. Carol Weyman and Ms. Allison Hunter.

Finally, I would like to dedicate this work to my wonderful parents, Ana and Aurelian Paduraru. I thank them for all their unconditional love and support, as well as for actually trying to understand thymic development. One of them still thinks that a double positive T cell is just "extra optimistic".

Abstract

The key feature of T cells is their T cell receptor (TCR), which renders them specific to antigen. Immature double positive (DP) T cells develop in the thymus into mature single positive (SP) cells. During this maturation process, developing T cells are positively selected if their receptors are able to receive a signal from self-antigen and negatively selected by the proapoptotic Bim-mediated mechanism if they bind self-antigen too strongly. Meanwhile, DP cells are lineage selected into either CD4 or CD8 SP cells. Some self-reactive cells are agonist-selected and upregulate *Foxp3* to become regulatory T cells (Treg), which suppress immune responses. The temporal order of these selection processes is not well understood due to a lack of tools to investigate temporal changes of T cell development *in vivo*. To determine the sequence of and relationship between these events, this project used the novel technology Timer of Cell Kinetics and Activity (Tocky), which analyses the maturation of a fluorescent timer (Timer) protein to show temporal changes in transcription. Here, Tocky was developed and used to study *in vivo* transcriptional dynamics of *Foxp3* and a gene immediately downstream TCR signalling, *Nr4a3*, to analyse Treg differentiation and TCR signalling downstream activities. In *Nr4a3*-Tocky mice, Timer^{+} cells were enriched with cells that undergo negative and agonist selection. *Nr4a3*-Tocky:*Bim*$^{\mathrm{KO/KO}}$ mice showed that Bim-mediated negative selection occurred rapidly at both DP and SP stages in the most immature Timer^{+} cells. *Foxp3* was detected after Bim transcription was downregulated in Timer^{+} cells, following persistent TCR signals. Intriguingly, in *Nr4a3*-Tocky:*Bim*$^{\mathrm{KO/KO}}$ mice Timer^{+} cells were enriched with cells that escaped negative selection and highly self-reactive *Foxp3*$^{+}$ cells were accumulated in both DP and SP fractions. Based on this work, a new model for the temporal order of thymic selection processes and T cell maturation is proposed.

Contents

Nomenclature

AIRE Autoimmune regulator

APECED Autoimmune polyendocrinopathy candidiasis ectodermal dystrophy

AP-1 Activator protein 1

APC Antigen-presenting cells

BAC Bacterial artificial chromosome

Bax Bcl-2-associated X protein

Bcl2 B-cell lymphoma 2

BH3 Bcl-2 Homology 3

Bim Bcl-2-like protein 11

CARMA1 Caspase recruitment domain-containing membrane-associated guanylate kinase protein-1

CCR7 C-C chemokine receptor type 7

CD Cluster of differentiation

cDNA complementary DNA

CNS Conserved noncoding sequencing

CRAC Ca^{2+} release-activated Ca^{2+}

cTEC Cortical thymic epithelial cell

CTLA-4 Cytotoxic T-lymphocyte-associated protein 4

DAG Diacylglycerol

DC Dendritic cell

DN Double negative

DNA Deoxyribonucleic acid

dNTP Deoxynucleoside triphosphate

DP Double positive

EDTA Ethylenediaminetetraacetic acid

EGFP Enhanced green fluorescent protein

Egr-1 Early growth response protein 1

Erk Extracellular signal-regulated kinases

FITC Fluorescein isothiocyanate

Foxp3 Forkhead box P3

GADs Grb2-related adaptor downstream of Shc

GATA-3 GATA-binding protein 3

GFP Green fluorescent protein

GITR Glucocorticoid-induced tumor necrosis factor

Grb2 Growth factor receptor-bound protein 2

HVEM Herpesvirus entry mediator

ID3 Inhibitor of DNA binding protein 3

IL Interleukin

ITAM Immunoreceptor tyrosine-based activation motif

IκB Inhibitor of NF-κB

IKK IκB kinase

IP3 Inositol-1,4,5-triphosphate

IPEX Immunodysregulation polyendocrinopathy enteropathy X-linked

JNK c-Jun N-terminal kinase

LAT Linker for activation of T cells

Lck Lymphocyte-specific protein tyrosine kinase

MALT1 Mucosa-associated lymphoid tissue lymphoma translocation protein 1

MAPK Mitogen-activated protein kinase

MFI Mean fluorescence intensity

MHC Major histocompatibility complex

mRNA Messenger RNA

mTEC Medullary thymic epithelial cell

mTORC Mammalian target of rapamycin complex (mTORC)

NF-κB nuclear factor-κB

NFAT Nuclear factor of activated T cells

NOD Non-obese diabetic

Nr4a Nuclear receptor 4A

OVA Ovalbumin

PCR Polymerase chain reaction

PD-1 Programmed death receptor 1

PKCθ Protein kinase C θ

PLC-γ Phospholipase C γ

RAG Recombination-activating gene

RasGRP Ras guanyl nucleotide-releasing protein

RIP-mOVA Rat insulin promoter-membrane-bound OVA

RNA Ribonucleic acid

RNAse Ribonuclease

RNAseq RNA sequencing

RT-qPCR Quantitative reverse transcription PCR

RUNX3 Runt-related transcription factor 3

S1PR1 Sphingosine 1-phosphate receptor 1

SH2 Src Homology 2

SHP-2 SH2 domain-containing protein tyrosine phosphatase-2

SLP-76 SH2 domain-containing leukocyte protein of 76 kDa

SOS1 Son of sevenless homolog 1

SP Single positive

TAE Tris acetate EDTA

TCR T cell receptor

ThPOK T-helper inducing POZ-Kruppel like factor

Timer Fluorescent timer

TNF Tumor necrosis factor

TNFRSF Tumor necrosis factor receptor superfamily

Tocky Timer of cell kinetics and activity

TRA Tissue-restricted antigen

Treg Regulatory T cells

TSO Template-switching oligos

ZAP-70 Zeta-chain-associated protein kinase 70

List of Figures

List of Tables

Introduction

In mammals, the immune system features an intricate network of organs, cells and proteins with the main role of protecting the host against pathogens. Two major branches of the immune system have been defined according to the specificity of the response: innate and adaptive. Innate immunity features fast-acting responses to infection and is carried out by neutrophils, macrophages and dendritic cells (DCs). Adaptive immunity, on the other hand, can provide long-lasting protection against a particular pathogen due to the ability of T and B cells to generate immunological memory. This study is centered around T cells, with a view to understanding the key developmental processes that must occur before they qualify as functionally mature. A fully developed T cell can either express the surface molecule cluster of differentiation (CD) 4 or CD8. CD4 T cells are also referred to as "helper" cells due to their role in promoting antibody production by B cells. They indirectly orchestrate an immune response by releasing small signalling molecules known as cytokines to recruit other cells. CD8 T cells, on the other hand, can mount a direct attack on cancerous or infected cells by secreting destructive molecules named cytotoxins, such as perforins, granzymes and granulysins. For this reason, CD8 T cells are also termed "killer" or "cytotoxic" T cells (Murphy et al., 2017).

1.1 The T cell Receptor

What distinguishes T cells from other immune components is their T cell receptor (TCR), a protein complex capable of recognising pathogen-derived peptide sequences, known as "antigens". These peptides are presented to them by other cells on a major histocompat-

ibility complex (MHC) molecule. All nucleated cells can make MHC class I molecules, which are exclusively recognised by CD8 T cells. CD4 T cells can only interact with MHC class II molecules, which are mainly found on the surface of professional antigen-presenting cells (APC), such as macrophages and DCs. Antigen recognition translates into a cascade of signalling events inside the cell, leading to transcription of the genes required for an appropriate response. Receptor activation followed by such intracellular processes are collectively referred to as "TCR signalling" (Murphy et al., 2017).

The structure of a TCR is illustrated in Fig.1.1. While the $\alpha\beta$ heterodimer is found on the surface of most T cells, a very small fraction of T cells express γ and δ chains instead. Regardless of type, these proteins confer TCR antigen specificity, but do not have any inherent signal transducing properties. However, they non-covalently associate with the CD3 complex, which can signal intracellularly. This is achieved by the presence of tyrosine-based activation motifs (ITAMs) on the CD3 subunits γ, δ, ϵ and ζ, which act as docking sites for Src Homology 2 (SH2) domain-containing signalling molecules (Gaud, Lesourne and Love 2018).

The extracellular domains of CD4 and CD8 bind to highly conserved regions on MHC molecules, while their intracellular structures bind lymphocyte-specific protein tyrosine kinase (Lck), which phosphorylates ITAMs and facilitates the recruitment and activation of another tyrosine kinase, Zeta-chain-associated protein kinase 70 (ZAP-70). The cytoplasmic domain of the CD8 co-receptor engages less efficiently with Lck than that of CD4, thus presumably promoting weaker signaling (Wiest 1993). Activated ZAP-70 then phosphorylates the transmembrane adaptor linker for activation of T cells (LAT), allowing for the docking of several adaptor and effector molecules and the subsequent formation of the LAT signalosome complex (Fig.1.1). The LAT signalosome facilitates TCR signal propagation through the major pathways involving Ca^{2+}-calcineurin, mitogen-activated protein kinase (MAPK) and nuclear factor-κB (NF-κB), leading to the respective ac-

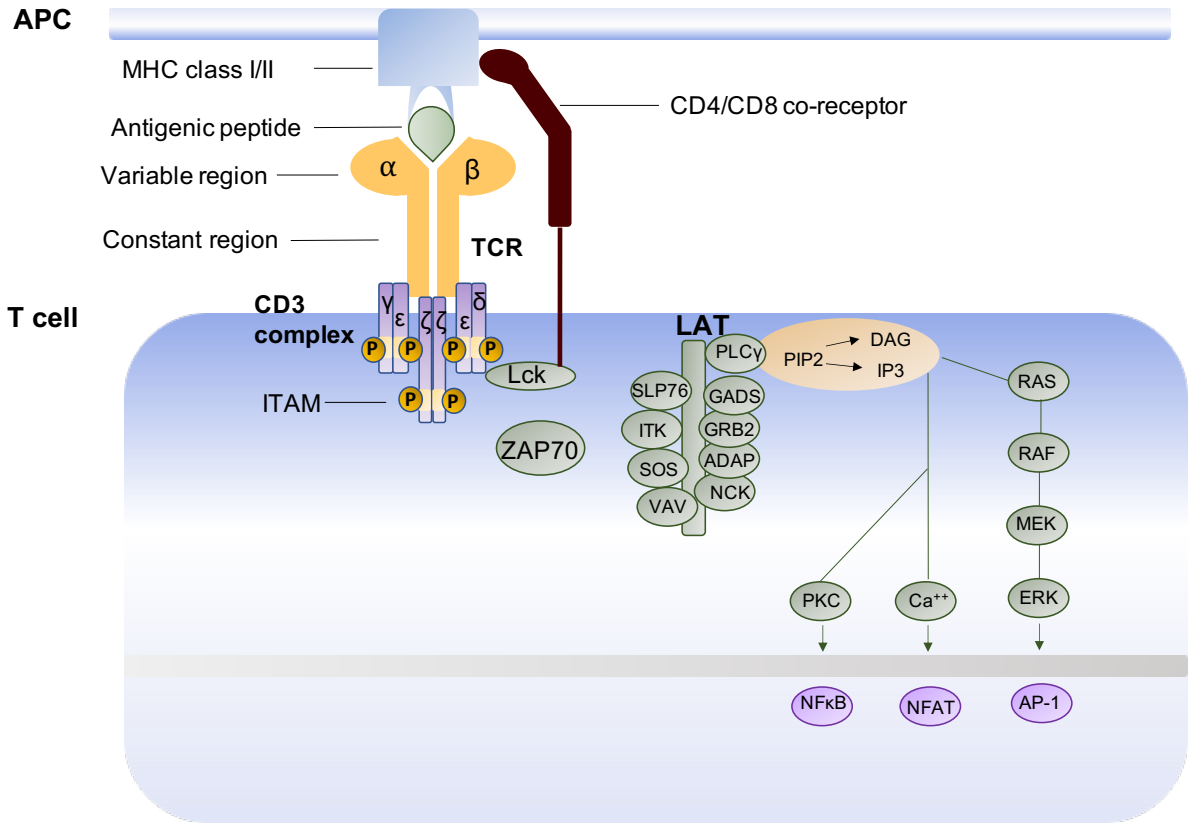

Figure 1.1: **The main elements involved in TCR signalling.**

tivation and nuclear translocation of transcription factors nuclear factor of activated T cells (NFAT), activator protein 1 (AP-1) and NF-κB/REL. Multiple T cell responses can thus be generated, including proliferation, cytokine production and migration (Gaud, Lesourne and Love 2018).

By modifying existing molecules already present in the cytoplasm, TCR signals can be conveyed rapidly, within seconds to minutes. New gene transcription, however, is a slower process, requiring around one hour. Newly transcribed genes involved in cell proliferation include the ones encoding the pleiotropic cytokine interleukin (IL) 2, which provides high affinity to the dimeric receptor IL2Rα (CD25) (Gaud, Lesourne and Love 2018). The cell also transcribes genes for molecules associated with pro-apoptotic effects, such as members of the nuclear receptor 4A (Nr4a) family (Thompson and Winoto, 2008). In this manner, TCR signalling dictates T cell response.

1.2 β-selection

Lymphoid progenitors of T cells originate in the bone marrow from hematopoetic stem cells. Their nomenclature, however, is owed to the fact that they are only able to mature upon migration to the thymus, a bilobed lymphoid organ that facilitates the necessary conditions for T cells to acquire their functional identity. The organ is divided into the cortical and medullary regions, surrounded by a capsule, and these highly complex microenvironments direct T cell development with the help of MHC-expressing cells, namely cortical thymic epithelial cells (cTEC), medullary thymic epithelial cells (mTEC), DCs, macrophages and B cells. Several checks are in place to assess whether a functional TCR has been assembled. Receptor diversity is achieved upon genetic recombination of germ-line encoded gene segments upon expression of the recombination-activating genes (RAG) 1 and 2. This process is, however, random and the T cell might either not be able to receive a signal or bear receptor specificity to self-antigens, which would result in autoimmune responses. Therefore, the process of T cell development also includes mechanisms for deletion of potentially harmful cells (Murphy et al., 2017).

The first screening process that cells are subjected to occurs in the cortex, where progenitors do not yet express either of the CD4 and CD8 co-receptors. They are designated as double negative (DN) stage, where they first upregulate RAG-1 and RAG-2. This stage is divided into four phases, ranging from DN1 to DN4, which have been characterised based on cell surface expression of CD25 and the adhesion molecule CD44, as illustrated in Fig.1.2. It is at this stage that T cells may become either $\alpha\beta$ or $\gamma\delta$, but complete lineage commitment is believed to only occur by the DN3 phase (Pereira, Boucontet and Cumano, 2012). This study will focus on $\alpha\beta$ T cells.

At the DN3 phase, $\alpha\beta$ T cell precursors undergo their first major selection process, known as β-selection. The name stems from the fact that in order to progress to DN4, the cell must have assembled a pre-TCR structure formed by an invariant pre-TCRα-chain and a fully re-arranged β-chain, which can receive a survival signal that leads to proliferation and subsequent progression to the DN4 phase. Since RAG-dependent recombination will probabilistically render many aberrant structures, this process specifically selects for successfully assembled β-chains (Carpenter and Bosselut, 2010). It has not yet been clarified, however, how the survival signal is delivered. The Saito lab proposed an oligomerisation mechanism for achieving pre-TCR signalling (Yamasaki et al., 2005), as no ligand had been found originally to be recognised by the pre-TCR structure (Irving, 1998). A decade later, however, specific interactions of low affinity were shown to occur between β-chains and peptide-MHC ligands (Mallis et al., 2015). These seemingly opposing studies were addressed by Yang and Mariuzza, who proposed that while the signal would be achieved via oligomerisation, this selection process may favour proliferation of pre-TCR-bearing cells which are also able to interact with peptide-bound MHC molecules with a view to optimising the final receptor repertoire (Yang and Mariuzza, 2015).

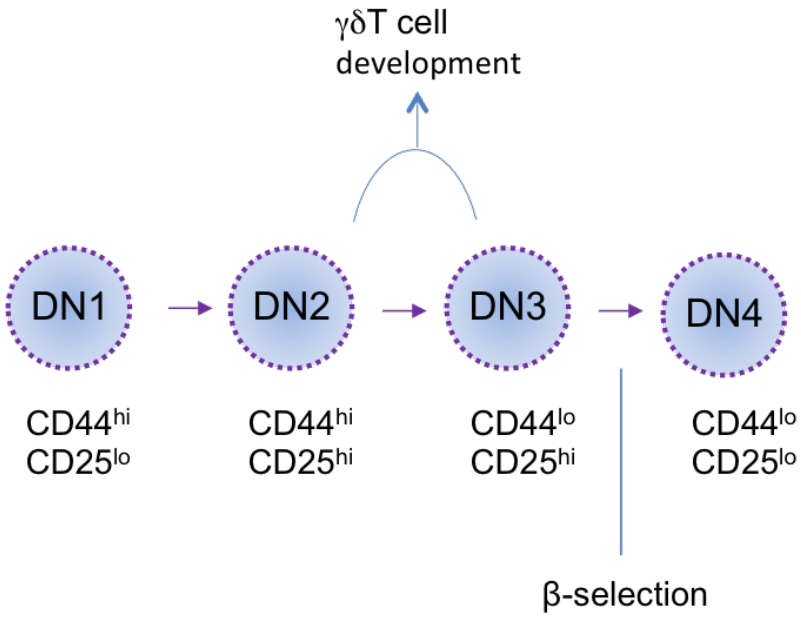

Figure 1.2: **T cell precursor progression through the double negative (DN) stage.** The four phases of development are defined according to surface expression of the markers CD44 and CD25.

1.3 Positive Selection

Proliferated DN4 thymocytes upregulate both CD4 and CD8 co-receptors, becoming double positive (DP) cells. RAG-1 and RAG-2 are once more activated to facilitate re-arrangement of the α-chain. Cells with fully formed $\alpha\beta$TCRs must then pass what is known as "positive selection" in order to continue their survival. A receptor is deemed as successfully assembled if it can recognise an antigen-MHC complex presented by cTECs. This leads to the propagation of a survival signal through the cell which activates its proliferation machinery. As few as 10% of DPs pass positive selection and become single positive (SP) T cells by downregulating either CD4 or CD8, while the majority never receive the signal to proliferate and undergo death by neglect (Murphy et al., 2017). Throughout this thesis, $CD4^{+}CD8^{-}$ and $CD4^{-}CD8^{+}$ T cells are referred to as CD4 SP and CD8 SP, respectively.

The transmembrane glycoprotein CD69 is an early activation marker closely associated with DP cells initiating positive selection (Chan et al., 1993), as well as with recent TCR signals (Sancho, Gomez and Sanchez-Madrid, 2005). It was argued that CD69 rather marks the end stages of positive selection, as its expression was associated with DP populations deemed as most differentiated, which would have selectively terminated synthesis of one of the two co-receptors (Punt et al., 1996). A more recent study identified a consistent drop in CD69 levels when culturing positive-selecting thymic sections. They concluded that the brief window during which CD69 expression failed to be maintained marked an early and late phase of positive selection (Ross et al., 2014).

1.4 Negative Selection

Positive selection ensures that a TCR is successfully re-arranged to be able to produce a signal. Since this effect is the result of T cell interactions with host-derived antigens,

positively selected cells now represent a potential risk, as they can become self-reactive when encountering the same antigen in the periphery and produce autoimmune responses. Only cells bearing TCRs that weakly bind self-antigen should therefore be allowed to mature, while T cells that have high affinity for host molecules must be deleted. In response to this, the thymic environment subjects all T cells to another screening process known as negative selection (Hogquist, Baldwin and Jameson, 2005).

Negative selection is thought to occur in the cortico-medullary juction, where professional APCs present developing T cells with endogenous antigen. Weak interactions between TCRs and peptide-MHC complexes qualify the cell for maturation, while very strong signalling results in clonal deletion. Thymocytes that surpassed all negative selection mechanisms briefly reside as mature CD4 or CD8 SP cells in the medulla, before migrating out of the thymus to occupy peripheral niches. There are cells that respond to self-antigen, however, with moderate affinity. It is believed that such cells are allowed to survive via what is known as agonist selection and develop into a unique lineage, namely regulatory T cells (Treg), with the unique role of suppressing other immune cells in the periphery (Hogquist, Baldwin and Jameson, 2005).

1.5 Regulatory T cells

CD25 was originally identified as a very sensitive marker for Treg in mice. (Takahashi et al., 2000). While it is still widely used, the hallmark of regulatory T cells is expression of the master regulator gene forkhead box P3 (*Foxp3*). This transcription factor is not only considered essential in committing a cell to the Treg lineage, but it is also believed to be the main contributor to their suppressive function (Ramsdell, 2003). The suppressive capacity of cells that express high levels of Foxp3 was found to be superior to that of intermediate expressers (Fujii et al., 2016). In humans, mutations in the *FOXP3* gene are a direct cause of the Immunodysregulation, polyendocrinopathy, enteropathy, X-linked

(IPEX) syndrome, a severe autoimmune disorder associated with a defective Treg pool (d'Hennezel et al., 2009). A similar condition can be induced in mice through a missense mutation in the *Foxp3* gene. The murine model is known as "scurfy" and develops multiorgan autoimmunity linked to absence of Treg (Ramsdell, 2003).

The most abundant and well studied suppressive T cells are those of the the CD4 lineage. Although $CD8^+$ Tregs were recognised as early as 1970 (Gershon and Kondo, 1970), they represent a very small and little understood population. Conventional $Foxp3^-CD4^+$ T cells and $Foxp3^+CD4^+$ Treg have different requirements for development. While conventional T cells pass negative selection through weak TCR interactions with self-antigen, Treg are only favoured if the strength of interaction lies between that required for positive selection and that promoting clonal deletion (Maloy and Powrie, 2001). The two populations have been widely considered to arise from a common precursor, yet little overlap was found between their TCR repertoires (Hsieh et al., 2004; Pacholczyk et al., 2006). Furthermore, the self-antigens associated with Treg selection appeared to be uncommon (Hsieh, Lee and Lio, 2012).

It is not fully established how early Treg selection occurs. While most Foxp3-expressing cells were found in the thymic medulla, about one fifth of them resided in the cortex (Owen et al., 2019). The cortex has been shown to allow for Treg development (Liston et al., 2008) and their precursors might emerge as early as the DP stage. These Treg precursors are identified by an increased expression of CD25 and glucocorticoid-induced tumor necrosis factor (GITR) compared to other DPs (Fontenot et al., 2005; Krishnamurthy et al., 2015). In fact, $Foxp3^+$ DP thymocytes are present in WT mice and can account for a quarter of the total $Foxp3^+$ thymocyte number. Phenotypically, they are high in CD69 and C-C chemokine receptor type 7 (CCR7), suggesting they have been positively selected and are able to enter the medulla (Liston et al., 2008). However, $Foxp3^+$ DPs are mainly found in the proximity of the cortico-medullary junction (Fontenot et al., 2005).

Therefore, it is yet to be clarified whether Treg differentiation successfully occurred or if Foxp3 expression at the DP stage is an aberrant expression by cells that are fated for deletion by negative selection. The existence of such Foxp3$^+$ DP cells suggests that the initiation of Foxp3 expression is a consequence of the TCR signals that they encounter, regardless of their stage of development. It was even suggested that some thymocytes are primed for Foxp3 expression as early as the DN stage (Pennington et al., 2006) and, indeed, a small GITR^{hi}Foxp3$^+$CD4$^-$CD8$^-$ population has been described by the Rudensky lab (Fontenot et al., 2005). The same study also proposed that Foxp3 upregulation occurs independently of CD4/CD8 lineage selection mechanisms upon identification of Foxp3$^+$ DPs in both MHC class I and MHC class II-deficient mice (Fontenot et al., 2005).

1.6 TCR signalling during T cell development

How signalling through the same TCR can lead to opposing developmental outcomes of cellular differentiation and death is not fully understood. However, significant progress has been made in understanding which intracellular molecules are required for induction of either positive or negative selection. Both selection processes require Lck phosphorylation of ZAP-70 and subsequent activation of LAT. However, it is possible that they rely on differential phosphorylation of LAT. Different tyrosine residues of LAT are required for the recruitment of Phospholipase C γ (PLC-γ) and Growth factor receptor-bound protein 2 (Grb2), which have been found to be involved in positive and negative selection, respectively (Starr, Jameson and Hogquist, 2003; Kappes and Soboloff, 2018).

Short-lasting, low-affinity ligand/TCR interactions likely induce partial LAT phosphorylation that results in the recruitment of Grb2-related adaptor downstream of Shc (GADs) and SH2 domain-containing leukocyte protein of 76 kDa (SLP-76), which in turn recruit PLC-γ. PLC-γ then generates the secondary messengers inositol-1,4,5-triphosphate (IP3) and diacylglycerol (DAG). IP3 binds the IP3 receptor on the endoplasmic reticulum and

mobilises the release of Ca^{2+} into the cytosol. In turn, intracytoplasmic Ca^{2+} activates calmodulin, which activates the phosphatase calcineurin. Calcineurin dephosphorylates the NFAT transcription factor family, allowing it to translocate to the nucleus and activate gene transcription (Starr, Jameson and Hogquist, 2003; Kappes and Soboloff, 2018). T cells express three NFAT isoforms, namely NFAT1, NFAT2 and NFAT4 (Macian, 2005). A study that analysed NFAT4-deficient mice found this isoform to be particularly involved in positive selection and DP cell survival (Oukka et al., 1998). DAG is also important in positive selection, as it promotes recruitment of Ras guanyl nucleotide-releasing protein (RasGRP) to the Golgi apparatus, where it activates Ras. Ras then triggers the MAPK cascade, resulting in low, sustained activation level of extracellular signal-regulated kinase (Erk). Erk then translocates to the nucleus, where it likely induces early growth response protein 1 (*egr-1*) gene expression. Transcription factor Egr-1 positively regulates expression of the inhibitor of deoxyribonucleic acid (DNA) binding protein 3 (ID3), which is involved in finalising TCRα chain rearrangement (Starr, Jameson and Hogquist, 2003; Kappes and Soboloff, 2018).

In the case of negative selection, sustained, high-affinity ligand/TCR interactions induce complete LAT phosphorylation. This allows LAT to activate the Grb2/son of sevenless homolog 1 (SOS1) complex, which was shown capable of recruiting Ras to the plasma membrane (Cheng et al., 1998). The MAPK cascade is triggered, resulting in Erk activation of a much higher magnitude and shorter duration than during positive selection-inducing TCR signalling. P38 and c-Jun N-terminal kinase (JNK) are concomitantly activated, both which are involved in negative selection. P38 promotes nuclear degradation via caspase-dependent and independent pathways. JNK can also trigger caspase-dependent cascades at the mitochondria, as well as activate pro-apoptotic members of the B-cell lymphoma 2 (Bcl2) family, such as Bcl-2-like protein 11 (Bim). Furthermore, JNK can translocate to the nucleus and increase the expression of pro-apoptotic genes by transactivating the c-Jun component of the AP-1 transcription factor (Rincón, Flavell and

Davis, 2000). Interestingly, the JNK signal transduction pathway was found to uniquely restrict nuclear translocation of NFAT4 amongst its family members (Chow et al., 1997).

Different localisation of Ras recruitment and subsequent MAPK pathway activation in cells undergoing positive and negative selection (at the Golgi and at the plasma membrane, respectively) may be one of the main distinguishing factors between the two outcomes. Another factor may be Ca^{2+} signalling. During negative selection, intracytoplasmic Ca^{2+} levels are sustained via Ca^{2+} release-activated Ca^{2+} (CRAC) channels. Positive selection, on the other hand, relies on voltage-gated Na^{+} channels and CRAC channels are dispensable. One study showed that Ca^{2+} signalling during negative selection promote protein kinase C θ (PKCθ) activation and subsequent production of Bim. The study proposed a model in which higher levels of intracytoplasmic Ca^{2+} lead to the activation of a dominant pathway over that required for positive selection, resulting in cellular apoptosis (Canté-Barrett et al., 2006).

Precisely how TCR signals propagate differently in response to agonist and negatively selecting ligands is not understood. TCR signals required for thymic Treg differentiation are believed to promote Ca^{2+}-dependent activation of PKCθ and subsequent activation of the caspase recruitment domain-containing membrane-associated guanylate kinase protein-1 (CARMA1)/Bcl10/mucosa-associated lymphoid tissue lymphoma translocation protein 1 (Malt1) complex, which activates inhibitor of NF-κB (IκB) kinase (IKK) and results in the ubiquitinylation of IκB. This frees NF-κB to translocate to the nucleus. Of all the Rel/NFκB transcription factor family, c-Rel is thought to be the most important in thymic Treg development. Evolutionarily conserved noncoding sequencing (CNS) located in the introns of the *Foxp3* gene have proven indispensable for efficient *Foxp3* expression. Of these, the enhancer element *Cns3* has been identified as the most important for thymic Treg selection. It has been suggested that following TCR interaction with agonist-selecting self-antigens, c-Rel binds to *Cns3*, resulting in *Foxp3* expression (Engel

et al., 2013; Li and Rudensky, 2016).

1.7 The TNF Receptor Superfamily

The tumor necrosis factor receptor superfamily (TNFRSF) features several cytokine receptors capable of binding tumor necrosis factors (TNFs), with main functional roles in cellular apoptosis, survival and development. High affinity receptor ligation initiates signal transduction cascades, which may generally lead to activation of either the death domain, followed by caspase-dependent pathways, or the ubiquitin E3 ligases family TRAF. While each TNFRSF molecule might signal via a different E3 ligase, the downstream effect is activation of the pro-survival NF-κB pathway (Ward-Kavanagh et al., 2016).

Both TNFR1 and TNFR2 bind TNF, generally with the opposing effects of cell death and survival, respectively. While TNFR1 is ubiquitously expressed, TNFR2 is only found on certain cell types, including T cells, and its ligation results in NF-κB activation. TNFR2 has also been implicated in thymic Treg development from precursor cells and its expression on naturally occurring Treg was dominant to TNFR1 (Faustman and Davis, 2013).

Another TNF receptor that is highly expressed on Treg precursors is GITR. Nishimura et al. showed that GITR expression on developing Treg precedes Foxp3 upregulation in vivo (Nishimura et al., 2004). Its ligand GITRL is present on the surface of mTECs and, upon receptor engagement, it promotes precursor maturation into Treg through upregulation of CD25 (Mahmud et al, 2014). GITR has also been proposed as a protective molecule against negative selection of developing Treg, as constitutive expression was shown to specifically inhibit TCR-induced apoptosis (Nocentini et al., 1997). Mature Treg then express GITR constitutively, while naïve T cells only show increased expression upon TCR stimulation (Kanamaru et al., 2004).

In addition to GITR and TNFR2, Treg progenitors were also shown to preferentially upregulate a third member of the TNFRSF, namely OX40. GITR-deficient and OX40-deficient mice generated a mature Treg pool that was smaller than that of wild-type mice by 30% and 50%, respectively. Since TNFR2-deficient mice do not develop any fatal disease, it was postulated that they are also able to produce mature Treg. When any two of the three TNFRSF members were absent, the mature Treg pool was significantly more affected and when expression of all three receptors was impaired, mature Tregs were nearly absent. Therefore, TNFR2, GITR and OX40 play a collective role in thymic Treg development (Mahmud et al, 2014).

1.8 CD4 and CD8 lineage choice

It is not fully known how a T cell may become either CD4 or CD8-restricted, but several theories have been studied. The instructive model proposes that lineage choice depends on which class of MHC molecule the cell is positively selected on at the DP stage (Robey et al. 1991). According to the stochastic model, T cells randomly downregulate CD4 or CD8 and survive if the resulting co-receptor corresponds to their TCR specificity (Chan et al. 1993; Davis et al. 1993). Both of these theories have been heavily disputed (He, Park and Kappes 2010) and a more refined view states that TCR strength is the actual determinant of lineage choice, where stronger signals promote CD4 SP differentiation, while weaker signals are associated with CD8 SP development. This is known as the qualitative instructive model (Matechak et al. 1996).

The prospect that lineage choice may happen beyond the DP stage gave rise to yet another perspective, the kinetic signalling model (Cibotti et al. 2000). All DP thymocytes appear to undergo an intermediate phase characterised by downregulation of CD8, becoming lineage uncommitted $CD4^{+}CD8^{lo}$. While MHC-II-restricted cells may then immediately transition to CD4 SP, MHC-I-restricted cells have to go through yet another

intermediate phenotype as $CD4^{lo}CD8^{lo}$ T cells before becoming CD8 SP (Lundberg et al. 1995; Suzuki et al. 1995; Lucas and Germain 1996). According to the kinetic signalling model, since loss of CD8 transcription in $CD4^{+}CD8^{lo}$ cells would terminate TCR signals induced by MHC-I but not by MHC-II, persistent TCR signals commit $CD4^{+}CD8^{lo}$ intermediates to a CD4 SP phenotype, while their cessation to that of CD8 SP. In this manner, longer or shorter duration of TCR signaling is associated with CD4 or CD8 SP lineage choice, respectively (Cibotti et al. 2000; Sarafova et al. 2005). Subsequent work by Sinclair and Seddon, however, found no link between premature termination of TCR signals in $CD4^{+}CD8^{lo}$ cells and choice of lineage. Using an inducible ZAP-70 mouse model, they showed that survival of both CD4 and CD8 cells was considerably affected by discontinued TCR signaling, but this did not appear to divert developing SP cells towards one phenotype or the other (Sinclair and Seddon, 2014).

There is evidence to suggest that co-receptor-Lck interaction during positive selection affects the developmental program of T cells (Hernandez-Hoyos et al. 2000). Following positive selection, lineage commitment to CD4 and CD8 SP occurs with the expression of the mutually repressive transcription factors T-helper inducing POZ-Kruppel like factor (ThPOK) (He et al. 2005) and Runt-related transcription factor 3 (Runx3) (Sato et al. 2005), respectively. ThPOK activity is dependent on another transcription factor, GATA-binding protein 3 (GATA-3) (Wang et al. 2008), which may play a role in T cell differentiation by suppressing Runx3 in order to allow ThPOK expression and therefore CD4 SP development (Xiong et al. 2013). In MHC-I-restricted $CD4^{+}CD8^{lo}$ cells, CD8-dependent TCR signalling is absent and cytokines such as IL-7 are believed to promote Runx3 expression and commit the cell to become CD8 SP (Cibotti et al. 2000; Park et al. 2010). The Singer lab identified two phases of MHC-I positive selection, characterised by dynamic changes in CD8 expression. The first phase and the second phase were exclusively dependent on TCR signaling and cytokine stimulation, respectively. The cell is believed to be committed to become CD8 SP only following the second

phase, where Runx3 transcription first occurs. Interestingly, artificial prolongation of normally observed MHC-I signaling duration led to ThPOK upregulation and erroneous commitment of these cells to the CD4 lineage (Kimura et al. 2016).

1.9 CD4 and CD8 expression dynamics

A model for the CD4/CD8 expression dynamics on a flow cytometry plot is shown in Fig.1.3. $CD4^{-}CD8^{-}$ cells that successfully re-arranged their TCR simultaneously upregulate both co-receptors to become $CD4^{+}CD8^{+}$. According to the kinetic model, TCR ligation with positively-selecting ligands leads to a selective reduction of CD8 expression. This results in a $CD4^{+}CD8^{lo}$ phenotype (Singer, Adoro and Park, 2008). Experimental data suggests that this is not a consequence of receptor internalisation, but of *Cd8* gene downregulation (Barthlott, Kohler and Eichmann, 1997; Bosselut et al., 2003). In spite of this, it has been accepted that $CD4^{+}CD8^{lo}$ cells are lineage uncommitted (Brugnera et al., 2000). If TCR signalling persists in the absence of *Cd8* transcription, then the cell becomes $CD4^{+}CD8^{-}$. Alternatively, if the cell is MHC-I-restricted, $CD4^{+}CD8^{lo}$ cells are able to terminate *Cd4* transcription and re-upregulate *Cd8*. This process is known as co-receptor reversal and only occurs in cells that no longer receive TCR signals (Yu et al., 2003). In this manner, cytokines such as IL-7 can help $CD4^{+}CD8^{lo}$ differentiate into $CD4^{-}CD8^{+}$ (Singer, Adoro and Park, 2008). As *Cd4* transcription ceases and until CD8 becomes fully re-upregulated, the MHC-I-restricted cell may temporarily adopt a $CD4^{lo}CD8^{lo}$ phenotype (Lucas and Germain 1996). A remarkable difference in the time required for reaching the single positive stage was found between the CD4 and CD8 cell lineages. Unlike $CD4^{+}CD8^{-}$ cells, which appeared 30 hours after induction of TCR signalling, $CD4^{-}CD8^{+}$ cells required up to 4 days to develop (Sinclair and Seddon, 2014).

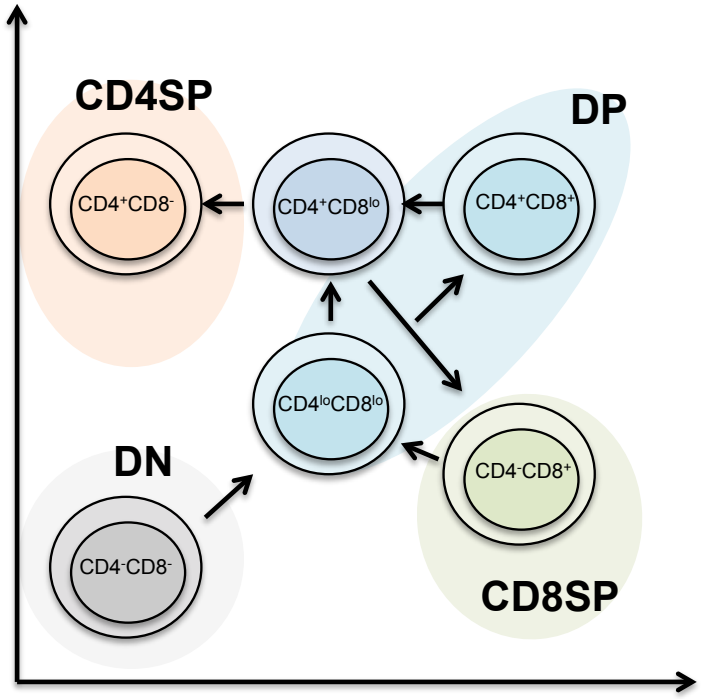

Figure 1.3: **CD4 and CD8 expression dynamics during T cell development.** Different stages of T cell development are characterised according to CD4 and CD8 co-receptor expression. DN cells have a $CD4^{-}CD8^{-}$ phenotype, while DP cells can be $CD4^{+}CD8^{+}$, $CD4^{+}CD8^{lo}$ or $CD4^{lo}CD8^{lo}$. Lineage committed CD4SP and CD8SP are $CD4^{+}CD8^{-}$ and $CD4^{-}CD8^{+}$, respectively. Figure was inspired by the kinetic signalling model for T cell development described by Singer, Adoro and Park, 2008.

1.10 Programmed Death Receptor-1

Programmed death receptor 1 (PD-1) is the most recently discovered member of the B7/CD28 family, which includes the co-stimulatory molecules CD28 and cytotoxic T-lymphocyte-associated protein 4 (CTLA-4) that augment and antagonise TCR signalling, respectively. The cytoplasmic domain of PD-1 features immunotyrosine-based motifs and their phosphorylation recruits the tyrosine phosphatase SH2 domain-containing protein tyrosine phosphatase-2 (SHP-2). In the case of activated T cells, tyrosine phosphorylation may be achieved by Lck. SHP-2 recruitment leads to dephosphorylation of molecules involved in TCR signal propagation, such as ZAP-70 and PKCθ, and inhibition of Ca^{2+} mobilisation. In this manner, PD-1 ligation blocks TCR signals (Okazaki et al., 2001; Sheppard et al., 2004).

Its inhibitory role in maintaining tolerance to self is highlighted by PD-1 deficient animal models which develop autoimmunity (Nishimura et al., 1999; Nishimura et al., 2001). PD-1 is believed to act by negatively regulating the signalling threshold of the TCR, therefore influencing TCR-induced thymocyte maturation. PD-1 deficient mice produce a population of DN cells which fail to upregulate any of the lineage co-receptors before migrating to the periphery (Blank et al., 2003). PD-1 deficiency has been associated with accelerated β-selection and a decreased efficiency in positive selection. The latter observation was attributed to the former effect, whereby many PD-1 deficient DN cells mature into DP by mounting a weaker signal through their pre-TCR than that required to pass positive selection (Nishimura, Honjo and Minato, 2000). RAG-deficient DP cells that lacked PD-1 protein expression were significantly more apoptotic than PD-1 sufficient ones, indicating augmented negative selection (Blank et al., 2003). According to microarray data from Baldwin and Hogquist, expression of the gene encoding PD-1 was induced by cells undergoing clonal deletion, but not positive selection (Baldwin and Hogquist, 2007). Collectively, these findings indicate a role for PD-1 in rescuing cells that

show a certain degree of self-affinity, while limiting their TCR signals in order to prevent autoimmune reactions.

1.11 The Nr4a Receptor Family

The Nr4a orphan nuclear receptor family comprises three members: Nur77 (Nr4a1), Nurr1 (Nr4a2) and Nor-1 (Nr4a3). Early studies involving T cell hybridomas identified Nr4a1 as an immediate early gene inducible by TCR signalling and an apoptosis mediator in developing thymocytes (Liu et al., 1994; Woronicz et al., 1994). Nr4a1 was further classified as a pro-apoptotic contributor to negative selection (Calnan et al., 1995). While constitutive expression of Nr4a1 leads to apoptosis, transient expression does not (Calnan et al., 1995; Winoto and Littman, 2002). Individual deletion of Nr4a1 does not lead to any phenotypic changes in thymocytes (Lee et al., 1995), while inhibition of all three Nr4a family members impairs negative selection (Calnan et al., 1995; Zhou et al., 1996). A plausible explanation for these phenomena is functional redundancy between Nr4a1 and Nr4a3. Structurally, Nr4a1 has the typical organisation of a steroid receptor, featuring a central DNA-binding domain with two zinc fingers, an N-terminal transactivation domain and a C-terminal ligand-binding domain (Carson-Jurica, Schrader and O'Malley, 1990). Functional redundancy between the Nr4a family members in thymocytes is very likely, since they show strong homology of their DNA-binding domains, with Nr4a1 and Nr4a3 sharing over 90% (Cheng et al., 1997). They lose this shared similarity towards the N and C termini, which might explain the observed differences in their levels of induction upon TCR signaling and nucleus-to-mitochondria translocation times (Cheng et al., 1997; Thompson and Winoto, 2008).

Recent work by the Bending lab identified differences in terms of TCR signalling requirements between Nr4a1 and Nr4a2-3. All Nr4a receptors required Lck activation following TCR signals and they were also reliant on Erk signalling for efficient transcription.

However, Nr4a2 and Nr4a3, but not Nr4a1, were shown to be absolutely dependent on calcineurin-mediated Ca^{+} signalling and subsequent activation of NFAT1. While this pathway appeared redundant for Nr4a1 transcription, overexpression of NFAT1 alone could induce both Nr4a2 and Nr4a3 (Jennings et al., 2019).

The Winoto lab compared the three Nr4a family members in terms of their transactivation mechanisms, DNA binding activity, ability to promote thymocyte apoptosis and induction kinetics during TCR-mediated apoptosis. Transactivation of all three receptors was inhibited by a dominant-negative Nur77 protein, leading to the conclusion that they share the same transactivation mechanisms. However, only Nr4a1 and Nr4a3 proteins were detected following TCR stimulation, showing mirrored kinetics of expression. The proteins were not present in resting, unstimulated cells and their constitutive expression was associated with massive thymocyte apoptosis (Cheng et al., 1997).

Following a data-oriented multidimensional analysis, Nr4a3 was identified as having the highest correlation with T cell activation among the members of the Nr4a family, followed by Nr4a1 (Bending at al., 2018). Using transgenic mice that constitutively express Nr4a1 or Nr4a3, the Winoto lab captured a dramatic decrease in the DP cell population. SP fractions were also lower compared to WT control (Cheng et al., 1997). In a murine model that expresses a dominant-negative Nr4a1, in which protein expression of all endogenous Nr4a receptors is blocked, negative selection is dysregulated. Positive selection, on the other hand, remains unaffected (Calnan et al., 1995; Zhou et al., 1996). Interestingly, negative selection in this case was inhibited when induced by antigen stimulation, but not when elicited by superantigens (Calnan et al., 1995).

Using BDC2.5 and OT-II/rat insulin promoter-membrane-bound ovalbumin (RIP-mOVA) mice, the Benoist and Mathis labs also showed a role for Nr4a1 in negative selection. In the BDC2.5 transgenic model, all T cells bear TCRs specific for the strongly agonis-

tic BDC2.5 peptide and become immediately deleted in its presence. Similarly, OT-II mice express MHC-II restricted TCRs that are reactive to ovalbumin (OVA). In the OT-II/RIP-mOVA double transgenic model, OVA is ectopically expressed at low levels by mTECs. In the presence of their cognate antigen, BDC2.5 mice deficient in Nr4a1 had more DP cells than WT, but this effect disappeared with increasing doses of antigen. Nr4a1 deficiency partially reversed the clonal deletion of OT-II/RIP-mOVA cells in the presence of ovalbumin, suggesting the receptor might be required for efficient negative selection. The authors also highlighted a role for Nr4a1 in agonist selection. Both transgenic and non-transgenic mice deficient in Nr4a1 showed a marked increase in $Foxp3^{+}CD25^{+}$ SP cells compared to WT. The authors concluded that while Nr4a1 influences agonist selection and limits Treg pool size, it has no functional implications in Treg development, as the excess $Foxp3^{+}$ cells observed in its absence developed normally (Fasset et al., 2012).

Sekiya et. al showed that Nr4a receptors are highly important for Treg development. Their findings suggested a large degree of redundancy between the three proteins, mainly due to homology of their DNA binding domains. Nr4a triple knockout mice are largely deficient in Treg and rapidly succumb to autoimmune disease induced death. The authors proposed that Nr4a receptors elicit their roles in T cell selection and development by acting as "translators" of TCR signal strength (Sekiya et. al, 2013). Fasset et al. found a remarkable increase in Foxp3 cells in the absence of Nr4a1 (Fasset et al, 2012). Sekiya et al. observed only a slight increase when Nr4a1 and Nr4a2 were deleted, but a marked decrease when Nr4a1 and Nr4a3 were deleted. In the triple KO they were almost absent. It is likely that the Nr4a receptors are required in regulating agonist selection, both positively and negatively, since they are associated with receipt of TCR signals and "translation" of its strength. They might "decide" if the signal qualifies the cell for agonist or negative selection (Sekiya et al, 2013).

The Hogquist lab identified Nr4a1 transcription to be upregulated during clonal dele-

tion. They captured different expression levels during positive and negative selection, in which Nr4a1 was increased 2-fold and 10-fold, respectively (Baldwin and Hogquist, 2007). The Hogquist lab later generated Nr4a1-GFP reporter mice, a model in which green fluorescent protein (GFP) expression is specifically induced upon TCR antigenic stimulation (and not by inflammatory stimuli) and its level of fluorescence directly correlates with TCR signal strength. Most fluorescence was captured in the medulla, while the cortex showed very little. Their investigations confirmed that GFP was expressed during positive selection *in vivo* (Moran et al., 2011) and the Hogquist lab followed up with a study that would use Nr4a1-GFP mice crossed with Bim-deficient mice in order to quantify thymocytes undergoing both positive and negative selection. Surprisingly, the study found that the majority of developing T cells that receive a signal are strongly self-reactive and undergo clonal deletion. It was estimated that six times more T cells undergo negative selection than positive selection. Furthermore, most cells succumb to clonal deletion in the cortex and only 25% of them in the medulla. Interestingly, the cells that were rescued from clonal deletion in Bim-deficient mice had similar GFP levels to Treg (Stritesky et al., 2013). This suggests that the self-reactivity spectrum distinguishing between negative and agonist selection is very narrow.

The mechanisms by which Nr4a receptors promote apoptosis during negative selection remain unclear. In a study by Cunningham et al., Nr4a1 phosphorylation and compartmentalisation were investigated in DP and SP cells. In DP cells, Nr4a1 was less phosphorylated than in SP cells and was only detected at the nuclear site, which led to the conclusion that its pro-apoptotic function in DP is confined to the nucleus. Unlike DP cells, SP cells featured a hyperphosphorylated form of Nr4a1 that was present in the nucleus, as well as in the cytoplasm. Nr4a1 was not identified, however, at the mitochondria (Cunningham et al., 2006). This final observation is consistent with earlier findings by the Winoto lab, which support a transcription-dependent role of Nr4a1 in the apoptosis of developing thymocytes (Kuang, Cado and Winoto, 1999; Rajpal et al., 2003).

The Winoto lab showed that transgenic expression of Nr4a1 results in a lower percentage of DP cells. Their microarray analysis identified a 2.6-fold increase in the expression of the PD-1-encoding gene, *Pdcd1*, in Nr4a1 transgenic mice when compared with non-transgenic. They ruled out a role for Nr4a1 in apoptosis by mitochondrial translocation when overexpression of the pro-survival protein Bcl-2 failed to antagonise the apoptotic effect of transgenic Nr4a1 expression on DP populations (Rajpal et al., 2003).

Restriction of Nr4a1 to the nucleus and cytoplasm was contradicted by a later study by Thompson and Winoto, who optimised the protocol for the difficult-to-study cytoplasmic environment of thymocytes and revealed the presence of Nr4a1 and Nr4a3 in DP T cells both at nuclear and mitochondrial sites upon TCR stimulation (an effect not observed in unstimulated thymocytes). Using a nuclear export inhibitor, the authors demonstrated that the presence of Nr4a1 and Nr4a3 in the mitochondria resulted from nuclear translocation. Both proteins were associated with Bcl-2 and because the pro-apoptotic Bcl-2 Homology 3 (BH3) domain was exposed following TCR stimulation, the authors proposed a mechanism by which Nr4a1 and Nr4a3 promote clonal deletion during negative selection by causing a conformational change in Bcl-2. Importantly, BH3 exposure was only found in $CD69^{+}$DP cells and not in DN or SP cells (Thompson and Winoto, 2008). This could indicate a specific mechanism for clonal deletion in the cortex. The fact that this effect was still captured in Nr4a1-deficient T cells can be explained by the redundancy between Nr4a1 and Nr4a3 previously proposed by the lab (Cheng et al., 1997). This study, however, analysed mitochondrial localisation of Nr4a receptors in thymocytes in bulk and only when looking at BH2/BH3 domain conformational changes does it separate them into subpopulations. Therefore, it is unclear whether Nr4a1 can translocate in DP cells. It also remains elusive whether this conformational change is an Nr4a1-specific mechanism of action, as a subsequent study by a different lab failed to observe the same effect (Hu and Baldwin, 2015).

Earlier work by the Winoto lab found a strong correlation between the transcriptional activity of Nr4a1 and its ability to induce apoptosis during negative selection. Two different C-terminal truncations rendered one form of Nr4a1 that had very mild transcriptional activity, and another that was very active. Mice transgenic for the former had an almost normal phenotype, while mice transgenic for the latter had almost no DP and SP cells and accumulated a large proportion of DN cells that were also CD3 negative (Kuang, Cado and Winoto, 1999). Hu and Baldwin showed that endogenous Nr4a1 cannot induce caspase-3-mediated apoptosis, but its transgenic expression can. They also showed that cell death associated with Nr4a1 expression first occurs between the DN3 and DN4 stages (Hu and Baldwin, 2015). Based on CD25 expression levels, the Winoto lab found that constitutive Nr4a1 expression negatively affects the transition from DN to the DP stage (Calnan et al., 1995).

1.12 Bim

The Bcl-2 family member protein Bim, short for "Bcl-2 interacting mediator of cell death", is structurally characterised by its highly conserved BH3 motif (Aouacheria et al., 2013), which allows it to heterodimerise with pro-survival proteins and is essential for its caspase-dependent pro-apoptotic function (O'Connor et al., 1998). Another structural characteristic of Bim is a hydrophobic transmembrane domain that facilitates its recruitment to intracellular membranes, independently of its interaction with anti-apoptotic members (O'Connor et al., 1998; Kelekar and Thompson, 1998).

An apoptotic stimulus, such as a strong TCR signal received by a highly self-reactive T cell, was thought to trigger Bim molecules to be released from the dynein motor complex where they are normally contained, enabling them to elicit their pro-apoptotic function (Puthalakath et al., 1999). It was later shown, however, that in the case of both healthy and apoptotic T cells, most Bim molecules are constitutively bound to pro-survival Bcl-2

family members at the mitochondria. The same study also revealed that T cell activation does not lead to a notable increase in the amount of Bim protein and proposed that the mechanism of action in the death of T cells is independent of both Bim movement and changes in its levels (Zhu et al., 2004). Rather, Bim may impact cellular survival by controlling the expression of pro-survival protein Bcl-2 (Jorgensen et al., 2007).

Several splicing isoforms with different cytotoxic properties have been identified for Bim (O'Connor et al., 1998), two of which were able not only to promote apoptosis by acting on pro-survival proteins, but also to directly cause a conformational change in the pro-apoptotic Bcl-2 family member Bcl-2-associated X protein (Bax) (Marani et al., 2002). Importantly, not all splice variants are co-localised (Puthalakath et al., 1999). Collectively, these findings support the possibility that unbound Bim proteins elicit their function directly by potentiating apoptosis agonists.

The requirement for Bim in the deletion of highly self-reactive T cells was strongly supported by six negative selection models (Bouillet et al., 2002). Bim was mainly induced in thymocytes at the DP stage, but was also found to be upregulated in SP cells (Schmitz, Clayton and Reinherz, 2003). Conflicting data suggest that only a very small proportion of self-reactive T cells are dependent on Bim for their elimination (Jorgensen et al., 2007). The Baldwin lab published a study in response to this controversy, stating that while Bim is important in cell deletion at the DP stage, it is not required for negative selection in the medulla (Hu et al., 2009).

A study by Daley, Hu and Goodnow showed that Bim-deficient mice accumulate a DP population of highly self-reactive T cells that express a $CD4^{lo}CD8^{lo}$ phenotype. The study also provided evidence for the occurrence of two waves of negative selection, one in the cortex and one in the medulla (Daley, Hu and Goodnow, 2013). The accumulated $CD4^{lo}CD8^{lo}$ population in Bim-deficient mice may be eventually deleted in a delayed

manner, as suggested by a later study that investigated $Bim^{-/-}$ mice transgenic for the ubiquitous male antigen HYCD4. Although $Bim^{-/-}$ mice accumulated highly reactive $CD4^{lo}CD8^{lo}$ DP thymocytes, there was a lack of SP cells reactive to HYCD4 in these models (Hu et al., 2009; Hu and Baldwin, 2015).

Bim-deficient mice have increased numbers of $Foxp3^{+}$ cells and it has been proposed that this may be a compensatory mechanism to suppress the activities of autoreactive T cells that survive in the absence of Bim, which causes them to upregulate Foxp3 and remain anergic to self-antigen (Zhan et al., 2011). A collaborative study between the Thomas and Kay labs found that Bim deficiency leads to complete protection against type 1 diabetes in Non-obese Diabetic (NOD) mice. Bim-defficient NOD mice were enriched with $CD69^{+}$DP thymocytes, which were also high in CD25 and GITR (Krishnamurthy et al., 2015), the phenotype associated with Treg precursors (Cabarrocas et al., 2006). Bim-deficient NOD mice also showed increased numbers of $GITR^{hi}Foxp3^{+}CD4^{+}$ cells that highly expressed Nur77, compared to Bim-sufficient mice. Insulin-specific, naturally occuring Treg were identified in the periphery to be functional and immunosuppressive. The authors concluded that the autoreactive cells allowed to survive in the absence of Bim were diverted to a Treg phenotype, which conferred protection from development of autoimmunity (Krishnamurthy et al., 2015). This study is consistent with previous observations in which Bim exclusively contributes to the deletion of cells reactive to tissue-specific antigen (Suen and Baldwin, 2012). A later study by a different lab showed that inhibition of the mammalian target of rapamycin complex (mTORC) pathway, which is known to promote effector T cell activation in the periphery, leads to a decrease in Foxp3-expressing cells in wild-type mice. This effect is nullified, however, when Bim is absent (Overall, van Driel and Gleeson, 2016). Collectively, these data support a possible role for Bim in restricting Treg differentiation by promoting apoptosis of highly self-reactive T-cells and thereby deciding the appropriate TCR signalling treshold for agonist selection.

A different scenario in which Foxp3 controls Bim has also been proposed. The Singer lab generated transgenic mice that express different levels of Foxp3 and showed that, while Foxp3 does not affect the amount of Bim protein, it does promote its phosphorylation (Tai et al., 2013). Depending on whether it is phosphorylated by Erk or JNK, it can be either targeted for ubiquitinylation, or disrupted from the dynein motor complex, respectively (Ley et al., 2005). According to the study, Foxp3 promotes the latter scenario, which allows Bim to translocate to the mitochondrial membrane and induce apoptosis (Tai et al., 2013). However, the significance of this effect is questionable, since in T cells most intracellular Bim proteins are not bound to the microtubules and T-cell activation does not lead to a marked increase in Bim relocalisation (Zhu et al., 2004). However, it is possible that the highly cytotoxic splice variant of Bim, BimS, which is not associated to the mitochondria, might be phosphorylated in certain Foxp3-expressing cells (O'Connor et al., 1998; Puthalakath et al., 1999; Marani et al., 2002). This supports the possibility that negative selection and Treg selection occur in a mutually exclusive manner, according to whether cytotoxic Bim splice variants become phosphorylated.

1.13 The Tocky System

All thymic T cell development processes are dependent on TCR signals. Nr4a1-GFP reporter mice proved a very useful tool in the study of antigenic receptor activation (Moran et al., 2011). However, due to the very long half-life of GFP of approximately 50 hours (Sacchetti et al., 2001), only transcriptional history can be analysed. Since TCR signalling is a highly dynamic process, a more sophisticated tool is required in order to capture the complex temporal sequences of thymic development.

Subach et al. described a fluorescent timer (Timer) mCherry mutant that spontaneously changes its emission spectrum from blue to red. The blue form of the protein is short-lived, having a reported half-life of approximately 7 hours, according to a pharmacological

kinetic model. It then becomes oxidised to its very stable red form, the half-life of which was estimated to be over 20 hours (Subach et al., 2009). Dr. Masahiro Ono used this Timer protein for the first time in mice as a reporter of transcriptional dynamics. Specifically, two mouse models were generated using a bacterial artificial chromosome (BAC) transgenic approach: *Foxp3*- and *Nr4a3*- Timer of cell kinetics and activity (Tocky), in order to facilitate the study of temporal dynamics of Treg development and TCR signalling, respectively. The short-lived blue Timer (Blue) protein would report real-time transcription, while the stable red Timer (Red) form would provide information regarding transcriptional history (Bending et al., 2018).

"Tocky" is a homonym of the Japanese word for time "toki" and is suggestive of the system's key feature of capturing the temporal dynamics of transcriptional events. By plotting Blue against Red fluorescence on the x and y axis, respectively, of a flow cytometry plot, the temporal events of transcription can be traced in a clockwise manner (Fig.1.4). $Blue^{+}Red^{-}$ cells segregate close to the y axis and represent a population that has recently commenced gene transcription. $Blue^{-}Red^{+}$ cells have recently terminated transcription, while $Blue^{+}Red^{+}$ cells are in a steady state characterised by persistent transcription. During persistent transcription, the cells have been expressing the gene for a long enough time for Blue protein to mature to Red, while new Blue proteins are being expressed. $Blue^{-}Red^{-}$ cells have either never expressed the gene, or terminated transcription long enough before Red protein completely decayed (Bending et al., 2018).

This clockwise distribution of transcriptional events on a flow cytometry plot can be further analysed in terms of two variables: Timer intensity and Timer angle. Timer intensity is defined by the Euclid distance of a cell from the origin and is a measure of signal strength. Timer angle is defined by the angular position of a cell from the Timer-Blue axis and is a measure of its trajectory and change in transcriptional history. Based on Timer angle values, five Timer loci can be defined in chronological order: New, New-

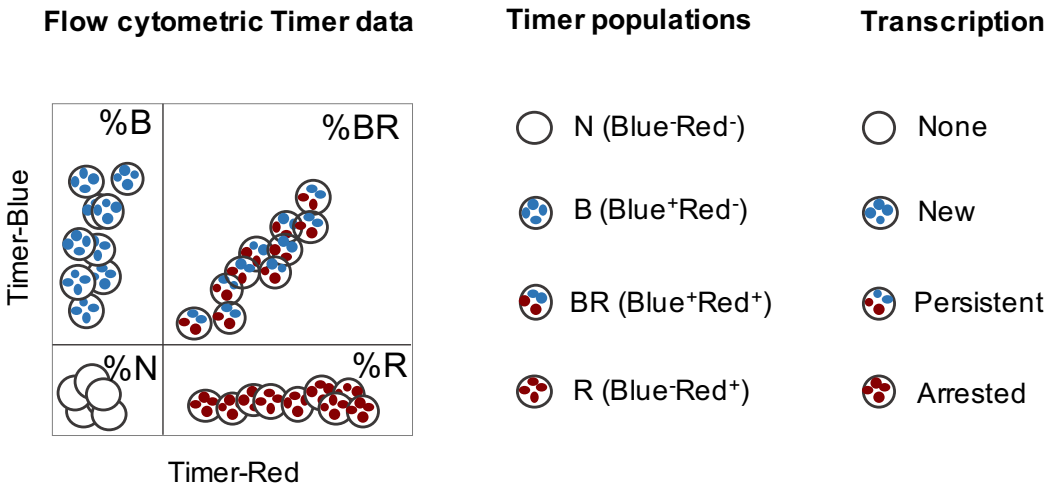

Figure 1.4: **Flow cytometry Timer data.** Figure shows a schematic representation of how cells distribute on a flow cytometry plot according to Timer protein expression. The quadrant gate defines four populations, termed N (cells that lack Timer expression and do not transcribe the reported gene), B (cells that have new transcription of the gene of interest and only express Blue protein), BR (cells that express Blue and Red proteins due to persistent expression of the reported gene) and R (cells that have recently terminated gene transcription and only express Red protein.

Persistent (NPt), Persistent, Persistent-Arrested (PAt) and Arrested. Their respective angular values are illustrated in (Fig.1.5). (Bending et al., 2018).

Although great progress has been made to understand thymic T cell development, many aspects regarding the temporal order of events and the relationships between different populations remain largely unclear. Since thymic T cell development is triggered by TCR signals, the Tocky system can be used to reveal the temporal sequences of events at single cell level. This technology can help untangle the apparently concurrent processes of positive, negative and CD4/CD8 lineage selection.

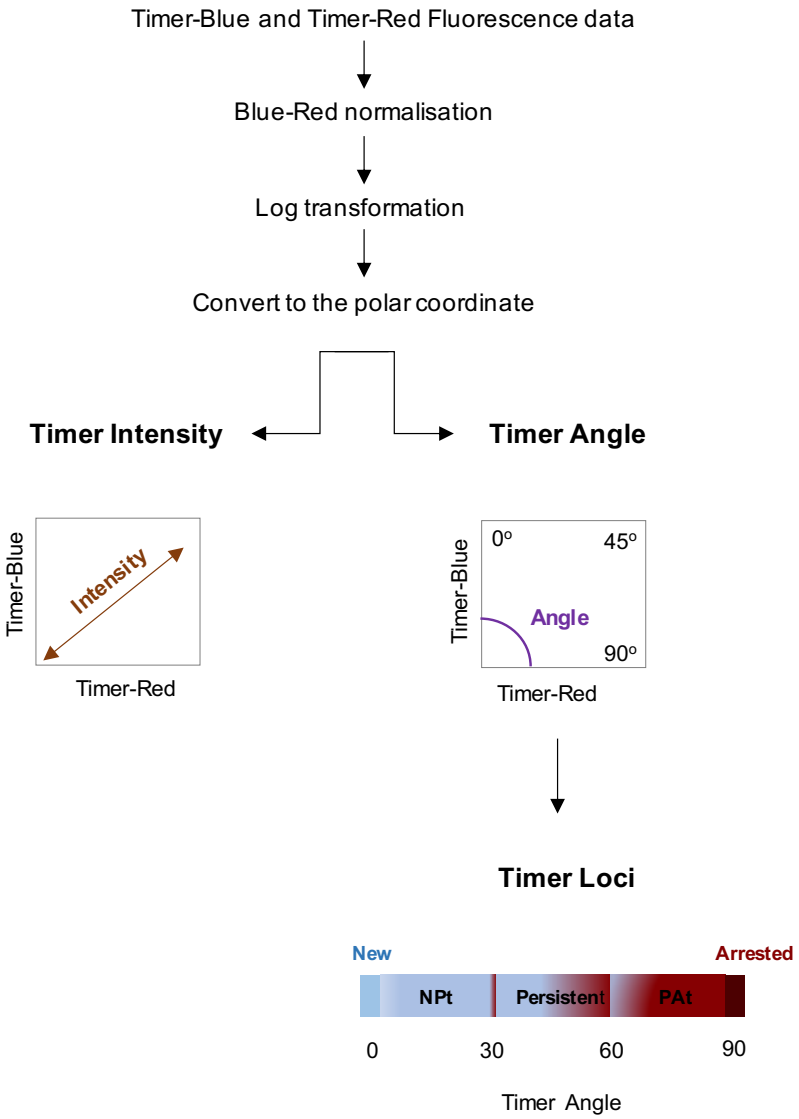

Figure 1.5: **Timer angle and intensity.** Figure shows the steps involved in trigonometric transformation of flow cytometric Timer data in order to calculate Timer intensity and Timer angle values. It is also shown how 5 Timer loci are defined according to Timer angle values: New, New-Persistent (NPt), Persistent, Persistent-Arrested (PAt) and Arrested.

1.14 Thesis structure and aims

The major aim of this work is to investigate the cellular and molecular mechanisms of thymic T cell development and selection events by analysing TCR signalling dynamics in individual T cells *in vivo* and the Tocky system will be extensively used in order to achieve this. This thesis is structured into four chapters with individual aims:

(I) To develop the Tocky system as an accurate tool for analysing transcriptional dynamics.

(II) To study the dynamic changes in transcription during Bim-mediated negative selection and CD4/CD8 lineage selection at the DP stage

(III) To compare between the developmental requirements of mature *Foxp3*$^{-}$CD4 and *Foxp3*$^{-}$CD8 SP cells

(IV) To investigate the TCR signalling requirements for and *Foxp3* transcriptional dynamics upon agonist selection of CD4 and CD8 SP cells.

Methods

2.1 Mice

Mice were bred and maintained under the UK Home Office regulations at Charles River and Imperial College London facilities. All transgenic mice used in this project were generated by Dr. Masahiro Ono and are detailed in Table 2.1. C57BL/6 mice were provided by Charles River and used for negative threshold flow cytometry gating of fluorescent protein-expressing cells throughout the study. All animal work was conducted in accordance with the UK Animals Scientific Procedures Act, 1986.

Strain Name	Short Name*	Description
Tg(BAC Foxp3-mCherry.v)	*Foxp3*-Tocky	The first coding exon of *Foxp3* is replaced by a transgene casette containing the Fast-FT *Timer* gene (Bending et al., 2018; Subach et al.,2009). This transgenic model reports *Foxp3* transcription.
Tg(BAC Foxp3-mCherry.v) × Tg(BAC Nr4a3-EGFP)	*Foxp3*-Tocky:*Nr4a3*-GFP	*Foxp3*-Tocky mice were crossed with *Nr4a3*-GFP, a BAC reporter transgenic in which the main coding exon of *Nr4a3* is replaced by EGFP. This double transgenic model reports *Foxp3* and *Nr4a3* transcription.
Tg(BAC Nr4a3-mCherry.v) × B6.Cg-Foxp3^{tm1Mal}/J	*Nr4a3*-Tocky	The first coding exon of *Nr4a3* is replaced by a transgene casette containing the Fast-FT *Timer* gene (Subach et al.,2009). These mice had been crossed with commercial Foxp3EGFP mice (Bending et al., 2018; Wang et al., 2008;JAX stock #018628). This double transgenic model reports *Nr4a3* and *Foxp3* transcription.
B6.129S1-Bcl2l11$^{tm1.1Ast}$/J × Tg(BAC Nr4a3-mCherry.v) × B6.Cg-Foxp3^{tm1Mal}/J	*Nr4a3*-Tocky:Bim	*Nr4a3*-Tocky mice were crossed with Bim KO mice (Bouillet et al., 1999; JAX stock #004525). This triple transgenic model lacks one or two *Bcl2l11* alleles and reports *Nr4a3* and *Foxp3* transcription.

Table 2.1: Transgenic mice used in this study. All animal models were generated by Dr. Masahiro Ono. *Troughout the study, animal models are referred to by their assigned short names

2.2 Genotype Screening

DNA Isolation. Ear notches were provided by Charles River or by Imperial College London facilities. Each biopsy was treated with a mixture containing 200 μl lysis buffer (100 mM Tris HCL pH = 8.5, 0.5 M ethylenediaminetetraacetic acid (EDTA), 5 M NaCl, 10% SDS) and 0.25 μg/ml proteinase K (Sigma) and subjected to an overnight incubation on a thermomixer block at 55^0C and 750 rpm to ensure tissue digestion. Enzymatic activity was inhibited by a subsequent incubation of 50 μl from each sample for 20 minutes at 95^0C on a polymerase chain reaction (PCR) block. The DNA solution was then diluted 1 in 3 in ribonuclease (RNAse)-free water (Sigma) and temporarily stored at -80^0C.

Transgenic sequence amplification. Mice were genotyped by PCR using the Standard Taq DNA Polymerase protocol (NEB) for 1 μl of DNA in 25 μl of total reaction volume. The template for each thermocycling program ran is described in Table 2.2. The oligonucleotide primers used corresponding to the transgenic sequences routinely genotyped for are detailed in Table 2.3. *Nr4a3*-Tocky mice were not routinely screened for their transgenes, as the colony was homogeneous.

Gel electrophoresis. Amplified DNA samples were loaded with loading buffer (Gel Loading Dye, Orange 6×, NEB) onto a 1.5% agarose gel made with Sigma agarose and 1x Tris acetate EDTA (TAE) buffer diluted in MiliQ water from 50x stock (242 g Trizma base, 0.5 M EDTA pH = 8, 57.1 ml glacial acetic acid in 1 L of MiliQ water) to which a nucleic acid gel stain was added for band visualisation (GelRed, Biotium). Gels were ran at 135 mV until clear band separation was observed. 100 bp DNA ladder (NEB) was used for molecular weight standards.

Genotype	Step	Temperature	Time	Cycles
Bcl2l11^{KO} *Bcl2l11*^{WT}	Initial Denaturation	95^0C	3 minutes	35
	Denaturation	95^0C	30 seconds	
	Annealing	58^0C	50 seconds	
	Extension	72^0C	50 seconds	
	Final Extension	72^0C	2 minutes	
	Hold	4^0C	∞	
Foxp3-Tocky *Nr4a3*-GFP	Initial Denaturation	94^0C	30 seconds	34
	Denaturation	94^0C	30 seconds	
	Annealing	63^0C	30 seconds	
	Extension	68^0C	20 seconds	
	Final Extension	68^0C	20 seconds	
	Hold	4^0C	∞	

Table 2.2: PCR thermocycling programs for transgenic sequence amplification.

Genotype	5'-3' Sequence	Sense	Product size (bp)
Bcl2l11^{KO}	CTCAGTCCATTCATCAACAG	Forward	540
	CATTCTCGTAAGTCCGAGTCT	Reverse	
Bcl2l11^{WT}	GTGCTAACTGAAACCAGATTAG	Forward	400
	CATTCTCGTAAGTCCGAGTCT	Reverse	
Foxp3-Tocky	CAGCTCCTCTGCCGTTATCC	Forward	370
	CCTCGCCCTCGATCTCGA	Reverse	
Nr4a3-GFP	GTGCAGGCTGCTAATCCTGT	Forward	1000
	GTCCTCCTTGAAGTCGATGC	Reverse	

Table 2.3: Oligonucleotide primers used for genotype screening.

2.3 Flow Cytometry Analysis and Cell Sorting

Flow Cytometry. Thymi from 4-8 weeks old mice were harvested and forced into single cell suspensions through a 70 μm cell strainer using a 10 mL syringe plunger. Cells were pelleted at the bottom of 15 ml FALCON tubes by a 7 minute centrifugation step at 500 g. Cells were then manually counted using a 0.4 mm depth Imp. Neubauer chamber (MARIENFIELD) and 20×10^6 cells were added to a 96-well V-bottom plate (Corning) for each sample to be stained for flow cytometry analysis. First, cells were stained with a fixable viability dye and incubated 15 minutes on ice in the dark. After washing the

plate with phosphate-buffered saline (PBS) containing 2% Foetal Bovine Serum (FBS) by a 3 minute centrifugation step at 500 g, a blocking solution containing anti-mouse CD16/32 antibody and 2% rat serum was added to prevent non-specific binding of subsequent conjugated antibodies. A cocktail of biotinylated antibodies was then added in order to create a dump channel for exclusion of non-T cells and allowed to bind for 30 minutes on ice. The antibody cocktail consisted of antibodies against markers present on B cells (CD19), DCs (CD11c), erythrocytes (Ter119), granulocytes (Ly6G/Ly6C), macrophages (CD11b), NKT cells (NK1.1) and $\gamma\delta$T (TCR$\gamma\delta$) cells. After being washed, samples were incubated with cocktails of fluorescently-labelled antibodies (and streptavidin) for at least 40 minutes on ice, in the dark. All conjugated antibodies used for the experiments described in this report are listed in Table 2.4. All thymic samples were kept on ice as much as possible in order to prevent maturation of the Blue protein before flow cytometry analysis on either a BD Fortessa III instrument or a Cytek Aurora Spectral Analyser. Blue amd Red proteins were excited off the 405 nm laser and the 561 nm laser, and detected in the 450/40 nm channel and 610/20 nm channel, respectively.

Cell sorting. Cells were prepared in a similar manner as described above before being sorted, using a BD ARIA III instrument, directly into Eppendorf tubes containing 100 μl lysis buffer (Arcturus PicoPure kit, Life Technologies). Sorted cells were then incubated at 42^0C for 30 minutes in order to ensure membrane disturbance and lysates were stored at -80^0C.

Data visualisation and analysis. Flow cytometry data was visualised, compensated and analysed using the FlowJo software. Tocky Locus data analysis and visualisation based on the resulting .fcs files were carried out in R using the approach described by Bending et al., 2018 in the Materials and Methods section "Timer Data Analysis" (Bending et al.,2018).

Antigen	Fluorochrome	Clone	Company
CD4	Alexa Fluor 700	RM4-5	BioLegend
CD4	BUV395	GK1.5	BD Horizon
CD4	BUV496	GK1.5	BD Horizon
CD4	PerCP-Cy5.5	RM4-5	BioLegend
CD8a	Alexa Fluor 700	53-6.7	BioLegend
CD8	BUV737	53-6.7	BD Horizon
CD8a	Brilliant Violet 785	53-6.7	BioLegend
CD8a	PE-Cy7	53-6.7	BioLegend
CD11b	Biotin	M1/70	eBioscience
CD11c	Biotin	N418	eBioscience
CD16/32 (TruStain FcX)TM		93	BioLegend
CD19	APC	6D5	BioLegend
CD19	Biotin	1D3	eBioscience
CD24	PerCP-Cy5.5	M1/69	BioLegend
CD25	Alexa Fluor 700	PC61.5	BioLegend
CD25	PerCP-Cy5.5	PC61.5	eBioscience
CD69	APC	H1.2F3	BioLegend
CD69	PE-Cy7	H1.2F3	BioLegend
CD134 (OX-40)	Brilliant Violet 711	OX-86	BioLegend
CD279 (PD-1)	APC	RMP1-30	BioLegend
CD357 (GITR)	BUV395	DTA-1	BD Horizon
CD357 (GITR)	PE-Cy7	DTA-1	BioLegend
Ly6G/Ly6C	Biotin	RB6-8C5	eBioscience
NK1.1	Biotin	PK136	eBioscience
Streptavidin	APC-Cy7		BioLegend
Streptavidin	PE-Cy5		BioLegend
TER-119	Biotin	TER-119	eBioscience
TCR$\gamma\delta$	Biotin	GL3	eBioscience
Viability Dye	APC-Cy7		eBioscience

Table 2.4: List of all antibodies used to prepare thymic samples for flow cytometry analysis.

2.4 In vitro culture

mRNA degradation assay. Naïve $CD4^+$ T cells were isolated from the spleens of *Foxp3*-Tocky mice using the immunomagnetic separation kit by StemCell Technologies, according to manufacturer's instructions. A total of 2×10^6 cells were cultured in RPMI 1640 media (Sigma-Aldrich) containing 10% FBS, penicillin/streptomycin (Thermo Fisher Scientific) and 55 μM β-mercaptoethanol (Gibco) at 37°C overnight on a 96-well U-bottom plate (Cornig) in the presence of plate-bound 2 μg/ml anti-CD3 (clone 145-2C11; eBioscience). The next day, the cells were re-plated at 4×10^5 cells per well together with 10 μg/ml actinomycin D (Sigma-Aldrich) in order to inhibit ribonucleic acid (RNA) polymerase activity. Cells were harvested every two hours and their pellets lysed in 350 μl RLT plus buffer (Qiagen) and stored at -80°C before RNA extraction, complementary DNA (cDNA) syntesis and quantitative reverse transcription PCR (RT-qPCR) analysis as described in a different section below.

Blue protein degradation assay. Splenocytes harvested from *Nr4a3*-Tocky mice were treated with RBC lysis buffer (eBioscience) and resuspended in RPMI 1640 media containing 10% FBS, penicillin/streptomycin and 55 μM β-mercaptoethanol. 4×10^5 cells in a final volume of 200 μl media were added to each well of a 96-well U-bottom plate in the presence of plate-bound 2 μg/ml anti-CD3 (clone 1452C11; eBioscience) for T cell stimulation. For polyclonal activation of B cells, an equivalent number of splenocytes was stimulated with 10 μg/ml F(ab')2 goat anti-mouse IgM (Thermo Fisher Scientific) instead. The plate was then incubated for 20 hours at 37°C, after which cells were harvested and re-plated with 100 μg/ml cyclohexamide (Sigma-Aldrich) in order to inhibit any new protein translation. Blue protein fluorescence was then measured every two hours by flow cytometry.

Red protein degradation assay. $Blue^-Red^+CD4^+$ splenocytes from *Nr4a3*-Tocky mice were

treated with RBC lysis buffer and sorted using the BD ARIA III instrument into RPMI 1640 media containing 10% FBS, penicillin/streptomycin and 55 μM β-mercaptoethanol. Nearly 10^5 cells were cultured without stimulation in each well of a 96-well U-bottom plate together with 500 U/ml recombinant human IL-2 (Roche), which does not induce Timer protein expression in *Nr4a3*-Tocky cells (Bending et al, 2018). The plate was then incubated at 37°C and cells were harvested every 24 hours for one week and analysed for Red fluorescence expression by flow cytometry.

2.5 Quantitative PCR

RNA extracted from lysates (Arcturus PicoPure kit, Life Technologies) was immediately converted to cDNA using the Superscript II kit (Life Technologies) according to manufacturer's instructions. For the messenger RNA (mRNA) degradation assay, SYBR green (BioRad) was used to quantify mRNA expression of *Timer*, *Foxp3* and the housekeeping gene *Hprt*. The following primer sequences were used: *Timer*-Forward CAGCTCCTCTGCCGTTATCC; *Timer*-Reverse CCTCGCCCTCGATCTCGA; *Foxp3*-Forward CAGCTCCTCTGCCGTTATCC; *Foxp3*-Reverse CCTCGCCCTCGATCTCGA; *Hprt*-Forward AGCCTAAGATGAGCGCAAGT, *Hprt*-Reverse TTACTAGGCAGATGGCCACA. For determining mRNA expression of thymocytes sorted according to their Timer fluorescence, TaqMan probes for *Nr4a3* and *Actin* provided by Thermo Fisher Scientific were used.

2.6 RNA sequencing

Thymic cell populations were sorted from *Nr4a3*-Tocky, *Nr4a3*-Tocky:Bim$^{WT/KO}$, *Nr4a3*-Tocky:Bim$^{KO/KO}$ mice as described in Fig.2.1 and 2.2. The Arcturus PicoPure kit (Life Technologies) was used according to instructions in order to extract RNA from cell lysates. RNaseZap (Thermo Fischer Scientific) was frequently used for decontamination of envi-

ronmental RNAses. Generation of cDNA libraries for RNA sequencing (RNAseq) was carried out according to the protocol designed by Picelli et al., 2014, using the Smart-Seq2 approach. All the reagents used were identical to the ones mentioned in their study (Picelli et al., 2014).

Sample ID	Mouse Number	Mouse Genotype	Sorted Population	Population Name	Chapter	Name in Chapter
1	1	*Nr4a3*-Tocky	Blue$^+$Red$^-$CD69$^+$ DP	DPB1	II	DP_B
2	1	*Nr4a3*-Tocky	Blue$^-$Red$^-$CD69$^+$ DP	DPN1	II	DP_N
3	1	*Nr4a3*-Tocky	Blue$^+$Red$^-$*Foxp3*$^-$CD69$^+$CD4 SP	CD4B1	III	CD4_B
4	1	*Nr4a3*-Tocky	Blue$^+$Red$^+$*Foxp3*$^-$CD69$^+$CD4 SP	CD4BR1	III	CD4_BR
5	1	*Nr4a3*-Tocky	Blue$^-$Red$^+$*Foxp3*$^-$CD69$^+$CD4 SP	CD4R1	III	CD4_R
6	1	*Nr4a3*-Tocky	Blue$^-$Red$^-$*Foxp3*$^-$CD69$^+$CD4 SP	CD4N1	III	CD4_N
7	1	*Nr4a3*-Tocky	Blue$^+$Red$^+$*Foxp3*$^+$CD69$^+$CD4 SP	FoxBR1	IV	Foxp3_BR
8	1	*Nr4a3*-Tocky	Blue$^-$Red$^+$*Foxp3*$^+$CD69$^+$CD4 SP	FoxR1	IV	Foxp3_R
9	2	*Nr4a3*-Tocky	Blue$^+$Red$^-$CD69$^+$ DP	DPB2	II	DP_B
10	2	*Nr4a3*-Tocky	Blue$^-$Red$^-$CD69$^+$ DP	DPN2	II	DP_N
11	2	*Nr4a3*-Tocky	Blue$^+$Red$^-$*Foxp3*$^-$CD69$^+$CD4 SP	CD4B2	III	CD4_B
12	2	*Nr4a3*-Tocky	Blue$^+$Red$^+$*Foxp3*$^-$CD69$^+$CD4 SP	CD4B2	III	CD4_BR
13	2	*Nr4a3*-Tocky	Blue$^-$Red$^+$*Foxp3*$^-$CD69$^+$CD4 SP	CD4R2	III	CD4_R
14	2	*Nr4a3*-Tocky	Blue$^-$Red$^-$*Foxp3*$^-$CD69$^+$CD4 SP	CD4N2	III	CD4_N
15	2	*Nr4a3*-Tocky	Blue$^+$Red$^+$*Foxp3*$^+$CD69$^+$CD4 SP	FoxBR2	IV	Foxp3_BR
16	2	*Nr4a3*-Tocky	Blue$^-$Red$^+$*Foxp3*$^+$CD69$^+$CD4 SP	FoxR2	IV	Foxp3_R
17	2	*Nr4a3*-Tocky	Blue$^+$Red$^-$CD69$^+$ DP	DPB3	II	DP_B
18	3	*Nr4a3*-Tocky	Blue$^-$Red$^-$CD69$^+$ DP	DPN3	II	DP_N
19	3	*Nr4a3*-Tocky	Blue$^+$Red$^-$*Foxp3*$^-$CD69$^+$CD4 SP	CD4B3	III	CD4_B
20	3	*Nr4a3*-Tocky	Blue$^+$Red$^+$*Foxp3*$^-$CD69$^+$CD4 SP	CD4BR3	III	CD4_BR
21	3	*Nr4a3*-Tocky	Blue$^-$Red$^+$*Foxp3*$^-$CD69$^+$CD4 SP	CD4R3	III	CD4_R
22	3	*Nr4a3*-Tocky	Blue$^-$Red$^-$*Foxp3*$^-$CD69$^+$CD4 SP	CD4N3	III	CD4_N
23	3	*Nr4a3*-Tocky	Blue$^+$Red$^+$*Foxp3*$^+$CD69$^+$CD4 SP	FoxBR3	IV	Foxp3_BR
24	3	*Nr4a3*-Tocky	Blue$^-$Red$^+$*Foxp3*$^+$CD69$^+$CD4 SP	FoxR3	IV	Foxp3_R

Figure 2.1: **List of sorted *Nr4a3*-Tocky samples for RNAseq analysis.** 24 populations were sorted from *Nr4a3*-Tocky mice according to Timer fluorescence and surface marker expression as shown and processed for RNAseq analysis as described in the methods. The chapter in which each population is first mentioned is also listed, followed by their assigned name in the respective chapter.

Sample ID	Mouse ID	Mouse Genotype	Sorted Population	Population Name	Chapter	Name in Chapter
1	1	*Nr4a3*-Tocky:Bim$^{WT/KO}$	Blue$^+$Red$^-$CD69$^+$ DP	DPB1_Het	II	Het_B
2	1	*Nr4a3*-Tocky:Bim$^{WT/KO}$	Blue$^-$Red$^-$CD69$^+$ DP	DPN1_Het	II	Het_N
3	1	*Nr4a3*-Tocky:Bim$^{WT/KO}$	Blue$^+$Red$^+$*Foxp3*$^-$CD69$^+$CD4$^+$ SP	CD4B1_Het	III	Het_B
4	1	*Nr4a3*-Tocky:Bim$^{WT/KO}$	Blue$^+$Red$^+$*Foxp3*$^-$CD69$^+$CD4$^+$ SP	CD4BR1_Het	III	Het_BR
5	1	*Nr4a3*-Tocky:Bim$^{WT/KO}$	Blue$^-$Red$^+$*Foxp3*$^-$CD69$^+$CD4$^+$ SP	CD4R1_Het	III	Het_R
6	1	*Nr4a3*-Tocky:Bim$^{WT/KO}$	Blue$^-$Red$^-$*Foxp3*$^-$CD69$^+$CD4$^+$ SP	CD4N1_Het	III	Het_N
7	1	*Nr4a3*-Tocky:Bim$^{WT/KO}$	Blue$^+$Red$^+$*Foxp3*$^+$CD69$^+$CD4$^+$ SP	FoxBR1_Het	IV	Het_BR
8	1	*Nr4a3*-Tocky:Bim$^{WT/KO}$	Blue$^-$Red$^+$*Foxp3*$^+$CD69$^+$CD4$^+$ SP	FoxR1_Het	IV	Het_R
9	2	*Nr4a3*-Tocky:Bim$^{KO/KO}$	Blue$^+$Red$^-$CD69$^+$ DP	DPB1_KO	II	KO_B
10	2	*Nr4a3*-Tocky:Bim$^{KO/KO}$	Blue$^+$Red$^+$CD69$^+$ DP	DPBR1_KO	II	KO_BR
11	2	*Nr4a3*-Tocky:Bim$^{KO/KO}$	Blue$^-$Red$^-$CD69$^+$ DP	DPN1_KO	II	KO_N
12	2	*Nr4a3*-Tocky:Bim$^{KO/KO}$	Blue$^+$Red$^-$*Foxp3*$^-$CD69$^+$CD4$^+$ SP	CD4B1_KO	III	KO_B
13	2	*Nr4a3*-Tocky:Bim$^{KO/KO}$	Blue$^+$Red$^+$*Foxp3*$^-$CD69$^+$CD4$^+$ SP	CD4BR1_KO	III	KO_BR
14	2	*Nr4a3*-Tocky:Bim$^{KO/KO}$	Blue$^-$Red$^+$*Foxp3*$^-$CD69$^+$CD4$^+$ SP	CD4R1_KO	III	KO_R
15	2	*Nr4a3*-Tocky:Bim$^{KO/KO}$	Blue$^-$Red$^-$*Foxp3*$^-$CD69$^+$CD4$^+$ SP	CD4N1_KO	III	KO_N
16	2	*Nr4a3*-Tocky:Bim$^{KO/KO}$	Blue$^+$Red$^+$*Foxp3*$^+$CD69$^+$CD4$^+$ SP	FoxBR1_KO	IV	KO_BR
17	2	*Nr4a3*-Tocky:Bim$^{KO/KO}$	Blue$^-$Red$^+$*Foxp3*$^+$CD69$^+$CD4$^+$ SP	FoxR1_KO	IV	KO_R
18	3	*Nr4a3*-Tocky:Bim$^{KO/KO}$	Blue$^+$Red$^-$CD69$^+$ DP	DPB2_KO	II	KO_B
19	3	*Nr4a3*-Tocky:Bim$^{KO/KO}$	Blue$^+$Red$^+$CD69$^+$ DP	DPBR2_KO	II	KO_BR
20	3	*Nr4a3*-Tocky:Bim$^{KO/KO}$	Blue$^-$Red$^-$CD69$^+$ DP	DPN2_KO	II	KO_N
21	3	*Nr4a3*-Tocky:Bim$^{KO/KO}$	Blue$^+$Red$^-$*Foxp3*$^-$CD69$^+$CD4$^+$ SP	CD4B2_KO	III	KO_B
22	3	*Nr4a3*-Tocky:Bim$^{KO/KO}$	Blue$^+$Red$^+$*Foxp3*$^-$CD69$^+$CD4$^+$ SP	CD4BR2_KO	III	KO_BR
23	3	*Nr4a3*-Tocky:Bim$^{KO/KO}$	Blue$^-$Red$^+$*Foxp3*$^-$CD69$^+$CD4$^+$ SP	CD4R2_KO	III	KO_R
24	3	*Nr4a3*-Tocky:Bim$^{KO/KO}$	Blue$^-$Red$^-$*Foxp3*$^-$CD69$^+$CD4$^+$ SP	CD4N2_KO	III	KO_N
25	3	*Nr4a3*-Tocky:Bim$^{KO/KO}$	Blue$^+$Red$^+$*Foxp3*$^+$CD69$^+$CD4$^+$ SP	FoxBR2_KO	IV	KO_BR
26	3	*Nr4a3*-Tocky:Bim$^{KO/KO}$	Blue$^-$Red$^+$*Foxp3*$^+$CD69$^+$CD4$^+$ SP	FoxR2_KO	IV	KO_R
27	4	*Nr4a3*-Tocky:Bim$^{WT/KO}$	Blue$^+$Red$^-$CD69$^+$ DP	DPB2_Het	II	Het_B
28	4	*Nr4a3*-Tocky:Bim$^{WT/KO}$	Blue$^-$Red$^-$CD69$^+$ DP	DPN2_Het	II	Het_N
29	4	*Nr4a3*-Tocky:Bim$^{WT/KO}$	Blue$^+$Red$^-$*Foxp3*$^-$CD69$^+$CD4$^+$ SP	CD4B2_Het	III	Het_B
30	4	*Nr4a3*-Tocky:Bim$^{WT/KO}$	Blue$^+$Red$^+$*Foxp3*$^-$CD69$^+$CD4$^+$ SP	CD4BR2_Het	III	Het_BR
31	4	*Nr4a3*-Tocky:Bim$^{WT/KO}$	Blue$^-$Red$^+$*Foxp3*$^-$CD69$^+$CD4$^+$ SP	CD4R2_Het	III	Het_R
32	4	*Nr4a3*-Tocky:Bim$^{WT/KO}$	Blue$^-$Red$^-$*Foxp3*$^-$CD69$^+$CD4$^+$ SP	CD4N2_Het	III	Het_N
33	4	*Nr4a3*-Tocky:Bim$^{WT/KO}$	Blue$^+$Red$^+$*Foxp3*$^+$CD69$^+$CD4$^+$ SP	FoxBR2_Het	IV	Het_BR
34	4	*Nr4a3*-Tocky:Bim$^{WT/KO}$	Blue$^-$Red$^+$*Foxp3*$^+$CD69$^+$CD4$^+$ SP	FoxR2_Het	*Removed as outlier*	
35	5	*Nr4a3*-Tocky:Bim$^{KO/KO}$	Blue$^+$Red$^-$CD69$^+$ DP	DPB3_KO	II	KO_B
36	5	*Nr4a3*-Tocky:Bim$^{KO/KO}$	Blue$^+$Red$^+$CD69$^+$ DP	DPBR3_KO	II	KO_BR
37	5	*Nr4a3*-Tocky:Bim$^{KO/KO}$	Blue$^-$Red$^-$CD69$^+$ DP	DPN3_KO	II	KO_N
38	5	*Nr4a3*-Tocky:Bim$^{KO/KO}$	Blue$^+$Red$^-$*Foxp3*$^-$CD69$^+$CD4$^+$ SP	CD4B3_KO	III	KO_B
39	5	*Nr4a3*-Tocky:Bim$^{KO/KO}$	Blue$^+$Red$^+$*Foxp3*$^-$CD69$^+$CD4$^+$ SP	CD4BR3_KO		
40	5	*Nr4a3*-Tocky:Bim$^{KO/KO}$	Blue$^-$Red$^+$*Foxp3*$^-$CD69$^+$CD4$^+$ SP	CD4R3_KO	III	KO_R
41	5	*Nr4a3*-Tocky:Bim$^{KO/KO}$	Blue$^-$Red$^-$*Foxp3*$^-$CD69$^+$CD4$^+$ SP	CD4N3_KO	III	KO_N
42	5	*Nr4a3*-Tocky:Bim$^{KO/KO}$	Blue$^+$Red$^+$*Foxp3*$^+$CD69$^+$CD4$^+$ SP	FoxBR3_KO	IV	KO_BR
43	5	*Nr4a3*-Tocky:Bim$^{KO/KO}$	Blue$^-$Red$^+$*Foxp3*$^+$CD69$^+$CD4$^+$ SP	FoxR3_KO	IV	KO_R
44	6	*Nr4a3*-Tocky:Bim$^{WT/KO}$	Blue$^+$Red$^-$CD69$^+$ DP	DPB3_Het	II	Het_B
45	6	*Nr4a3*-Tocky:Bim$^{WT/KO}$	Blue$^-$Red$^-$CD69$^+$ DP	DPN3_Het	II	Het_N
46	6	*Nr4a3*-Tocky:Bim$^{WT/KO}$	Blue$^+$Red$^-$*Foxp3*$^-$CD69$^+$CD4$^+$ SP	CD4B3_Het	III	Het_B
47	6	*Nr4a3*-Tocky:Bim$^{WT/KO}$	Blue$^+$Red$^+$*Foxp3*$^-$CD69$^+$CD4$^+$ SP	CD4BR3_Het	III	Het_BR
48	6	*Nr4a3*-Tocky:Bim$^{WT/KO}$	Blue$^-$Red$^+$*Foxp3*$^-$CD69$^+$CD4$^+$ SP	CD4R3_Het	III	Het_R
49	6	*Nr4a3*-Tocky:Bim$^{WT/KO}$	Blue$^-$Red$^-$*Foxp3*$^-$CD69$^+$CD4$^+$ SP	CD4N3_Het	*Removed as outlier*	
50	6	*Nr4a3*-Tocky:Bim$^{WT/KO}$	Blue$^+$Red$^+$*Foxp3*$^+$CD69$^+$CD4$^+$ SP	FoxBR3_Het	IV	Het_BR
51	6	*Nr4a3*-Tocky:Bim$^{WT/KO}$	Blue$^-$Red$^+$*Foxp3*$^+$CD69$^+$CD4$^+$ SP	FoxR3_Het	IV	Het_R

Figure 2.2: **List of sorted *Nr4a3*-Tocky:Bim$^{WT/KO}$ and *Nr4a3*-Tocky:Bim$^{KO/KO}$ samples for RNAseq analysis.** 51 populations were sorted from *Nr4a3*-Tocky:Bim$^{WT/KO}$ and *Nr4a3*-Tocky:Bim$^{KO/KO}$ mice according to Timer fluorescence and surface marker expression as shown and processed for RNAseq analysis as described in the methods. Sample 39, highlighted in grey, was not successfully processed and could not be included in the data set. Samples 34 and 49 were removed as outliers. The chapter in which each population is first mentioned is also listed, followed by their assigned name in the respective chapter.

cDNA synthesis and amplification. A mixture of 2.6 μl mRNA, 1 μl oligo-dT primers and 1 μl deoxynucleoside triphosphate (dNTP) was centrifuged in RNAse-free 0.2 μl PCR tubes (Star-Lab) at 700 g for 10 seconds incubated at 72°C for 3 minutes. To this, 5.4 μl containing 100 U SuperScript II reverse transcriptase, 10 U RNAse inhibitor, 1× Superscript II first-strand buffer, 5 mM dithiothreitol, 1 M Betaine, 6 mM $MgCl_2$ and 1 μM template-switching oligos (TSO) were added and the tubes were incubated in a thermal cycler, as shown in Table 2.5. The product was then amplified by adding a mixutre of 12.5 μl KAPA HiFi Hot Start ReadyMix 2×, 0.5 μl of 0.1 μM biotinylated ISPCR primers and 2.25 μl of nuclease free water (Sigma) to each tube, which was incubated according to the program described in Table 2.6.

Temperature (°C)	Time (minutes)	Number of Cycles
42	90	1
50 42	2 2	11
70 4	15 ∞	1

Table 2.5: Reverse Transcription.

Temperature (°C)	Time	Number of Cycles
98	3 minutes	1
98 67 72	20 seconds 15 seconds 6 minutes	13
72 4	5 minutes ∞	1

Table 2.6: PCR Preamplification.

PCR product purification. Thoroughly vortexed Agentcourt AMPure XP Beads were mixed with each sample in a 1:1 ratio and the entire volume was transferred to a 96-well plate that was placed on a magnetic stand. DNA was allowed to bind the beads and all the liquid was carefully pipetted out. Following two wash steps with 200 μl 80% molecular grade ethanol (Sigma), Elution Buffer solution (Quiagen) was added and the DNA was carefully collected in 15 μl liquid to avoid bead contamination.

Library construction and amplification. Sequencing libraries were obtained via tagmentation. 1 ng/μl purified cDNA was added to a mixture of 10 μl Tagment DNA buffer (2×) and 5 μl amplicon tagment mix for a final volume of 20 μl, which was incubated at 55ºC for 5 minutes. Tagmented DNA was incubated for 5 minutes at room temperature with 5 μl NT buffer in order to stop enzymatic activity before indexing each sample with a unique set of primers for identification during sequencing. The adapter-ligated fragments were then amplified as shown in Table 2.7. The PCR product was then purified as described above, only this time adding the AMPure XP Beads to DNA in a 0.6:1 ratio.

Temperature (°C)	Time	Number of Cycles
72	3 minutes	1
95	30 seconds	
95	10 seconds	16
55	30 seconds	
72	30 seconds	
72	5 minutes	1
4	∞	

Table 2.7: Amplification of adapter-ligated fragments.

Quality Check. The Qubit ssDNA Assay kit and the Agilent D5000 ScreenTape system were used according to the manufacturer's instructions to confirm the size and quality of amplified cDNA. One of the samples failed this quality check step, as shown in Fig.2.3. The quality of amplified libraries was determined using the Agilent D1000 ScreenTape system. Samples were ultimately diluted to 1 ng/μl in buffer TE (Quiagen), pooled into a single low-bind Eppendorf tube and sent for HiSeq analysis, Paired End (75bp).

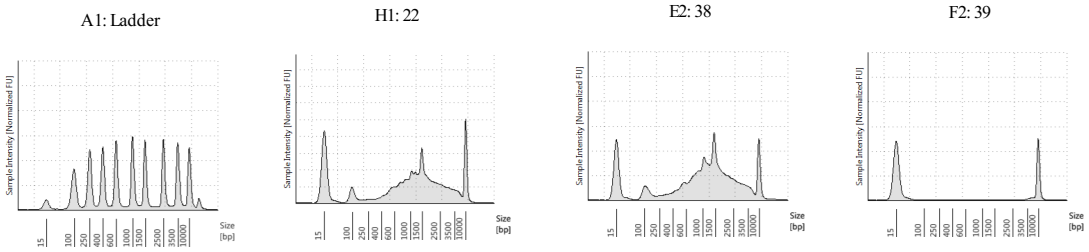

Figure 2.3: **Quality check of cDNA fragments**. 51 samples of amplified, bead-purified cDNA fragments were processed from cells sorted from *Nr4a3*-Tocky:Bim$^{WT/KO}$ and *Nr4a3*-Tocky:Bim$^{KO/KO}$ mice as described in Fig.2.2. The samples were subjected to a quality check step using the Agilent 4200 TapeStation System. TapeStation results show the D5000 screen tape ladder, followed by two arbitrarily chosen samples that passed the quality check step (Sample ID 22 and 38) and the only sample that was not amplified and failed the quality check (Sample ID 39).

Data Analysis and Visualisation. The Salmon software was used in order to index RNAseq data and to count the reads. The Bioconductor tools GenomicFeatures and Tximport were then used for alignment to wild-type mouse genome. The Timer gene was also annotated to the genome. All read count data were stored in the DESeqDataSet object class of the R package DESeq2. Normalisation and transformation of data were carried out using the DESeq2 function normTransform. Pre-processing of data by quality check was also carried out using DESeq2. Because of the small replicate number for each sample (n = 3), quantitative statistics could not be performed to identify potential outliers. Instead, quality check was done by calculating sample-to-sample distances (Fig. 2.4 and 2.6) and by principal component analysis (PCA) of transcriptomes (Fig. 5.6 and 4.16) to ensure replicates cluster together. The Euclidean distances between

samples were calculated using the R function dist. The sample-to-sample distances were then visualised in a heatmap using the R package pheatmap. A blue colour palette was applied to the heatmap using the colorRampPalette function of the RColorBrewer package. PCA plots were generated using the function plotPCA. Two samples were identified as outliers (CD4N_Het3 and FoxR_Het2, Fig.2.2) based on the large deviation from their replicates, both on the sample-to-sample distance heatmap (Fig.2.6) and on the PCA plot (Fig.4.16). Genome wide annotation was carried out by another Bioconductor package, org.Mm.eg.db. Differential gene expression between samples adjusted p value of <0.05 was determined using the DESeq2 function results. Heatmaps of differentially expressed genes were generated using the R package gplots. The matrix of normalised values was extracted using the function assay and normalised count data were then reported on scatter plots on a logarithmic scale to base 2 using the GraphPad Prism software.

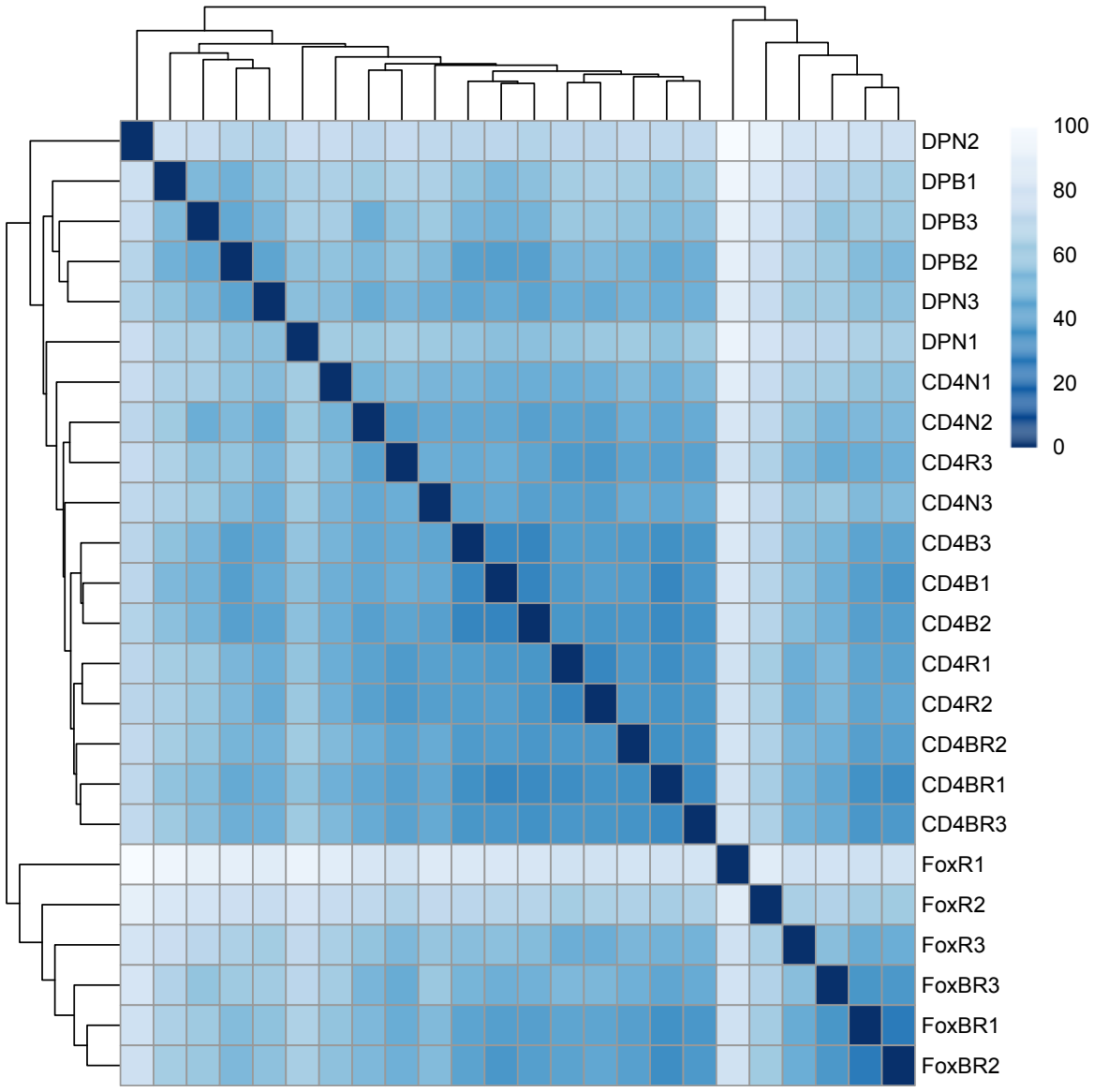

Figure 2.4: Heatmap of sample-to-sample distances for all populations sorted from *Nr4a3*-Tocky mice as shown in Fig.2.1 and processed for RNAseq analysis as described in the methods.

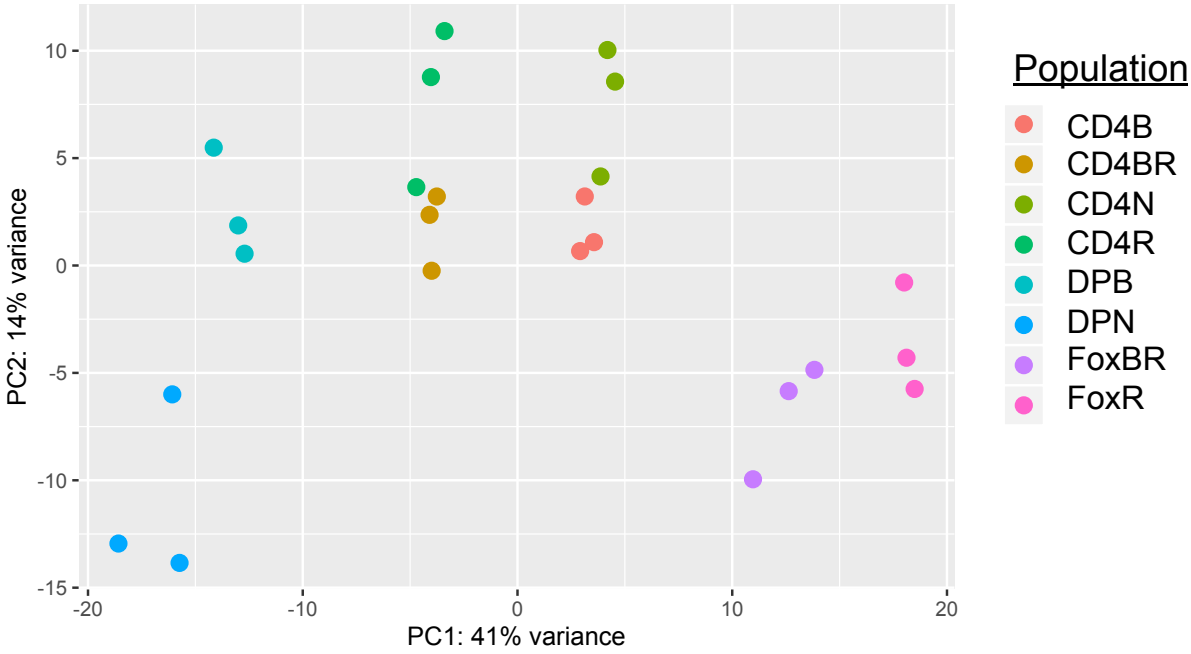

Figure 2.5: Cluster analysis of the transcriptomes of all populations sorted from *Nr4a3*-Tocky mice as shown in Fig.2.1 and processed for RNAseq analysis as described in the methods.

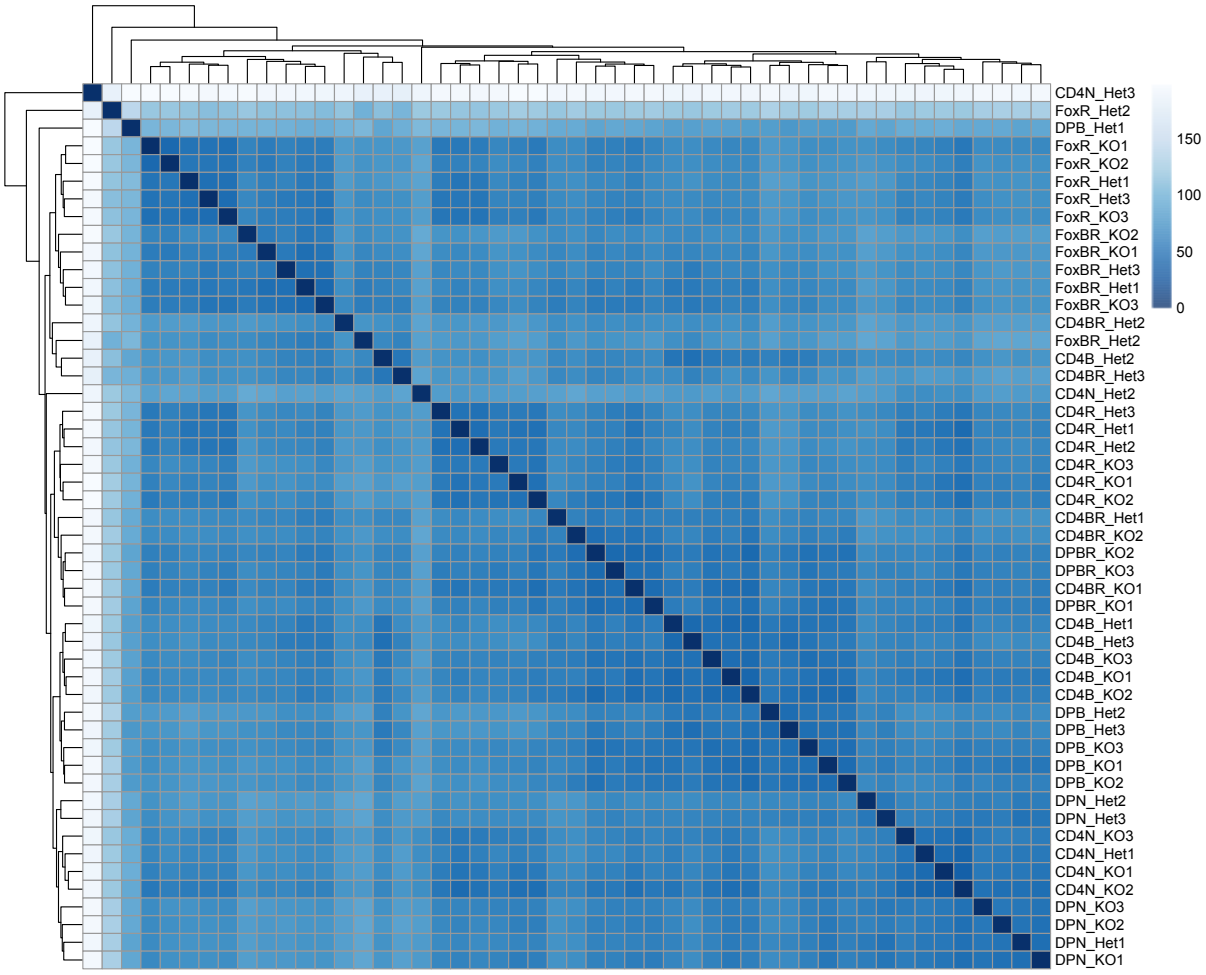

Figure 2.6: Heatmap of sample-to-sample distances for all populations sorted from *Nr4a3*-Tocky:Bim$^{WT/KO}$ and *Nr4a3*-Tocky:Bim$^{KO/KO}$ mice as shown in Fig.2.2 and processed for RNAseq analysis as described in the methods.

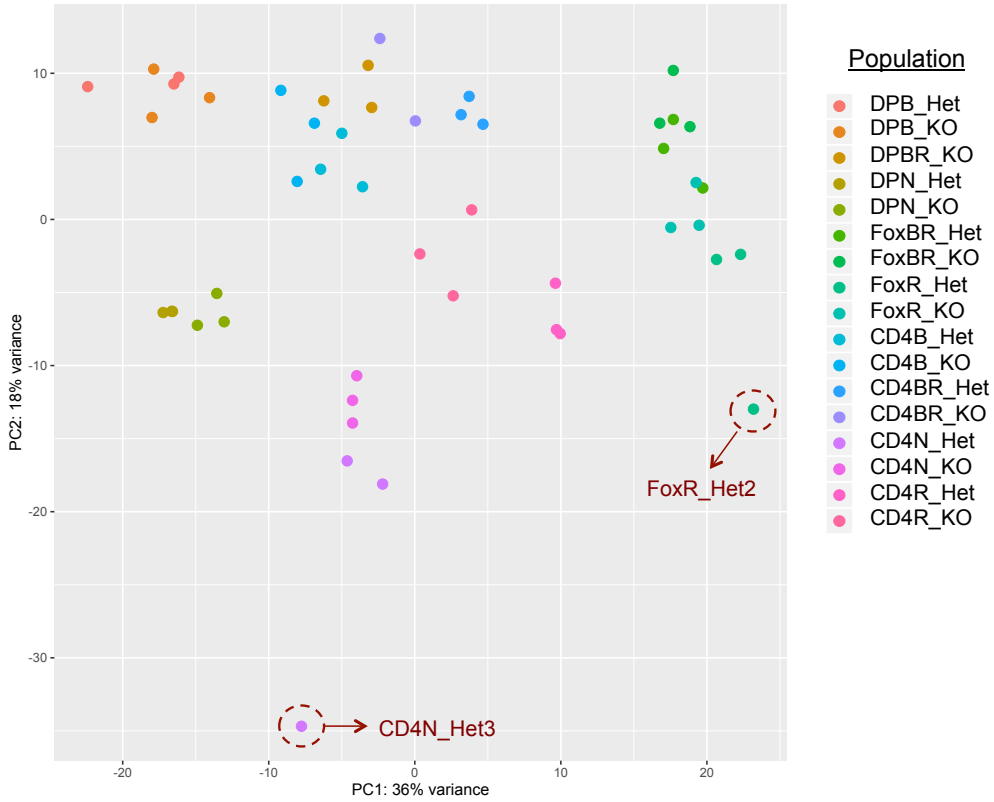

Figure 2.7: Cluster analysis of the transcriptomes of all populations sorted from *Nr4a3*-Tocky:Bim$^{WT/KO}$ and *Nr4a3*-Tocky:Bim$^{KO/KO}$ mice as shown in Fig.2.2 and processed for RNAseq analysis as described in the methods, where red dotted circles mark the samples identified as outliers (CD4N_Het3 and FoxR_Het2).

2.7 Statistical Analysis

Statistical analyses were performed either in R using built-in functions (or the DESeq2 package for RNAseq data to obtain adjusted p values) or in GraphPad Prism. Unpaired Student's t-test or Mann-Whitney U test analysis were used to compare between two groups. Multiple group comparisons were carried out by Kruskal-Wallis test or by one-way ANOVA. In the case of one-way ANOVA, Tukey's post-hoc test was applied to compare between individual groups. Normal distribution was assumed for mean fluorescence intensity (MFI) data and for RNAseq normalised count data on a logarithmic scale to base 2 and either t-test or ANOVA followed by Tukey's post-hoc analyses were carried out. Assumption of Gaussian distribution for these data sets was confirmed by D'Agostino & Pearson normality test, or by Shapiro-Wilk normality test where $n < 8$. In the case of percentage data, normal distribution was not assumed because the data are bounded and non-parametric Mann-Whitney U test or Kruskal-Wallis analyses were carried out instead. Statistically significant differences are reported as * for $p<0.05$, ** for $p<0.01$, *** for $p<0.001$ **** for $p<0.0001$ and n.s. ("not significant") for $p>0.05$.

Chapter I: Development of the Tocky System

3.1 Introduction

An immune response ultimately consist of gene expression in the form of proteins. For a gene to become expressed, it needs to first be transcribed to mRNA. Aided by transcription factors, RNA polymerase binds to the promoter region of the gene and causes DNA strand separation. The enzyme then moves along the nucleotide sequence in the 3'-5' direction from the transcriptional start site and generates an mRNA strand complimentary to the sequence that grows from the 5' end by attaching the appropriate nucleotides. Once it has reached a termination signal, RNA polymerase detaches. The resulting mRNA then leaves the nucleus and relocates to the cytoplasm to be translated into protein. Ribosomes are part of the translational machinery of the cell and they convert mRNA into a polypeptide sequence by attributing the corresponding amino acid to each three-letter base pair codon of the transcript. Hydrogen bonds formed between amino acids cause the chain to fold onto itself and subsequent intramolecular interactions result in a three-dimensional structure. A fully mature protein is the result of post-translational modifications, which can occur spontaneously or following enzymatic activities by other proteins. Intracellular proteins are eventually degraded, either by proteolysis in the lysosome or via ubiquitinylation, where the protein is tagged for degradation in the proteasome. The rate of decay can vary from minutes to weeks, depending on the function, structure and intramolecular properties of the protein (Alberts, 2015).

3.1.1 Green Fluorescent Protein

Following post-translational modifications involving cyclisation, oxidation and dehydration mechanisms, GFP matures into a visibly green fluorescent light-emitting structure. Cyclisation of three amino acids, followed by dehydrogenation at one of the side chains results in the formation of double bonds that absorb violet-blue light and emit green fluorescence (Craggs, 2009). By virtue of this property, GFP has become a frequently used biological marker ever since it was first purified in the 1970s from the jellyfish species *Aequorea Victoria* (Reviewed by Phillips, 2001). Single point mutation S65T not only enhanced its fluorescence and photostability, but it also shifted its main excitation peak, rendering it detectable by commercially available fluorescein isothiocyanate (FITC) filter sets (Orm et al., 1996), allowing scientists to easily use them in flow cytometry. This mutant was further optimised to fold at 37°C (Cormack, Valdivia and Falkow, 1996), facilitating its use in mammalian studies. It is referred to as enhanced GFP (EGFP) and it is routinely used to generate reporter transgenic mice, which allow scientists to study the expression of a gene of interest. While these reporters have been very helpful in the field (Moran et al., 2011), EGFP is a very stable protein with a half life of approximately 56 hours (Fig.3.1A; Sacchetti et al., 2001). Therefore, it can only report transcription history, which serves as limited information when investigating a highly dynamic environment such as the thymus. In order to fully address complex matters such as the mechanisms of thymic T cell development, alternative methods are required that enable the visualisation of real-time transcription *in vivo*.

3.1.2 Fluorescent Timer Proteins

DsRed is a fluorescent protein, originally purified from the sea anaemone Discosoma striata (Matz et al., 1999), which emits a red-orange light when excited. Its post-translational cycle is similar to that of GFP, except for an additional oxidation step, which causes its emission spectrum to shift from green to red (Strack et al., 2010). The Siebert lab gener-

ated a mutant of this protein to enhance the fluorescence of its dim green light-emitting intermediate and referred to it as a "fluorescent Timer". The slow maturation of DsRed (over 24 hours) would facilitate the study of genetic activity over time, where green emission reflects more recent expression than the fully mature red fluorescent form, which could reflect gene downregulation (Terskikh et al., 2000). Although the concept of a Timer is very attractive for *in vivo* studies, the tetrameric structure of DsRed renders it unsuitable for the generation of fusion proteins, as it could disrupt localisation and endogenous function. In response to this, the monomeric mutant mRFP1 was generated (Campbell et al., 2002) and the lab carried out further work to improve its photostability, fusion properties and maturation capacity, which gave rise to a variety of new monomers (Shaner et al., 2004). Among these, mCherry was chosen by the Verkhusha lab as a candidate for developing Timers. Because mCherry spontaneously changes its emission spectrum from a very short-lived blue form to a very stable red form, it can be used in combination with GFP, making it a very promising reporter. The lab described three mCherry mutants which had a delay in their maturation process, qualifying them as potential Timers. By fitting data derived from purified Timer proteins into a pharmacological kinetics model, Subach et al. estimated the time required for protein maturation to the red form, where the blue form of the Fast-FT variant had a half-life of approximately 7 hours (Fig.3.1B; Subach et al., 2009).

3.1.3 The Tocky System

Dr. Masahiro Ono chose the Fast-FT mCherry-derived mutant and pioneered the use of Timer proteins in mice in order to capture transcriptional dynamics *in vivo* of genes of interest (Bending et al., 2018). Timer reporter mice are designated as "Tocky", which stands for Timer of cell kinetics and activity, where [toki] is a word for "Time" in Japanese, a fit nomenclature for a reporter that is informative of the temporal dynamics of gene transcription. A modified BAC containing the *Timer* gene was randomly integrated un-

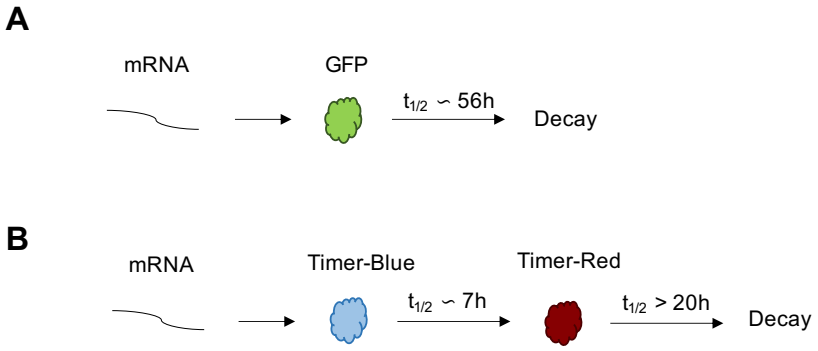

Figure 3.1: Schematic representations of (A) GFP maturation and (B) Timer protein maturation. The $t_{1/2}$ values of Timer protein featured in this figure were not determined following direct experimental measurements, but by model fitting by Subach et al., 2009.

der the regulatory sequences of the target gene of interest. This approach avoids any interference of the transgenic reporter with the endogenous transcription of the reported gene (Bending et al., 2018). The Tocky system enables visualisation of transcription dynamics on a flow cytometry plot. The Blue^{+}Red^{-} and Blue^{-}Red^{+} phenotypes indicate new and arrested transcription, respectively. Some cells, however, may appear as Blue^{+}Red^{+}. This means that while Blue protein matures to Red, the cell is still transcribing the gene, producing more Blue proteins. When Red and Blue flourescence are plotted on the x and y axes, respectively, of a flow cytometry plot, the temporal dynamics of transcription can be observed in a clockwise manner (Bending et al., 2018).

3.1.4 Chapter aims

Before making use of this promising technology, it is imperative to experimentally validate the Tocky system as an accurate reporter of endogenous transcriptional dynamics *in vivo*. This chapter will aim to develop the Tocky system by:

(I) Investigating the biochemical properties of the *Timer* transcript

(II) Experimentally measuring the half-life of Blue and Red proteins

(III) Correlating transcript variation to protein maturation

3.2 Results

3.2.1 *Timer* mRNA products accurately report gene transcriptional activity

It was hypothesised that in the *Foxp3*-Tocky model, expression of *Timer* and endogenous *Foxp3* are correlated. To verify this, an RNA degradation assay was performed, where actinomycin D was used to block further transcriptional activity. *Timer* mRNA exhibited a similar half-life to that of *Foxp3* and of the constitutively expressed gene *Hprt* (Fig.3.2). This correlation between transcripts demonstrates that in *Foxp3*-Tocky mice, the kinetics of *Timer* transcripts are largely determined by those of *Foxp3* transcripts, as long as transcriptional activities of the *Timer* gene are synchronised with those of the *Foxp3* gene.

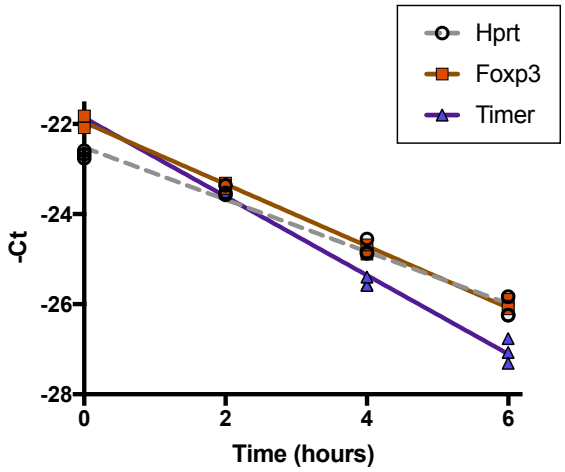

Gene	*Hprt*	*Foxp3*	*Timer*
R^2	0.99	0.99	0.99
$t_{1/2}$	1.73	1.46	1.14

Figure 3.2: **mRNA degradation assay.** CD4 SP splenocytes from *Foxp3*-Tocky mice were cultured in the presence of actinomycin D and RNA was extracted at the indicated time points. mRNA expression of *Hprt*, *Foxp3* and *Timer* was measured by RT-qPCR to obtain the plotted raw Ct values. The half-life of each species was determined using linear regression analysis by Pearson's correlation, where n = 3 culture replicates. The results were confirmed by two independent experiments, one of which was performed by Dr. David Bending, University of Birmingham.

3.2.2 Characterising Timer-expressing populations on flow cytometry plots

By plotting Red against Blue fluorescence of cells from an *Nr4a3*-Tocky mouse model, four different populations were defined according to their endogenous Timer expression: Blue$^-$Red$^-$, Blue$^+$Red$^-$, Blue$^+$Red$^+$ and Blue$^-$Red$^+$ (Fig.3.3). The quadrant gate was set against cell populations from a mouse lacking the Timer construct. Blue$^-$Red$^-$ cells do not transcribe *Nr4a3*, while Blue$^+$Red$^-$ cells have recently upregulated it. Blue$^+$Red$^+$ are persistently transcribing *Nr4a3*, while Blue$^-$Red$^+$ cells have ceased transcription.

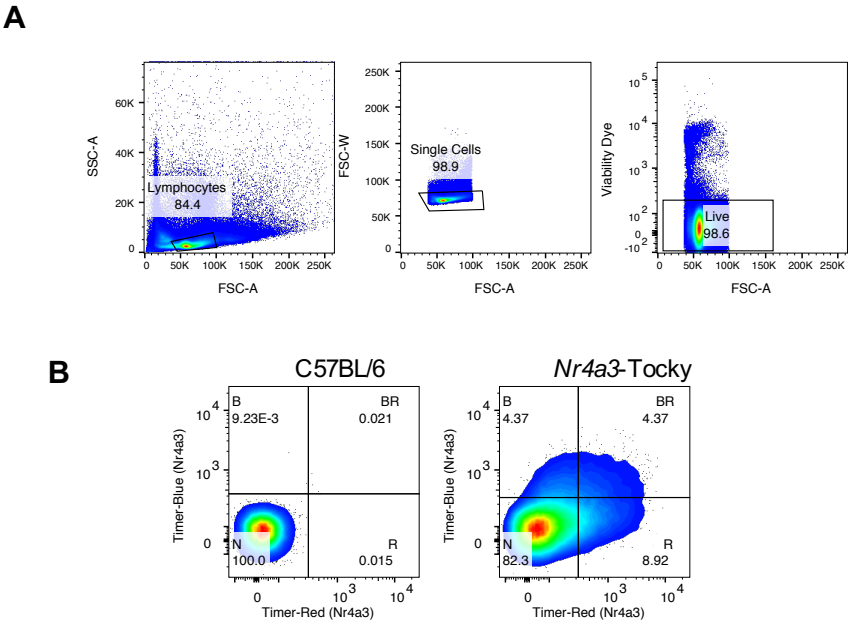

Figure 3.3: **Gating strategy for characterising Timer-expressing populations on flow cytometry plots.** Thymocytes from C57BL/6 or *Nr4a3*-Tocky mice were stained for flow cytometry analysis. (A) 2-D plots show the gating strategy for removing doublets and dead cells. (B) Quadrant gate for Timer-expressing populations was set against the Blue$^-$Red$^-$ population of the C57BL/6 mouse model and the four Timer populations were assigned a one letter name on flow cytometry plots, where N = Blue$^-$Red$^-$, B = Blue$^+$Red$^-$, BR = Blue$^+$Red$^+$ and R = Blue$^-$Red$^+$.

3.2.3 Blue protein reports real-time transcription

The half-life of Blue protein was originally estimated at approximately 7 hours (Subach et al., 2009). Because this was established by fitting data from purified Timer proteins to a pharmacological kinetic model, it was desirable to determine it experimentally. It was also of interest to verify whether Timer protein maturation is affected by cell type. To test this, T cells and B cells from *Nr4a3*-Tocky mice had their TCR and BCR stimulated overnight with anti-CD3 and goat anti-mouse IgM, respectively, in order to induce Blue protein expression. The next day, cells were treated with cyclohexamide in order to inhibit further protein synthesis and Blue fluorescence was measured every two hours by flow cytometry. In all three population tested (B cells, CD4 SP and CD8 SP cells), Blue protein decayed with a half-life of approximately 4 hours, much quicker than originally reported (Subach et al., 2009). This suggests that Timer protein maturation is not affected by cell type and that Blue fluorescence reports real-time transcription.

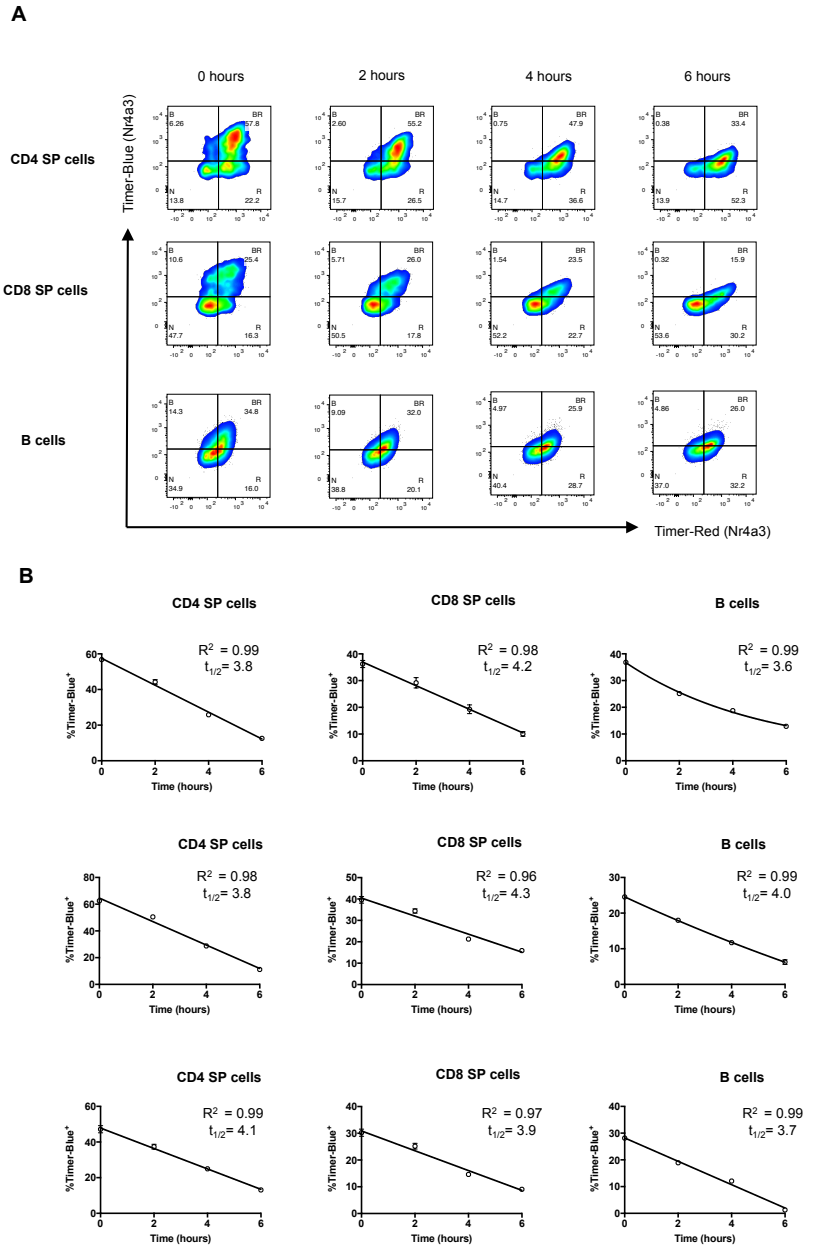

Figure 3.4: **Blue protein degradation assay.** Splenocytes from *Nr4a3*-Tocky mice were stimulated overnight with plate-bound anti-CD3 to induce T cells stimulation, or with goat anti-mouse IgM for B cell stimulation, and cultured the next day for the indicated time points in the presence of cyclohexamide. Blue protein expression was then measured by flow cytometry in CD4 SP or CD8 SP cells and in $CD3^{-}CD19^{+}$ B cells. (A) Flow cytometry plots show blue protein expression by each cell population for each culture time point. (B) Graphs show blue protein expression measurements and the half-life of fluorescent protein for each population in three independent experiments (one experiment per row), where n = 3 culture replicates. Data were analysed using the GraphPad Prism software one phase exponential decay model.

3.2.4 Red protein reports transcription history

Blue^{-}Red^{+}CD4 SP cells from *Nr4a3*-Tocky mice were sorted in order to measure the half-life of Red protein (Fig.3.5A). Since Timer protein would only be expressed following TCR engagement, the cells were cultured in the absence of stimulation and Red protein MFI was measured roughly every 24 hours (Fig.3.5B). Red protein slowly decayed with a half life of 113 hours (Fig.3.5C). This indicates that in Tocky mice, Red fluorescence reports the accumulation of *Nr4a3* transcripts over a period of approximately 5 days.

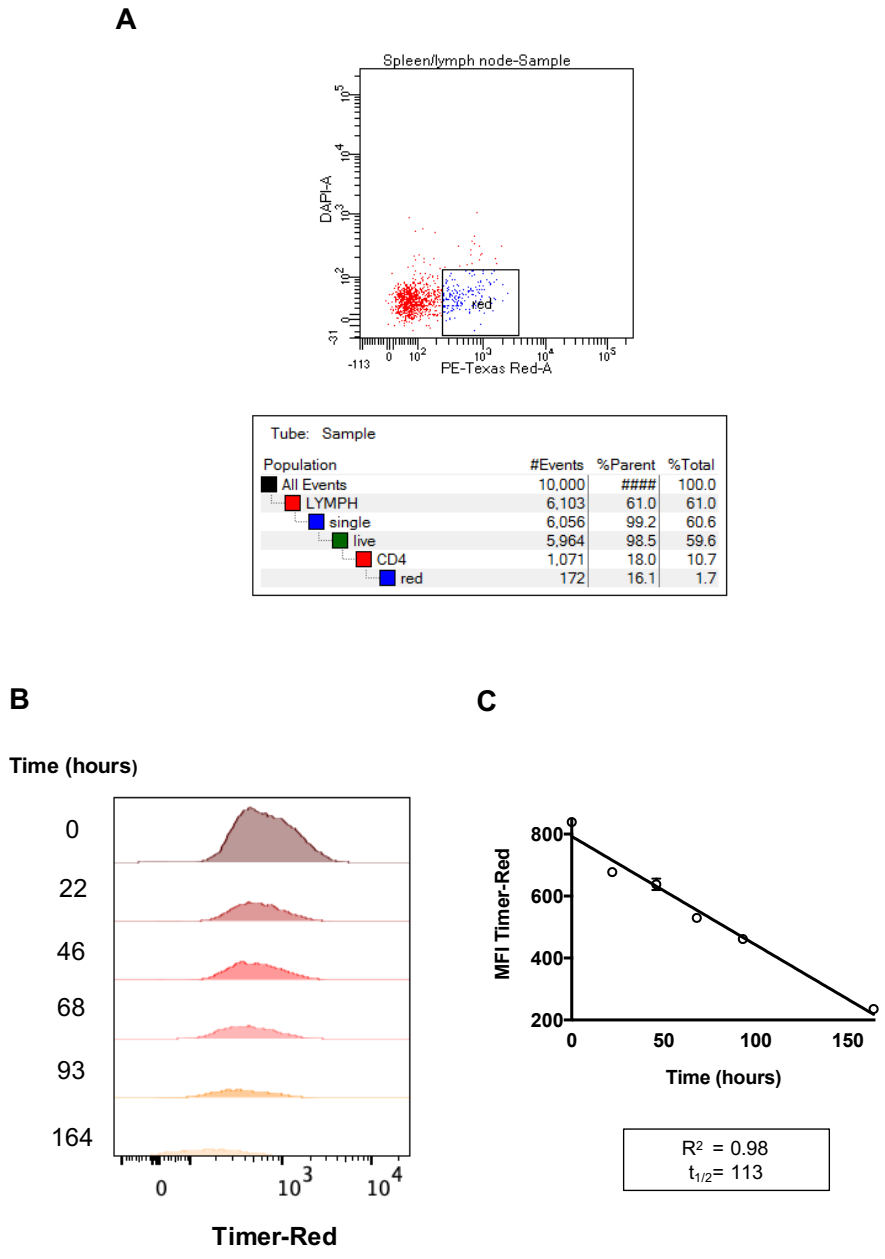

Figure 3.5: **Red protein degradation assay.** Blue^{-}Red^{+}CD4 SP cells from *Nr4a3*-Tocky mice were sorted using a BD Aria III machine as shown in (A) and cultured without stimulation for the time points indicated in (B). MFI values of Red protein were measured by flow cytometry and its half-life was determined using linear regression analysis by Pearson's correlation, as shown in (C), where n = 3 culture replicates. The calculations were confirmed by two independent experiments.

3.2.5 Transcribed *Nr4a3* quantitatively correlates with Timer protein dynamics

In order to determine *Nr4a3* mRNA variation in relationship to protein maturation, cells from the thymus of *Nr4a3*-Tocky mice were sorted according to Timer expression and mRNA levels were measured by RT-qPCR (Fig.3.6). As expected, the largest quantity of *Nr4a3* mRNA was observed in the Blue^{+}Red^{-} population, followed by Blue^{-}Red^{+}. Blue^{-}Red^{+} cells, which would have ceased *Nr4a3* transcription, had similarly low levels of *Nr4a3* as the Blue^{-}Red^{-} population. Together, these findings show that Timer protein maturation accurately reflects the quantity of *Nr4a3* mRNA present in the cell.

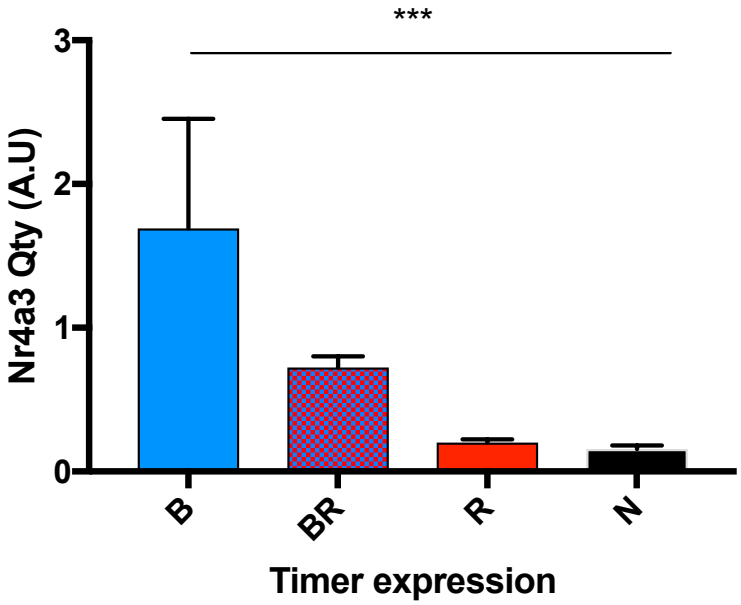

Figure 3.6: ***Nr4a3* levels in Timer-expressing thymocytes.** Four thymic CD4SP populations from *Nr4a3*-Tocky mice were defined according to their endogenous Timer expression, where B = Blue^{+}Red^{-}, BR = Blue^{+}Red^{+}, R = Blue^{-}Red^{+} and N = Blue^{-}Red^{-} and sorted directly into lysis buffer. mRNA levels were measured by RT-qPCR and normalised for cell number by dividing the resulting value by that of the housekeeping gene Actin. Error bars are representative of mean ± s.d, where n = 3 biological replicates and ***p = 0.003 according to Kruskal-Wallis non-parametric test.

3.3 Discussion

In this chapter, the Tocky system was developed as an accurate reporter of transcriptional dynamics *in vivo* by determining critical parameters for the maturation and degradation properties of Timer transcripts and proteins. The mRNA degradation assay showed that the degradation rates of *Timer* and *Foxp3* mRNA were very similar. Therefore, the degradation factor does not contribute to the dynamics of Timer fluorescence expression. In addition, in *Nr4a3*-Tocky, RT-qPCR data further demonstrated that Blue fluorescence accurately predicted the quantity of mRNA. This is especially relevant when sorting cells according to Timer protein expression for RNAseq analysis.

Since the half-lives of Timer proteins had only been estimated using a pharmacological kinetic model (Subach et al., 2009), it was important to measure them experimentally in order to accurately determine the relative age of cells maturing *in vivo*. While the half-lives of Blue and Red proteins were originally estimated to be 7 hours and 20 hours, respectively, flow cytometry data showed different results. The half-life of Blue protein was approximately 4 hours and that of Red was approximately 5 days (Fig.3.7). This means that Blue fluorescence very nicely captures real-time transcription, which is an important requirement when investigating fast-occurring events, such as TCR signalling. The very long half-life of Red protein helps capture cells that have ceased transcription over several days and distinguishes them from Blue$^-$Red$^-$ cells.

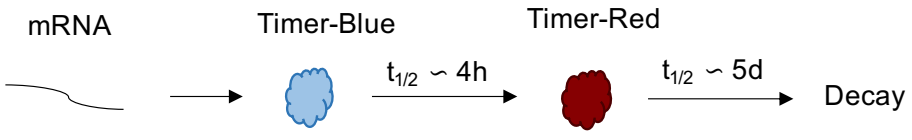

Figure 3.7: Schematic representation Timer protein maturation according to experimental results.

The Tocky system is a powerful tool for the study of the highly complex and fast-changing

thymic environment. In the following chapters, the *Nr4a3*- and *Foxp3*-Tocky models will be used in order to study the dynamics of thymic T cell development and selection. Since Timer protein maturation did not appear to be affected by cell type, the Tocky system can be used to investigate the fate of thymocytes during all stages of development.

Chapter II: Investigation of T cell development at the DP stage

4.1 Introduction

DP cells are unique in their co-expression of CD4 and CD8 lineage markers, which allows them to interact with both MHC-I and MHC-II molecules. DPs that survive the process of positive selection upregulate CD69 and are the first thymocytes to express a fully functional $\alpha\beta$TCR.

4.1.1 Selection processes in the cortex

The general consensus regarding T cell selection is that self-antigens required to induce positive selection are presented by cTECs, while self-antigens that promote negative and agonist selection are mainly presented by medullary APCs, particulary mTECs and DCs. There is ample evidence, however, that negative selection also occurs in the cortex, induced by cTEC antigen presentation and carried out in a Bim-mediated manner (Ahn et al., 2008; McCaughtry et al., 2008; Daley, Hu and Goodnow, 2013; Stritesky et al., 2013). In fact, twice as many cells are estimated to become negatively selected in the cortex than in the medulla (Stritesky et al., 2013). T cells with strong affinity to tissue-restricted antigens (TRAs), which are only encountered in specialised perhipheral organs, are indeed exclusively removed in the medulla (McCaughtry and Hogquist, 2008). However, negative selection of cells with very strong affinity to ubiquitous self-antigen occurs in the cortex, without any contribution from the medullary compartment (McCaughtry et al., 2008).

The cortex was also shown to support Treg development. It is not known whether the fate of any suppressive T cells is pre-determined by interactions with cortical antigens, but it has been suggested that as many as 20% of Foxp3$^+$ T cells could be selected on cTECs (Owen et al., 2019). Two independent studies showed that suppressive T cells can develop from cortical interactions alone, without the involvement of the medulla (Bensinger et al., 2001; Liston et al., 2008).

The *Prss16* gene, encoding a serine protease exclusively expressed in the thymus, was found to be cTEC-specific and the lysosomal localisation of the resulting protein indicates a role in antigen processing. Interestingly, PRSS16 polymorphisms are associated with type I diabetes in humans (Viken et al., 2009). This suggests that complete tolerance to self-antigen requires efficient antigen processing and presentation in the cortex.

4.1.2 Antigen presentation by cTECs

What distinguishes cTECs from other APCs is their characteristic antigen processing machinery, which results in unique antigen-MHC complexes. While antigen presented on MHC-II molecules by most APCs is derived from extracellular sources, the one presented by cTECs is the endogenous by-product of macroautophagy, a bulk protein degradation process. Macroautophagy is particularly abundant in cTECs and contributes to efficient positive selection (Nedjic et al., 2009).

When an MHC-II molecule is produced, its antigen binding site is temporarily blocked by a structure known as the invariant chain. If processed antigen is ready to be loaded, the lysosomal proteases cathepsins degrade the invariant chain. They are also involved in the generation of self-antigens. While most APCs mainly express cathepsin S, cTECs predominantly express cathepsin L. Inactivation of the gene encoding cathepsin L reduced the CD4 SP thymic population by up to 80%. The severely diminished polyclonal TCR

repertoire highlights the essential role of cTEC-derived antigens for T cell development from the DP stage (Nakagawa et al., 1998). A study in NOD mice found that Cathepsin L deficiency is associated with attenuated onset of diabetes and disease progression, promoted by an imbalance between Treg and pathogenic T cells. The authors concluded that this protease supports self-reactive T cell development (Maehr et al., 2005).

cTECs also provide unique self-antigens for MHC-I molecule presentation. The proteasome is the organelle responsible for generating antigens presented on MHC-I molecules by all eukaryotic cells. The thymoproteasome is a derivative of it, which features the unique catalytic subunit β5t and is exclusively found in cTECs (Murata, Takahama and Tanaka, 2008). β5t subunit deficiency results in severe diminishment of the CD8 SP pool (Murata et al., 2007) and qualitatively altered TCR repertoires (Nitta et al., 2010). A gene-replacement experiment that engineered β5t-deficient animals to produce a set of antigens for MHC-I molecule loading that differs from that normally generated by cTECs or other APCs could not rescue the CD8 SP compartment. The study also showed that of the few surviving CD8 SP cells, most displayed high affinity to self-antigen, characterised by elevated levels of Nr4a1 (Xing, Jameson and Hogquist, 2013). This, together with the findings presented above, highlights the unique role cTECs have in antigen processing for proper T cell development from the DP stage.

4.1.3 Chapter aims

Significant progress has been made in understanding how lineage-committed SP cells with diverse TCR repertoires tolerant to self-antigens develop from the DP stage. However, the TCR signalling requirements for negative selection and CD4/CD8 lineage fate decision are not well understood and the temporal dynamics of T cell development at the DP stage remain elusive. The work presented in this chapter aims to clarify this by using the *Nr4a3*-Tocky system in order to:

(I) Investigate the dynamic changes in transcription and surface protein expression in DP cells upon receiving TCR signals from cognate antigen

(II) Study the TCR signalling requirements associated with CD4/CD8 lineage marker downregulation

(III) Capture cells which escape negative selection in *Nr4a3*-Tocky:Bim$^{KO/KO}$ mice and investigate the dynamic changes in transcription and surface protein expression associated with their development

(IV) Address how impaired negative selection affects CD4/CD8 lineage selection in Timer^{+} DP cells

4.2 Results

4.2.1 CD69 and *Nr4a3* are expressed in a synchronised manner following strong TCR signalling

DP cells that are able to recognise self-antigen pass the process of positive selection, which is associated with the surface marker CD69. *Nr4a3*-Tocky mice, in which Timer expression is induced upon cognate antigen signalling (Bending et al., 2018), were used to study T cell development at the DP stage. While there was not much Timer expression in the bulk DP population (Fig.4.1A), when gating on cells that express CD69, a Blue^{+}Red^{-} population was observed. Timer^{+} cells were almost exclusively captured in this quadrant, suggesting that positively selected cells that receive strong signals either immediately proceed to the next stage of development, or undergo clonal deletion before Timer protein has a chance to mature. Furthermore, Blue protein was detected only when CD69 expression was highly expressed and most of it was detected in a very small population characterised by the cells highest in CD69 (Fig.4.1B). This indicates a close dependency between CD69 upregulation and *Nr4a3* transcription for DP maturation, where CD69 expression likely precedes *Nr4a3* transcription. If CD69 is an exclusive marker for positively selected cells at the DP stage, then CD69^{+}Blue^{-}Red^{-} cells have passed this stage of development by receiving a signal through their receptor of too weak affinity to induce *Nr4a3* transcription. Blue^{+}Red^{-} cells, on the other hand, have either encountered their cognate antigen immediately after positive selection, or were positively selected on their cognate antigen.

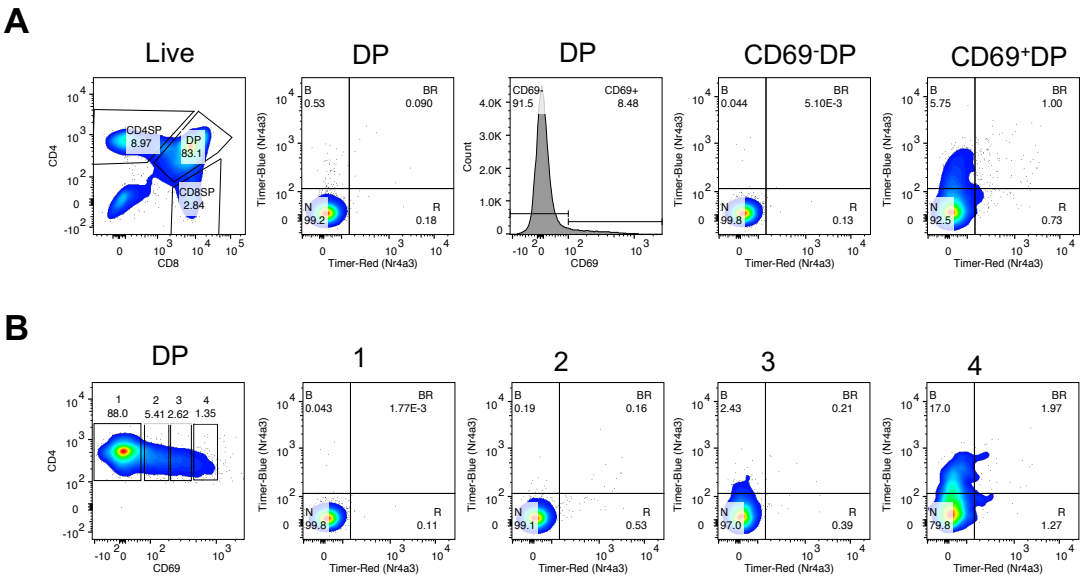

Figure 4.1: ***Nr4a3* Timer protein expression by DP populations**. Thymocytes from 4 weeks old *Nr4a3*-Tocky mice were analysed by flow cytometry on a Fortessa III instrument. (A) Gating strategy for CD69^{-} and CD69^{+} DP cells, followed by their respective Timer protein expression. (B) Gating strategy for four DP populations expressing different CD69 MFI values, followed by their respective Timer expression. Data shown are typical of at least 4 independent experiments that used 2-4 mice.

4.2.2 DP cells receiving strong TCR signals upregulate PD-1, GITR and CD25

Next, $CD69^{+}Blue^{-}Red^{-}$ DP (DP_N) and $CD69^{+}Blue^{+}Red^{-}$ DP (DP_B) cells were further analysed at protein level (Fig.4.2). Compared to DP_N, DP_B showed downregulated expression of both CD4 and CD8 co-receptors, indicating active involvement in the T cell lineage selection process. They were also enriched with PD-1, which has been shown to have a protective role from clonal deletion at the DP stage (Blank et al., 2003). GITR and CD25, which have been previously identified as markers of Treg precursors at the DP stage (Fontenot et al., 2005; Krishnamurthyet al., 2015), were also compared between DP_N and DP_B to determine whether this phenotype is induced upon cognate antigen recognition at the DP stage. While DP_B showed significantly higher GITR levels compared to DP_N, CD25 expression was comparable between the two populations. However, $CD25^{+}$ DP_B cells had higher Blue MFI than $CD25^{-}$ DP_B (Fig.4.3). A similar effect was observed in $PD\text{-}1^{hi}$ and $GITR^{hi}$ populations upon comparison against $PD\text{-}1^{lo}$ and $GITR^{lo}$ cells, respectively. This suggests that cells expressing the three markers receive stronger TCR signals.

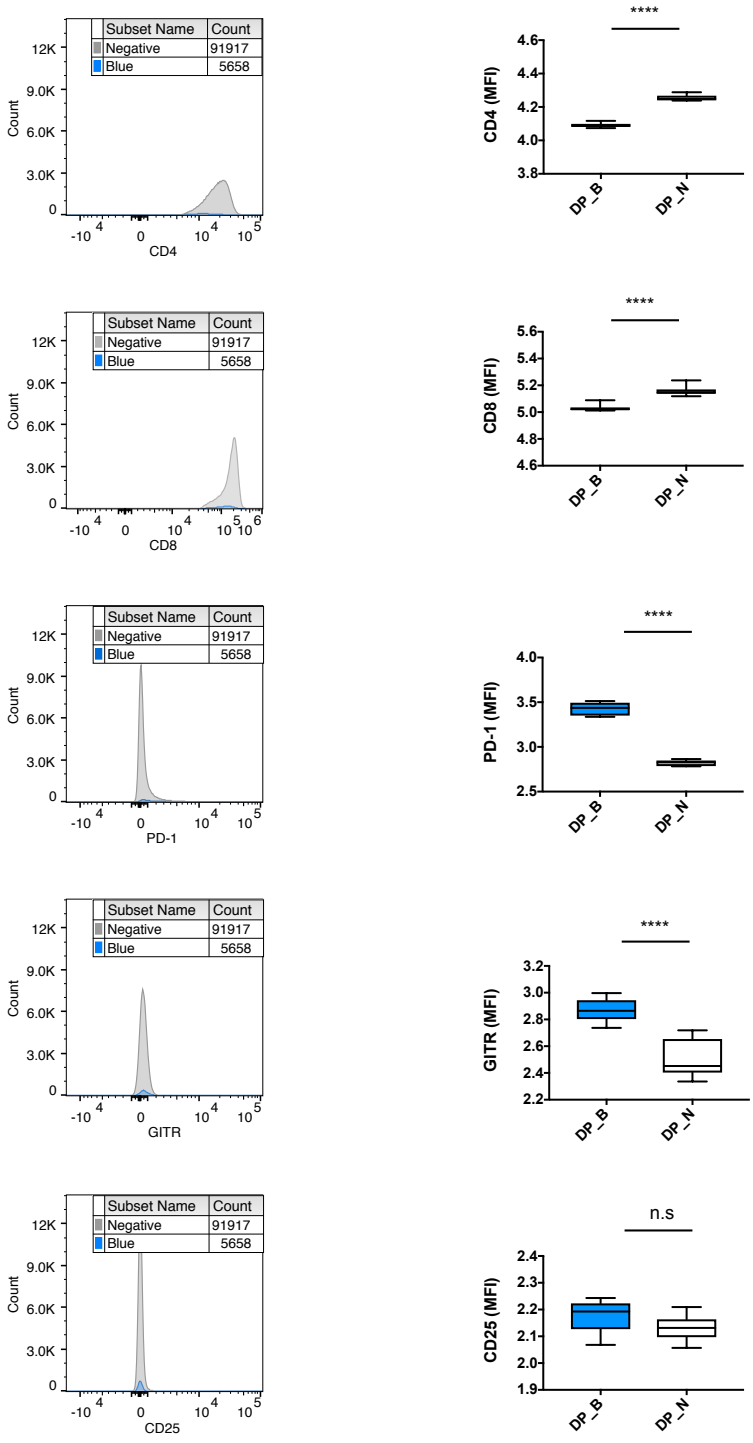

Figure 4.2: **Marker expression in CD69^{+}DP populations**. Thymocytes from 4 weeks old *Nr4a3*-Tocky mice were analysed on a Cytek Aurora spectral analyser. Left panel shows expression of several surface markers by CD69^{+}Blue^{-}Red^{-} DP (DP_N) and CD69^{+}Blue^{+}Red^{-} DP (DP_B) cells. On the right, the MFI of each marker is shown as box plots and compared between DP_N and DP_B cells. Error bars are representative of mean ± s.d, where n = 8 biological replicates. Two independent experiments were combined and summary data are shown. The experiments were performed two days apart and the instrument settings were not changed. Statistically significant differences from unpaired Student's t-test are shown as **** for p<0.0001.

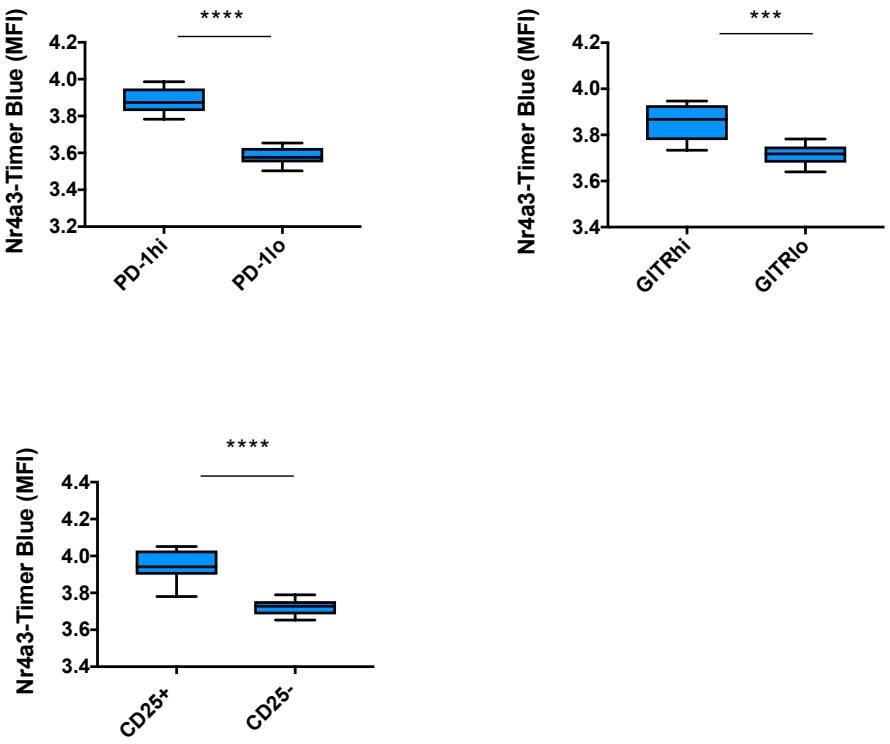

Figure 4.3: **Blue fluorescence intensity in CD69^{+}DP populations**. Thymocytes from 4 weeks old *Nr4a3*-Tocky mice were analysed on a Cytek Aurora spectral analyser and the MFI of Blue protein is shown as box plots and compared between DP_B cells that express different levels of the markers PD-1, GITR and CD25. Error bars are representative of mean ± s.d, where n = 8 biological replicates. Two independent experiments were combined and summary data are shown. The experiments were performed two days apart and the instrument settings were not changed. Statistically significant differences from unpaired Student's t-test are shown as *** for p<0.001 and **** for p<0.0001.

To examine the observed differences between DP_N and DP_B cells at transcript level, the two populations were sorted for RNAseq analysis. 1000 cells from each population were sorted from three 8 weeks old *Nr4a3*-Tocky mice and subjected to RNAseq. The DESeq2 algorithm was used to determine differentially expressed genes based on normalised counts. Expectedly, both *Nr4a3* and *Timer* genes were similarly upregulated in DP_B cells (Fig.4.4).

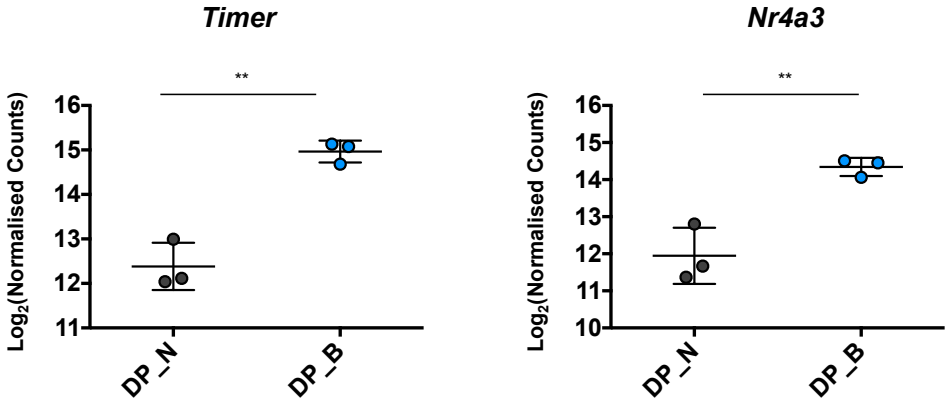

Figure 4.4: ***Timer* expression reflects *Nr4a3* transcription.** 1000 cells per population were sorted from the thymus of 8 weeks old *Nr4a3*-Tocky mice. RNA was extracted from cells and subjected to RNAseq as described in the methods. Normalised counts of expressed genes were obtained using the algorithm DESeq2. Data are shown as $\log_2$ of normalised counts. Error bars are representative of mean ± s.d, where n = 3 biological replicates. Statistically significant differences from unpaired Student's t-test are shown as ** for $p<0.01$.

Consistent with marker expression data (Fig.4.2), RNAseq analysis showed that *Cd4* and *Cd8a* transcription was significantly lower in DP_B cells than in DP_N (Fig.4.5). Transcript levels of the genes *Pdcd1* and *Tnfrsfr18*, coding for the markers PD-1 and GITR, respectively, also matched the phenotypical differences observed between DP_N and DP_B, where the latter population was enriched with both (Fig.4.6). While no significant differences in CD25 protein expression were detected between the two populations (Fig.4.2), at transcript level DP_B cells had significantly higher *Il2ra* levels compared to DP_N (Fig.4.6). The relatively low transcript levels, together with the large variation between samples suggests that there is a very small population which encountered cognate

antigen at the DP stage and upregulated *Il2ra* in a heterogeneous manner. There were no significant differences in terms of *Foxp3* transcription between DP_N and DP_B, suggesting that *Foxp3* upregulation does not immediately follow cognate antigen recognition.

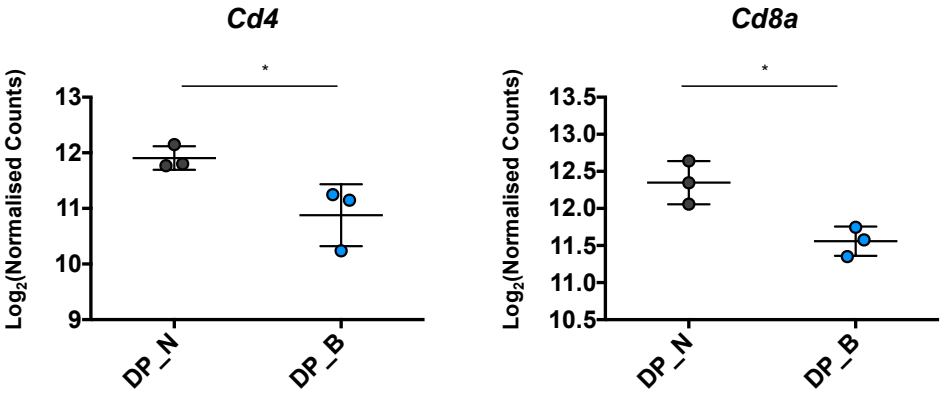

Figure 4.5: **Transcript levels of lineage markers.** 1000 cells per population were sorted from the thymus of 8 weeks old *Nr4a3*-Tocky mice. RNA was extracted from cells and subjected to RNAseq as described in the methods. Normalised counts of expressed genes were obtained using the algorithm DESeq2. Data are shown as $\log_2$ of normalised counts. Error bars are representative of mean ± s.d, where n = 3 biological replicates. Statistically significant differences from unpaired Student's t-test are shown as ** for $p<0.01$.

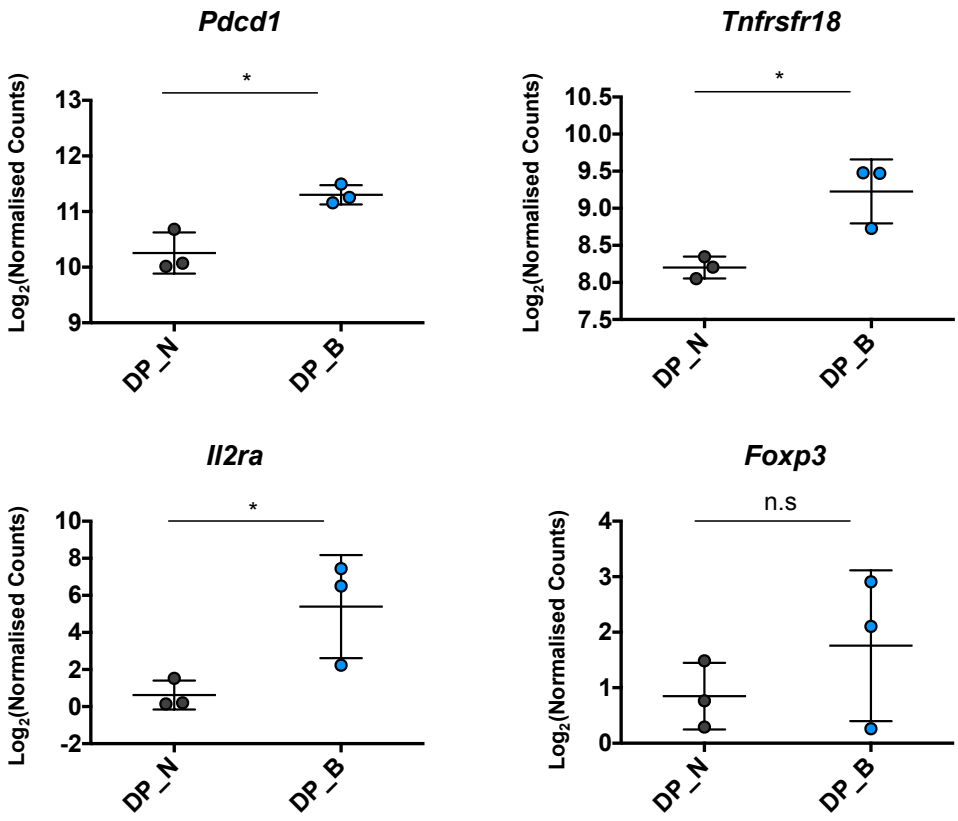

Figure 4.6: **Differentially expressed genes in Timer-expressing populations.** 1000 cells per population were sorted from the thymus of 8 weeks old *Nr4a3*-Tocky mice. RNA was extracted from cells and subjected to RNAseq as described in the methods. Normalised counts of expressed genes were obtained using the algorithm DESeq2. Data are shown as $\log_2$ of normalised counts. Error bars are representative of mean ± s.d, where n = 3 biological replicates. Statistically significant differences from unpaired Student's t-test are shown as * for $p<0.05$.

4.2.3 Blue^{+}Red^{-}DP cells likely undergo negative selection at this stage

DP_B cells were enriched with the transcript *Bcl2l11*, which encodes the pro-apoptotic molecule Bim that is involved in clonal deletion of potentially pathogenic, self-reactive T cells (Fig.4.7). Transcript levels of *Ccr7*, coding for the chemokine CCR7, which is required for migration to the medulla, were double in DP_N compared to DP_B cells (Fig.4.8). These findings, together with their marked downregulation of CD4 and CD8 lineage markers (Fig.4.2) and the nearly absent Red fluorescence in the overall CD69^{+}DP population (Fig.4.1), suggest that, on average, fewer DP_B cells reach the medulla compared to DP_N. Some DP_B may become deleted in a Bim-mediated manner, while others very quickly change their phenotype upon reaching the next stage of development.

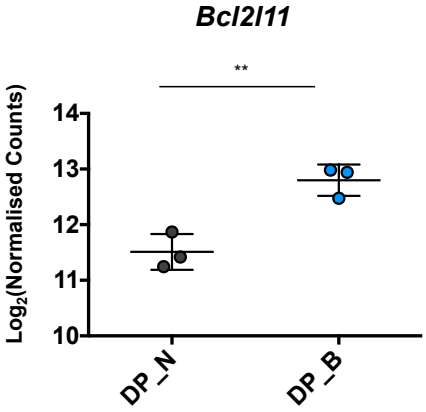

Figure 4.7: ***Bcl211* is actively transcribed by cells receiving strong signals.** 1000 cells per population were sorted from the thymus of 8 weeks old *Nr4a3*-Tocky mice. RNA was extracted from cells and subjected to RNAseq as described in the methods. Normalised counts of expressed genes were obtained using the algorithm DESeq2. Data are shown as $\log_2$ of normalised counts. Error bars are representative of mean ± s.d, where n = 3 biological replicates. Statistically significant differences from unpaired Student's t-test are shown as ** for $p<0.01$.

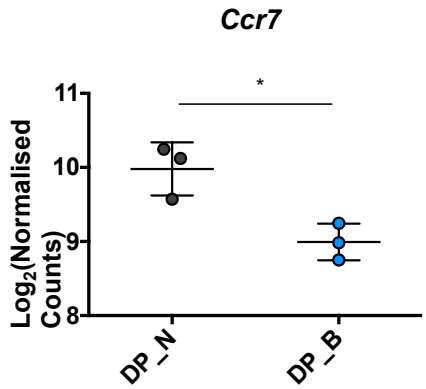

Figure 4.8: **Transcript levels of *Ccr7*.** 1000 cells per population were sorted from the thymus of 8 weeks old *Nr4a3*-Tocky mice. RNA was extracted from cells and subjected to RNAseq as described in the methods. Normalised counts of expressed genes were obtained using the algorithm DESeq2. Data are shown as $\log_2$ of normalised counts. Error bars are representative of mean ± s.d, where n = 3 biological replicates. Statistically significant differences from unpaired Student's t-test are shown as * for $p<0.05$.

4.2.4 CD69^{+}CD4^{lo}CD8^{lo} cells represent a unique developing population

In order to address the significance of the observed co-receptor downmodulation by DP_B (Fig.4.2) in the context of CD4/CD8 selection, four CD69^{+}DP cell populations were defined according to relative CD4 and CD8 expression: CD4^{hi}CD8^{hi}, CD4^{hi}CD8^{lo}, CD4^{lo}CD8^{hi} and CD4^{lo}CD8^{lo} (Fig.4.9). All populations which had downregulated at least one co-receptor consisted of a significantly higher fraction of Blue^{+} cells than CD4^{hi}CD8^{hi} (Fig.4.10). The literature states that all DPs first undergo an intermediate phase as lineage-uncommitted CD4^{+}CD8^{lo} cells, which either progress to the CD4 SP stage or undergo a subsequent intermediary phase characterised by a CD4^{lo}CD8^{lo} phenotype before becoming CD8 SP (Lundberg et al. 1995; Suzuki et al. 1995; Lucas and Germain 1996). Here, a third intermediary phase was defined as CD4^{lo}CD8^{hi} and showed very similar *Nr4a3* expression as CD4^{hi}CD8^{lo}. Both of these populations had significantly smaller proportions of Blue^{+} cells compared to the CD4^{lo}CD8^{lo} population.

The mean Timer angle value of a population is an average measurement of its timing after receiving TCR signals (Bending et al., 2018). All four populations had low angle values, which are within the time domain of Tocky and therefore the temporal sequence of the differentiation events that involve the regulation of CD4 and CD8 expression can be addressed. By comparing the calculated values between all populations (Fig.4.11A), the results show CD4^{hi}CD8^{hi} as having the highest angle, although this population had only a few Timer^{+} cells, followed by CD4^{lo}CD8^{hi}. There was no significant difference between CD4^{hi}CD8^{lo} and CD4^{lo}CD8^{lo} cells, which showed the lowest angle value.

Mean Timer intensity provides information regarding TCR signal strength. According to the results (Fig.4.11B), CD4^{lo}CD8^{lo} cells received the strongest signals, followed by CD4^{hi}CD8^{lo} and CD4^{lo}CD8^{hi} populations, which had similar intensities. Timer intensity

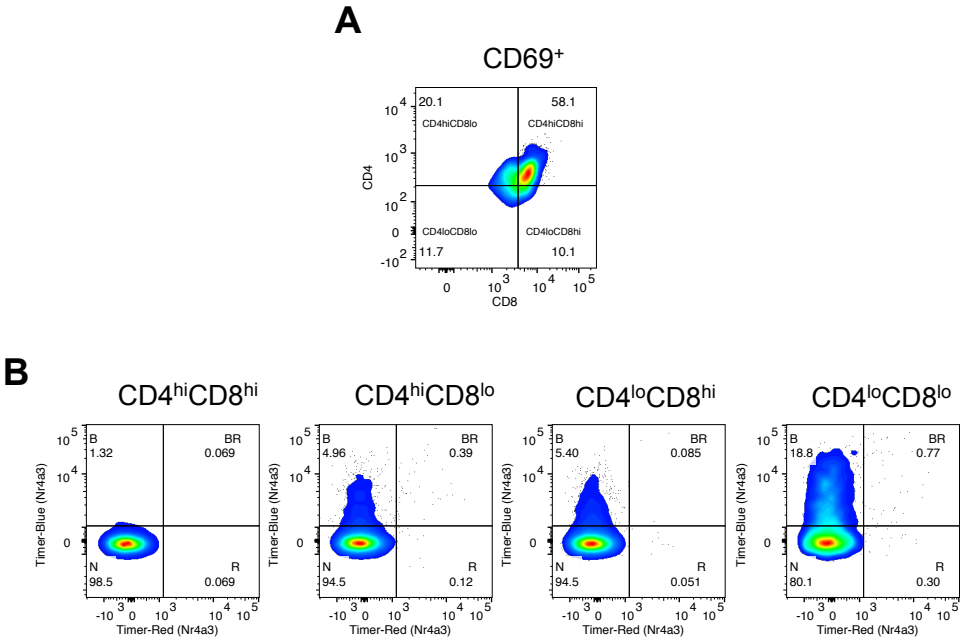

Figure 4.9: **CD69^{+}DP populations defined according to CD4/CD8 lineage marker expression**. Thymocytes from 4 weeks old *Nr4a3*-Tocky mice were analysed on a Cytek Aurora spectral analyser. (A) Gating strategy for defining CD69^{+}DP according to CD4 and CD8 co-receptor expression: CD4^{hi}CD8^{hi}, CD4^{hi}CD8^{lo}, CD4^{lo}CD8^{hi} and CD4^{lo}CD8^{lo}. (B) *Nr4a3*-Timer protein expression patterns of the four defined populations. Data shown are typical of at least 3 independent experiments that used 2-4 mice.

of CD4^{hi}CD8^{hi} was very low compared to the other populations. These cells only had a small number of Timer^{+} cells that likely received weak signals and maintained their high CD4 and CD8 expression for a relatively long time, as shown by their relatively high Timer angle (Fig.4.11B).

As it was shown that *Nr4a3* expression levels correlate with CD69 accumulation, CD69 MFI was measured for each of the four defined populations (Fig.4.12). CD4^{hi}CD8^{hi} had the lowest CD69 MFI. This was immediately followed by CD4^{lo}CD8^{hi} cells, which had significantly lower levels of CD69 expression than CD4^{hi}CD8^{lo} and CD4^{lo}CD8^{lo} cells. This suggests that CD4^{hi}CD8^{lo} precursors received more prolonged TCR signals compared to CD4^{lo}CD8^{hi}, which allowed them to accumulate CD69. This is further supported by their significantly higher Timer angle value (Fig.4.11). CD4^{lo}CD8^{lo} cells also showed

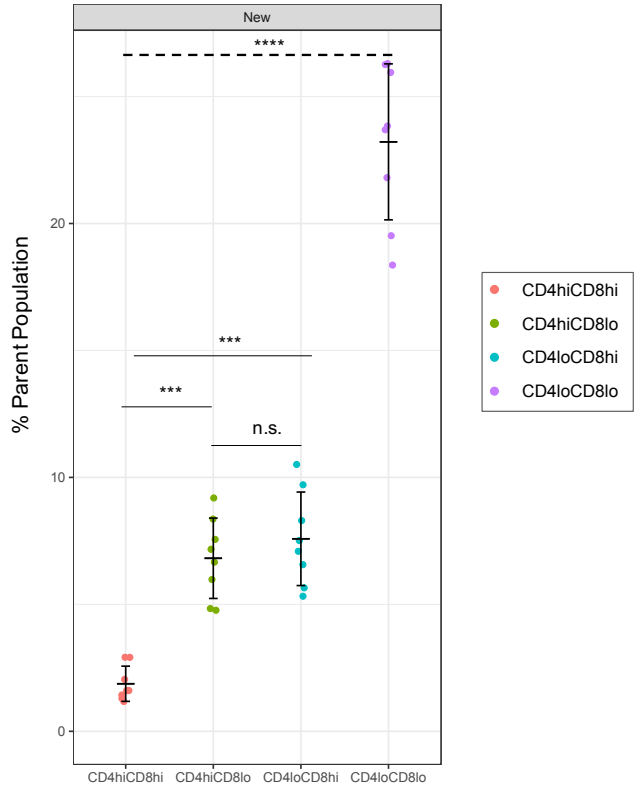

Figure 4.10: **Frequency of CD69^{+}DP populations in the New locus**. Thymocytes from 4 weeks old *Nr4a3*-Tocky mice were analysed on a Cytek Aurora spectral analyser in two independent experiments and data were combined. The experiments were performed two days apart and the instrument settings were not changed. The percentage of cells in each Timer locus among their parent cell population is shown by scatter plots for four CD69^{+}DP populations defined according to CD4 and CD8 co-receptor expression: CD4^{hi}CD8^{hi}, CD4^{hi}CD8^{lo}, CD4^{lo}CD8^{hi} and CD4^{lo}CD8^{lo}. Statistically significant differences from ANOVA (dashed line) and Tukey's post-hoc analysis results that yielded different results from ANOVA (solid lines) are shown as * for p<0.05, ** for p<0.01, *** for p<0.001 and **** for p<0.0001. Error bars are representative of mean ± s.d, where n = 8 biological replicates.

high CD69 expression, similar to that of CD4^{hi}CD8^{lo} cells. This suggests that they also receive more prolonged TCR signals.

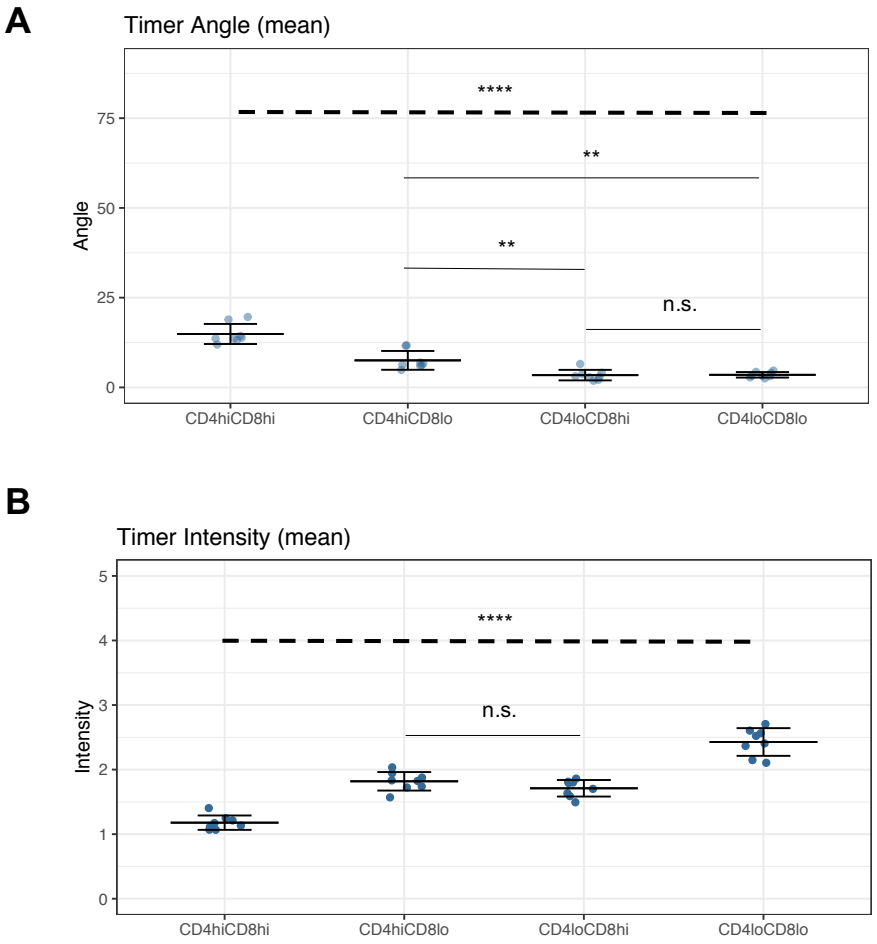

Figure 4.11: **Mean Timer angle and intensity of four CD69^{+}DP populations**. Thymocytes from 4 weeks old *Nr4a3*-Tocky mice were analysed on a Cytek Aurora spectral analyser in two independent experiments and data were combined. The experiments were performed two days apart and the instrument settings were not changed. Mean *Nr4a3*-Timer angle (A) and intensity (B) are shown for four CD69^{+}DP populations defined according to CD4 and CD8 co-receptor expression: CD4^{hi}CD8^{hi}, CD4^{hi}CD8^{lo}, CD4^{lo}CD8^{hi} and CD4^{lo}CD8^{lo}. Statistically significant differences from ANOVA and Tukey's post-hoc analysis are shown as ** for $p<0.01$ and **** for $p<0.0001$. Dashed line represents comparison by ANOVA. Solid lines show individual comparisons by Tukey's post-hoc analysis that yielded different results from the ANOVA analysis. Error bars are representative of mean ± s.d, where n = 8 biological replicates.

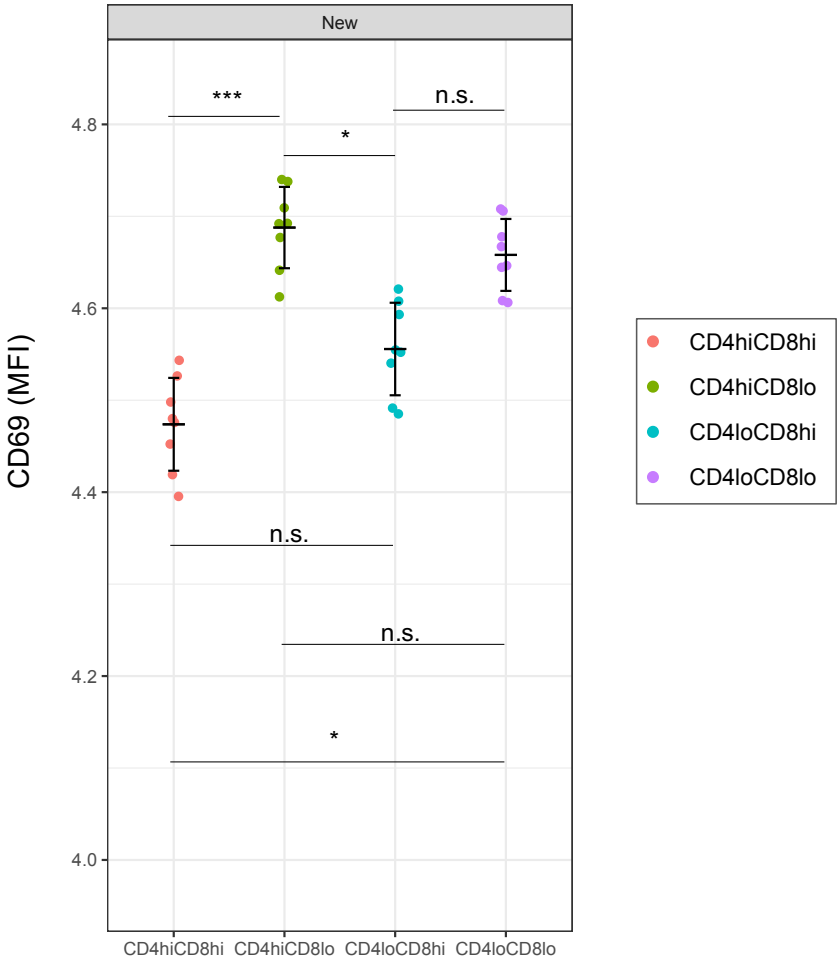

Figure 4.12: **CD69 expression by Blue^{+}Red^{-}CD69^{+}DP populations**. Thymocytes from 4 weeks old *Nr4a3*-Tocky mice were analysed on a Cytek Aurora spectral analyser in two independent experiments and data were combined. The experiments were performed two days apart and the instrument settings were not changed. MFI of the surface marker CD69 is shown for four CD69^{+}DP populations present in the New Timer locus and defined according to CD4 and CD8 co-receptor expression: CD4^{hi}CD8^{hi}, CD4^{hi}CD8^{lo}, CD4^{lo}CD8^{hi} and CD4^{lo}CD8^{lo}. Statistically significant differences from Tukey's post-hoc analysis are shown as * for $p<0.05$ and *** for $p<0.001$. Error bars are representative of mean $\pm$ s.d, where n = 8 biological replicates.

Since high GITR, PD-1 and, to some extent, CD25 expression was found to be associated with stronger TCR signals (Fig.4.3), it was of interest to determine how their expression varies between the four defined populations. The MFI of GITR and CD25 were similar between all four populations (Fig.4.13). PD-1, on the other hand, was preferentially expressed by $CD4^{lo}CD8^{lo}$ cells. No significant differences were observed between the $CD4^{hi}CD8^{lo}$ and $CD4^{lo}CD8^{hi}$ intermediates, although they both expressed it at significantly higher levels than $CD4^{hi}CD8^{hi}$ cells. This finding, together with the observation that $CD4^{lo}CD8^{lo}$ cells express significantly more $Timer^{+}$ cells of higher intensity, distinguishes this population as a unique DP intermediate. The data so far presented indicates that strong TCR signals immediately downregulate one or both co-receptors. Since the population that downregulated both received the strongest TCR signals, it is likely that some $CD4^{lo}CD8^{lo}$ cells become deleted in a Bim-mediated manner, while others survive and express PD-1.

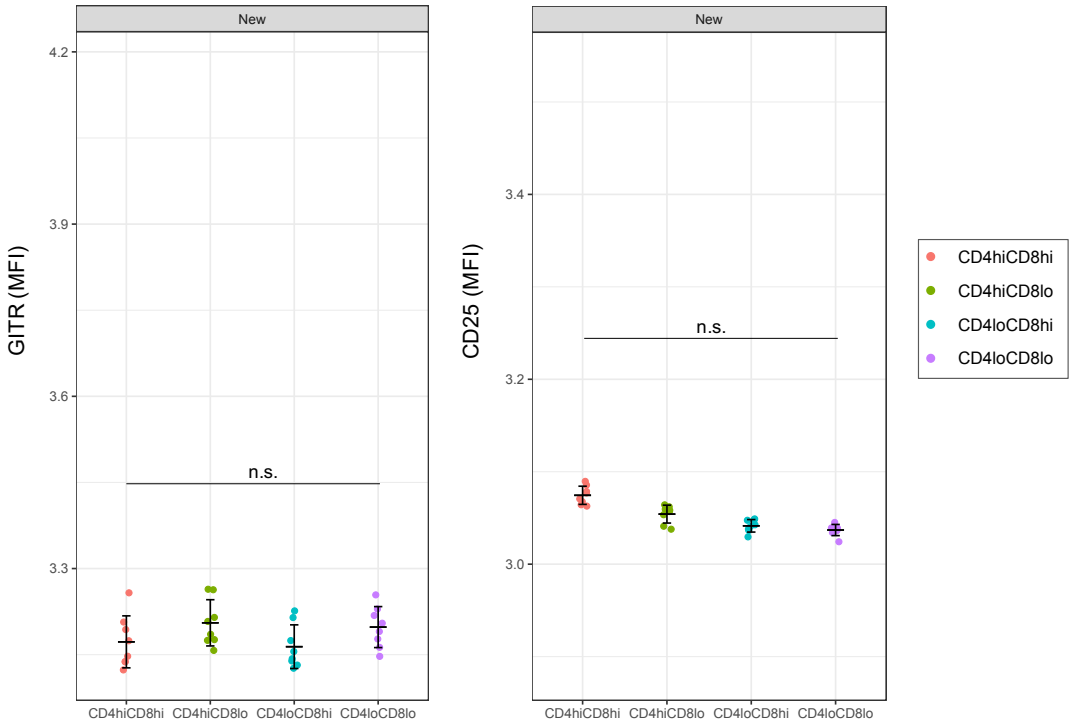

Figure 4.13: **GITR and CD25 expression by Blue^{+}Red^{-}CD69^{+}DP populations**. Thymocytes from 4 weeks old *Nr4a3*-Tocky mice were analysed on a Cytek Aurora spectral analyser in two independent experiments and data were combined. The experiments were performed two days apart and the instrument settings were not changed. MFI of the surface markers GITR and CD25 are shown for four CD69^{+}DP populations present in the New Timer locus and defined according to CD4 and CD8 co-receptor expression: CD4^{hi}CD8^{hi}, CD4^{hi}CD8^{lo}, CD4^{lo}CD8^{hi} and CD4^{lo}CD8^{lo}. No statistically significant differences from ANOVA analysis were observed. Error bars are representative of mean ± s.d, where n = 8 biological replicates.

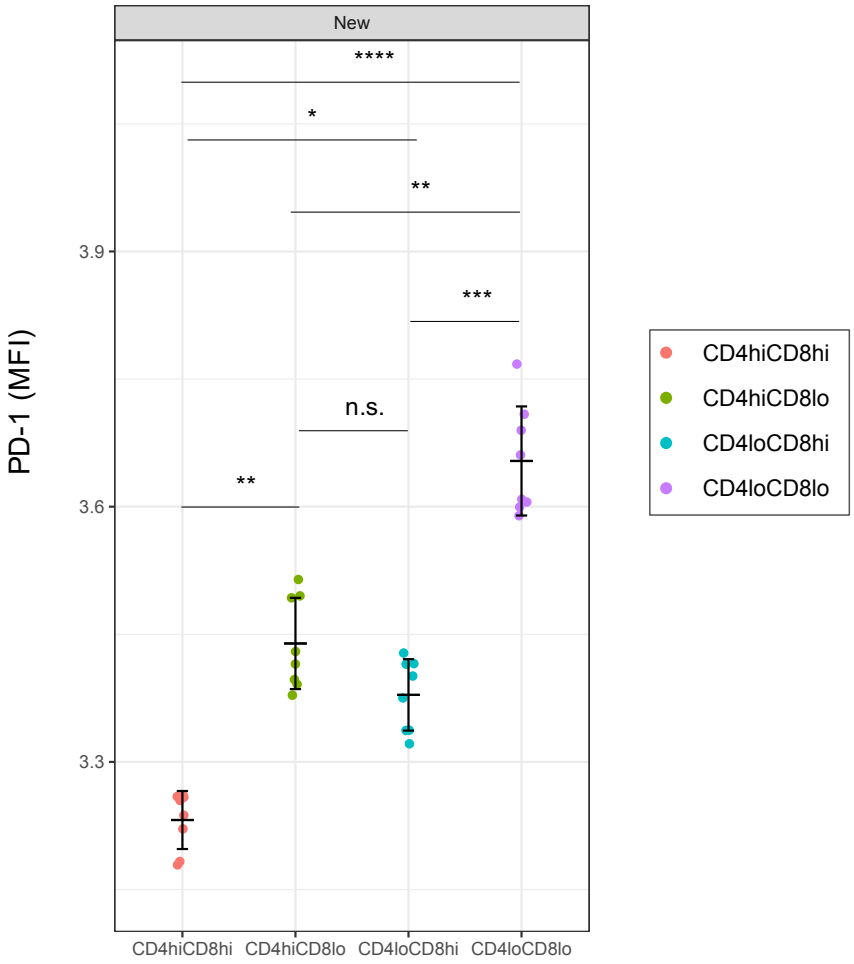

Figure 4.14: **PD-1 expression by Blue^{+}Red^{-}CD69^{+}DP populations**. Thymocytes from 4 weeks old *Nr4a3*-Tocky mice were analysed on a Cytek Aurora spectral analyser in two independent experiments and data were combined. The experiments were performed two days apart and the instrument settings were not changed. MFI of the surface marker PD-1 is shown for four CD69^{+}DP populations present in the New Timer locus and defined according to CD4 and CD8 co-receptor expression: CD4^{hi}CD8^{hi}, CD4^{hi}CD8^{lo}, CD4^{lo}CD8^{hi} and CD4^{lo}CD8^{lo}. Statistically significant differences from Tukey's post-hoc analysis are shown as * for p<0.05, ** for p<0.01, *** for p<0.001 and **** for p<0.0001. Error bars are representative of mean ± s.d, where n = 8 biological replicates.

4.2.5 DP cells that escape Bim-mediated deletion have B^+R^+ and B^-R^+ phenotypes

Nr4a3-Tocky mice that lack one or both Bim alleles were used to further investigate DP cell development. The *Bim*$^{KO/KO}$ phenotype accumulates DP cells that would have normally been deleted in Bim-sufficient mice, allowing for the study of self-reactive cells. In this chapter, cells derived from *Nr4a3*-Tocky:Bim$^{KO/KO}$ mice are referred to as Bim$^{KO/KO}$ or simply "KO", while cells from *Nr4a3*-Tocky:Bim$^{WT/KO}$ mice, here used as control, are referred to as Bim$^{WT/KO}$ or "Het".

Upon flow cytometry analysis, while Bim$^{WT/KO}$ DP cells resembled the *Nr4a3*-Timer patterns previously observed in WT *Nr4a3*-Tocky mice (Fig.4.1), CD69$^+$ DPs from Bim$^{KO/KO}$ mice distributed in each Timer locus (Fig.4.15). This suggests that in Bim-sufficient mice, DP cells are deleted before acquiring a potentially pathogenic Blue$^+$Red$^+$ phenotype.

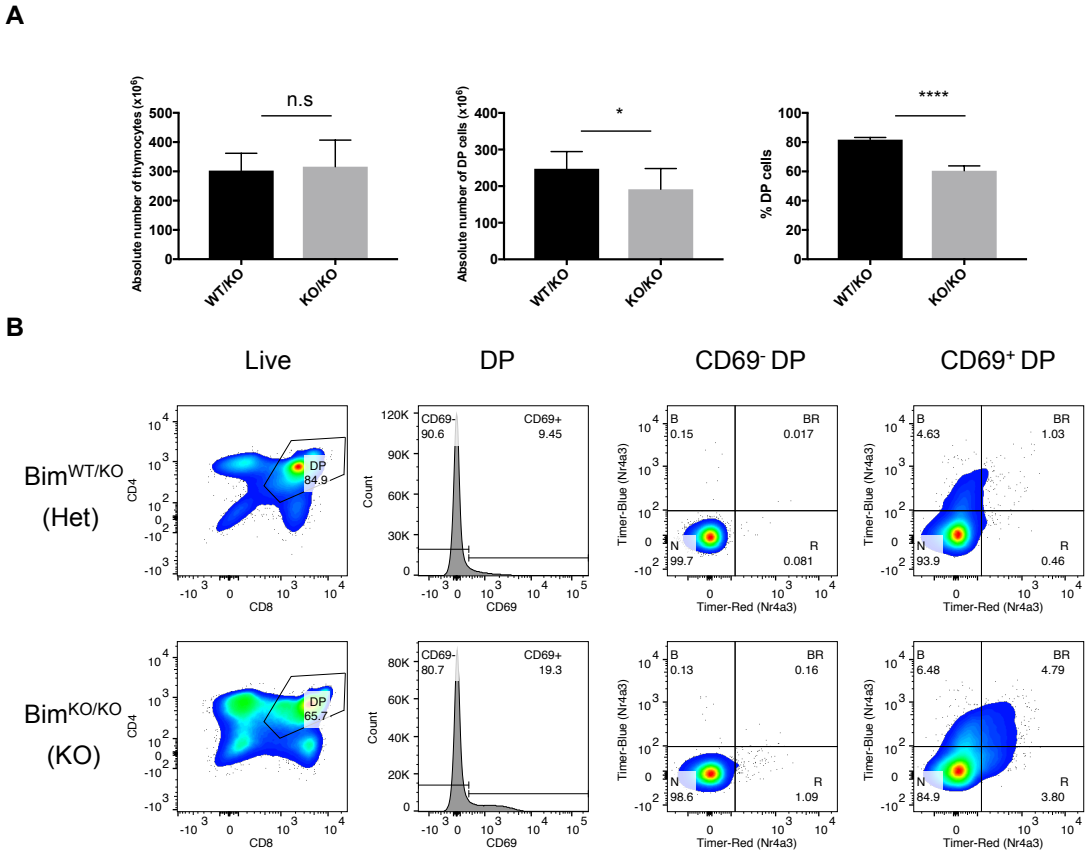

Figure 4.15: ***Nr4a3*-Timer expression in Bim-deficient DP cells.** Thymocytes were harvested from 5 weeks old *Nr4a3*-Tocky:Bim$^{WT/KO}$ or *Nr4a3*-Tocky:Bim$^{KO/KO}$ mice and were analysed by flow cytometry on a Fortessa III instrument. For simplicity, *Nr4a3*-Tocky:Bim$^{WT/KO}$ genotype is referred to as Bim$^{WT/KO}$ or Het, while *Nr4a3*-Tocky:Bim$^{KO/KO}$ is referred to as Bim$^{KO/KO}$ or KO. (A) Absolute cell numbers of thymocytes and DP cells are shown for each genotype, followed by the absolute percentage of DP cells in the thymus. Data are a summary of four independent experiments, where 2-4 mice per group were used. Error bars are representative of mean ± s.d, where n = 12 total biological replicates. Statistically significant differences from unpaired Student's t-test are shown as * for $p<0.05$ (performed on absolute count data) and from Mann-Whitney U test as **** for $p<0.0001$ (performed on percentage data). (B) Flow cytometry plots and histogram show gating strategy for CD69^{-} and CD69^{+} DP populations and *Nr4a3*-Timer expression in CD69^{-} and CD69^{+} DP populations is shown for each genotype. Data shown are typical of at least 4 independent experiments that used 2-4 mice per group.

4.2.6 B^+R^+DPs are enriched with PD-1 and *Foxp3*

Next, CD69$^+$DP populations were sorted for RNAseq analysis from both $Bim^{WT/KO}$ and $Bim^{KO/KO}$ mice based on Timer protein fluorescence as shown in Table 4.1, using the gating strategy in Fig.4.15. In the $Bim^{KO/KO}$ model, only the third exon of the gene encoding the BH3 domain is deleted. While the resulting protein is truncated and not functional, transcription of its gene, *Bcl2l11*, occurs normally (Bouillet et al., 1999).

Genotype	Timer Protein Expression	Assigned Name
$Bim^{WT/KO}$	$Blue^-Red^-$	Het_N
$Bim^{KO/KO}$	$Blue^-Red^-$	KO_N
$Bim^{WT/KO}$	$Blue^+Red^-$	Het_B
$Bim^{KO/KO}$	$Blue^+Red^-$	KO_B
$Bim^{KO/KO}$	$Blue^+Red^+$	KO_BR

Table 4.1: CD69$^+$ DP cells sorted for RNAseq analysis from 6-7 weeks old $Bim^{WT/KO}$ and $Bim^{KO/KO}$ mice as described in the methods, according to *Nr4a3*-Timer expression. 2000 cells were sorted for each population and subjected to RNAseq.

PCA of RNAseq data showed that Timer$^-$ samples have the most different transcriptomes compared to the other populations, as captured by the PC1 axis (Fig.4.16.). The PC2 axis mostly separated the two genotypes and captured the features of KO_BR cells, which clustered away from the rest.

Bcl2l11 transcription was significantly higher in KO populations compared to the control, regardless of Timer protein expression (Fig.4.17A). This suggests that a certain amount of Bim protein is always required by developing T cells and, in its absence, transcript becomes accumulated. *Bcl2l11* transcription became downregulated as KO_B cells matured to KO_BR (Fig.4.17B). *Pdcd1*, on the other hand, was significantly upregulated (Fig.4.18B). At protein level, once KO_BR cells no longer received TCR signals and aquired a $Blue^-Red^+$ phenotype as KO_R, PD-1 became downregulated (Fig.4.18C). This suggests that if DP cells which receive strong TCR signals are not immediately deleted

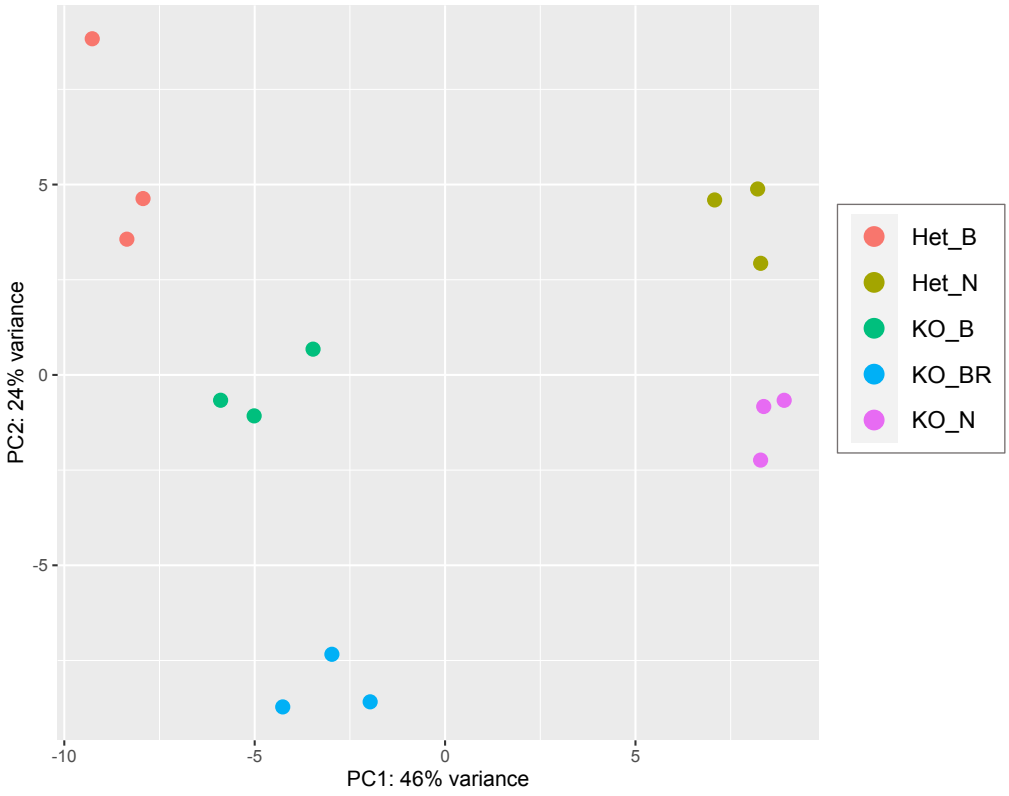

Figure 4.16: **PCA of the transcriptomes of populations sorted. CD69^{+} DP cells were sorted for RNAseq analysis from 6-7 weeks old Bim$^{WT/KO}$ and Bim$^{KO/KO}$ mice according to *Nr4a3*-Timer expression as described in Table 4.1. 2000 cells were sorted for each population and subjected to RNAseq. Normalised counts of expressed genes were obtained using the algorithm DESeq2 and a PCA plot of their transcriptomes is shown.**

by Bim, PD-1 is induced and, consequently, *Bcl2l11* transcription is repressed. Once the cell no longer receives TCR signals that could trigger apoptotic mechanisms, PD-1 becomes downregulated.

In WT *Nr4a3*-Tocky mice, DP_N cells expressed significantly higher levels of *Ccr7* than DP_B (Fig.4.8). This observation led to the hypothesis that DP_B are either immediately deleted or quickly progress to the next stage of development, accumulating overall lower levels of *Ccr7*. Het_N and Het_B cells had similar *Ccr7* levels to KO_N and KO_B, respectively (Fig.4.19A). KO_BR expressed significantly higher transcript levels than KO_B, very similar to KO_N (Fig.4.19). This supports the hypothesis that the difference in *Ccr7*

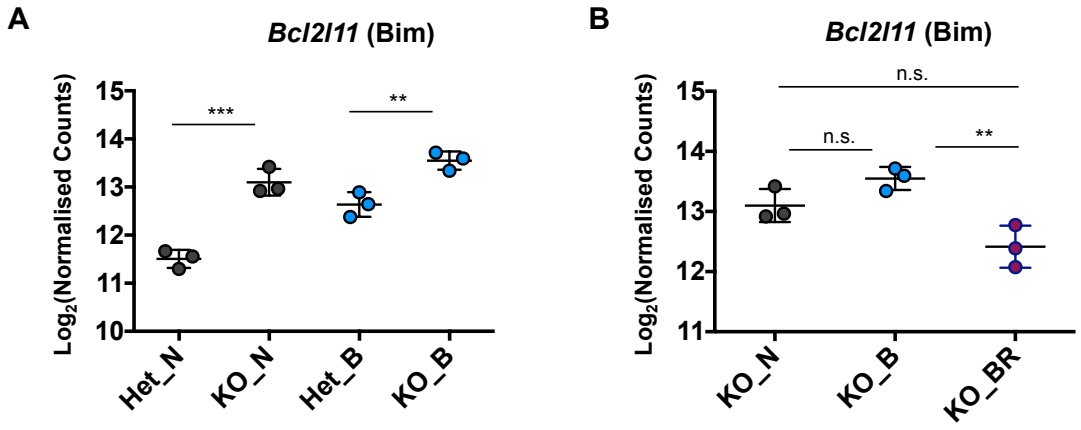

Figure 4.17: **Summary data of *Bcl211* transcription by Bim-sufficient and Bim-deficient cell populations.** CD69$^+$ DP cells were sorted for RNAseq analysis from 6-7 weeks old Bim$^{WT/KO}$ and Bim$^{KO/KO}$ mice according to *Nr4a3*-Timer expression as described in Table 4.1. 2000 cells were sorted for each population and subjected to RNAseq. Normalised counts of the gene *Bcl2l11* coding for the pro-apoptotic molecule Bim were obtained using the algorithm DESeq2. Data are shown as $\log_2$ of normalised counts. Error bars are representative of mean $\pm$ s.d, where n = 3 biological replicates. Statistically significant differences from Tukey's post-hoc analysis are shown as ** for $p<0.01$.

transcript levels between DP_N and DP_B cells is due to the latter population either undergoing apoptosis or progressing to the next stage.

Bim-deficient mice were previously shown to be enriched with *Foxp3*$^+$CD4 SP cells (Zhan et. al, 2011) and it was proposed that their precursors at the DP stage have a GITR^{hi}CD25$^+$CD69$^+$DP phenotype (Krishnamurthy et. al, 2015). Here, there was no detectable genotype effect on transcription of *Tnfrsfr18* (Fig.4.20A) and *Il2ra* (Fig.4.21A), the genes encoding GITR and CD25, respectively. There were also no significant differences in either *Tnfrsfr18* or *Il2ra* levels between KO_B and KO_BR (Fig.4.20B and 4.21B). Both GITR and CD25 protein expression became downregulated as KO_BR matured to KO_R, although this difference was not significant in the case of CD25 (Fig.4.20C and 4.21C). *Foxp3* transcription, on the other hand, while similar between genotypes (Fig.4.22A), was significantly upregulated in KO_BR cells (Fig.4.22B) and its expression was maintained in KO_R cells as well (Fig.4.22C). Collectively, these findings suggest

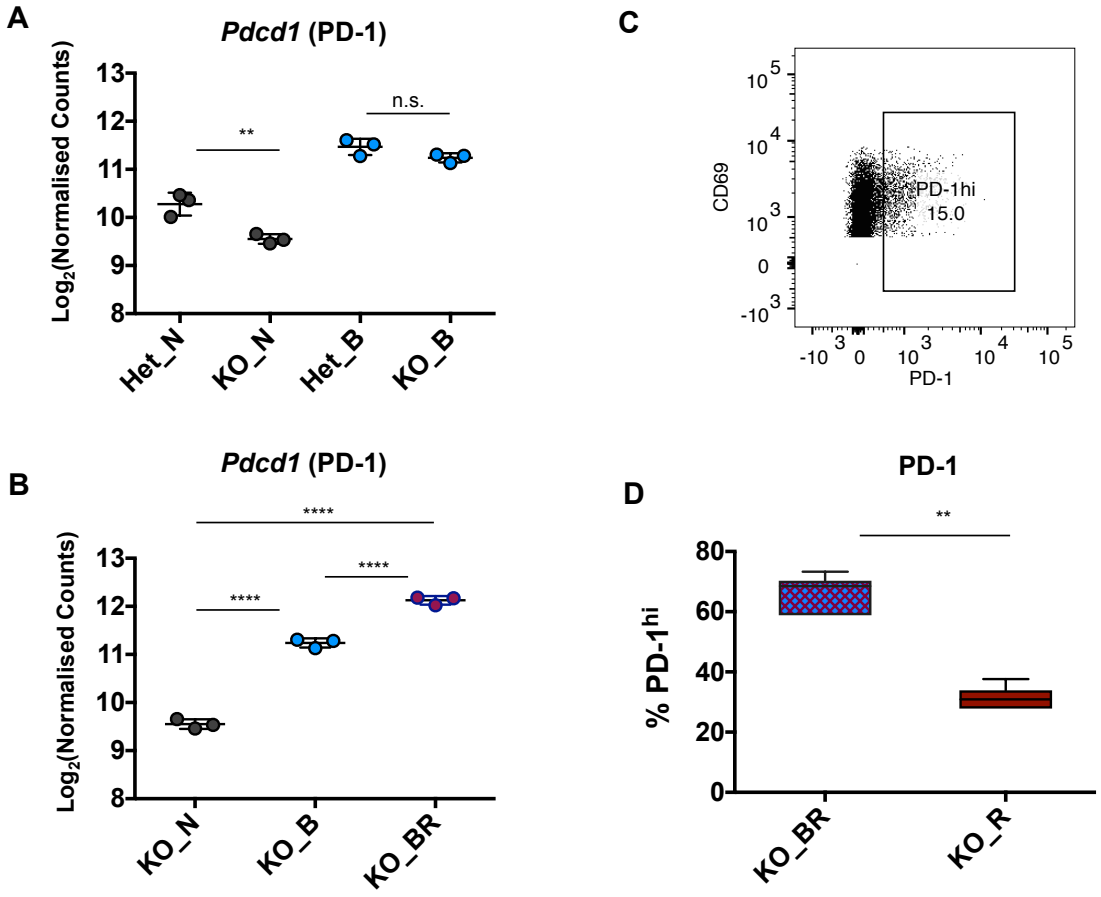

Figure 4.18: **Summary data of PD-1 expression by Bim-sufficient and Bim-deficient cell populations**.

(A);(B) CD69$^+$ DP cells were sorted for RNAseq analysis from 6-7 weeks old Bim$^{WT/KO}$ and Bim$^{KO/KO}$ mice according to *Nr4a3*-Timer expression as described in Table 4.1. 2000 cells were sorted for each population and subjected to RNAseq. Log_2 of normalised counts of the gene transcript *Pdcd1* coding for PD-1 are shown for several populations, where n = 3 biological replicates.

(C);(D) Blue$^+$Red$^+$CD69$^+$DP (KO_BR) and Blue$^-$Red$^+$CD69$^+$DP (KO_R) cells from 6 weeks old Bim$^{KO/KO}$ mice were analysed by flow cytometry on a Fortessa III instrument and the proportions of cells expressing high PD-1 MFI values are compared between the two populations, where n = 4 biological replicates. Data shown are typical of at least 3 independent experiments that used 2-4 mice per group.

In all plots, error bars are representative of mean ± s.d. Statistically significant differences by Tukey's post-hoc analysis **(A);(B)** and Mann-Whitney U test **(D)** are shown as * for p<0.05, ** for p<0.01, *** for p<0.001 and **** for p<0.0001.

.

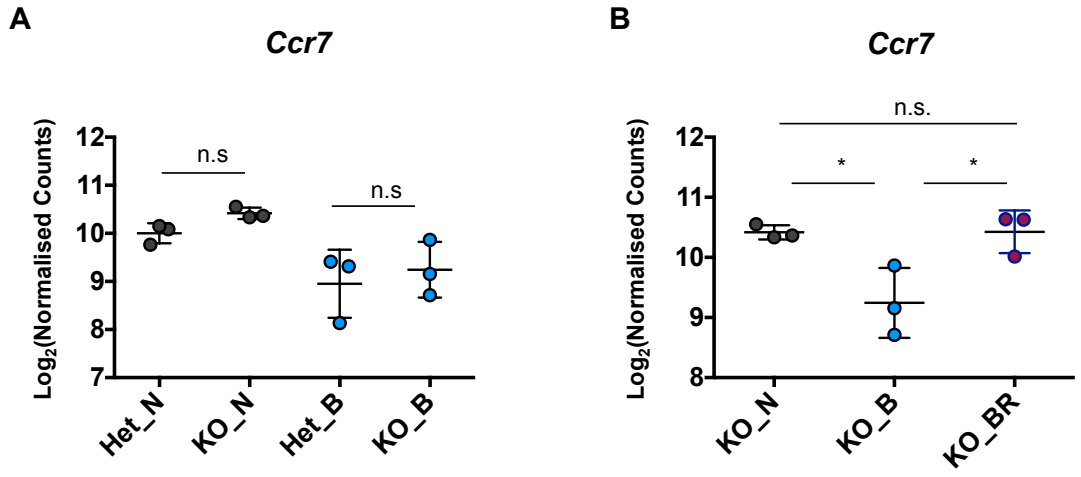

Figure 4.19: **Summary data of *Ccr7* transcription by Bim-sufficient and Bim-deficient cell populations.** CD69$^+$ DP cells were sorted for RNAseq analysis from 6-7 weeks old Bim$^{WT/KO}$ and Bim$^{KO/KO}$ mice according to *Nr4a3*-Timer expression as described in Table 4.1. 2000 cells were sorted for each population and subjected to RNAseq. Normalised counts of the gene *Ccr7* coding for the chemokine CCR7 were obtained using the algorithm DESeq2. Data are shown as $\log_2$ of normalised counts. Error bars are representative of mean $\pm$ s.d, where n = 3 biological replicates. Statistically significant differences from Tukey's post-hoc analysis are shown as * for $p<0.05$.

that Bim-deficient mice accumulate a *Foxp3*$^+$DP population following strong TCR signals and this phenotype is maintained once signals are no longer received. The data does not support a particular relationship between GITR and CD25 expression and the accumulation of *Foxp3*$^+$ cells in Bim-deficient mice, but rather suggests that they are both induced upon cognate antigen recognition and their expression is maintained for as long as TCR signals are sustained.

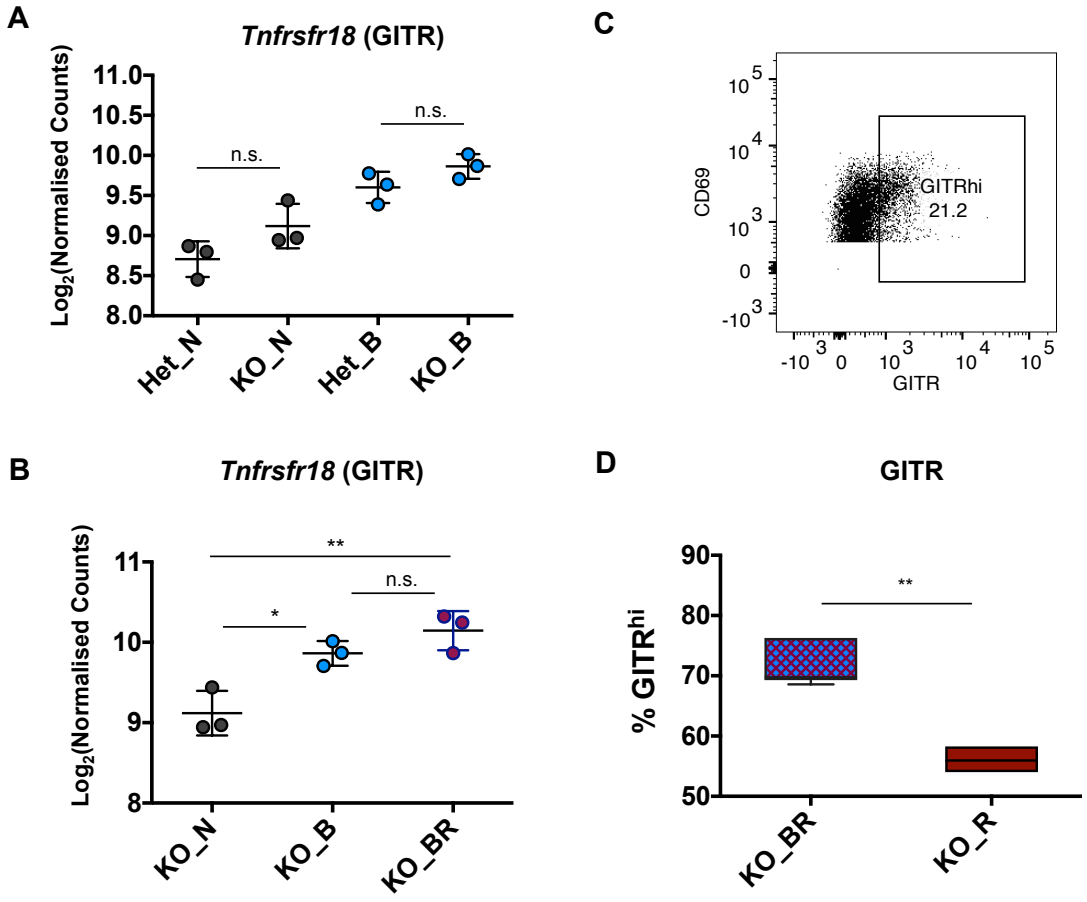

Figure 4.20: **Summary data of GITR expression by Bim-sufficient and Bim-deficient cell populations**.

(A);(B) CD69^{+} DP cells were sorted for RNAseq analysis from 6-7 weeks old Bim$^{WT/KO}$ and Bim$^{KO/KO}$ mice according to *Nr4a3*-Timer expression as described in Table 4.1. 2000 cells were sorted for each population and subjected to RNAseq. Log_2 of normalised counts of the gene transcript *Tnfrsfr18* coding for GITR are shown for several populations, where n = 3 biological replicates.

(C);(D) Blue^{+}Red^{+}CD69^{+}DP (KO_BR) and Blue^{-}Red^{+}CD69^{+}DP (KO_R) cells from 6 weeks old Bim$^{KO/KO}$ mice were analysed by flow cytometry on a Fortessa III instrument and the proportions of cells expressing high GITR MFI values are compared between the two populations, where n = 4 biological replicates. Data shown are typical of at least 3 independent experiments that used 2-4 mice per group.

In all plots, error bars are representative of mean ± s.d. Statistically significant differences by Tukey's post-hoc analysis **(A);(B)** and Mann-Whitney U test **(D)** are shown as * for $p<0.05$, ** for $p<0.01$, *** for $p<0.001$ and **** for $p<0.0001$.

.

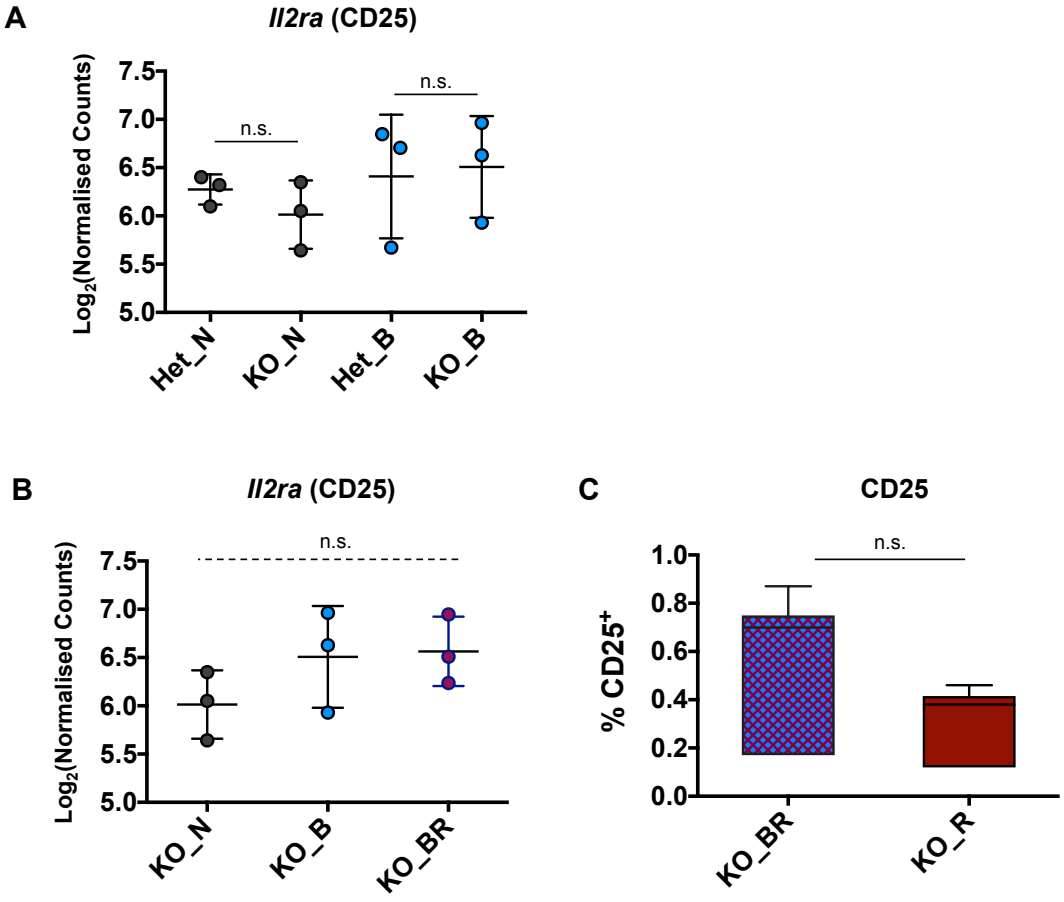

Figure 4.21: **Summary data of CD25 expression by Bim-sufficient and Bim-deficient cell populations**.

(A);(B) CD69$^+$ DP cells were sorted for RNAseq analysis from 6-7 weeks old Bim$^{WT/KO}$ and Bim$^{KO/KO}$ mice according to *Nr4a3*-Timer expression as described in Table 4.1. 2000 cells were sorted for each population and subjected to RNAseq. Log_2 of normalised counts of the gene transcript *Il2ra* coding for CD25 are shown for several populations, where n = 3 biological replicates.

(C) Blue$^+$Red$^+$CD69$^+$DP (KO_BR) and Blue$^-$Red$^+$CD69$^+$DP (KO_R) cells from 6 weeks old Bim$^{KO/KO}$ mice were analysed by flow cytometry on a Fortessa III instrument and the proportions of CD25$^+$ cells are compared between the two populations, where n = 4 biological replicates. Data shown are typical of at least 3 independent experiments that used 2-4 mice per group.

In all plots, error bars are representative of mean ± s.d. Statistically significant differences by Tukey's post-hoc analysis **(A);(B)** and Mann-Whitney U test **(C)** are shown as * for $p<0.05$, ** for $p<0.01$, *** for $p<0.001$ and **** for $p<0.0001$.

.

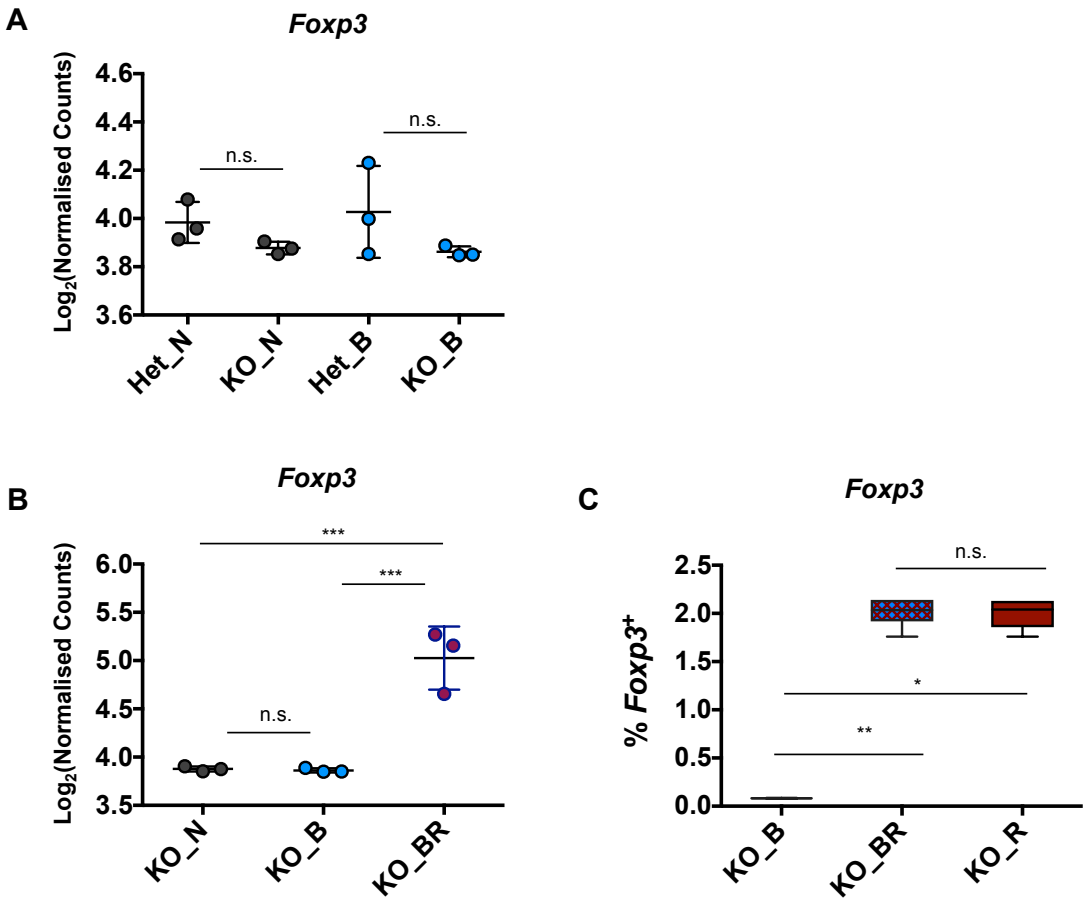

Figure 4.22: **Summary data of *Foxp3* expression by Bim-sufficient and Bim-deficient cell populations**.

(A);(B) CD69$^+$ DP cells were sorted for RNAseq analysis from 6-7 weeks old Bim$^{WT/KO}$ and Bim$^{KO/KO}$ mice according to *Nr4a3*-Timer expression as described in Table 4.1. 2000 cells were sorted for each population and subjected to RNAseq. Log_2 of normalised counts of the gene transcript *Foxp3* are shown for several populations, where n = 3 biological replicates.

(C) Blue$^+$Red$^+$CD69$^+$DP (KO_BR) and Blue$^-$Red$^+$CD69$^+$DP (KO_R) cells from 6 weeks old Bim$^{KO/KO}$ mice were analysed by flow cytometry on a Fortessa III instrument and the proportions of *Foxp3*-GFP$^+$ cells are compared between the two populations, where n = 4 biological replicates. Data shown are typical of at least 4 independent experiments that used 2-4 mice per group.

In all plots, error bars are representative of mean ± s.d. Statistically significant differences by Tukey's post-hoc analysis **(A);(B)** and Kruskal-Wallis test **(C)** are shown as * for $p<0.05$, ** for $p<0.01$, *** for $p<0.001$ and **** for $p<0.0001$. All mice used were *Foxp3*-GFP

4.2.7 Bim deficiency has an impact on CD4/CD8 selection

As DP cells start transcribing *Nr4a3*, the lineage markers CD4 and CD8 become down-regulated, as shown earlier in this chapter (Fig.4.2). KO_B cells had higher *Cd4* levels than Het_B (Fig.4.23A). *Cd8a* transcription, however, was similar between genotypes (Fig.4.24A). This raises the possibility that in the absence of Bim, more cells can recognise MHC-II molecules. KO_BR cells showed similar *Cd4* and *Cd8a* expression (Fig.4.23B and 4.24B). In KO_R cells, surface expression of both lineage markers was significantly higher that that of KO_BR. This suggests that CD4 and CD8 become re-upregulated in Bim-deficient DPs that no longer receive persistent TCR signals.

To further investigate the possible impact of Bim deficiency on CD4/CD8 selection, the four populations that had been previously defined according to lineage marker expression ($CD4^{hi}CD8^{hi}$, $CD4^{hi}CD8^{lo}$, $CD4^{lo}CD8^{hi}$ and $CD4^{lo}CD8^{lo}$) were analysed in $Bim^{KO/KO}$ mice.

Fig.4.25A shows the frequency of the four defined $CD69^{+}$DP populations in the $Bim^{WT/KO}$ model, which does not have many cells beyond the New locus (Fig.4.15). Their distribution in the New locus was very similar to that observed in WT *Nr4a3*-Tocky mice (Fig.4.10), where $CD4^{lo}CD8^{lo}$ was the dominant population in $Timer^{+}$ cells and no significant differences were found between the percentages of $B^{+}R^{-}$ $CD4^{hi}CD8^{lo}$ and $CD4^{lo}CD8^{hi}$ cells. A very similar population distribution in the New locus was observed in $Bim^{KO/KO}$ mice (Fig.4.25B). Since in this model DP cells can express both Blue and Red fluorescence (Fig.4.15), the fate of these four $CD69^{+}$DP populations can be further investigated.

In $Bim^{KO/KO}$ mice, proportional distribution of the four populations was mostly maintained in each Timer locus (Fig.4.25B). There was a consistent increase in $CD4^{hi}CD8^{lo}$ proportions compared to $CD4^{lo}CD8^{hi}$ as Timer protein matured, until they were signifi-

cantly higher in the Arrested locus. This is consistent with the increase in *Cd4* transcription observed in $Bim^{KO/KO}$ mice (Fig.4.23B). Both in the Persistent and the Arrested loci, the dominant population was $CD4^{lo}CD8^{lo}$, suggesting that most cells which become deleted in a Bim-mediated manner express this phenotype.

Nr4a3-Tocky data revealed that $CD4^{lo}CD8^{lo}$ cells express significantly higher levels of PD-1 than other populations in the New locus (Fig.4.14). Bim-deficient $CD4^{lo}CD8^{lo}$ cells further upregulated PD-1 as *Nr4a3* transcription was sustained, with levels peaking in the PAt locus and becoming decreased in cells that had terminated transcription (Fig.4.26). While a slight increase in PD-1 was also observed in the other three populations from the New to the Persistent locus, PD-1 was particularly high in $CD4^{lo}CD8^{lo}$ cells.

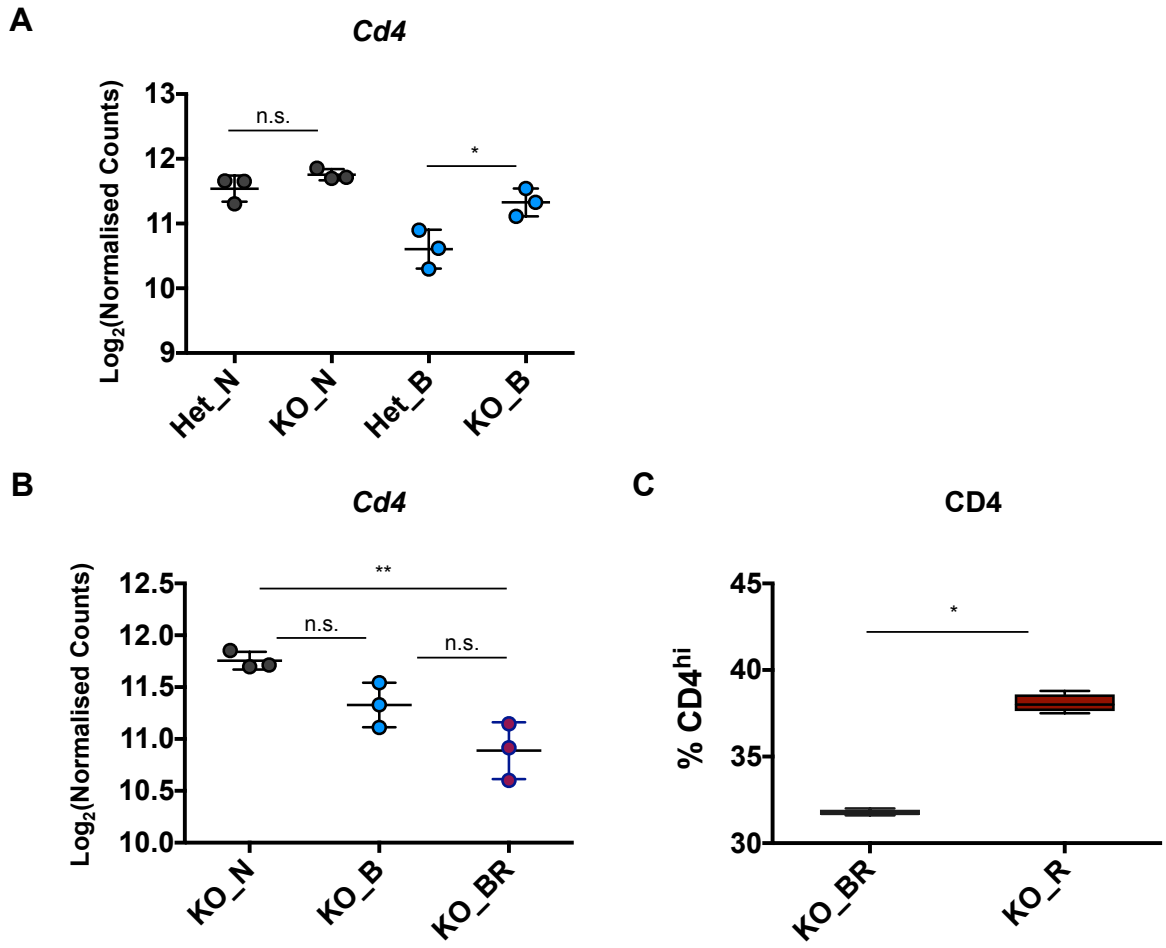

Figure 4.23: **Summary data of CD4 expression by Bim-sufficient and Bim-deficient cell populations**.

(A);(B) CD69$^+$ DP cells were sorted for RNAseq analysis from 6-7 weeks old Bim$^{WT/KO}$ and Bim$^{KO/KO}$ mice according to *Nr4a3*-Timer expression as described in Table 4.1. 2000 cells were sorted for each population and subjected to RNAseq. Log_2 of normalised counts of the gene transcript *Cd4* coding for the co-receptor CD4 are shown for several populations, where n = 3 biological replicates.

(C) Blue$^+$Red$^+$CD69$^+$DP (KO_BR) and Blue$^-$Red$^+$CD69$^+$DP (KO_R) cells from 6 weeks old Bim$^{KO/KO}$ mice were analysed by flow cytometry on a Fortessa III instrument and the proportions of cells expressing high CD4 MFI values are compared between the two populations, where n = 4 biological replicates. Data shown are typical of at least 4 independent experiments that used 2-4 mice per group.

In all plots, error bars are representative of mean ± s.d. Statistically significant differences by Tukey's post-hoc analysis **(A);(B)** and Mann-Whitney U test **(C)** are shown as * for $p<0.05$, ** for $p<0.01$, *** for $p<0.001$ and **** for $p<0.0001$.

.

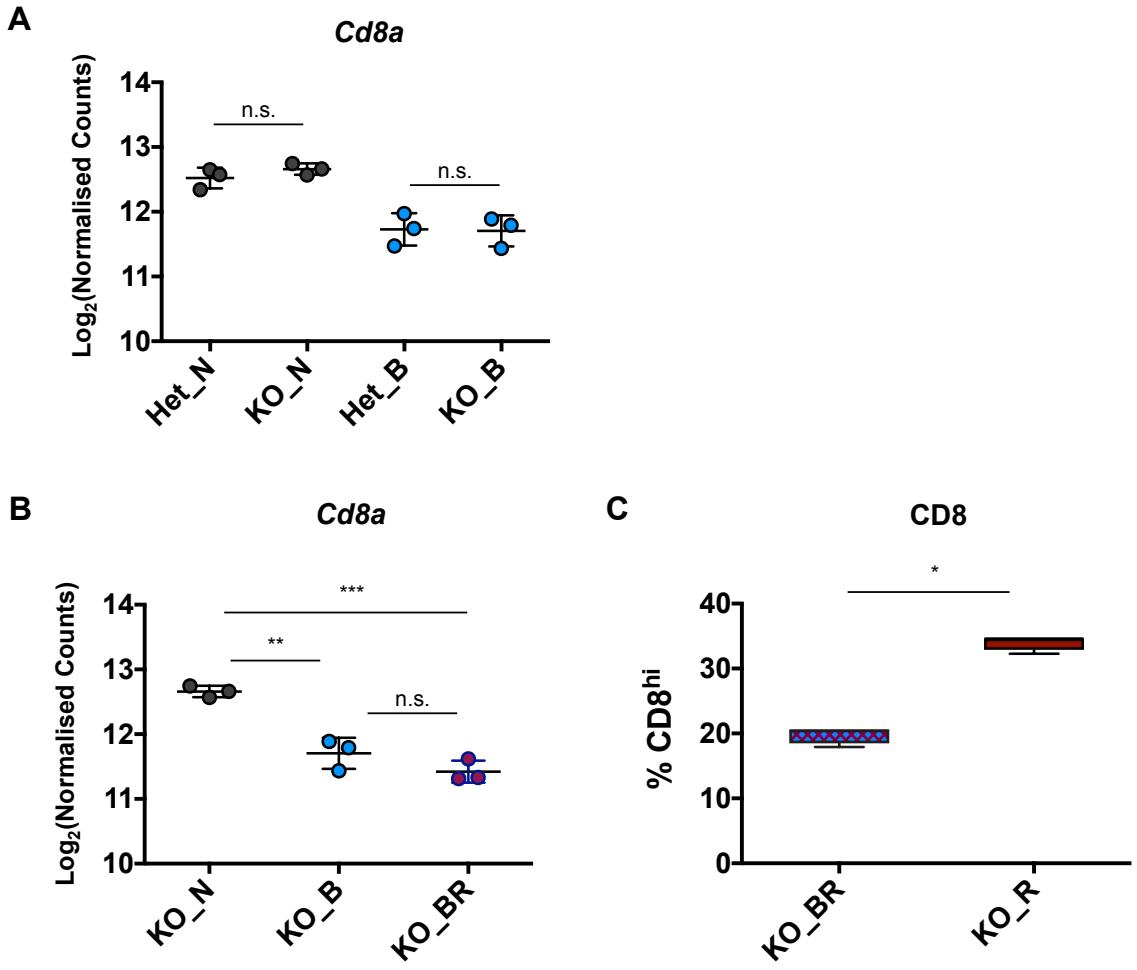

Figure 4.24: **Summary data of CD8 expression by Bim-sufficient and Bim-deficient cell populations**.

(A);(B) CD69$^+$ DP cells were sorted for RNAseq analysis from 6-7 weeks old Bim$^{WT/KO}$ and Bim$^{KO/KO}$ mice according to *Nr4a3*-Timer expression as described in Table 4.1. 2000 cells were sorted for each population and subjected to RNAseq. Log_2 of normalised counts of the gene transcript *CD8a* coding for the co-receptor CD8 are shown for several populations, where n = 3 biological replicates.

(C) Blue$^+$Red$^+$CD69$^+$DP (KO_BR) and Blue$^-$Red$^+$CD69$^+$DP (KO_R) cells from 6 weeks old Bim$^{KO/KO}$ mice were analysed by flow cytometry on a Fortessa III instrument and the proportions of cells expressing high CD8 MFI values are compared between the two populations, where n = 4 biological replicates. Data shown are typical of at least 4 independent experiments that used 2-4 mice per group.

In all plots, error bars are representative of mean ± s.d. Statistically significant differences by Tukey's post-hoc analysis **(A);(B)** and Mann-Whitney U test **(C)** are shown as * for p<0.05, ** for p<0.01, *** for p<0.001 and **** for p<0.0001.

.

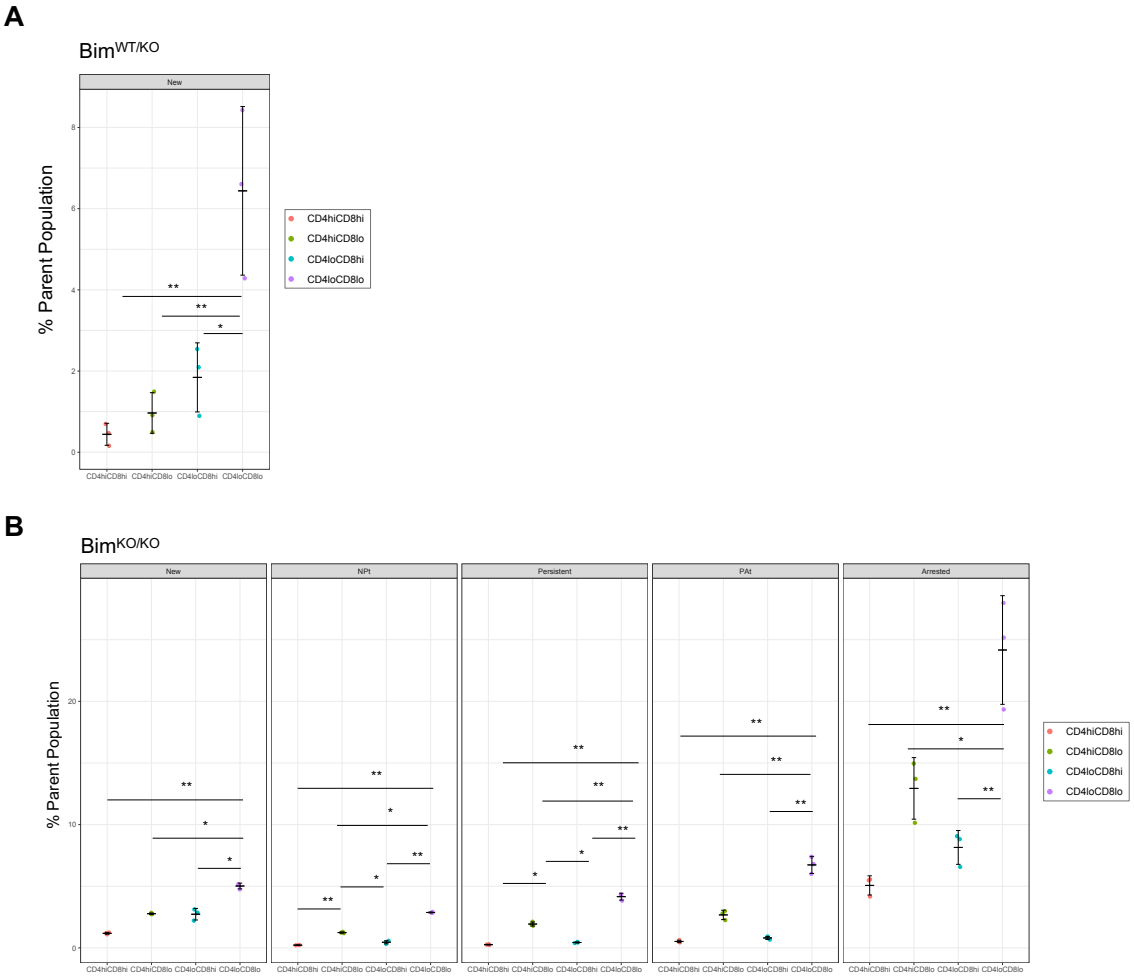

Figure 4.25: **Timer locus analysis of CD69$^+$DP populations in Bim-deficient mice**. CD69$^+$DP cells from 6 weeks old Bim$^{WT/KO}$ and Bim$^{KO/KO}$ mice were analysed by flow cytometry on a Fortessa III instrument. The percentage of cells in each Timer locus among their parent cell population is shown by scatter plots for four CD69$^+$DP populations defined according to CD4 and CD8 co-receptor expression: CD4^{hi}CD8^{hi}, CD4^{hi}CD8^{lo}, CD4^{lo}CD8^{hi} and CD4^{lo}CD8^{lo}. (A) Population frequencies in the New locus in Bim$^{WT/KO}$ mice. In this genotype, Timer$^+$ cells are too rare to analyse beyond the New locus. (B) Population frequencies in each Timer locus in Bim$^{KO/KO}$ mice. Statistically significant differences from Tukey's post-hoc analysis are shown as * for $p<0.05$, ** for $p<0.01$, *** for $p<0.001$ and **** for $p<0.0001$. Error bars are representative of mean $\pm$ s.d, where n = 3 biological replicates. Data shown are representative of at least 4 independent experiments that used 2-4 mice per group.

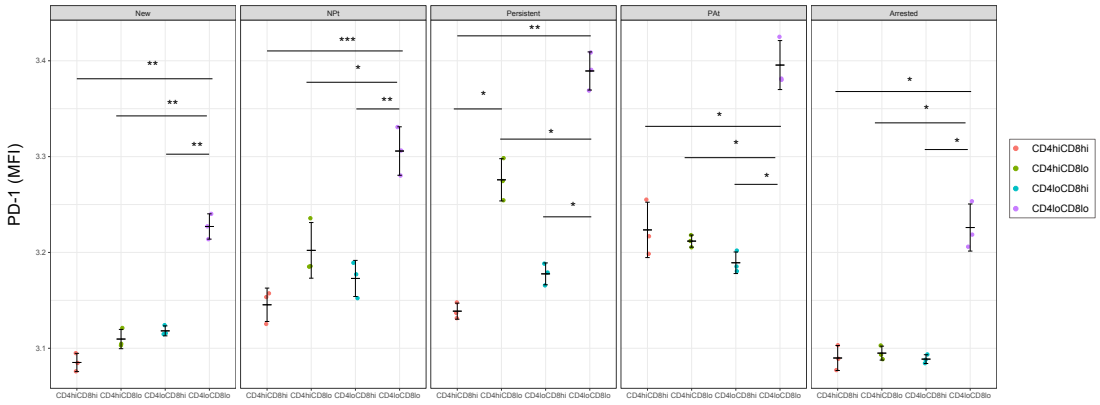

Figure 4.26: **PD-1 expression by Bim-deficient CD69^{+}DP populations in each Timer locus**. CD69^{+}DP cells from 6 weeks old Bim$^{KO/KO}$ mice were analysed by flow cytometry on a Fortessa III instrument. MFI of the surface marker PD-1 is shown for four CD69^{+}DP populations present in the New Timer locus and defined according to CD4 and CD8 co-receptor expression: CD4^{hi}CD8^{hi}, CD4^{hi}CD8^{lo}, CD4^{lo}CD8^{hi} and CD4^{lo}CD8^{lo}. Statistically significant differences from Tukey's post-hoc analysis are shown as * for $p<0.05$, ** for $p<0.01$, *** for $p<0.001$ and **** for $p<0.0001$. Error bars are representative of mean $\pm$ s.d, where n = 3 biological replicates. Data shown are representative of at least 3 independent experiments that used 2-4 mice per group.

4.2.8 Timer^{+}GITR^{hi}*Foxp3*$^{+}$CD4^{hi}CD8^{lo} DP cells develop in the absence of Bim

Bim$^{KO/KO}$ mice accumulated Blue^{+}Red^{+} and Blue^{-}Red^{+} DPs that expressed *Foxp3* (Fig.4.22). In order to identify whether these populations express a particular CD4/CD8 phenotype, *Foxp3*-GFP MFI was compared between the four DP populations (Fig.4.27). Although CD4^{lo}CD8^{lo} cells were the most abundant population accumulated in the absence of Bim (Fig.4.25), *Foxp3*-GFP expression was predominantly upregulated by the CD4^{hi}CD8^{lo} intermediate and was absent in CD4^{lo}CD8^{lo} cells (Fig.4.27). Timer intensity data showed that there were no significant differences between CD4^{hi}CD8^{lo} and CD4^{lo}CD8^{hi} cells in Bim$^{WT/KO}$ mice. In Bim$^{KO/KO}$, however, CD4^{hi}CD8^{lo} showed a significantly higher mean Timer intensity value than CD4^{lo}CD8^{hi}. These findings suggest that in the absence of Bim, a *Foxp3*$^{+}$CD4^{lo}CD8^{hi} population accumulates in response to high intensity TCR signalling.

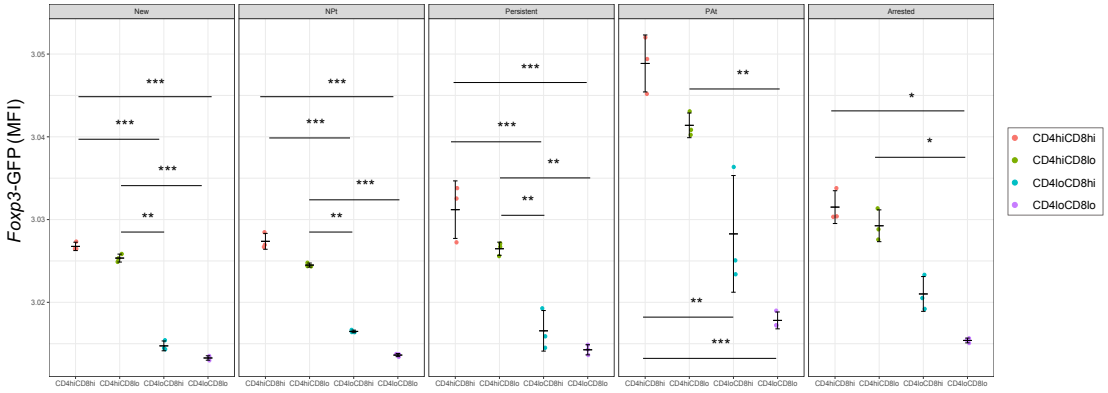

Figure 4.27: ***Foxp3* expression by Bim-deficient CD69^{+}DP populations in each Timer locus**. CD69^{+}DP cells from 6 weeks old Bim$^{KO/KO}$ mice were analysed by flow cytometry on a Fortessa III instrument. MFI of *Foxp3*-GFP is shown for four CD69^{+}DP populations present in the New Timer locus and defined according to CD4 and CD8 co-receptor expression: CD4^{hi}CD8^{hi}, CD4^{hi}CD8^{lo}, CD4^{lo}CD8^{hi} and CD4^{lo}CD8^{lo}. Statistically significant differences from Tukey's post-hoc analysis are shown as * for $p<0.05$, ** for $p<0.01$, *** for $p<0.001$ and **** for $p<0.0001$. Error bars are representative of mean $\pm$ s.d, where n = 3 biological replicates. Data shown are representative of at least 4 independent experiments that used 2-4 mice per group. All mice used were *Foxp3*-GFP.

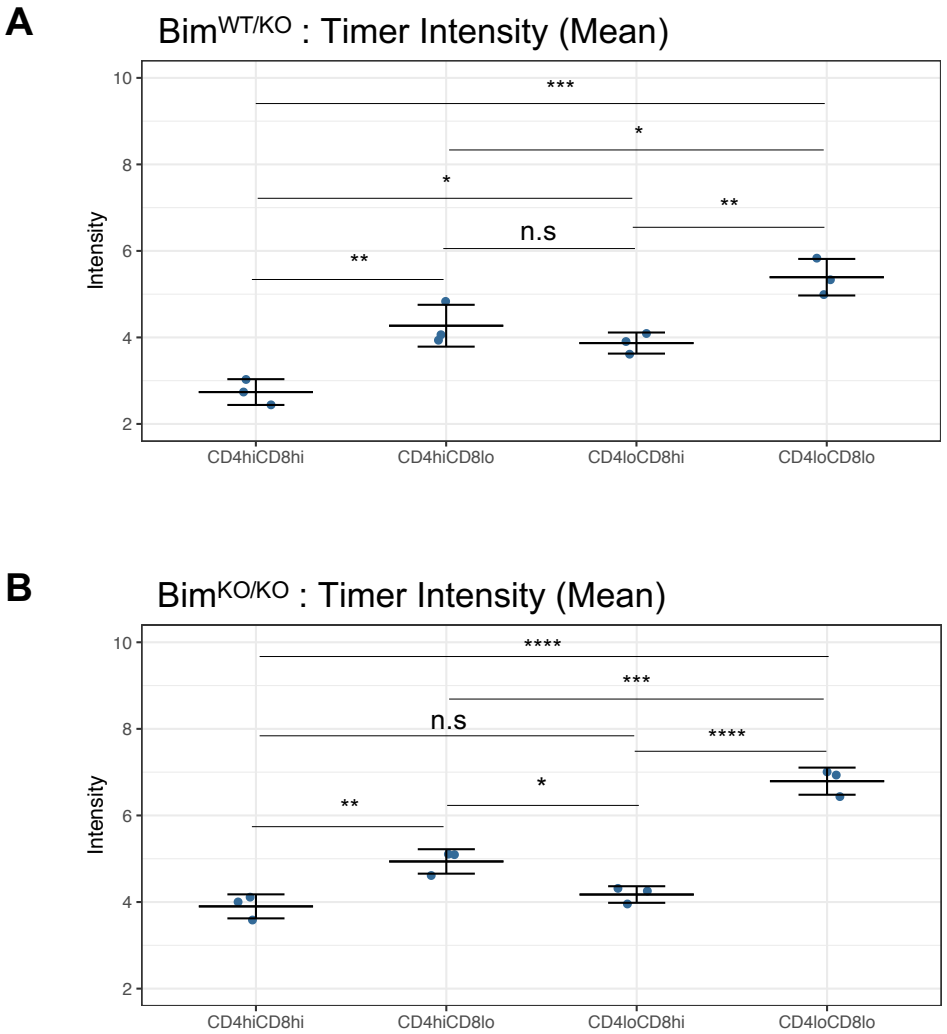

Figure 4.28: **Mean Timer intensity of four Bim-deficient CD69^{+}DP populations**. Thymocytes from 6 weeks old Bim$^{WT/KO}$ **(A)** or Bim$^{KO/KO}$ **(B)** mice were analysed by flow cytometry on a Fortessa III instrument. Mean *Nr4a3*-Timer intensity is shown for four CD69^{+}DP populations defined according to CD4 and CD8 co-receptor expression: CD4^{hi}CD8^{hi}, CD4^{hi}CD8^{lo}, CD4^{lo}CD8^{hi} and CD4^{lo}CD8^{lo}. Statistically significant differences from Tukey's post-hoc analysis are shown as * for $p<0.05$, ** for $p<0.01$, *** for $p<0.001$ and **** for $p<0.0001$. Error bars are representative of mean $\pm$ s.d, where $n = 3$ biological replicates. Data shown are representative of at least 4 independent experiments that used 2-4 mice per group.

All four DP populations upregulated GITR as Timer protein matured, with levels peaking in the PAt locus (Fig.4.29). The levels decreased in the Arrested locus, consistent with the earlier observation that GITR upregulation is sustained by ongoing *Nr4a3* transcription and protein levels decrease when TCR signals are no longer received (Fig.4.20).

Across the Timer loci, $CD4^{hi}CD8^{lo}$ were consistently more enriched with GITR than the other intermediates. CD25 expression was mainly found in $CD4^{hi}CD8^{hi}$ and $CD4^{lo}CD8^{hi}$ cells (Fig.4.30). Collectively, these findings suggest that the most likely precursors of accumulated Treg previously observed in Bim-deficient mice (Zhan et al., 2011) have a $GITR^{hi}$ *Foxp3*$^{+}CD4^{hi}CD8^{lo}$ phenotype.

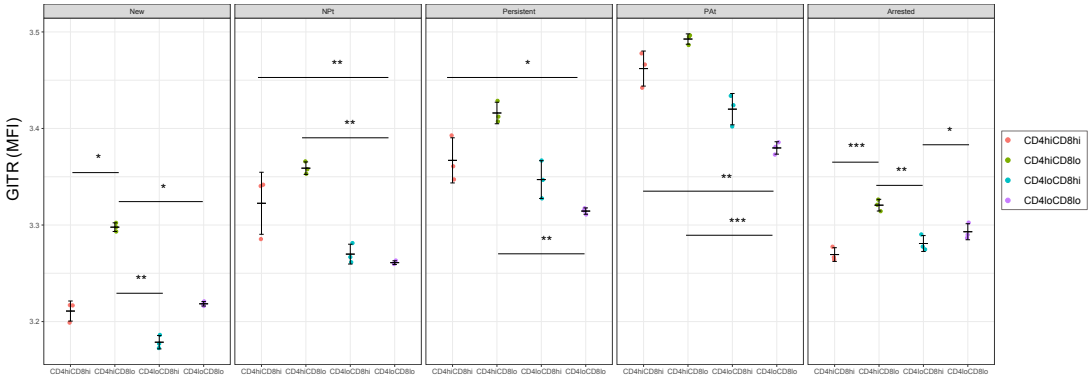

Figure 4.29: **GITR expression by Bim-deficient $CD69^{+}$DP populations in each Timer locus**. $CD69^{+}$DP cells from 6 weeks old $Bim^{KO/KO}$ mice were analysed by flow cytometry on a Fortessa III instrument. MFI of the surface marker GITR is shown for four $CD69^{+}$DP populations present in the New Timer locus and defined according to CD4 and CD8 co-receptor expression: $CD4^{hi}CD8^{hi}$, $CD4^{hi}CD8^{lo}$, $CD4^{lo}CD8^{hi}$ and $CD4^{lo}CD8^{lo}$. Statistically significant differences from Tukey's post-hoc analysis are shown as * for $p<0.05$, ** for $p<0.01$, *** for $p<0.001$ and **** for $p<0.0001$. Error bars are representative of mean $\pm$ s.d, where $n = 3$ biological replicates. Data shown are representative of at least 3 independent experiments that used 2-4 mice per group.

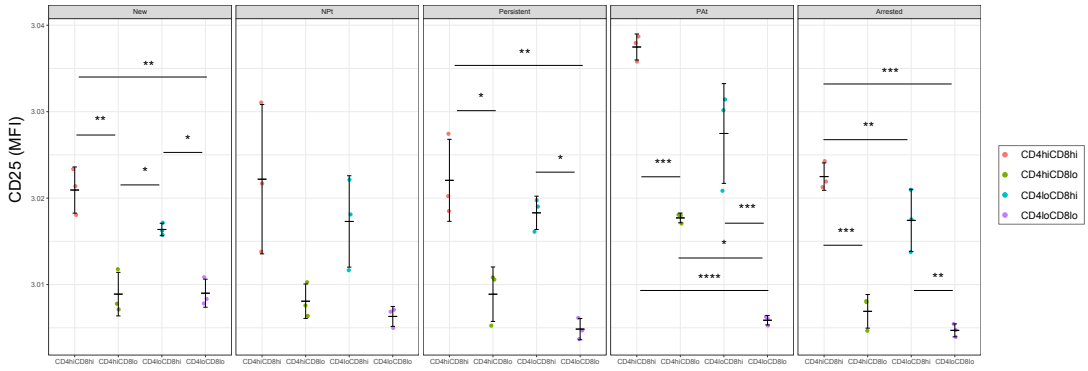

Figure 4.30: **CD25 expression by Bim-deficient CD69^{+}DP populations in each Timer locus**. CD69^{+}DP cells from 6 weeks old Bim$^{KO/KO}$ mice were analysed by flow cytometry on a Fortessa III instrument. MFI of the surface marker CD25 is shown for four CD69^{+}DP populations present in the New Timer locus and defined according to CD4 and CD8 co-receptor expression: CD4^{hi}CD8^{hi}, CD4^{hi}CD8^{lo}, CD4^{lo}CD8^{hi} and CD4^{lo}CD8^{lo}. Statistically significant differences from Tukey's post-hoc analysis are shown as * for $p<0.05$, ** for $p<0.01$, *** for $p<0.001$ and **** for $p<0.0001$. Error bars are representative of mean $\pm$ s.d, where n = 3 biological replicates. Data shown are representative of at least 3 independent experiments that used 2-4 mice per group.

4.3 Discussion

In this chapter, the *Nr4a3*-Tocky system was used to analyse the phenotype and transcriptome of thymic T cells with a polyclonal repertoire, which receive strong TCR signals at the DP stage. The study focused on the CD69^{+} DP cells that are considered to have received TCR signals and completed positive selection. Based on *Nr4a3*-Timer protein expression, CD69^{+} DP were composed of either Blue^{-}Red^{-} (DP_N) or Blue^{+}Red^{-} (DP_B). DP_N cells likely interacted with antigen on cTECs, but the TCR signal was not strong enough to induce Timer expression. Some of these cells may encounter their cognate antigen as they migrate towards the medulla to become CD4 or CD8 SP.

Since *Nr4a3*-Timer fluorescence is induced only by cognate antigen signalling (Bending et. al, 2018), DP_B must be enriched with cells that have encountered their cognate antigen in the cortex. This study showed that Blue^{+}Red^{-} cells express very high levels of CD69, which raises two possibilities regarding the ontogeny of DP_B. One is that they have undergone positive selection as DP_N and then they encountered their cognate antigen, becoming DP_B. Alternatively, they were positively selected on their cognate antigen and, as *Nr4a3* transcript accumulated enough to be detected by Timer fluorescence, CD69 also reached high MFI levels.

No DP cells were detected beyond the New Timer locus in WT and Bim$^{WT/KO}$ *Nr4a3*-Tocky mice. This means that once a cell has received strong TCR signals, it does not maintain a DP phenotype for long. DP_B cells in Bim-sufficient mice therefore either mature to the SP stage or rapidly undergo apoptosis. This study showed that Bim is responsible for eliminating at least some Timer^{+} DP cells, given the accumulation of Red fluorescence in Bim-deficient DPs. Since Blue matures to Red in approximately 4 hours and there is hardly any Red fluorescence expressed by Bim-sufficient DP, Bim-mediated negative selection must be a very quick process. Based on this study, a model is pro-

posed for the development of cells at the DP stage in *Nr4a3*-Tocky mice, as illustrated in Fig.4.31.

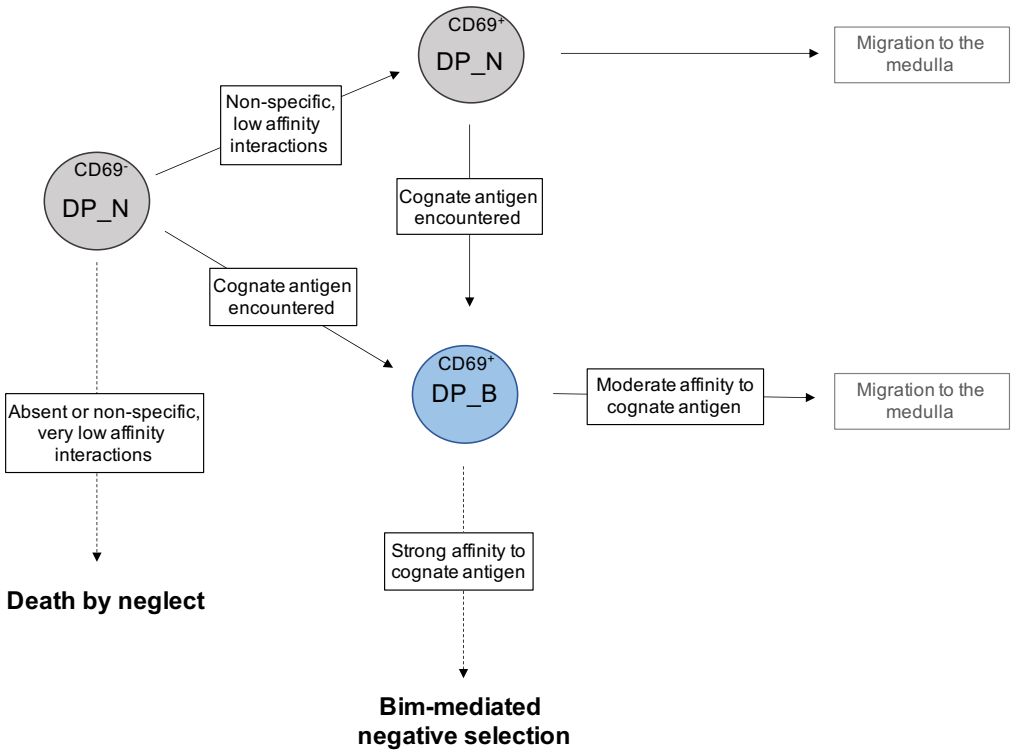

Figure 4.31: **Proposed model for thymic T cell development at the DP stage in *Nr4a3*-Tocky mice.** Figure shows a new model of thymic selection processes at the DP stage, where CD69 expression and *Nr4a3*-Timer maturation are used to identify key developmental events.

$Bim^{KO/KO}$ mice accumulated a smaller fraction of $Blue^{-}Red^{+}$ DP cells (DP_R) than $Blue^{+}Red^{+}$ (DP_BR). It is therefore likely that some DP_BR cells directly join the SP fraction, before *Nr4a3* transcription has ceased. This scenario is supported by their particularly high expression of *Ccr7* compared to other DPs (Fig.4.19). Kovalovsky et al. identified $CD4^{lo}CD8^{lo}$ self-reactive T cells, which are immediately deleted in Bim-sufficient mice. In the absence of Bim, however, they accumulate in close proximity to the medulla and their removal is delayed. The authors postulated that this is the result of a secondary, Bim-independent deletion process, which likely occurs in a different location and is mediated by other cells than those involved in the primary, immediate,

Bim-dependent negative selection (Kovalovsky et al., 2010). Taking this possibility into consideration, a model for DP cell development in Bim-deficient *Nr4a3*-Tocky mice is proposed in Fig.4.32.

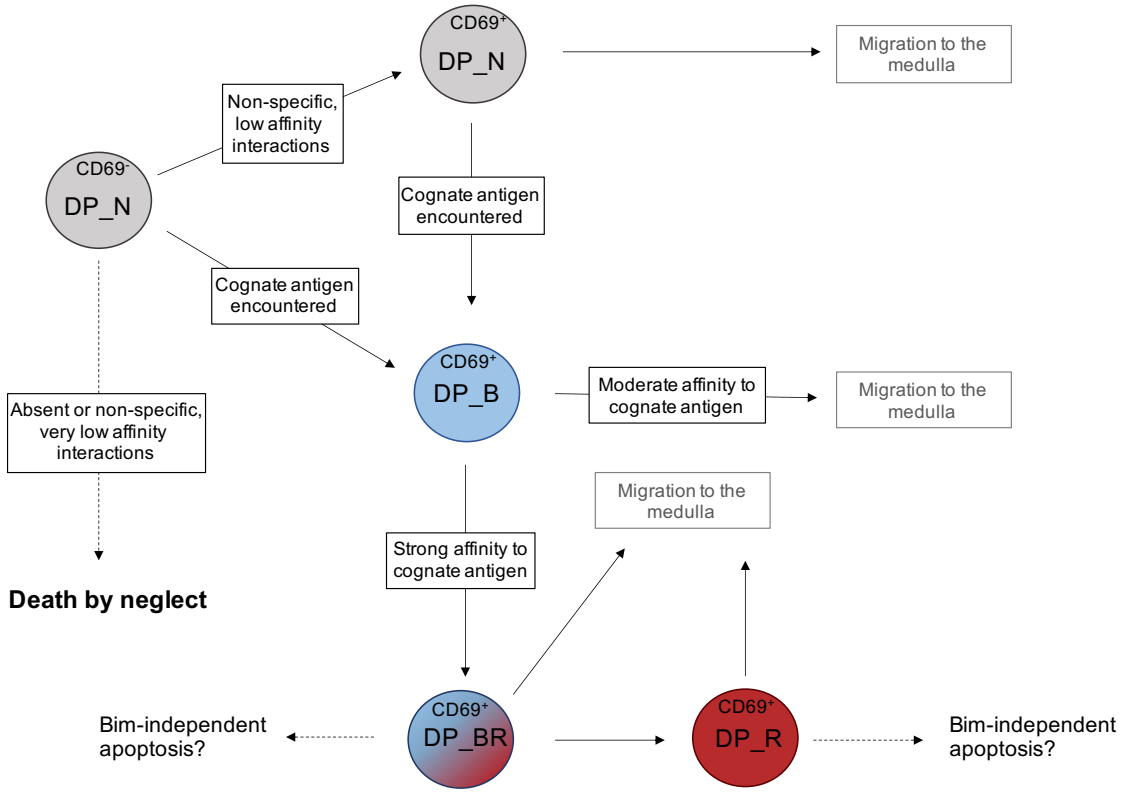

Figure 4.32: **Proposed model for thymic T cell development at the DP stage in Bim-deficient *Nr4a3*-Tocky mice.** Figure shows a new model of thymic selection processes at the DP stage in Bim-deficient mice, where CD69 expression and *Nr4a3*-Timer maturation are used to identify key developmental events.

Compared to DP_N, DP_B had lower surface levels of the CD4 and CD8 lineage markers. $CD4^{hi}CD8^{lo}$ and $CD4^{lo}CD8^{hi}$ cells likely encountered their cognate antigen on MHC-II and MHC-I molecules, respectively. This would render them as the immediate precursors of CD4 and CD8 SP cells, respectively. $CD4^{hi}CD8^{lo}$ cells were, on average, slightly older than $CD4^{lo}CD8^{hi}$ according to Timer angle data, despite receiving signals of the same Timer intensity. They also expressed higher levels of CD69. One explanation for this could be that CD4 SP development requires slightly prolonged TCR signals, resulting in a higher Timer angle and an accumulation of CD69. One study in support of this

scenario showed that DP cells selected on MHC-I molecules had a higher percentage of CCR7^{+} cells than cells selected on MHC-II. Furthermore, CCR7 overexpression by ThPOK-deficient mice resulted in CD8-lineage commitment of some MHC-II restricted T cells (Yin et al., 2007). Therefore, it could also be that CD4^{hi}CD8^{lo} cells migrate slower to the medulla than CD4^{lo}CD8^{hi}, thus residing for longer at the DP stage and accumulating both Timer and CD69 expression. Another possibility is that that CD8 becomes internalised much slower than CD4. However, this is challenged by the fact that CD4^{lo}CD8^{lo} cells were as young as CD4^{lo}CD8^{hi}. If CD8 required a longer time to become internalised, their angle would be expected to be slightly higher.

CD4^{lo}CD8^{lo} cells received much stronger signals than other DPs. They might T cells that recognise both MHC-I and MHC-II molecules, leading to their downregulation of both CD4 and CD8. Receiving TCR signals from antigens presented on both MHC-I and MHC-II molecules would justify their more rapid Blue protein accumulation and to higher intensities than other DP populations. Given that they become highly accumulated in Bim$^{KO/KO}$ mice, they are most probably enriched with the highly self-reactive cells that undergo negative selection before reaching the medullary zones. This study showed that Bim and PD-1 expression are mutually exclusive in Timer^{+} cells. Since high PD-1 expression was detected in CD4^{lo}CD8^{lo} cells, many are likely to survive. Surviving cells would then completely downregulate one of the co-receptors and upregulate the other, becoming SP. It is unlikely that they would acquire a CD4^{lo}CD8^{hi} or CD4^{hi}CD8^{lo} phenotype, otherwise Bim-deficient mice would preferentially accumulate them, instead of CD4^{lo}CD8^{lo} cells. The significance behind synchronised co-receptor downmodulation in this population could also be that some self-reactive T cells selected on MHC-I and MHC-II molecules may survive by being diverted towards a CD4 and a CD8 phenotype instead, respectively. Single cell RNAseq analysis would be very useful in determining whether there is heterogenous expression of Bim, ThPOK and Runx3 in this population.

The fact that $CD4^{lo}CD8^{lo}$ cells are the most accumulated Timer-expressing DP population in Bim-deficient mice indicates that this is the cell phenotype most associated with TCR repertoires of the strongest affinity to self-antigen. Although to a lesser extent, $CD4^{hi}CD8^{lo}$ and $CD4^{lo}CD8^{hi}$ are also captured in the Arrested Timer locus in Bim-deficient mice, which implies that at least some of them bear TCR repertoires of sufficient self-reactivity to become removed at the DP stage in a Bim-mediated manner.

In $Bim^{KO/KO}$ mice, *Foxp3* expression was detected in $Blue^{+}Red^{+}$ and $Blue^{-}Red^{+}$ DP cells. If *Foxp3* expression requires a narrow spectrum of self-reactivity, it is possible that in the absence of Bim, cells which are quite close to the upper limit of this range are diverted towards a Treg phenotype, an idea that was previously suggested by Krishnamurthy et al. upon analysing Bim-deficient DP and $Foxp3^{+}$ SP cells in NOD mice. The study proposed that the precursors of accumulated $Foxp3^{+}$ SP in Bim-deficient mice have a $GITR^{hi}CD25^{+}$ phenotype at the DP stage (Krishnamurthy et al., 2015). In this study, the *Foxp3*$^{+}$DP cells uniquely detected in $Bim^{KO/KO}$ mice had a $CD4^{hi}CD8^{lo}$ lineage marker expression, high GITR levels and received TCR signals of higher intensity than the $CD4^{hi}CD8^{lo}$ population in control mice. CD25, however, was not particularly expressed and was in fact comparatively more abundant in $CD4^{lo}CD8^{hi}$ cells. Therefore, this study proposes that in the absence of Bim, a population of self-reactive T cells become *Foxp3*$^{+}$ CD4 SP and their precursors at the DP stage have a $GITR^{hi}$*Foxp3*$^{+}CD4^{hi}CD8^{lo}$ phenotype.

Chapter III: Investigation of early stages of SP T cell development and their negative selection

5.1 Introduction

After DP cells undergo positive selection and become CD4 or CD8 lineage-committed, they upregulate CCR7 to migrate to the medulla and complete their differentiation programme. CD4 and CD8 SP cells are estimated to occupy the medullary zones for approximately 5 days before thymic egress, a process associated with high expression of the Sphingosine 1-phosphate receptor 1 (S1PR1) (McCaughtry, Wilken and Hogquist, 2007).

In the previous chapter, it was shown that some cells encounter their cognate antigen at the DP stage of development. Importantly, a significant proportion of DP cells expressed the marker of positive selection CD69, but did not express Timer (Fig.4.1A). Therefore, these $CD69^{+}Timer^{-}$ cells have not recognised cognate antigen, or have not accumulated sufficient Timer proteins to be detected. Once becoming CD4 or CD8 SP, they can become mature $Foxp3^{-}$ T cells, or Treg if they encounter their cognate antigen on medullary APCs and express Foxp3 to survive negative selection.

5.1.1 Antigen presentation in the medulla

The medulla is essential for generating the TCR repertoire that is tolerant to self-antigen. Expression of TRAs is characteristic of mTECs and is directed by the autoimmune regulator (AIRE) gene. Mutations in the gene encoding AIRE cause autoimmune polyendocrinopathy candidiasis ectodermal dystrophy (APECED) in humans and similar pathological autoimmune features in mice. While there are several differences in disease manifestations between humans and mice, both conditions are associated with mononuclear cell infiltration, organ-specific autoimmunity and autoantibodies to TRAs (Peterson, Org and Rebane, 2008).

Although mTECs are an essential self-antigen reservoir, only a very small number of mTECs express a particular TRA (1-3% of the mature pool). Furthermore, they have a very rapid turnover rate, where up to 20% of mTECs undergo apoptosis and are replaced by new cells each day. These aspects render them as inefficient APCs (Derbinski et al.,2008; Gray etal., 2007). To compensate for this, mTECs unidirectionally transfer MHC-II-antigen complexes to DCs via direct cell contact (Millet, Naquet and Guinamard, 2008). mTEC-derived self-antigen presented by DCs can be nuclear, cytosolic and membrane-bound (Koble and Kyewski, 2009).

While most medullary DCs originate in the thymus, up to one third of them are derived from peripheral sites. Such migratory DCs are capable of inducing negative selection in the medulla and induce Treg development, both *in vitro* and *in vivo* (Bonasio et al., 2006; Proietto et al., 2008). It has not been clarified whether their peptide range differs from that presented by thymus-derived DCs, but it has been postulated that they might induce tolerance to innocuous antigens derived from foreign sources such as food and commensal gut bacteria (Klein et al., 2009). This idea is supported by evidence showing that circulating DCs can transport soluble and particulate circulating antigens to the

thymus (Li et al., 2009).

Around 0.3% of the total thymic population is constituted by B cells. Most thymic B cells immigrate from the periphery and, upon reaching the thymus, they upregulate MHC-II, CD80 and AIRE expression, which are phenotypic properties of thymic APCs (Yamano et al., 2015). Thymic B cells are capable of inducing negative selection (Frommer and Waisman, 2010) and might also be involved in Treg selection (Walters et al., 2014).

5.1.2 Chapter aims

In this chapter, the TCR signalling dynamics characteristic of *Foxp3*$^{-}$ T cells which mature or become negatively selected in the medulla will be investigated using the *Nr4a3*-Tocky system. This work aims to:

(I) identify and study the Timer^{+} cells that are undergoing negative selection

(II) address the possible involvement of Bim in negative selection at the SP stage

(III) compare between the TCR signalling dynamics and relative marker expression of *Foxp3*$^{-}$ T cells of the CD4 and CD8 lineages

(IV) investigate the consequences of Bim deficiency on SP cell development, with a focus on the CD4 T cell lineage

5.2 Results

5.2.1 Developing SP stage T cells have different *Nr4a3* transcriptional dynamics according to lineage marker and *Foxp3* expression

Once reaching the SP stage, T cells undergo TCR signalling-dependent selection processes in order to become fully mature. The *Nr4a3*-Tocky system is used here to study the TCR signalling dynamics of $CD4^+CD8^-$ and $CD4^-CD8^+$ T cells. The flow cytometry plots in Fig.5.1 show Timer protein expression patterns of each population. The two SP populations were further divided into *Foxp3*$^-$ and *Foxp3*$^+$ cells. In flow cytometry plots, *Foxp3*$^-$$CD4^+CD8^-$ cells show different cell distributions in the Blue-Red plot of *Nr4a3*-Timer protein expression to *Foxp3*$^-$$CD4^-CD8^+$, where the former has a higher fraction of B^+R^- cells and a lower fraction of B^-R^+.

Regardless of CD4 or CD8 expression, cells that have upregulated *Foxp3* show different *Nr4a3*-Timer fluorescence patterns compared to *Foxp3*$^-$ populations. Although *Foxp3*$^+$$CD4^-CD8^+$ T cells constitute a very rare population, their Timer dynamics are very similar to those of *Foxp3*$^+$$CD4^+CD8^-$ T cells. Specifically, most *Foxp3*$^+$ cells show either persistent or arrested *Nr4a3* transcription and a very small number are $Timer^-$. $Blue^+Red^-$ expression is nearly absent in *Foxp3*$^+$ cells at the SP stage (Fig.5.1).

Timer locus analysis was applied to *Foxp3*$^-$ $CD4^+CD8^-$ or $CD4^-CD8^+$ (hereafter CD4SP or CD8SP in this chapter) and to *Foxp3*$^+$ $CD4^+CD8^-$ or $CD4^-CD8^+$ (hereafter CD4Foxp3 or CD8Foxp3 in this chapter). In Fig.5.2 and 5.3 statistical comparisons are only drawn between CD4SP and CD8SP, as well as between CD4SP and CD4Foxp3. It was not considered biologically relevant at this point to compare between CD4Foxp3 and CD8SP,

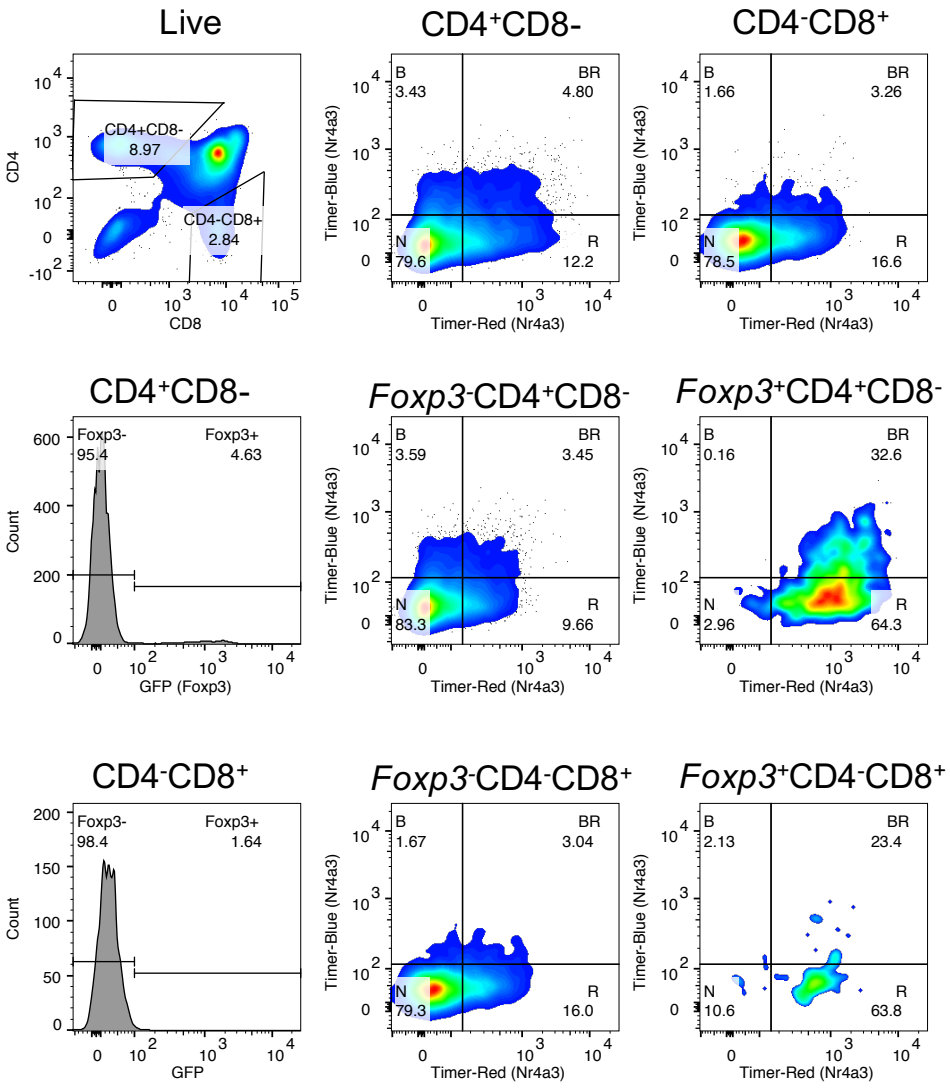

Figure 5.1: **Timer expression in thymic SP cells from *Nr4a3*-Tocky mice**. Thymocytes from 4 weeks old *Nr4a3*-Tocky mice were analysed by flow cytometry on a Fortessa III instrument. Gating strategies to identify cell populations based on their expression of CD4, CD8 and *Foxp3* are shown on the leftermost column and Blue-Red 2-D plots show their Timer protein expression. Data shown are typical of at least 4 independent experiments that used 2-4 mice and all mice were *Foxp3*-GFP.

therefore any existing significance between the two populations is not shown. Because CD8Foxp3 was a very rare population, it was not further discussed in this chapter and will be later addressed in Chapter IV. CD4/CD8 selection and the development of Foxp3-CD4$^+$ T cells are the main focus of this analysis.

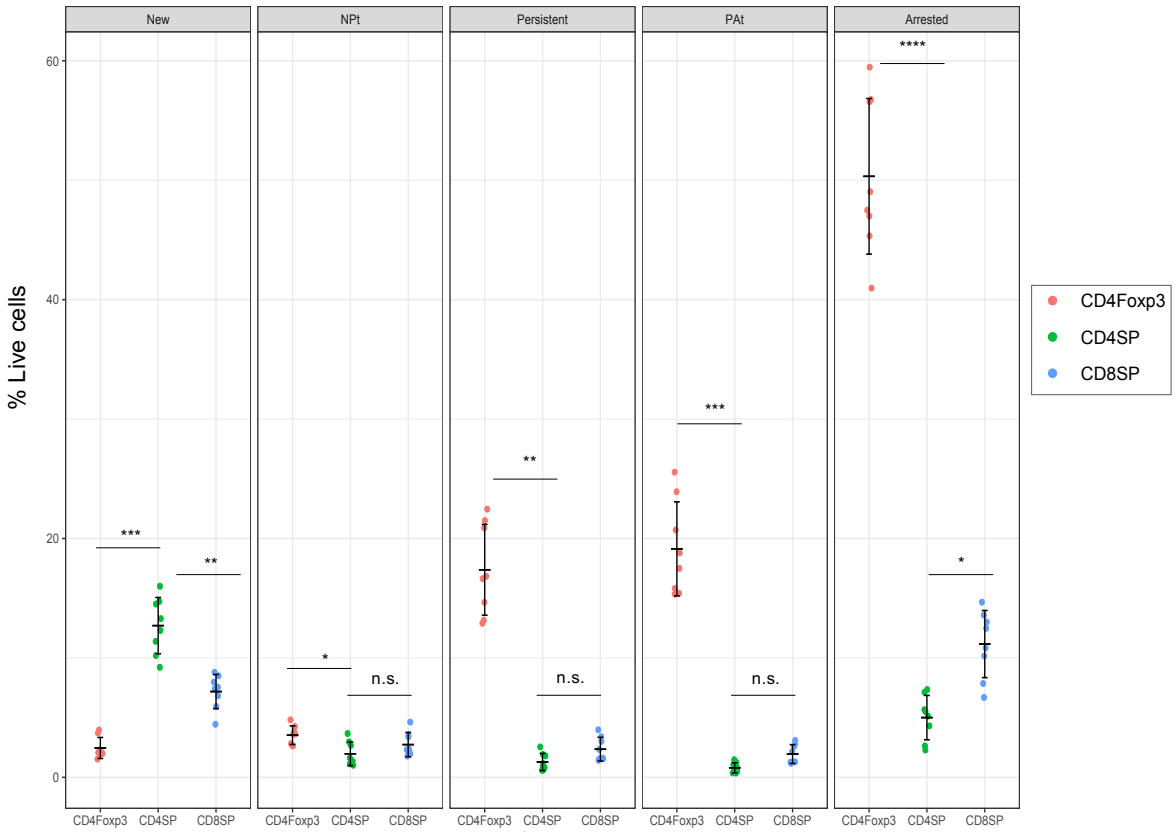

Figure 5.2: **Frequency of SP populations in each Timer locus**. Thymocytes from 4 weeks old *Nr4a3*-Tocky mice were analysed by a Cytek Aurora spectral analyser in two independent experiments and data was combined. The experiments were performed two days apart and the instrument settings were not changed. The percentage of cells in each Timer locus among their parent cell population is shown by scatter plot for three populations: *Foxp3*$^{-}$CD4^{+}CD8^{-} (CD4SP), *Foxp3*$^{+}$CD4^{+}CD8^{-} (CD4Foxp3) and *Foxp3*$^{-}$CD4^{-}CD8^{+} (CD8SP). Statistically significant differences from Tukey's post-hoc analysis are only shown for CD4SP vs CD4Foxp3 and CD4SP vs CD8SP populations as * for $p<0.05$, ** for $p<0.01$, *** for $p<0.001$ and **** for $p<0.0001$. Statistical differences between CD4Foxp3 and CD8SP are not shown, as comparison between the two populations was not considered biologically relevant. Error bars are representative of mean ± s.d, where n = 8 biological replicates. All mice used were *Foxp3*-GFP.

According to Timer locus analysis, CD4SP cells show significantly higher proportions of cells in the New locus than the other two populations (Fig.5.2). This fraction includes relatively immature CD4SP, mature CD4SP, as well as CD4Foxp3 precursors. Only a very small fraction of CD4Foxp3 are found in the New Timer locus. Compared to CD4SP, CD4Foxp3 show significantly higher proportions of cells in the Persistent locus and have higher Timer intensities overall. Collectively, this suggests that Treg differentiation oc-

curs only after receiving cognate antigen signals and accumulating *Nr4a3*-Timer proteins (Fig.5.3B).

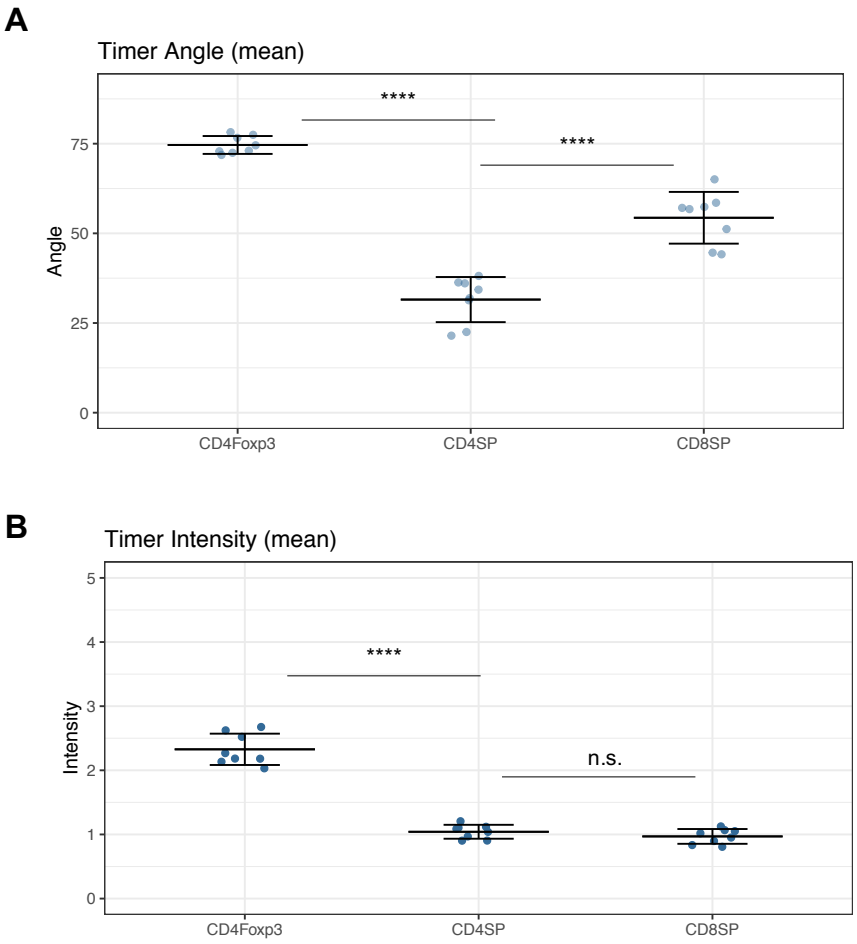

Figure 5.3: **Mean Timer angle and intensity of SP populations**. Thymocytes from 4 weeks old Nr4a3-Tocky mice were analysed by flow cytometry on a Cytek Aurora spectral analyser in two independent experiments and data was combined. The experiments were performed two days apart and the instrument settings were not changed. Mean *Nr4a3*-Timer angle (A) and intensity (B) are shown for three populations: *Foxp3*$^{-}$CD4^{+}CD8^{-} (CD4SP), *Foxp3*$^{+}$CD4^{+}CD8^{-} (CD4Foxp3) and *Foxp3*$^{-}$CD4^{-}CD8^{+} (CD8SP). Statistically significant differences from Tukey's post-hoc analysis are only shown for CD4SP vs CD4Foxp3 and CD4SP vs CD8SP populations as * for $p<0.05$, ** for $p<0.01$, *** for $p<0.001$ and **** for $p<0.0001$. Statistical differences between CD4Foxp3 and CD8SP are not shown, as comparison between the two populations was not considered biologically relevant. Error bars are representative of mean ± s.d, where n = 8 biological replicates. All mice used were *Foxp3*-GFP.

While CD4SP and CD8SP had similar *Nr4a3* transcription dynamics (Fig.5.1) and Timer

intensities (Fig.5.3B), overall, CD4SP cells had significantly more Blue^{+}Red^{-} cells, while CD8SP had more Blue^{-}Red^{+}, also reflected by the significantly higher Timer angle (Fig.5.3A). When levels of the maturation marker CD69 were compared between populations (Fig.5.4), they were much lower in CD8SP compared to CD4SP and this was consistent in most Timer loci. Collectively, these findings suggest that DP cells differentiate into CD8SP upon receiving shorter and weaker TCR signals than CD4SP, resulting in the observed larger fraction of cells with arrested *Nr4a3* transcription and lower accumulation of CD69 protein.

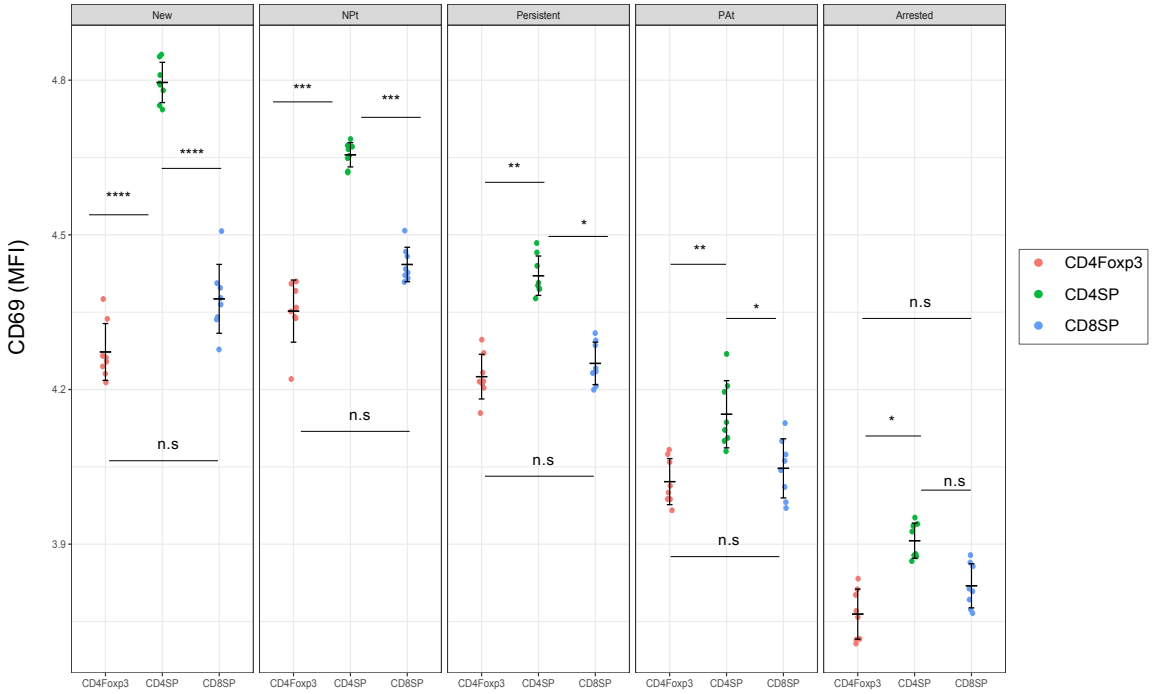

Figure 5.4: **CD69 expression by Timer^{+} populations**. Thymocytes from 4 weeks old *Nr4a3*-Tocky mice were analysed by a Cytek Aurora spectral analyser in two independent experiments and data was combined. The experiments were performed two days apart and the instrument settings were not changed. Plots show mean fluorescence intensity of the marker CD69 expressed in each Timer locus by three populations: *Foxp3*$^{-}$CD4^{+}CD8^{-} (CD4SP), *Foxp3*$^{+}$CD4^{+}CD8^{-} (CD4Foxp3) and *Foxp3*$^{-}$CD4^{-}CD8^{+} (CD8SP). Statistically significant differences from Tukey's post-hoc analysis are only shown for CD4SP vs CD4Foxp3 and CD4SP vs CD8SP populations as * for $p<0.05$, ** for $p<0.01$, *** for $p<0.001$ and **** for $p<0.0001$. Error bars are representative of mean ± s.d, where n = 8 biological replicates. All mice used were *Foxp3*-GFP.

5.2.2 CD69^{+} SP cells most recently received TCR signals

Complete CD69 downregulation is associated with the most mature state of thymic SP populations (Xing et al., 2016). To test if CD69^{+} T cells are enriched with cells that have recently received TCR signals, SP cell populations were divided according to its surface expression into CD69^{-} and CD69^{+} and their Timer protein expression patterns were studied using flow cytometry. The 2-D plots unambiguosly show that Timer^{+}CD69^{-} cells are mostly Red^{+}, with little to no Blue protein expression (Fig.5.5). High CD69 expression levels, however, capture both new and persistent transcription. Blue^{-}Red^{+} cells, which have completely ceased *Nr4a3* transcription, are also present, but in smaller percentages than those captured in CD69^{-} populations. These findings indicate that high CD69 expression is associated with developing SP cells that most recently received TCR signals and are actively transcribing *Nr4a3*.

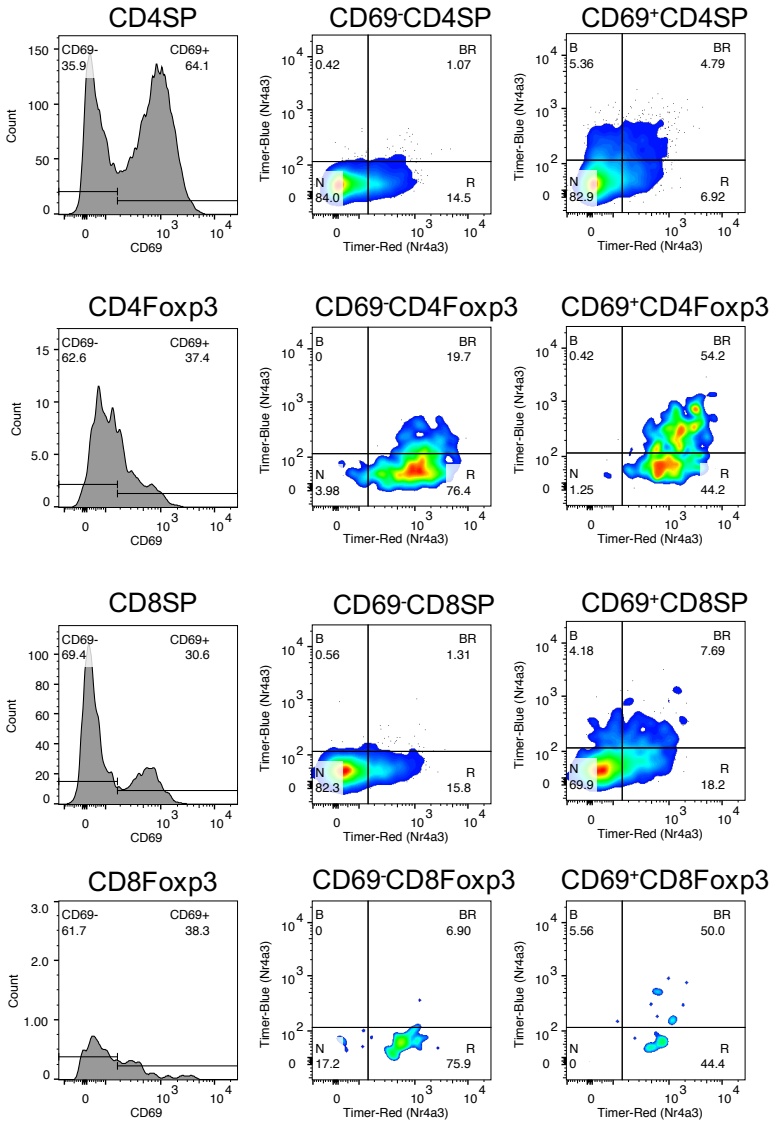

Figure 5.5: **The relationship between CD69 expression and *Nr4a3*-Timer patterns**. Thymocytes from 4 weeks old *Nr4a3*-Tocky mice were analysed by flow cytometry on a Fortessa III instrument. Gating strategies to identify $CD69^+$ and $CD69^-$ populations are shown in histograms on the leftermost column and the Blue-Red 2-D plots show their Timer expression. All mice used were *Foxp3*-GFP. Data shown are representative of at least 4 independent experiments that used 2-4 mice per group.

5.2.3 Bim-dependent negative selection occurs at both DP and SP stages of development

Having confirmed CD69 as a reliable marker for the T cells that have most recently received TCR signals from their cognate antigen, both at DP stage (in Chapter II) and at SP stage, $CD69^+$ T cell populations were sorted for RNAseq analysis based on *Nr4a3*-Timer protein expression as described in Table 5.1, in order to determine the temporal dynamics of TCR signalling required for negative selection.

Cell Population	Timer Protein Expression	Assigned Name
$CD69^+CD4^+CD8^+$	$Blue^+Red^-$	DP_B
$CD69^+$ *Foxp3*$^-CD4^+CD8^-$	$Blue^+Red^-$	CD4_B
$CD69^+$ *Foxp3*$^-CD4^+CD8^-$	$Blue^+Red^+$	CD4_BR
$CD69^+$ *Foxp3*$^-CD4^+CD8^-$	$Blue^-Red^+$	CD4_R
$CD69^+$ *Foxp3*$^-CD4^+CD8^-$	$Blue^-Red^-$	CD4_N.

Table 5.1: Thymic T cell populations sorted for RNAseq analysis from 8 weeks old *Nr4a3*-Tocky mice as described in the metods, according to *Nr4a3*-Timer protein expression. 1000 cells were sorted for each population.

On a principal component analysis (PCA) plot of gene expression data, DP_B were a very distinct population from the rest, clustering to the far left of the PC1 axis (Fig.5.6). The PC2 axis separated CD4 cells according to *Nr4a3*-Timer protein maturation.

Bcl2l11, the gene encoding the pro-apoptotic molecule Bim, was highly transcribed by both DP_B and CD4_B cells, with no significant difference between the two populations (Fig.5.7A). This suggests that Bim-mediated deletion mechanisms are most active in cells that have very recently received TCR signals and upregulated *Nr4a3*, irrespective of DP or SP development stage. In either case, Bim-mediated deletion must be an immediate process, as its transcription becomes significantly downregulated as Blue protein matures to Red. Gene expression data show that *Ccr7* transcription is low in DP_B and highly

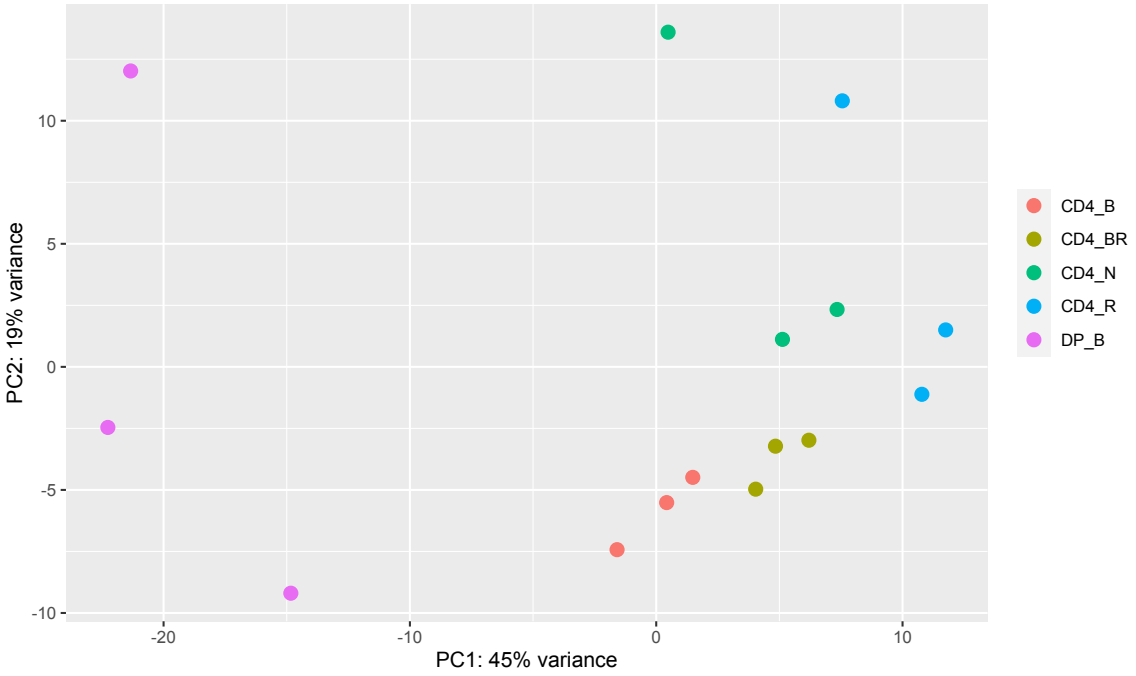

Figure 5.6: **PCA result of developing T cell populations transcriptomes.** Cells were sorted for RNAseq analysis from the thymus of 8 weeks old *Nr4a3*-Tocky mice according to *Nr4a3*-Timer expression as described in Table 5.1. 1000 cells were sorted for each population and subjected to RNAseq. Normalised counts of expressed genes were obtained using the algorithm DESeq2 and a PCA plot of their transcriptomes is shown.

upregulated in CD4_B cells, suggesting that Bim-mediated negative selection in response to strong affinity to self-antigen occurs not only in the cortex, but also in the medulla (Fig.5.7B).

Since Bim transcription becomes significantly downregulated in CD4_BR cells, it was hypothesised that CD4_BR cells are less apoptotic than DP_B and CD4_B cells. To test this, a heatmap was generated to include several pro-apoptotic members of the Bcl2 family, as well as the Nr4a family (Fig.5.8). DP_B and CD4_B showed a similar pro-apoptotic profile, where most genes included in the heatmap were highly expressed in these two populations. Compared to DP_B and CD4_B, CD4_BR had much lower levels of most pro-apoptotic genes. This suggests that negative selection mainly occurs in Blue^{+}Red^{-} cells, before Timer protein matures to Red.

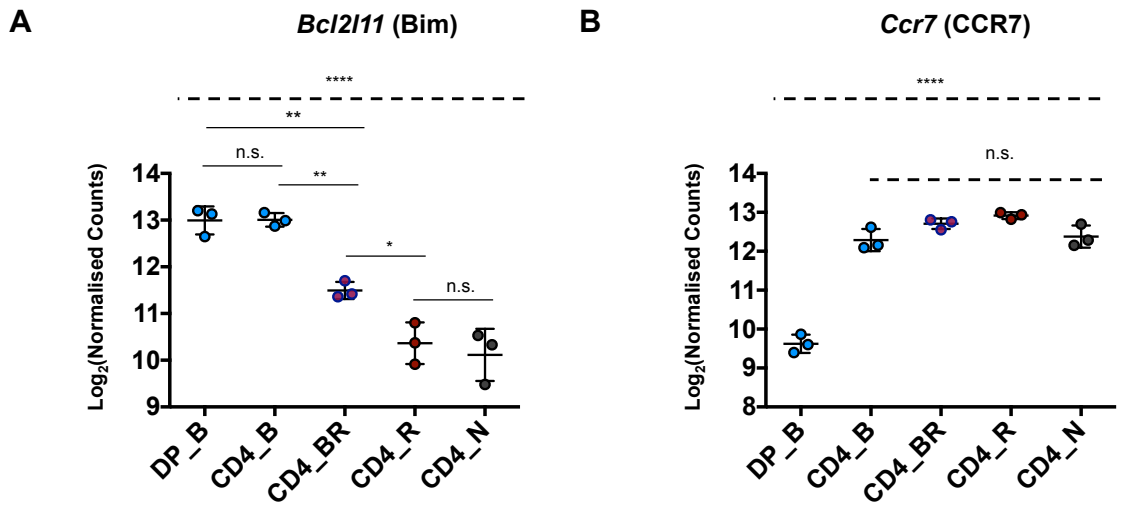

Figure 5.7: ***Bcl2l11* and *Ccr7* transcription by *Nr4a3*-Tocky T cell populations undergoing negative selection.** Cells were sorted for RNAseq analysis from the thymus of 8 weeks old *Nr4a3*-Tocky mice according to *Nr4a3*-Timer expression as described in Table 5.1. 1000 cells were sorted for each population and subjected to RNAseq. Normalised counts of the genes *Bcl2l11* coding for the pro-apoptotic molecule Bim (A) and *Ccr7* coding for the chemokine receptor CCR7 (B) were obtained using the algorithm DESeq2. Data are shown as $\log_2$ of normalised counts. Error bars are representative of mean ± s.d, where n = 3 biological replicates. Dashed lines show significance by one-way ANOVA. Individual comparisons by Tukey's post-hoc analysis where significance was different from the ANOVA result are shown by solid lines as * for $p<0.05$, ** for $p<0.01$, *** for $p<0.001$ and **** for $p<0.0001$.

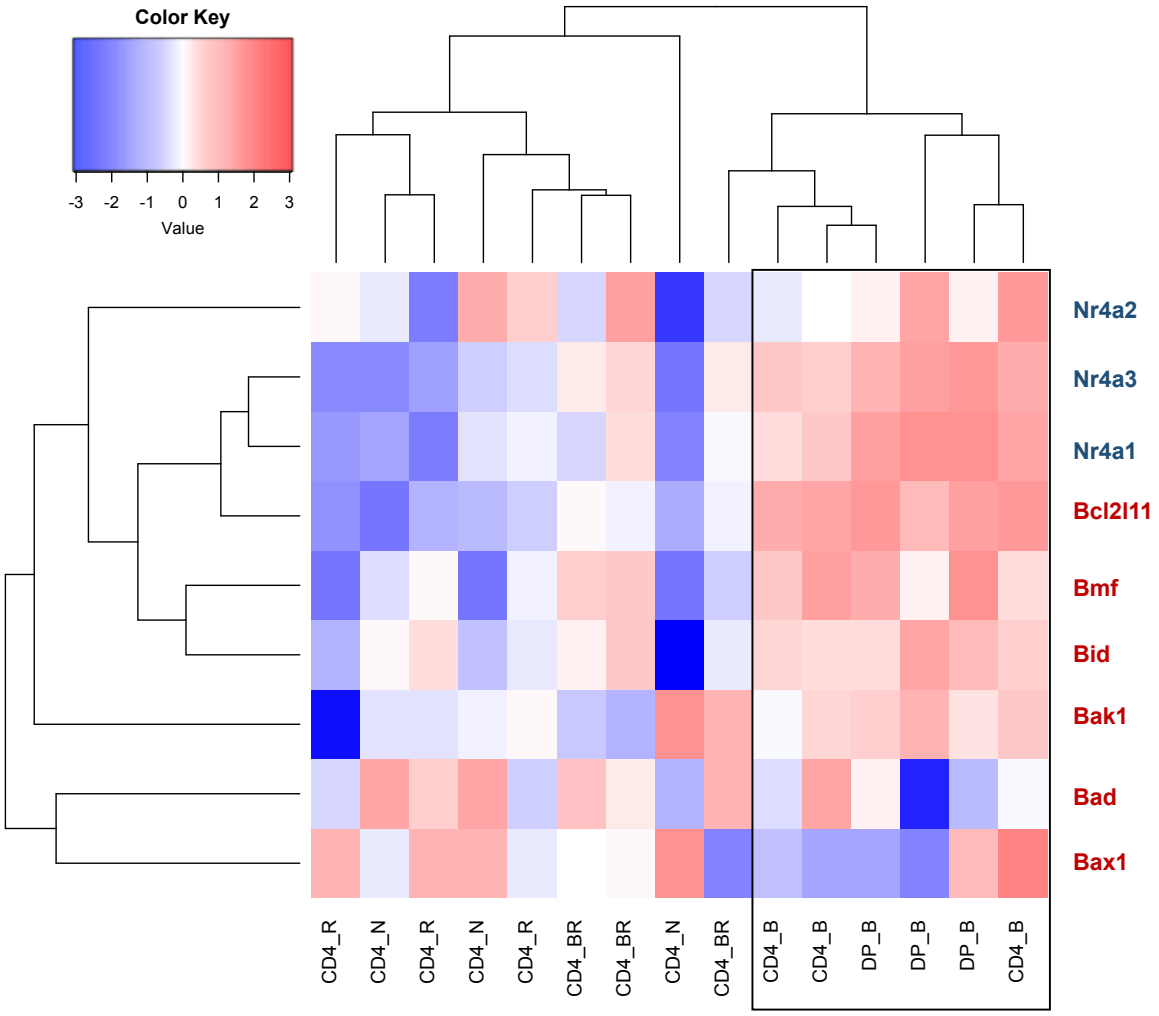

Figure 5.8: **Pro-apoptotic transcript profiles of developing T cells**. Cells were sorted for RNAseq analysis from the thymus of 8 weeks old *Nr4a3*-Tocky mice according to *Nr4a3*-Timer expression as described in Table 5.1. 1000 cells were sorted for each population and subjected to RNAseq. Normalised counts of expressed genes were obtained using the algorithm DESeq2. Heatmap analysis of differential gene expression of select pro-apoptotic members of the Bcl2 family (labelled in red font) and of the Nr4a family members (labelled in blue font) is shown. The heatmap was scaled across subpopulations.

5.2.4 High PD-1 expression marks cells rescued from Bim-mediated negative selection

PD-1 was reported as a marker of cells driven to tolerance following interaction with self-antigen (Blank et al., 2003). To test whether cells that matured past the New locus ($Blue^{+}Red^{-}$) and acquired Red fluorescence in the DP and CD4SP populations were mainly rescued from negative selection, transcript levels of *Pdcd1*, the gene encoding PD-1, were compared (Fig.5.9). *Pdcd1* was very highly upregulated in DP_B and CD4_BR cells, with no significant difference between the two populations. Comparatively, the other three populations showed little expression. This suggests that DP_B and CD4_BR are enriched with self-reactive cells that are nevertheless rescued from negative selection.

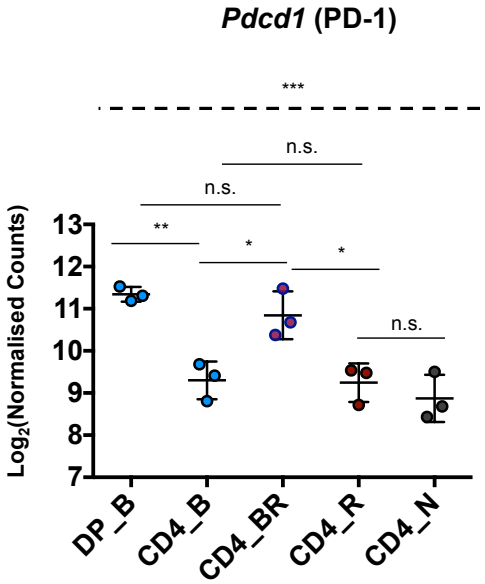

Figure 5.9: ***Pdcd1* transcription by *Nr4a3*-Tocky populations.** Cells were sorted for RNAseq analysis from the thymus of 8 weeks old *Nr4a3*-Tocky mice according to *Nr4a3*-Timer expression as described in Table 5.1. 1000 cells were sorted for each population and subjected to RNAseq. Normalised counts of the gene *Pdcd1* coding for PD-1 were obtained using the algorithm DESeq2. Data are shown as $\log_2$ of normalised counts. Error bars are representative of mean ± s.d, where n = 3 biological replicates. Dashed line shows significance by one-way ANOVA as *** for $p<0.001$. Results of individual comparisons between several populations by Tukey's post-hoc analysis are shown by solid lines as * for $p<0.05$ and ** for $p<0.01$.

At protein level, surface PD-1 expression of CD4SP and CD8SP cells peaks when cells are in the NPt and Persistent loci and becomes downregulated in the Arrested (Fig.5.10). No significant differences were found between PD-1 MFI of CD4SP and CD8SP cells (Fig.5.10). This indicates that PD-1 expression is increased in CD4SP and CD8SP while they recognise cognate antigen. It is therefore possible that PD-1 acts to rescue self-reactive T cells that accumulate Timer protein independently of CD4 or CD8 lineage.

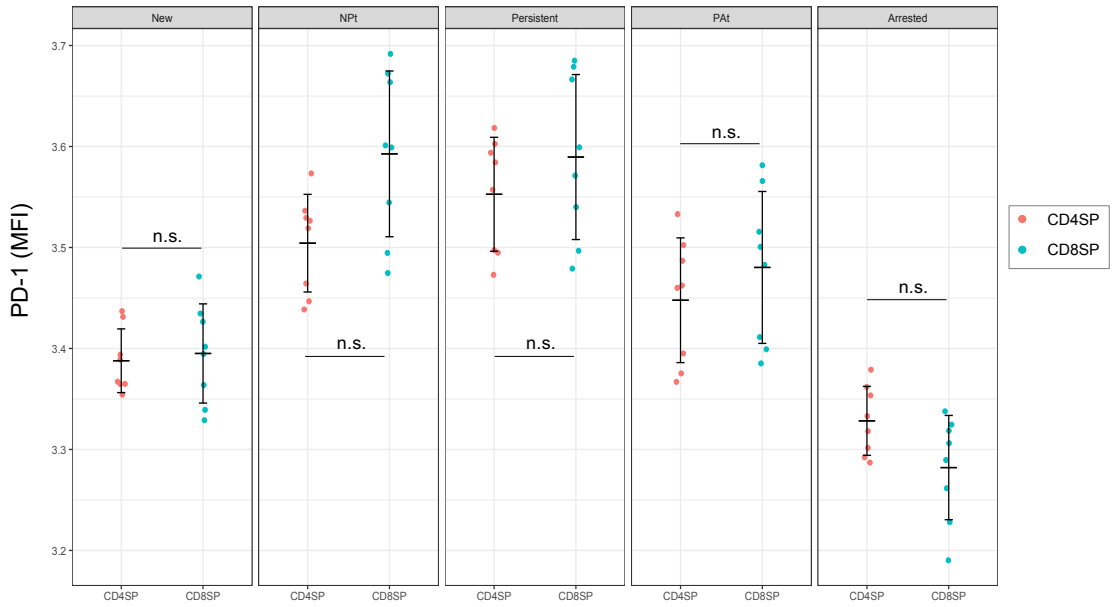

Figure 5.10: **PD-1 expression by developing T cells at the SP stage**. Thymocytes from 4 weeks old *Nr4a3*-Tocky mice were analysed by a Cytek Aurora spectral analyser in two independent experiments and data was combined. The experiments were performed two days apart and the instrument settings were not changed. Plots show mean fluorescence intensity of the marker PD-1 expressed in each Timer locus by *Foxp3*$^{-}$CD4^{+}CD8^{-} (CD4SP) and *Foxp3*$^{-}$CD4^{-}CD8^{+} (CD8SP). No statistically significant were found between the two populations upon performing unpaired Student's t-test analysis. Error bars are representative of mean ± s.d, where n = 8 biological replicates.

5.2.5 Blue$^-$Red$^-$CD69$^+$ cells are a heterogeneous population

CD4_N cells were the closest to CD4_R on the PCA plot (Fig.5.6), as well as on a heatmap of pro-apoptotic genes (Fig.5.8). It is, however, unlikely that CD4_N would be derived from the CD4_R pool when considering that CD69$^-$CD4SP cells express Red fluorescence (Fig.5.5). Therefore, CD4_R would first downregulate CD69 before completely losing Red fluorescence. Given that T cells that are going to emigrate the thymus have high S1PR1 expression, normalised counts of the gene encoding it, *S1pr1*, were compared between the sorted CD69$^+$CD4SP populations, where high expression is associated with preparation for thymic egress. The four populations were ordered on the summary plot from Fig.5.11 according to their mean transcript levels. CD4_R cells had significantly higher levels of *S1pr1* compared to the rest of the populations. CD4_B and CD4_N had similarly low levels. These findings suggest that CD4_R cells are in the process of thymic egress, while CD4_N are not developed enough for this step.

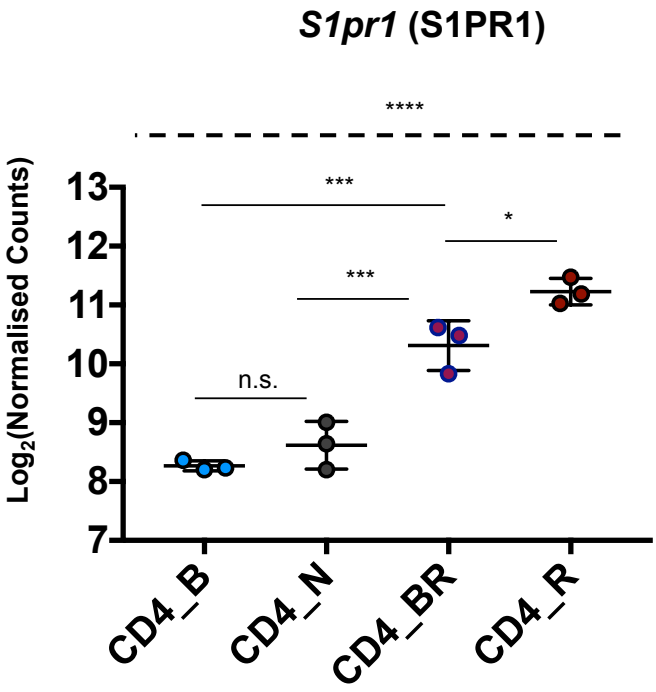

Figure 5.11: ***S1pr1* transcription by *Nr4a3*-Tocky CD4SP populations.** Cells were sorted for RNAseq analysis from the thymus of 8 weeks old *Nr4a3*-Tocky mice according to *Nr4a3*-Timer expression as described in Table 5.1. 1000 cells were sorted for each population and subjected to RNAseq. Normalised counts of the gene *S1pr1* coding for S1PR1 were obtained using the algorithm DESeq2. Data are shown as $\log_2$ of normalised counts. Error bars are representative of mean ± s.d, where n = 3 biological replicates. Dashed line shows significance by one-way ANOVA as **** for $p<0.0001$. Individual comparisons by Tukey's post-hoc analysis where significance was different from the ANOVA result are shown by solid lines as * for $p<0.05$ and ** for $p<0.01$.

5.2.6 T-cell development at the SP stage in the absence of Bim

The development of *Nr4a3*-Timer^{+} CD4SP and CD8SP was investigated in Bim$^{KO/KO}$ mice (KO) in order to better understand the role of Bim in negative selection at the SP stage. Compared to Bim$^{WT/KO}$ mice (Het), which were used as control, the KO model accumulates a larger fraction of both CD4SP and CD8SP cells (Fig.5.12). In the case of CD4SP, KO mice also accumulate significantly higher proportions of Timer^{+} cells (Fig.5.13 and 5.14A). This effect was not observed in Bim-deficient CD8SP cells (CD8_KO) (Fig.5.14B). Although CD8SP_KO cells were increased in the Arrested locus compared to Bim-sufficient CD8SP (CD8SP_Het), the difference was not significant. Overall, these findings indicate a more disruptive effect of Bim deficiency on the development of CD4 lineage T cells than CD8 lineage T cells.

CD4SP_KO expressed significantly higher levels of PD-1 in the PAt and the Arrested loci (Fig.5.15A) compared to CD4SP_Het. The accumulation of Timer^{+}PD-1^{hi}CD4SP in KO mice supports that self-reactive T cells survive in the absence of Bim (Fig.5.12 and 5.14).

PD-1 expression is overall lower in KO mice compared to Het in the CD8SP fraction, although the differences were not significant in most Timer loci (Fig.5.15B). CD8SP_KO cells in the Persistent locus, however, expressed significantly lower levels of PD-1 than Bim-sufficient ones. The fact that PD-1 expression is higher in CD4_KO compared to control, but lower in CD8SP_KO suggests that the former are more enriched with self-reactive cells. Low PD-1 expression in CD8SP_KO that receive persistent signals contributes to the stronger genotype effect observed on the CD4 lineage (Fig.5.14).

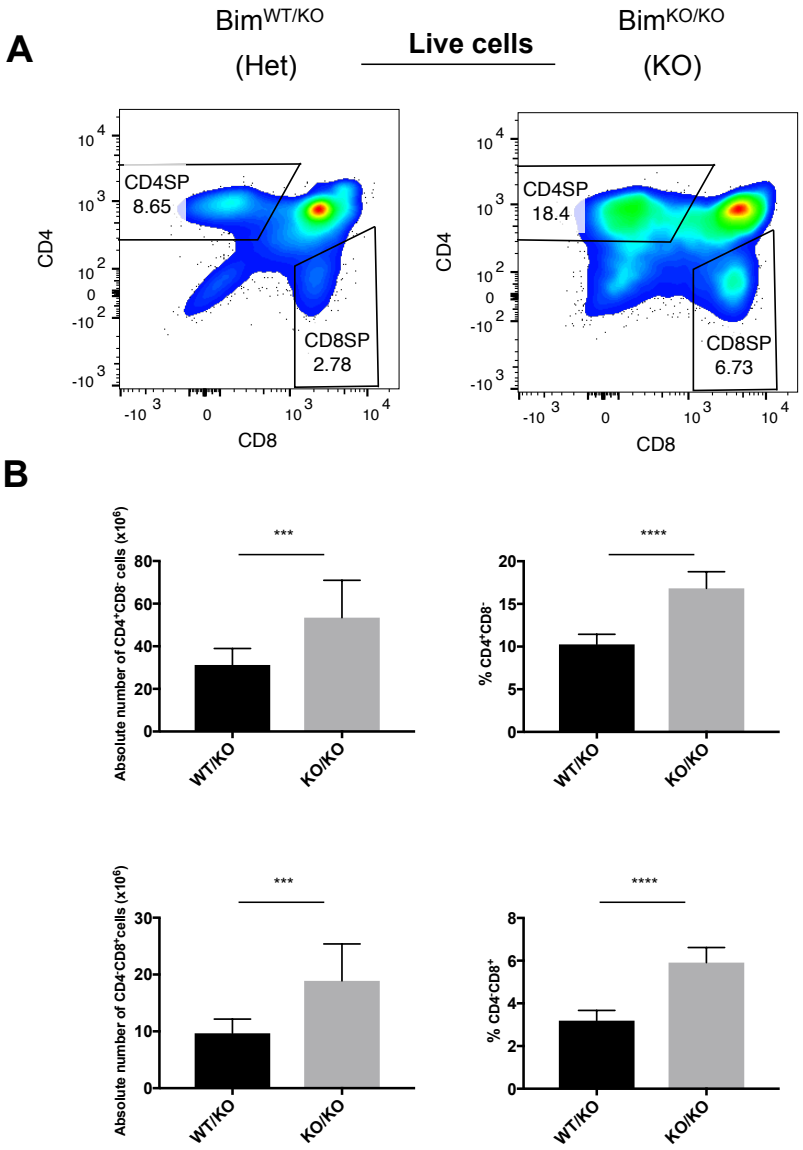

Figure 5.12: **SP fractions in Bim$^{WT/KO}$ and Bim$^{KO/KO}$ mice**. Thymocytes were harvested from 6 weeks old *Nr4a3*-Tocky:Bim$^{WT/KO}$ (Bim$^{WT/KO}$ or Het) and *Nr4a3*-Tocky:Bim$^{KO/KO}$ mice (Bim$^{KO/KO}$ or KO) and were analysed by flow cytometry on a Fortessa III instrument. **(A)** Gating strategy to identify CD4$^+$CD8$^-$ and CD4$^-$CD8$^+$ populations is shown by 2-D plots. Data shown are representative of at least 4 independent experiments that used 2-4 mice per group. **(B)** Absolute cell numbers (right) and absolute percentages (left) of CD4$^+$CD8$^-$ and CD4$^-$CD8$^+$ populations are shown for each genotype by bar charts. Data are a summary of three independent experiments, where 2-3 mice per group were used. Error bars are representative of mean ± s.d, where n = 8 total biological replicates. Statistically significant differences from unpaired Student's t-test are shown as *** for p<0.001 (performed on absolute count data) and from Mann-Whitney U test as **** for p<0.0001 (performed on percentage data).

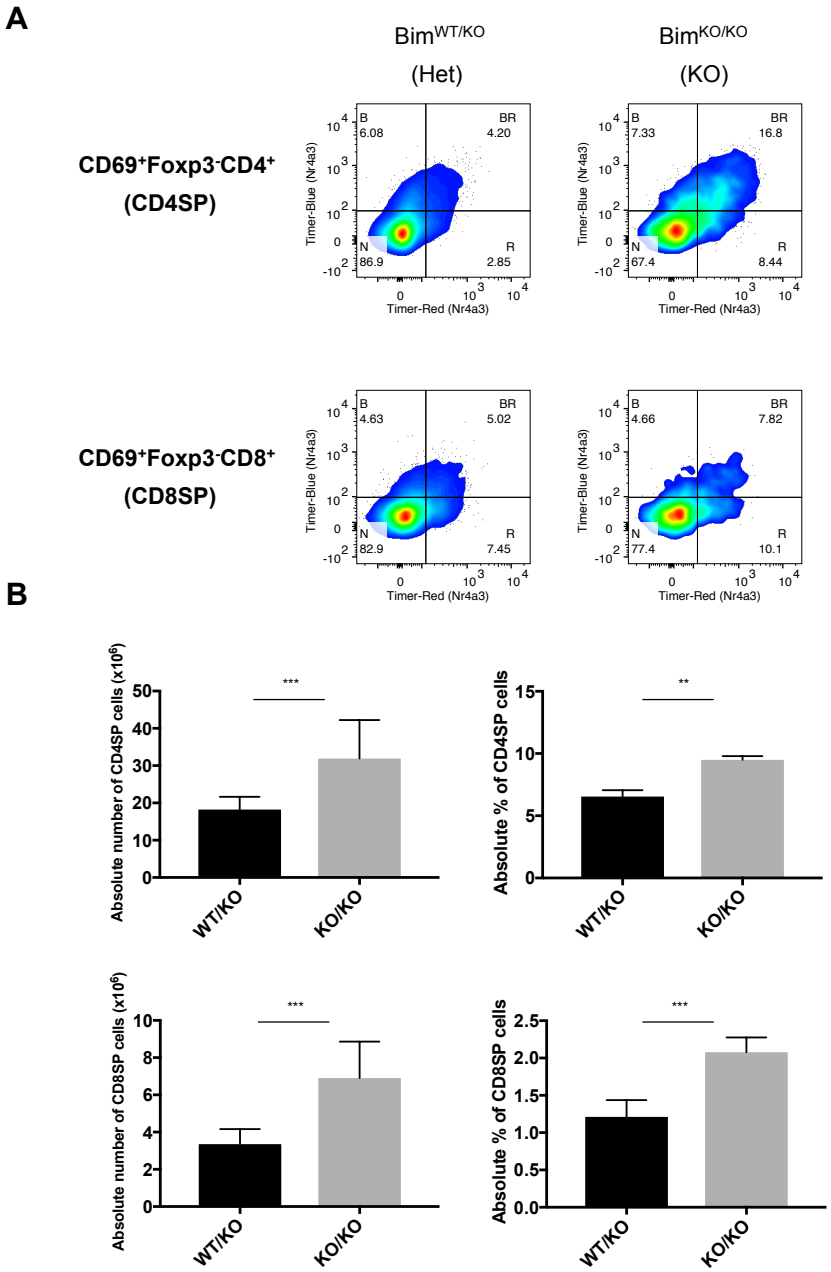

Figure 5.13: ***Nr4a3*-Timer expression in Bim-deficient SP cells**. Thymocytes were harvested from 6 weeks old *Nr4a3*-Tocky:Bim$^{WT/KO}$ or *Nr4a3*-Tocky:Bim$^{KO/KO}$ mice and were analysed by flow cytometry on a Fortessa III instrument. **(A)** 2-D Blue-Red plots show *Nr4a3*-Timer expression by CD69$^+$*Foxp3*$^-$CD4$^+$CD8$^-$ (CD4SP) and CD69$^+$*Foxp3*$^-$CD4$^-$CD8$^+$ (CD8SP) fractions. Data shown are representative of at least 4 independent experiments that used 2-4 mice per group. **(B)** Absolute cell numbers (right) and absolute percentages (left) of CD4SP and CD8SP populations are shown for each genotype by bar charts. Data are a summary of three independent experiments, where 2-3 mice per group were used. Error bars are representative of mean ± s.d, where n = 8 total biological replicates. Statistically significant differences from unpaired Student's t-test (performed on absolute count data) and from Mann-Whitney U test (performed on percentage data) are shown as ** for $p<0.01$ and *** for $p<0.001$. All mice used in these experiments were *Foxp3*-GFP.

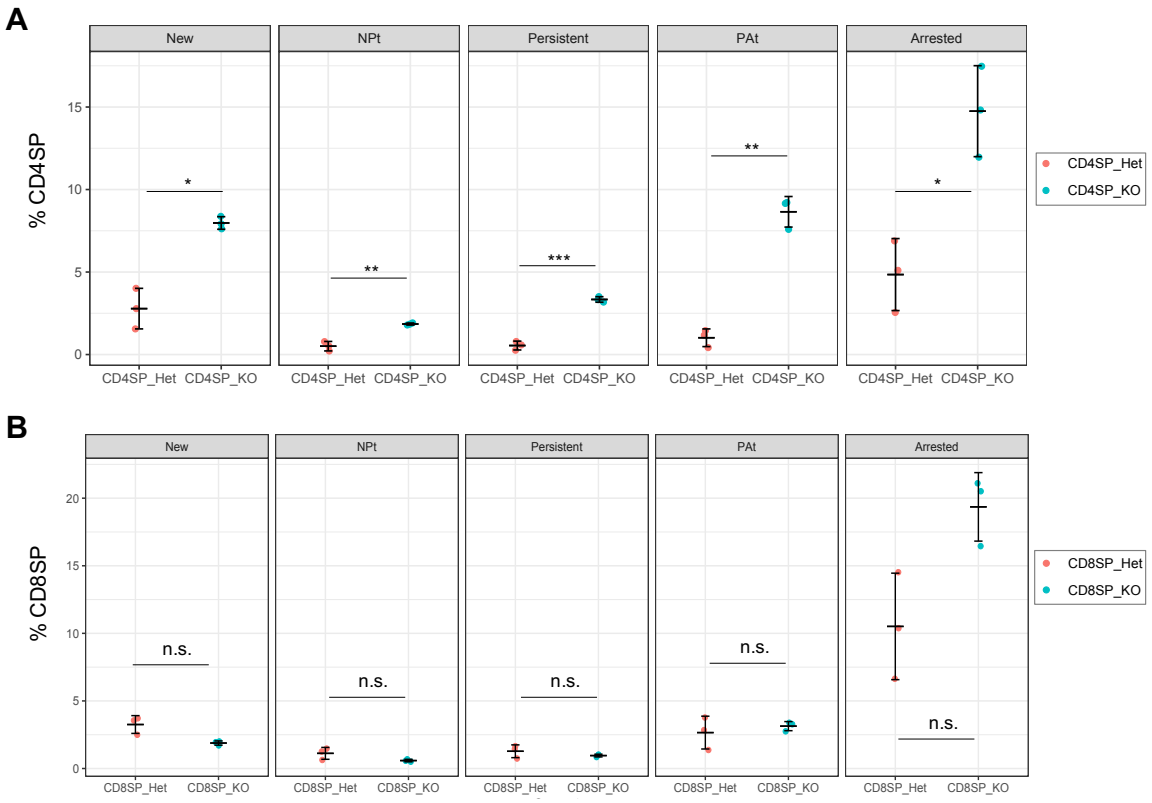

Figure 5.14: **Frequency of Timer expressing cells in each Timer locus**. CD69^{+}*Foxp3*$^{-}$ cells from 6 weeks old Bim$^{WT/KO}$ (_Het) and Bim$^{KO/KO}$ mice (_KO) were analysed by flow cytometry on a Fortessa III instrument. The percentage of cells in each Timer locus among their parent cell population is shown for (A) CD4SP and (B) CD8SP fractions. Statistically significant differences from unpaired Student's t-test analysis are shown as * for p<0.05, ** for p<0.01, *** for p<0.001 and **** for p<0.0001. Error bars are representative of mean ± s.d, where n = 3 biological replicates for each genotype. Data shown are typical of at least 4 independent experiments that used 2-4 mice per group.

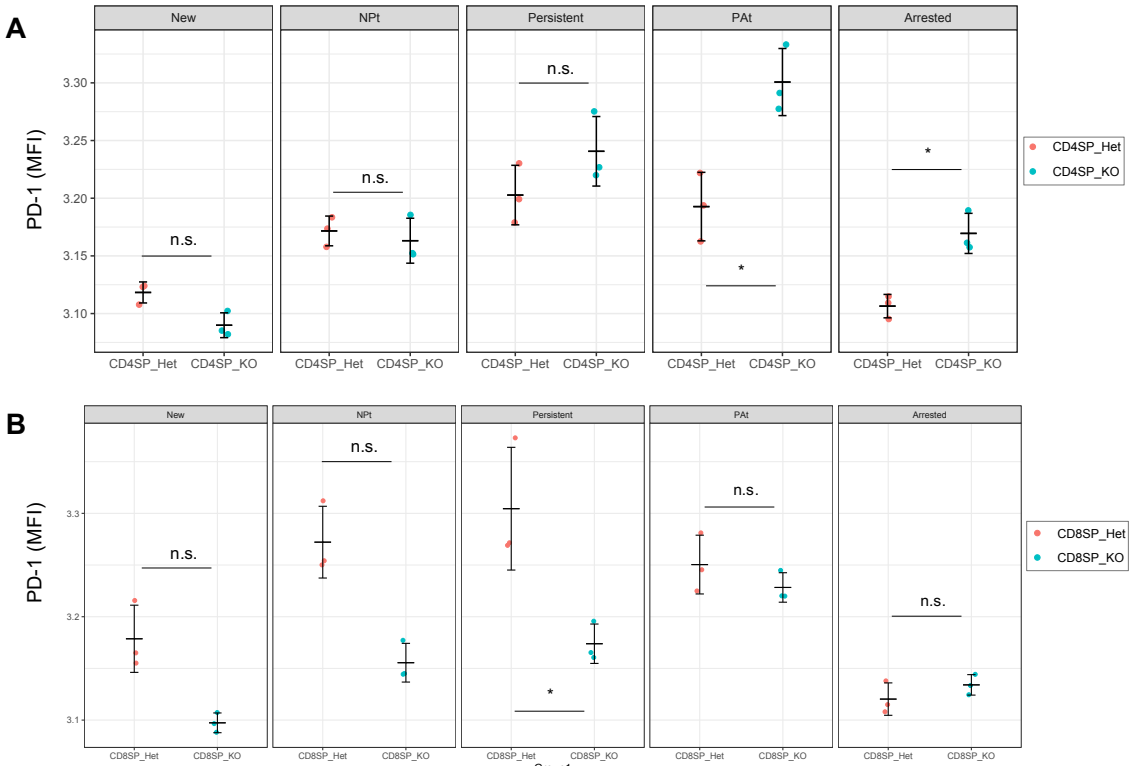

Figure 5.15: **PD-1 expression by Bim-deficient SP populations in each Timer locus**. CD69^{+}*Foxp3*$^{-}$ cells from 6 weeks old Bim$^{WT/KO}$ (_Het) and Bim$^{KO/KO}$ mice (_KO) were analysed by flow cytometry on a Fortessa III instrument. The MFI of PD-1 expressed by cells in each Timer locus is shown for (A) CD4SP and (B) CD8SP fractions. Statistically significant differences from unpaired Student's t-test analysis are shown as * for p<0.05, ** for p<0.01, *** for p<0.001 and **** for p<0.0001. Error bars are representative of mean ± s.d, where n = 3 biological replicates for each genotype. Data shown are typical of at least 3 independent experiments that used 2-4 mice per group.

5.2.7 The effects of Bim deficiency on CD4SP trancript profile

To further understand the mechanisms of Bim-mediated apoptosis in CD4SP development, CD69$^+$CD4SP cells from Bim$^{WT/KO}$ and Bim$^{KO/KO}$ mice were sorted according to Timer protein expression for RNAseq analysis, as shown in Table 5.2.

Genotype	Cell population	Timer Protein Expression	Assigned Name
Bim$^{WT/KO}$	CD69$^+$*Foxp3*$^-$CD4$^+$CD8$^-$	Blue$^-$Red$^-$	Het_N
Bim$^{KO/KO}$	CD69$^+$*Foxp3*$^-$CD4$^+$CD8$^-$	Blue$^-$Red$^-$	KO_N
Bim$^{WT/KO}$	CD69$^+$*Foxp3*$^-$CD4$^+$CD8$^-$	Blue$^+$Red$^-$	Het_B
Bim$^{KO/KO}$	CD69$^+$*Foxp3*$^-$CD4$^+$CD8$^-$	Blue$^+$Red$^-$	KO_B
Bim$^{WT/KO}$	CD69$^+$*Foxp3*$^-$CD4$^+$CD8$^-$	Blue$^+$Red$^+$	Het_BR
Bim$^{KO/KO}$	CD69$^+$*Foxp3*$^-$CD4$^+$CD8$^-$	Blue$^+$Red$^+$	KO_BR
Bim$^{WT/KO}$	CD69$^+$*Foxp3*$^-$CD4$^+$CD8$^-$	Blue$^-$Red$^+$	Het_R
Bim$^{KO/KO}$	CD69$^+$*Foxp3*$^-$CD4$^+$CD8$^-$	Blue$^-$Red$^+$	KO_R

Table 5.2: CD69$^+$CD4SP cells sorted for RNAseq analysis from 6-7 weeks old Bim$^{WT/KO}$ and Bim$^{KO/KO}$ mice as described in the methods, according to *Nr4a3*-Timer expression. 2000 cells were sorted for each population.

On a PCA plot of RNAseq data, the PC1 axis separated cells that actively transcribe *Nr4a3*-Timer from cells that do not to the left and right sides, respectively (Fig.5.16). According to the PC2 axis, the distance between the two genotypes for each population is smaller than the distance between different *Nr4a3*-Timer expressing populations. This indicates that between-genotype variations are largely dominated by between-population variations. Notably, B$^-$R$^+$ cells were the least distinct between genotypes, followed by B$^-$R$^-$.

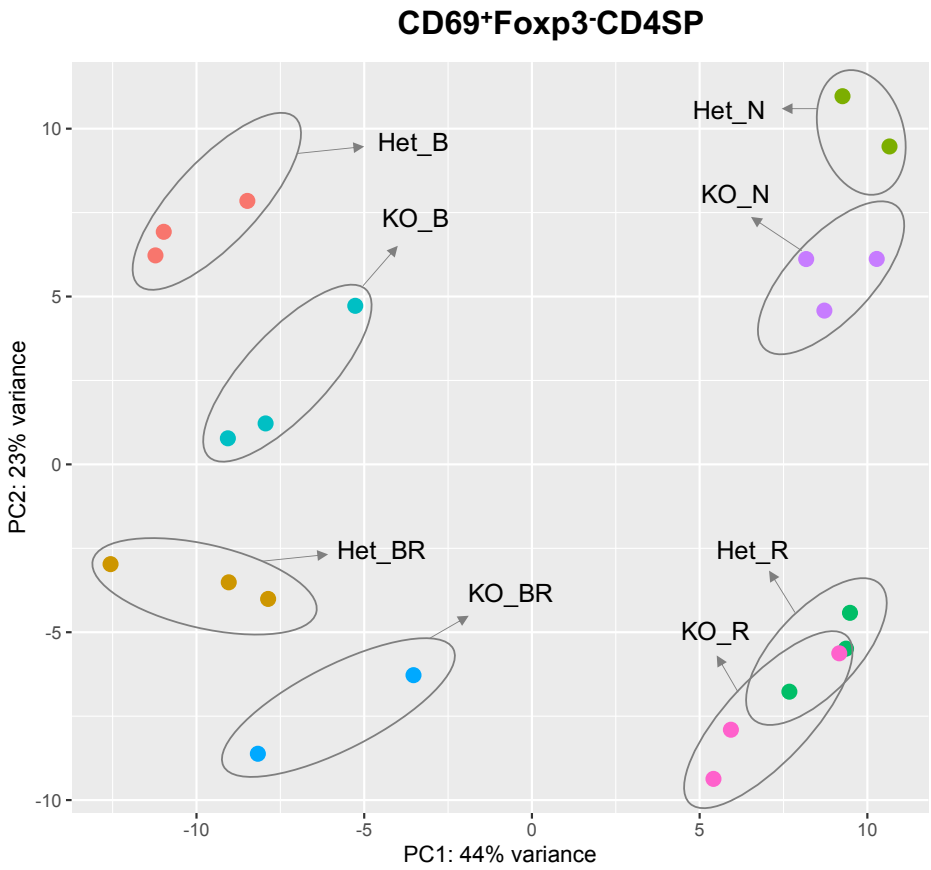

Figure 5.16: **PCA result of the transcriptomes of Bim-deficient and Bim-sufficient populations.** Cells were sorted for RNAseq analysis from 6-7 weeks old $Bim^{WT/KO}$ and $Bim^{KO/KO}$ mice according to *Nr4a3*-Timer expression as described in Table 5.2. 2000 cells were sorted for each population and subjected to RNAseq. Normalised counts of expressed genes were obtained using the algorithm DESeq2 and a PCA plot of their transcriptomes is shown.

Regardless of Timer protein expression, KO populations transcribe significantly more *Bcl2l11* than Het. (Fig.5.17). KO_R cells, which no longer receive TCR signals, were especially enriched with Bim transcript compared to the control. If Bim-mediated effects trigger negative feedback mechanisms to inhibit its own transcription, then, in its absence, the longer cells mature, the more *Bcl2l11* trasncript they accumulate. KO_R cells were also the only population where a genotype effect was detected in terms of PD-1 trancript levels (Fig.5.18). They expressed significantly higher levels of *Pdcd1* compared to the control, suggesting that the self-reactive CD4SP cells which would express PD-1 after receiving TCR signals are deleted in a Bim-mediated manner. Therefore, Bim deficiency leads to the development of a PD-1^{hi}, self-reactive CD4SP cell population.

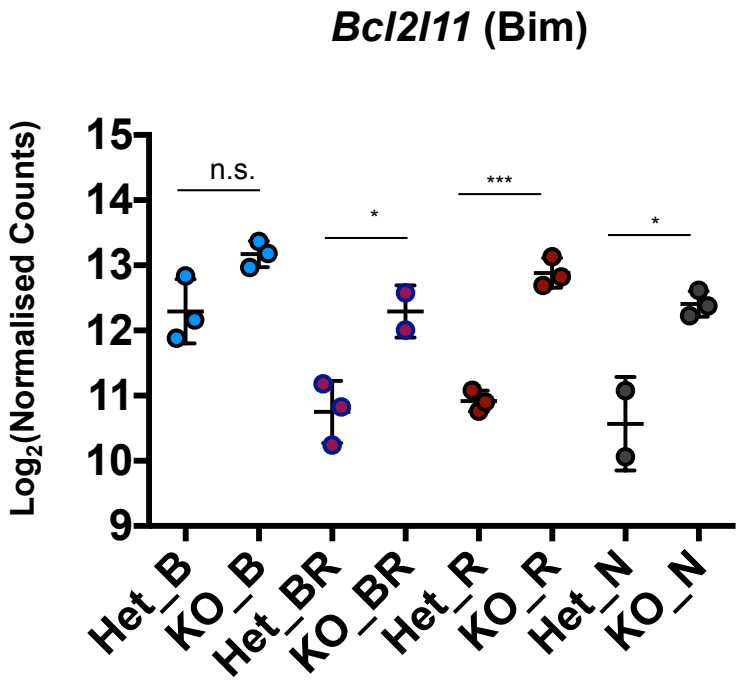

Figure 5.17: **Expression of *Bcl211* in Bim-sufficient and Bim-deficient cell populations.** Cells were sorted for RNAseq analysis from 6-7 weeks old $Bim^{WT/KO}$ and $Bim^{KO/KO}$ mice according to *Nr4a3*-Timer expression as described in Table 5.2. 2000 cells were sorted for each population and subjected to RNAseq. Normalised counts of the gene *Bcl2l11* coding for the pro-apoptotic molecule Bim were obtained using the algorithm DESeq2. Data are shown as $\log_2$ of normalised counts. Error bars are representative of mean ± s.d, where n = 3 biological replicates. Individual comparisons between the two genotypes by Tukey's post-hoc analysis are shown as * for $p<0.05$, ** for $p<0.01$, *** for $p<0.001$ and **** for $p<0.0001$.

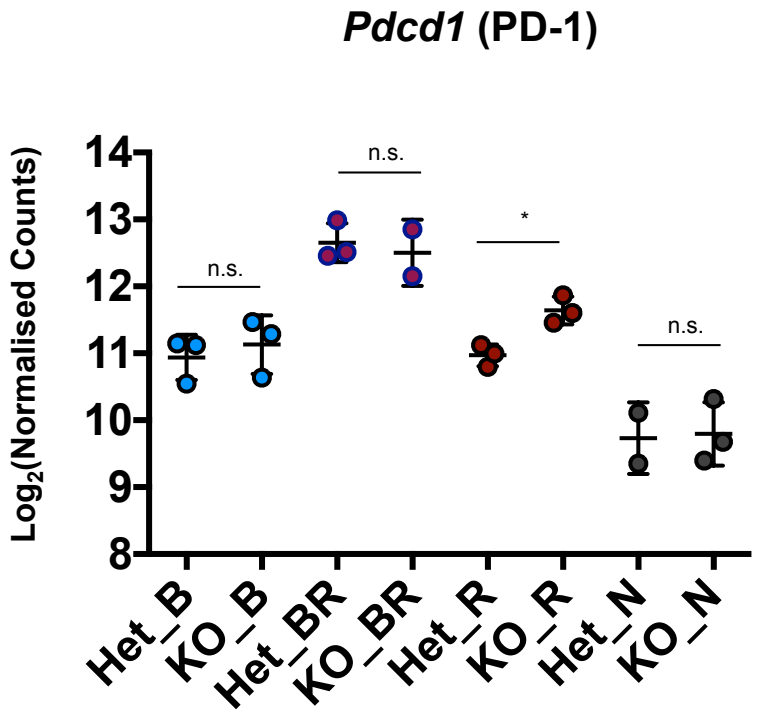

Figure 5.18: **Expression of *Pdcd1* in Bim-sufficient and Bim-deficient cell populations.** Cells were sorted for RNAseq analysis from 6-7 weeks old $Bim^{WT/KO}$ and $Bim^{KO/KO}$ mice according to *Nr4a3*-Timer expression as described in Table 5.2. 2000 cells were sorted for each population and subjected to RNAseq. Normalised counts of the gene *Pdcd1* coding for the surface marker PD-1 were obtained using the algorithm DESeq2. Data are shown as $\log_2$ of normalised counts. Error bars are representative of mean ± s.d, where n = 3 biological replicates. Individual comparisons between the two genotypes by Tukey's post-hoc analysis are shown as * for $p<0.05$, ** for $p<0.01$, *** for $p<0.001$ and **** for $p<0.0001$.

With the exception of Timer$^-$ cells, KO populations had significantly lower levels of *Ccr7* than the control (Fig.5.19). Furthermore, KO_R had much lower levels of *S1pr1* and *Cd24a* than Het_R (Fig.5.21 and 5.20). The latter gene encodes the CD24 molecule, a marker highly expressed on immature T cells, which becomes downregulated during their maturation (Crispe and Benvan, 1987). These findings suggest that cells which erroneously survive negative selection in the absence of Bim are in a more immature state and may be retained in the thymus for longer.

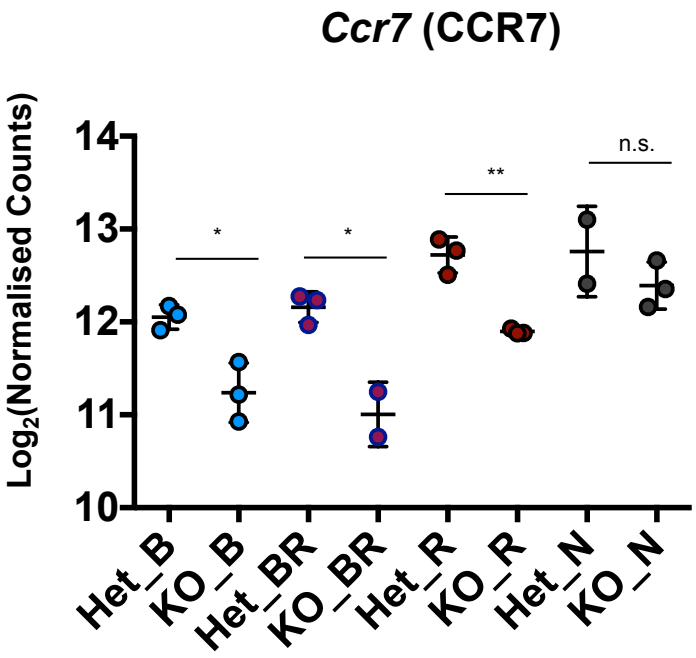

Figure 5.19: **Expression of *Ccr7* in Bim-sufficient and Bim-deficient cell populations.** Cells were sorted for RNAseq analysis from 6-7 weeks old Bim$^{WT/KO}$ and Bim$^{KO/KO}$ mice according to *Nr4a3*-Timer expression as described in Table 5.2. 2000 cells were sorted for each population and subjected to RNAseq. Normalised counts of the gene *Ccr7* coding for the chemokine receptor CCR7 were obtained using the algorithm DESeq2. Data are shown as $\log_2$ of normalised counts. Error bars are representative of mean ± s.d, where n = 3 biological replicates. Individual comparisons between the two genotypes by Tukey's post-hoc analysis are shown as * for $p<0.05$, ** for $p<0.01$, *** for $p<0.001$ and **** for $p<0.0001$.

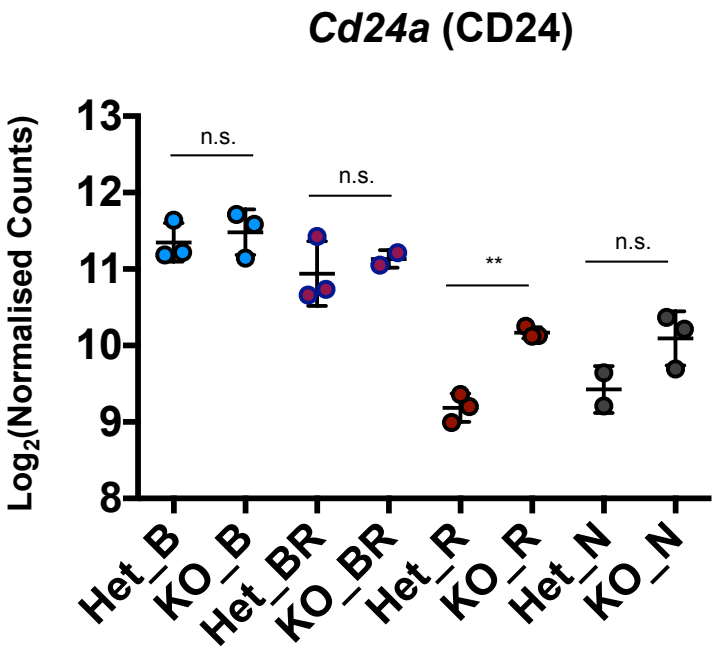

Figure 5.20: **Expression of *Cd24a* in Bim-sufficient and Bim-deficient cell populations.** Cells were sorted for RNAseq analysis from 6-7 weeks old $Bim^{WT/KO}$ and $Bim^{KO/KO}$ mice according to *Nr4a3*-Timer expression as described in Table 5.2. 2000 cells were sorted for each population and subjected to RNAseq. Normalised counts of the gene *Cd24a* coding for the CD24 molecule were obtained using the algorithm DESeq2. Data are shown as $\log_2$ of normalised counts. Error bars are representative of mean ± s.d, where n = 3 biological replicates. Individual comparisons between the two genotypes by Tukey's post-hoc analysis are shown as * for $p<0.05$, ** for $p<0.01$, *** for $p<0.001$ and **** for $p<0.0001$.

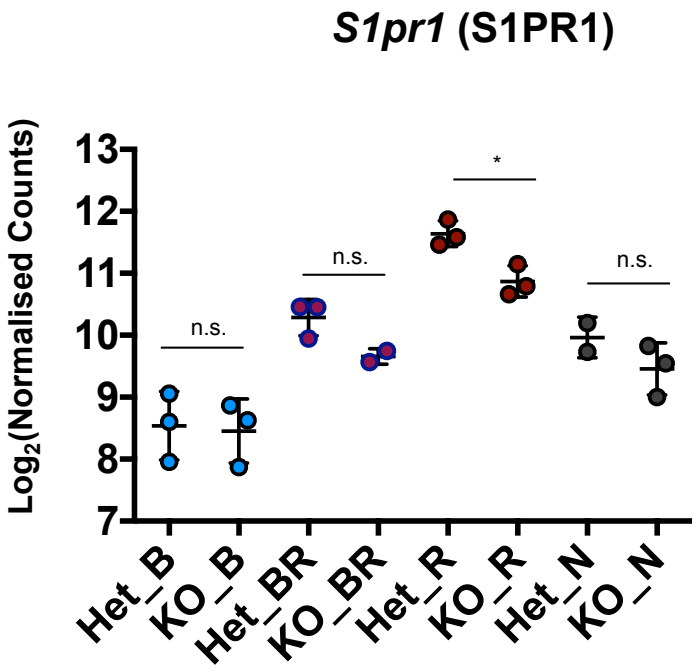

Figure 5.21: **Expression of *S1pr1* in Bim-sufficient and Bim-deficient cell populations.** Cells were sorted for RNAseq analysis from 6-7 weeks old $Bim^{WT/KO}$ and $Bim^{KO/KO}$ mice according to *Nr4a3*-Timer expression as described in Table 5.2. 2000 cells were sorted for each population and subjected to RNAseq. Normalised counts of the gene *S1pr1* coding for S1PR1 were obtained using the algorithm DESeq2. Data are shown as $\log_2$ of normalised counts. Error bars are representative of mean ± s.d, where n = 3 biological replicates. Individual comparisons between the two genotypes by Tukey's post-hoc analysis are shown as * for $p<0.05$, ** for $p<0.01$, *** for $p<0.001$ and **** for $p<0.0001$.

5.3 Discussion

The findings included in this chapter provide an overview of the temporal dynamics of T cell development at the SP stage. *Nr4a3*-Timer expression was detected in both CD4 and CD8 lineages and *Foxp3* was expressed by T cells with unique TCR signalling dynamics. While only 15-20% of the *Foxp3*$^-$ T cell pool expressed Timer proteins, almost all *Foxp3*$^+$ cells were Timer$^+$ and showed either persistent or arrested transcription of *Nr4a3*. Although T cells of the CD8 lineage consisted of a very small population of *Foxp3*$^+$ cells, their Timer expression pattern was similar to that of CD4 Treg. This suggests that *Foxp3* upregulation requires very specific TCR signalling dynamics, regardless of cell lineage.

Developing *Foxp3*$^-$ cells were the main focus of this chapter. CD69 was found to be a very good marker of immature T cells that most recently encountered their cognate antigen (Fig.5.5). Most CD69$^-$ T cells have been removed from antigen, terminating their Timer transcription. Some T cells may go through positive selection without expressing high levels of CD69. However, this is unlikely because CD69$^-$ T cells have Blue$^-$Red$^+$, but not Blue$^+$Red$^-$ cells, indicating that those cells joined the CD69$^-$ fraction after expressing Blue protein in the CD69$^+$ fraction.

There was a very remarkable difference in CD69 expression between CD4SP and CD8SP T cells, where the latter showed much lower levels (Fig.5.4). By using MHC-I-restricted TCR transgenic mice deficient in MHC-II ligands and CD5, a potent TCR signalling inhibitor, the Singer lab reported that artificially prolonged signalling erroneously diverts MHC-I restricted T cells to the CD4 lineage (Kimura et al. 2016). In Chapter II, it was shown that CD69 MFI increases as Blue protein becomes accumulated (Fig.4.1B). If the duration of TCR signals required for CD8 selection is much shorter than CD4SP, it is possible that CD8SP, on average, do not accumulate as many CD69 molecules as CD4SP, resulting in lower MFI values.

CD69^{+}CD4SP cells were sorted for RNAseq analysis to study their early stages of development at transcript level. Although Bim was shown to be upregulated in both DP and SP cells (Schmitz, Clayton and Reinherz, 2003), it was argued that Bim-mediated deletion is only required at the DP stage (Hu et al., 2009). The findings presented in this chapter disagree with this. Equivalently high Bim transcript levels were uniquely detected in DP and CD4SP cells that newly transcribe *Nr4a3*. Both populations showed nearly overlapping gene expression profiles on a heatmap that featured pro-apoptotic genes. Levels of CCR7 transcript differed greatly between Blue^{+}Red^{-} DP and CD4SP cells, where the former showed very little. This further highlights the fact that Bim-mediated negative selection occurs not only in the medulla, but also in the cortex (Stritesky et al., 2013). The reason why Bim-mediated deletion did not appear to have a great impact at the SP stage in the study by Hu et al. (Hu et al., 2009) could be attributed to the fact that Blue^{+}Red^{-} SP cells are a very small population, accounting for only about 3.5% of the total CD4SP T cell fraction and less that 2% in the case of CD8 (Fig.5.1). Given that only 1-3% of mature mTECs express one particular TRA (Derbinski et al., 2008) and the antigens they express frequently change due as many mTECs are removed and replaced each day (Gray et al., 2007), it is likely that only a very small T cell population encounters their cognate antigen at this stage. Therefore, if CD4SP are analysed in bulk, the effect of Bim on negative selection at the SP stage can be easily missed. Since DP cells in WT *Nr4a3*-Tocky mice only express Blue fluorescence, as shown in Chapter II, they can be analysed in bulk in order to detect Bim-mediated effects.

Based on the work so far presented in this thesis, a model for Timer^{+}CD4SP T cell development is proposed, where each cell that has strong affinity to its cognate antigen undergoes Bim-mediated negative selection, either in the cortex or in the medulla (Fig.5.22). CD4_N are a heterogenous population enriched with CD4_B precursors and cells with TCRs of too low affinity to express Timer proteins before migrating out of the

thymus. While CD4_R cells will eventually lose Timer protein expression and become Timer$^-$, the probability of this occuring in the thymus is quite small. The half-life of Red protein is approximately 5 days and mature CD4 T cells have been shown to vacate the medulla within a time-frame of 4-7 days, depending on the experimental design, where the latest studiest give more support to a shorter window (Rooke et al., 1997; McCaughtry, Wilken and Hogquist, 2007; Jin et al., 2008). Taken together with the fact that CD69$^-$CD4SP do express Red fluorescence (Fig.5.5), it is more likely that CD4_R cells downregulate CD69 and migrate out of the thymus before Red protein is completely decayed.

CD4_BR cells downregulated Bim transcription and highly expressed PD-1. Therefore, if self-reactive T cells that receive persistent TCR signals do not undergo apoptosis within approximately 4 hours, before Blue protein matures to Red, PD-1 becomes upregulated and further Bim transcription is repressed. DP_B cells were similarly enriched with PD-1 transcript, which was much lower in CD4_B. The fact that DP_B and CD4_BR have similar levels of PD-1 transcript that are significantly higher than CD4_B supports the possibility that some DP_B cells are the precursors of CD4_BR. CD4_B most likely arise from CD4_N cells that were positively selected following low-affinity antigen interactions and encountered their cognate antigen in the medulla. This implies that DP_B and CD4_B have different TCR repertoires.

At protein level, PD-1 was expressed in a similar manner by both CD4SP and CD8SP cells. PD-1 expression peaked in the Persistent locus became downregulated once cells terminated *Nr4a3* transcription. This implies that PD-1 contributes to the survival of cells that receive persistent signals irrespective of lineage. However, it is still unclear if PD-1 is directly involved in rescuing both CD4SP and CD8SP cells from Bim-mediated apoptosis, or if it acts in the same manner in both lineages. Bim-deficient CD4SP T cells behaved quite differently from CD8SP T cells. They showed a significant accumulation of

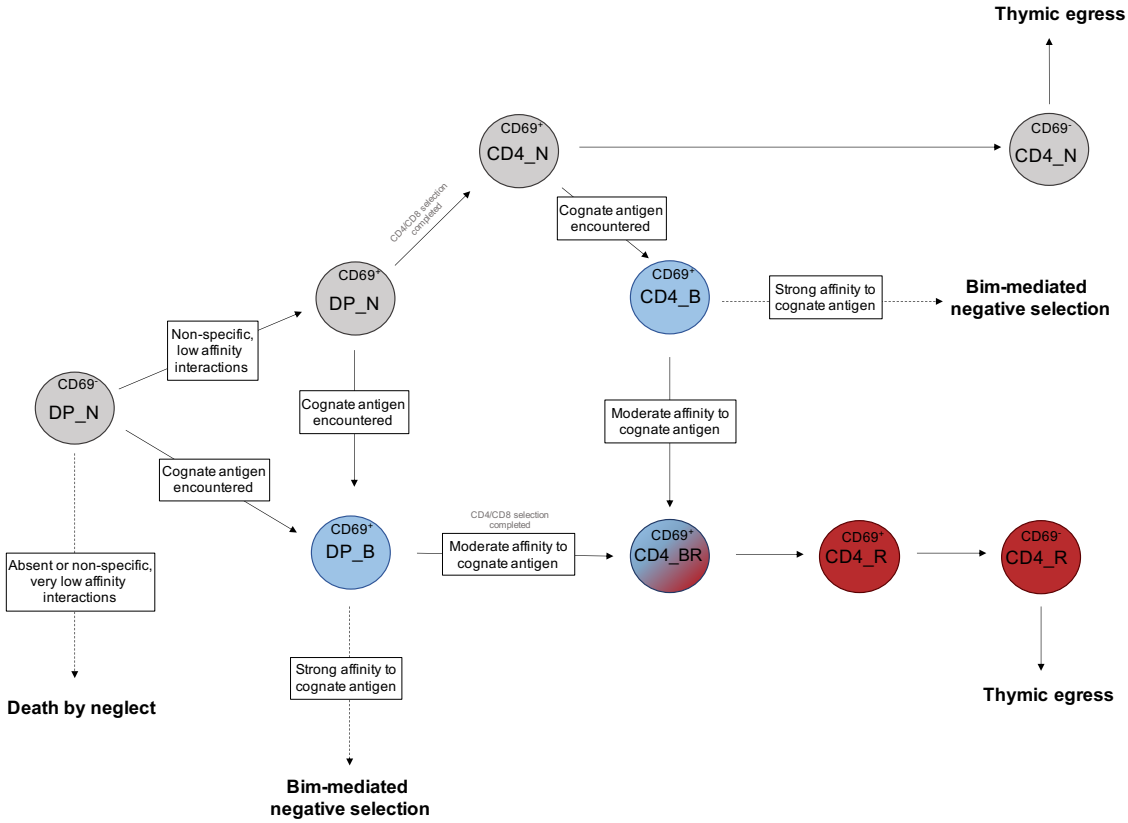

Figure 5.22: **Proposed model for *Nr4a3*-Timer^{+}CD69^{+}CD4SP thymic T cell development**. Figure shows a new model of Foxp3^{-}CD4 SP cell differentiation from the DP stage, where CD69 expression and *Nr4a3*-Timer maturation are used to identify key thymic developmental stages.

Timer^{+} cells in each Timer locus compared to the control, while in CD8SP the differences were not significant. PD-1 expression also differed. While in Bim-deficient CD4SP T cells it was slightly higher than the control, in CD8SP T cells it was lower. In the absence of Bim, DP cells that should have undergone apoptosis might preferentially join the CD4 lineage. This is supported by the fact that aberrantly prolonged TCR signals can trigger CD4SP T cell development from MHC-I-restricted cells (Kimura et al. 2016). If surface CD4 expression is dependent on the nature of TCR signals, this may be partly sensed by Bim. The different effect of Bim deficiency between cell lineage could also be the result of a slightly different scenario, in which the Bim-mediated negative selection pressure normally pushes some self-reactive cells towards the CD8 lineage and in its absence they become CD4.

In the absence of Bim, developing CD4SP had lower *Ccr7* transcript levels. In a study that used two-photon time-lapse microscopy imaging, positively selecting TCR-self-antigen interactions were associated with continuous migration of developing thymic T cells, while negatively selecting ones led to migratory arrest (Melichar et al., 2013). According to these findings, although in the absence of Bim some cells erroneously survive negative selection, their migratory properties are still affected, resulting in the observed diminished levels of *Ccr7* compared to the control. Bim-deficient Blue$^-$Red$^+$ cells also had less transcript levels of CD24 and S1PR1. This suggests that although self-reactive cells that receive very strong TCR signals survive in Bim-deficient mice, they are in a more immature state and their thymic egress is therefore delayed. This may contribute to the observed accumulation of Blue$^-$Red$^+$ cells in Bim-deficient mice (Fig.5.13).

What is rather surprising about the Bim-deficient populations is their aberrant upregulation of Bim transcript by cells that no longer receive TCR signals. Although very little, some Bim transcript was detected even in Timer$^-$, Bim-sufficient cells. It is therefore possible that low-level constitutive expression might be required by all developing thymocytes for housekeeping purposes. Since in the absence of Bim these effects would not be induced and cannot inhibit its further transcription, it is possible that by the time cells have completely ceased *Nr4a3* transcription, Bim transcript would have accumulated to the levels detected in this study.

Based on the collective data presented in chapters II and III, a model is proposed for the development of Bim-deficient CD4 lineage-committed thymocytes (Fig.5.23). In this model, CD4_R cells are a heterogenous population comprised of the cells which naturally survive negative selection, as well as highly self-reactive thymocytes that are fated for Bim-mediated apoptosis at the DP_B or CD4_B stages of development.

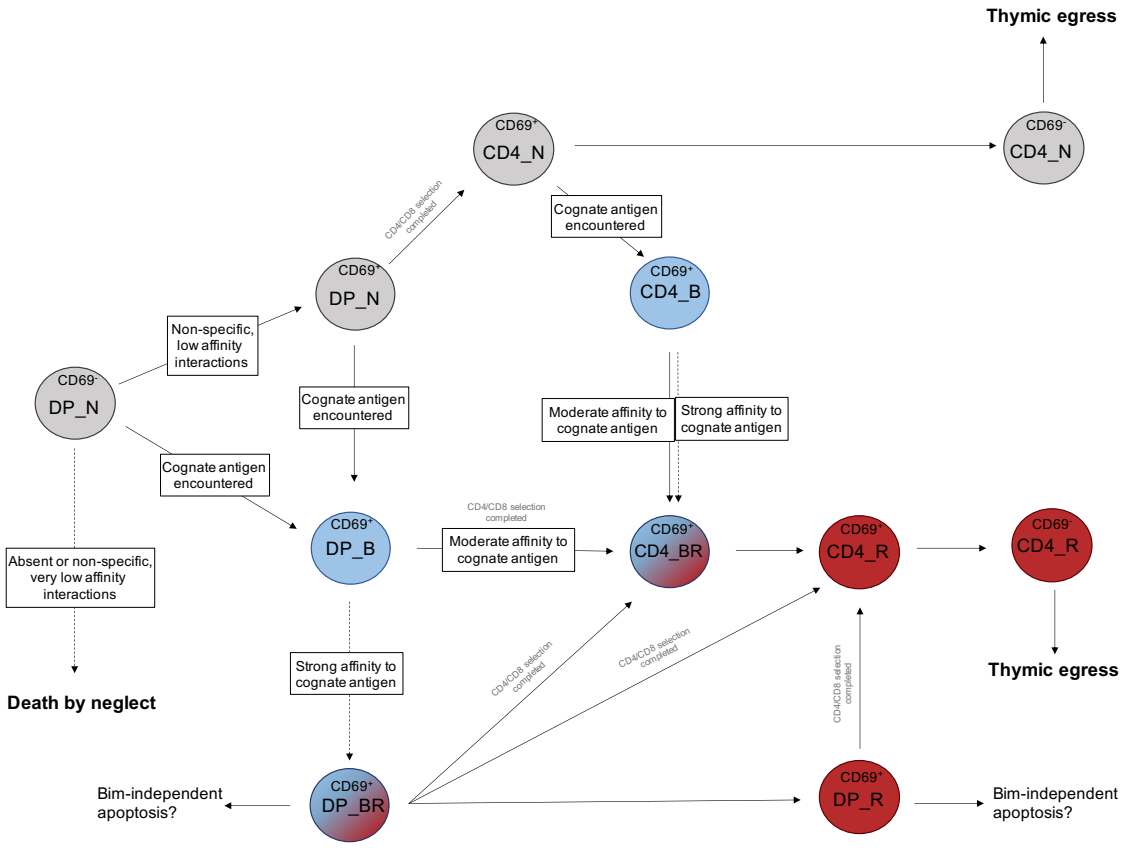

Figure 5.23: **Proposed model for Bim-deficient *Nr4a3*-Timer^{+}CD69^{+}CD4SP thymic T cell development.** Figure shows a new model of Foxp3^{-}CD4 SP cell differentiation from the DP stage in Bim-deficient mice, where CD69 expression and *Nr4a3*-Timer maturation are used to identify key thymic developmental stages.

Chapter IV: TCR signalling and *Foxp3* transcription dynamics of developing thymic Treg

6.1 Introduction

A small fraction of developing T cells differentiate into Treg in the thymus and migrate to the periphery, where they play different roles in maintaining homeostasis. The $CD25^{+}Foxp3^{+}$ phenotype is associated with their suppressive functions in preventing misdirected immune responses and ablation of either marker results in fatal autoimmune disease (Chinen et al., 2016; Ramsdell, 2003). Foxp3-expressing $CD25^{-}$ cells with regulatory properties have also been reported in the literature (Annacker et al., 2001; Lehmann et al., 2002; Alyanakian et al., 2003), but their ontogeny and functional significance are not well understood. Although they were less potent than $CD25^{+}Foxp3^{+}$ populations, $CD25^{-}Foxp3^{+}$ cells were shown to be actively involved in suppressing autoimmunity in the periphery (Ono et al., 2006). Peripheral $CD25^{-}Foxp3^{+}$ cells were also shown to acquire the $CD25^{+}Foxp3^{+}$ phenotype during homeostatic expansion and activation, becoming fully functional. Based on this finding, it was postulated that they act as a natural reservoir of differentiated Treg (Zelenay et al., 2005).

The studies mentioned so far exclusively investigated CD4 SP populations. $Foxp3^{+}$CD8 SP also develop naturally in the thymus. However, this population is very small in comparison and its significance is far less understood (Vuddamalay et al., 2016). This chapter

will mainly focus on CD4$^+$ Treg, while also addressing the developmental requirements of the less studied *Foxp3*$^+$CD8 SP cell pool.

6.1.1 CD4$^+$ Treg

The Palmer lab classified thymic, *de novo* generated, self-reactive CD4$^+$ Treg into Triple^{hi} and Triple^{lo} populations based on their expression of GITR, PD-1 and CD25. Their TCR repertoires were significantly different from *Foxp3*$^-$ T cells, as well as from each other. Triple^{hi} cells expressed higher levels of Nr4a1-GFP and overall appeared more self-reactive and proliferative than Triple^{lo} Treg. The two populations were also functionally distinct, with non-overlapping properties: Triple^{hi} cells limited lymphoproliferation in peripheral lymph nodes, while Triple^{lo} cells suppressed colitis in lymphopenic conditions by promoting conversion of *Foxp3*$^-$ T cells into Treg. The authors concluded that Treg precursors can have stronger or weaker TCR affinity to self-antigen, which promotes the development of Foxp3$^+$ populations with different properties (Wyss et al., 2016).

Notably, the Farrar lab recently proposed the existence of two distinct developmental thymic CD4$^+$ Treg programs based on major differences observed between the CD25$^+$Foxp3$^-$ and CD25$^-$Foxp3^{lo}/Foxp3$^+$ thymic populations (Owen et al., 2019), previously identified as Treg precursor candidates (Lio and Hsieh, 2008; Tai et al., 2013). This is an attractive explanation for the development of the previously described Triple^{hi} and Triple^{lo} Treg (Wyss et al., 2016). Not only were the precursors found to have distinct TCR repertoires, but also the ones positive for CD25 expressed higher Nr4a1-GFP levels and had higher affinity to self-antigen. They also showed functional differences, when CD25$^+$Foxp3$^-$ cells could suppress EAE, while CD25$^-$Foxp3^{lo} failed to do so (Owen et al., 2019). It is therefore possible that some CD25$^+$Foxp3$^-$ cells develop into Triple^{hi} Treg and CD25$^-$Foxp3^{lo} into Triple^{lo} Treg.

Once major challenge to this theory is the fact that, unlike Triple^{lo} Treg, the CD25$^-$Foxp3^{lo}

population was originally found to express high levels of GITR and OX40 (Tai et al., 2013). Another issue is the fact that CD25^{-}Foxp3^{lo} cells were defined as Treg precursors based on their ability to upregulate Foxp3 upon stimulation with very little amounts of IL-2 in vitro and upon intrathymic injection in vivo (Tai et al., 2013; Owen et al., 2019). However, this does not necessarily render them as *de novo* precursors and leaves open the possibility that they are mature cells with different developmental requirements.

Using Nr4a3-Tocky, the Ono lab showed that CD25^{+}Foxp3^{-}CD4^{+} cells temporally precede the CD25^{+}Foxp3^{+}CD4^{+} and CD25^{-}Foxp3^{+}CD4^{+} populations in receiving TCR signals and that they are the major precursor of mature Treg that have received strong, persistent signals. The study also revealed that the CD25^{-}Foxp3^{+}CD4^{+} pool featured aborted TCR signals and likely comprised of Foxp3^{+} cells that had received weaker and less sustained TCR signals (Bending et al., 2018). Surface marker analysis also showed that CD25^{-}Foxp3^{+}CD4^{+} cells are in a more mature state than CD25^{+}Foxp3^{-}CD4^{+} cells and according to a RAG2-GFP reporter, they develop at the same time as CD25^{+}Foxp3^{+}CD4^{+} cells (Owen et al., 2019).

6.1.2 CD8^{+} Treg

"CD8^{+} suppressor cells" is an umbrella term for T cells of the CD8 lineage that elicit immunosuppressive functions. Only a small subset express Foxp3 and no specific marker that unambiguously distinguishes them from effector CD8^{+} cells has been found. It was demonstrated that they develop in the thymus and require MHC-I expression on stromal cells. The same study found them to develop concomitantly with the other CD8^{+} T cells (Vuddamalay et al., 2016). The Annunziato lab identified a subset of CD25^{+}CD8^{+} T cells in human thymi that shared transcriptional characteristics with CD25^{+}CD4^{+} T cells, including constitutive mRNA expression of FOXP3 and GITR. In CD4 and CD8 T cells that were negative for CD25 the two transcripts were barely, if at all, detected (Cosmi et al., 2003). Churlaud et al. characterised CD25^{+}Foxp3^{+}CD8^{+} T

cells in both mice and humans. Their surface expression of CD25 molecules was lower than that of $CD25^{+}Foxp3^{+}CD4^{+}$ T cells. Using an in vitro culture assay in mice, they found them to be slightly more suppressive of effector $CD4^{+}$ T cell proliferation than $CD25^{+}Foxp3^{+}CD4^{+}$ T cells (Churlaud et al., 2015).

6.1.3 Chapter aims

Treg have unique developmental properties, where their differentiation relies on TCR signals that are much stronger than the ones received by mature *Foxp3*$^{-}$ T cells, but not potent enough to trigger negative selection. However, the relationship between their TCR signalling and *Foxp3* transcriptional dynamics has not been clarified. Precisely how CD4/CD8 lineage choice, CD25 expression levels and disrupted negative selection affect TCR signalling requirements and *Foxp3* transcriptional dynamics is also ambiguous. In this chapter, the *Nr4a3* and *Foxp3*-Tocky systems are used to clarify these aspects by addressing the following aims:

(I) To study the transcriptome of CD4 Treg according to their temporally dynamic changes in *Nr4a3* transcription

(II) To assess the temporally dynamic changes in *Nr4a3* and *Foxp3* transcription according to the level of CD25 expressed by Treg

(III) To compare the developmental requirements of CD4 and CD8 Treg

(IV) To investigate the impact of Bim deficiency on CD4 and CD8 Treg development

6.2 Results

6.2.1 Transcript analysis of developing *Foxp3*$^+$CD4 SP populations

The *Nr4a3*-Tocky system was used to study the development of *Foxp3*$^+$CD4 SP cells at transcript level according to temporally dynamic changes in transcription. Since CD69 was found to be upregulated in SP cells which most recently received TCR signals from their cognate antigens (Chapter III), the following CD69$^+$ populations were sorted for RNAseq analysis (gating strategy shown in Fig.6.1): Blue$^+$Red$^-$*Foxp3*$^-$CD4 SP (CD4_B), Blue$^+$Red$^+$*Foxp3*$^-$CD4 SP (CD4_BR), Blue$^+$Red$^+$*Foxp3*$^+$CD4 SP (Foxp3_BR) and Blue$^-$Red$^+$*Foxp3*$^+$CD4 SP (Foxp3_R). Because *Foxp3* is only induced after Timer proteins become accumulated (Chapter III), CD4_B and CD4_BR are enriched with early and immediate Fox_BR precursors, respectively.

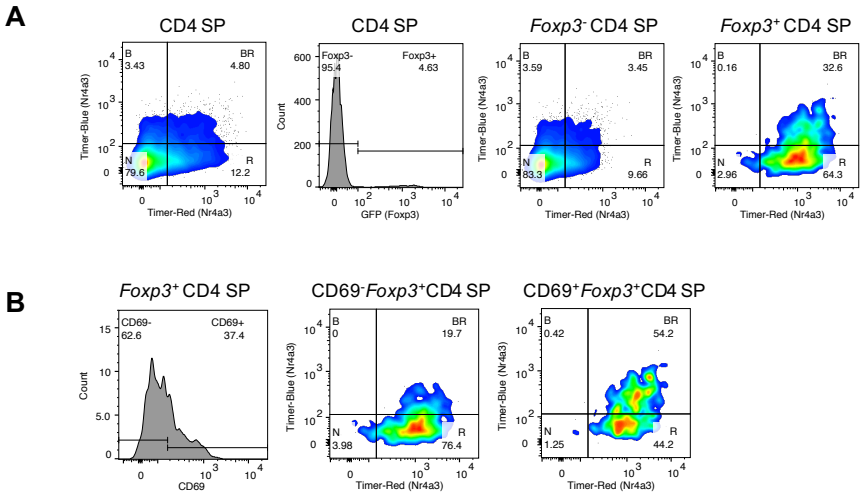

Figure 6.1: ***Nr4a3*-Timer protein expression by *Foxp3*$^+$CD4 SP cells**. Thymocytes from 4 weeks old *Nr4a3*-Tocky mice were analysed by flow cytometry on a Fortessa III instrument. Histograms show gating by strategy for (A) *Foxp3*$^-$ and *Foxp3*$^+$CD4SP and for (B) CD69$^-$ and CD69$^+$*Foxp3*$^+$ CD4SP. 2-D plots show *Nr4a3*-Timer protein expression of each defined population. Data shown are representative of at least 4 independent experiments that used 2-4 mice per group.

On a PCA plot of gene expression data, cell populations clustered most closely according to *Foxp3* expression, not Timer fluorescence. This suggests that *Foxp3* transcription leads to more transcriptomic changes in CD4 SP populations than persistent *Nr4a3* transcription.

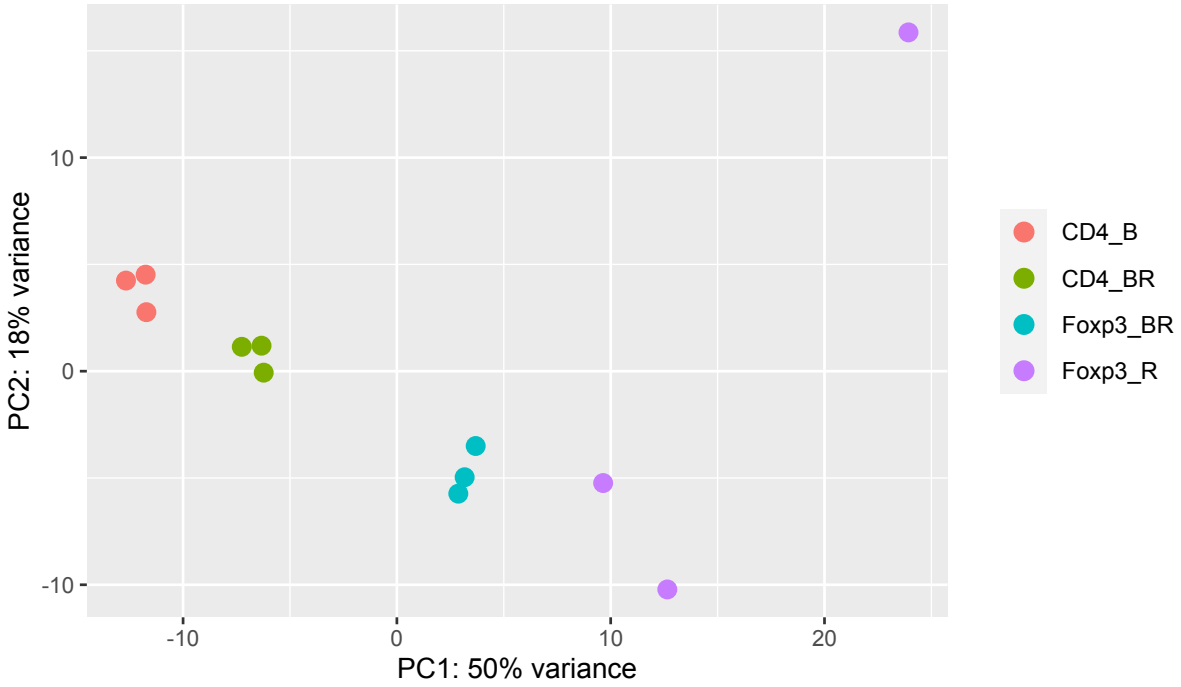

Figure 6.2: **PCA of the transcriptome of developing *Foxp3*$^+$ CD4SP cells.** CD69$^+$ T cell populations were sorted from 8 weeks old *Nr4a3*-Tocky mice for RNAseq analysis according to *Foxp3*-GFP and *Nr4a3*-Timer protein expression as follows: Blue$^+$Red$^-$*Foxp3*$^-$CD4 SP (CD4_B), Blue$^+$Red$^+$*Foxp3*$^-$CD4 SP (CD4_BR), Blue$^+$Red$^+$*Foxp3*$^+$CD4 SP (Foxp3_BR) and Blue$^-$Red$^+$*Foxp3*$^+$CD4 SP (Foxp3_R). 1000 cells were sorted for each population and subjected to RNAseq. Normalised counts of expressed genes were obtained using the algorithm DESeq2 and a PCA plot of their transcriptomes is shown.

The levels of *Nr4a3* transcript were similar between CD4_BR and Foxp3_BR (Fig.6.3). They also shared similar PD-1 transcript levels (Fig.6.4). PD-1 transcript was shown in the previous chapter to become downregulated once *Foxp3*$^-$CD4 SP cells no longer transcribe *Nr4a3*. Foxp3_R cells, however, maintained its expression. This suggests that self-reactive *Foxp3*$^+$CD4 SP cells require constitutive PD-1 expression for complete de-

velopment. The gradual increase in *Ccr7* from CD4_B to CD4_BR to Foxp3_BR suggests that *Foxp3* becomes upregulated as cells migrate deeper into the medulla.

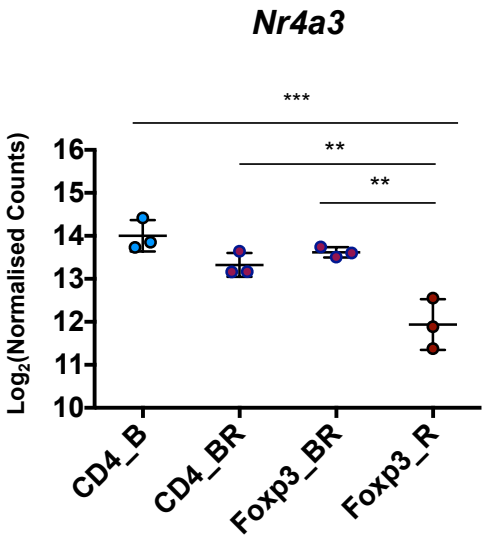

Figure 6.3: **Summary data of *Nr4a3* transcript levels in developing *Foxp3*$^+$CD4 SP cells.** Cells were sorted for RNAseq analysis from the thymus of 8 weeks old *Nr4a3*-Tocky mice according to *Nr4a3*-Timer expression as described in Fig.6.2. 1000 cells were sorted for each population and subjected to RNAseq. Normalised counts of the gene *Nr4a3* were obtained using the algorithm DESeq2. Data are shown as $\log_2$ of normalised counts. Error bars are representative of mean ± s.d, where n = 3 biological replicates. Only statistically significant differences by Tukey's post-hoc analysis are shown as solid lines as ** for $p<0.01$ and *** for $p<0.001$.

Where CD4_BR and Foxp3_BR cells differed considerably was in their transcript levels of TNFRSF members. The heatmap in Fig.6.6 shows all family members that were upregulated by any of the investigated populations. DR3, CD30, GITR and OX40 transcripts were much more highly expressed by *Foxp3*$^+$ cells. Herpesvirus entry mediator (HVEM) was preferentially upregulated by Foxp3_R, while 4-1BB was exclusively induced by cells receiving TCR signals. TNFR2 transcript expression appeared quite heterogenous, despite its associated role with Treg development (Faustman and Davis, 2013).

In the previous chapter, it was shown that Bim-deficient *Foxp3*$^-$CD4SP cells constitutively transcribe *Bcl2l11*, even after TCR signals have ceased. Here, *Foxp3*$^+$ cells had the lowest

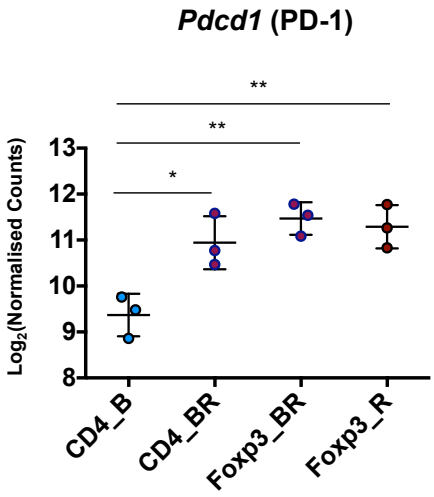

Figure 6.4: **Summary data of *Pdcd1* transcription by developing *Foxp3*$^+$CD4 SP cells.** Cells were sorted for RNAseq analysis from the thymus of 8 weeks old *Nr4a3*-Tocky mice according to *Nr4a3*-Timer expression as described in Fig.6.2. 1000 cells were sorted for each population and subjected to RNAseq. Normalised counts of the gene coding *Pdcd1* for PD-1 were obtained using the algorithm DESeq2. Data are shown as $\log_2$ of normalised counts. Error bars are representative of mean ± s.d, where n = 3 biological replicates. Only statistically significant differences by Tukey's post-hoc analysis are shown as solid lines as * for $p<0.05$ and ** for $p<0.01$.

levels of Bim transcript, but these were maintained between Foxp3_BR and Foxp3_R stages of development (Fig.6.7). This led to the question of whether Bim deficiency has an impact on *Foxp3*$^+$CD4 SP development.

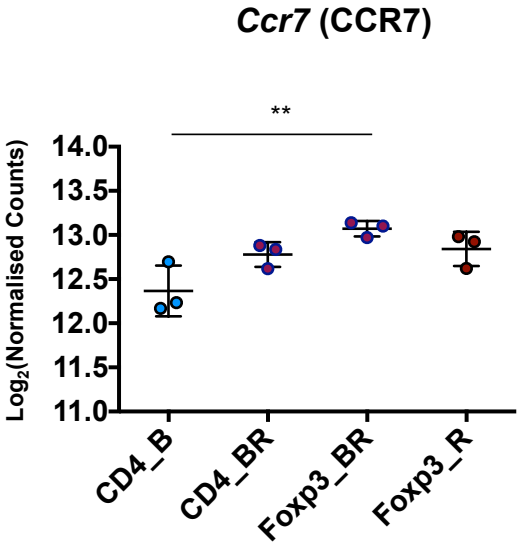

Figure 6.5: **Summary data of *Ccr7* transcription by developing *Foxp3*$^+$ CD4SP cells.** Cells were sorted for RNAseq analysis from the thymus of 8 weeks old *Nr4a3*-Tocky mice according to *Nr4a3*-Timer expression as described in Fig.6.2. 1000 cells were sorted for each population and subjected to RNAseq. Normalised counts of the gene *Ccr7* encoding the chemokine CCR7 were obtained using the algorithm DESeq2. Data are shown as $\log_2$ of normalised counts. Error bars are representative of mean ± s.d, where n = 3 biological replicates. Only statistically significant differences by Tukey's post-hoc analysis are shown as solid lines as ** for $p<0.01$.

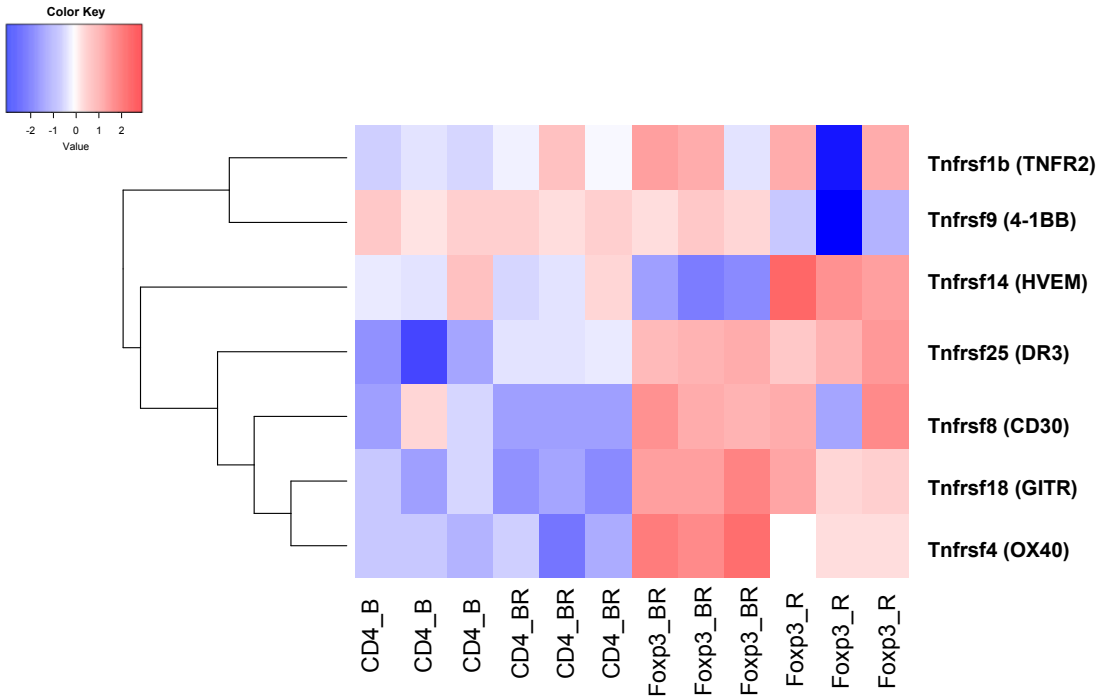

Figure 6.6: **Differentially expressed TNFRSF members by developing *Foxp3*$^+$ CD4SP cells.** Cells were sorted for RNAseq analysis from the thymus of 8 weeks old *Nr4a3*-Tocky mice according to *Nr4a3*-Timer expression as described in Fig.6.2. 1000 cells were sorted for each population and subjected to RNAseq. Normalised counts of expressed genes were obtained using the algorithm DESeq2. Heatmap analysis of differential gene expression of several members of the TNFRSF is shown. The heatmap was scaled across genes.

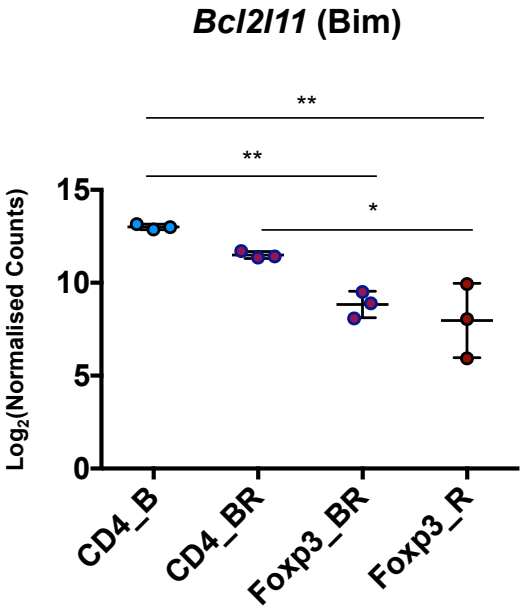

Figure 6.7: **Summary data of *Bcl2l11* transcription by developing *Foxp3*$^+$ CD4SP.** RNA was extracted from CD69$^+$ cells from 8 weeks old *Nr4a3*-Tocky mice according to *Foxp3*-GFP and Timer protein expression, as described in Fig.6.2. Normalised counts of the gene *Bcl2l11* encoding the pro-apoptotic molecule Bim were obtained using the algorithm DESeq2. Error bars are representative of mean ± s.d, where n = 3 biological replicates. Only statistically significant differences by Tukey's post-hoc analysis are shown as solid lines as * for $p<0.05$ and ** for $p<0.01$.

6.2.2 The effect of Bim deficiency on developing *Foxp3*$^+$ CD4SP cells

Bim$^{KO/KO}$ *Nr4a3*-Tocky mice (KO) were used to investigate any possible implications of Bim expression in the development of *Foxp3*$^+$CD4SP cells. Their Timer protein expression patterns are compared in Fig.6.8A against Bim$^{WT/KO}$ mice (Het), which were used as control. From these data alone, Bim deficiency appeared to have a much more dramatic impact on *Foxp3*$^-$ cells compared to *Foxp3*$^+$ ones, which did not seem to be much affected in terms of Timer expression patterns. There was a significant increase, however, in both the absolute cell number and percentage of *Foxp3*$^+$CD4SP cells in KO mice compared to Het (Fig.6.8B).

Although Timer angle values of Het and KO *Foxp3*$^+$CD4 SP populations were very similar (Fig.6.9A), Timer intensity, was significantly higher in KO cells (Fig.6.9B). Timer locus analysis revealed that KO *Foxp3*$^+$CD4 SP cells have slightly different *Nr4a3*-Timer expression dynamics. Specifically, a significantly higher proportion of cells were captured in the PAt locus of KO cells (Fig.6.10). Collectively, this indicates that a part of *Foxp3*$^+$CD4 SP that receive persistent TCR signals are deleted in a Bim dependent manner.

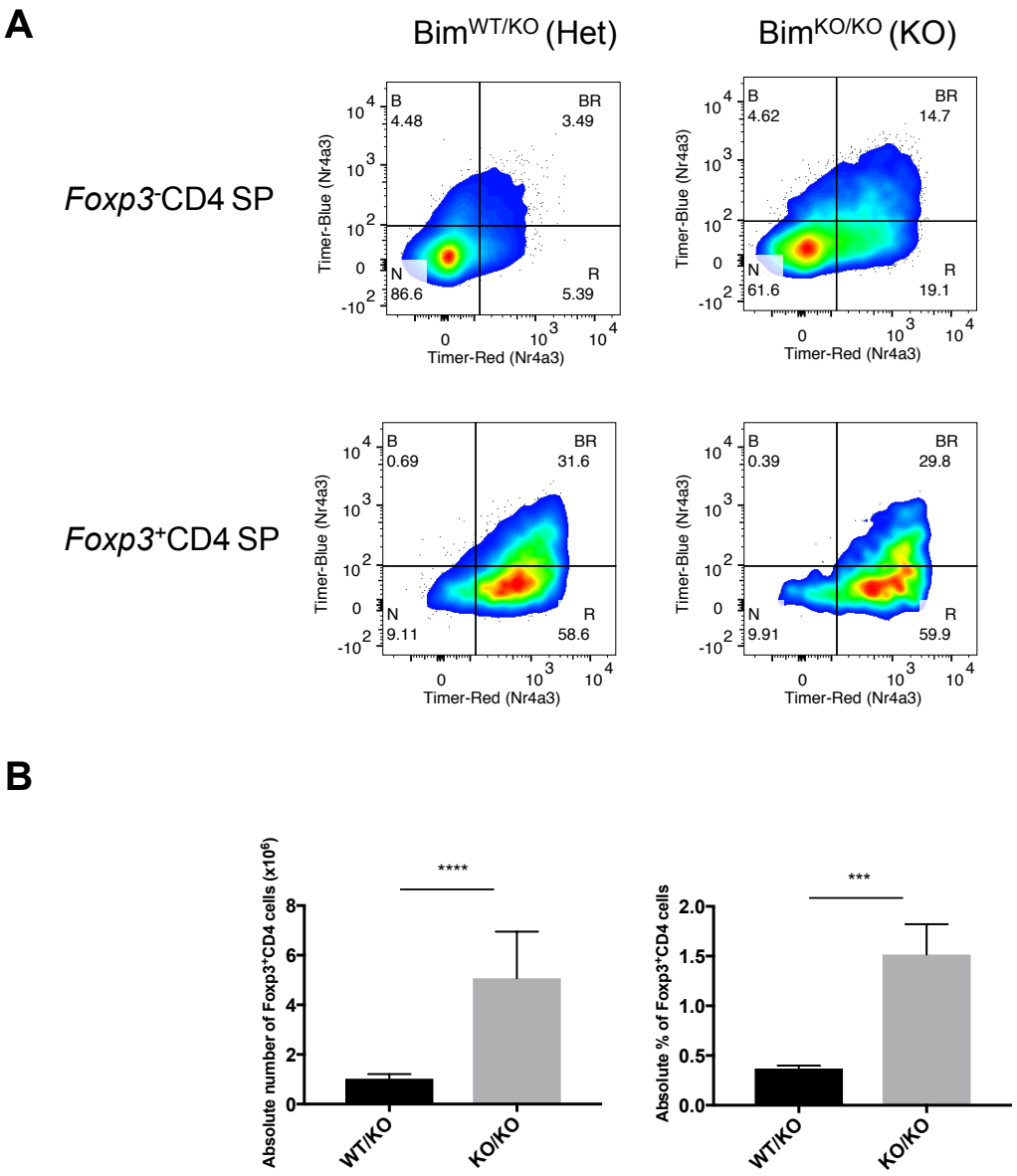

Figure 6.8: ***Nr4a3*-Timer protein expression by Bim-deficient developing CD4SP cells**. Thymocytes were harvested from 6 weeks old *Nr4a3*-Tocky:Bim$^{WT/KO}$ or *Nr4a3*-Tocky:Bim$^{KO/KO}$ mice and were analysed by flow cytometry on a Fortessa III instrument. **(A)** For each genotype, *Nr4a3*-Timer expression is shown in *Foxp3*$^-$CD4 SP and *Foxp3*$^+$CD4 SP fractions. Data shown are representative of at least 4 independent experiments that used 2-4 mice per group. All mice used were *Foxp3*-GFP. **(B)** Absolute numbers of *Foxp3*$^+$CD4 cells are shown for each genotype, followed by their absolute percentage in the thymus. Data are a summary of three independent experiments, where 2-3 mice per group were used. Error bars are representative of mean ± s.d, where n = 8 total biological replicates. Statistically significant differences from unpaired Student's t-test are shown as *** for $p<0.001$ (performed on absolute count data) and from Mann-Whitney U test as **** for $p<0.0001$ (performed on percentage data).

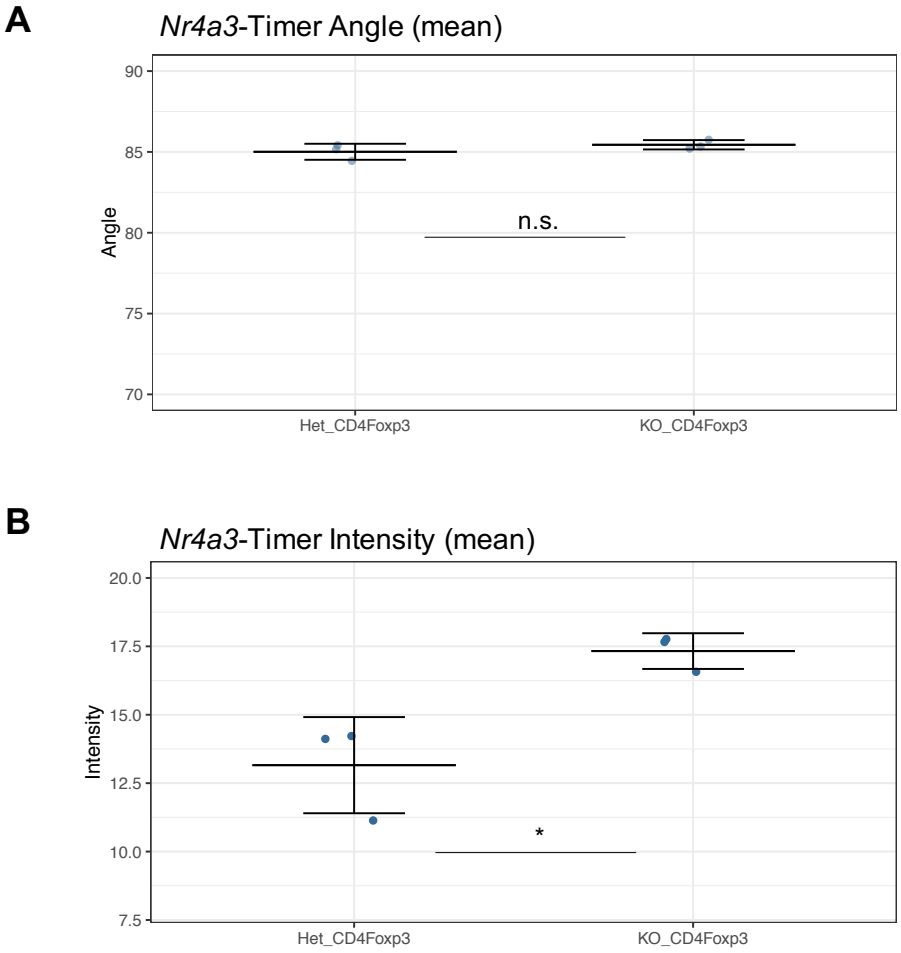

Figure 6.9: **Mean Timer angle and intensity of Bim-deficient *Foxp3*$^+$CD4SP cells**. Thymocytes were harvested from 6 weeks old *Nr4a3*-Tocky:Bim$^{WT/KO}$ or *Nr4a3*-Tocky:Bim$^{KO/KO}$ mice and were analysed by flow cytometry on a Fortessa III instrument. Mean *Nr4a3*-Timer angle (A) and intensity (B) are shown for two populations: *Foxp3*$^+$CD4 SP Bim$^{WT/KO}$ (Het_CD4Foxp3) and *Foxp3*$^+$CD4 SP Bim$^{KO/KO}$ (KO_CD4Foxp3). Statistically significant differences from unpaired Student's t-test are shown as * for $p<0.05$. Error bars are representative of mean ± s.d, where n = 3 biological replicates for each genotype. Data shown are representative of at least 4 independent experiments that used 2-4 mice per group. All mice used were *Foxp3*-GFP.

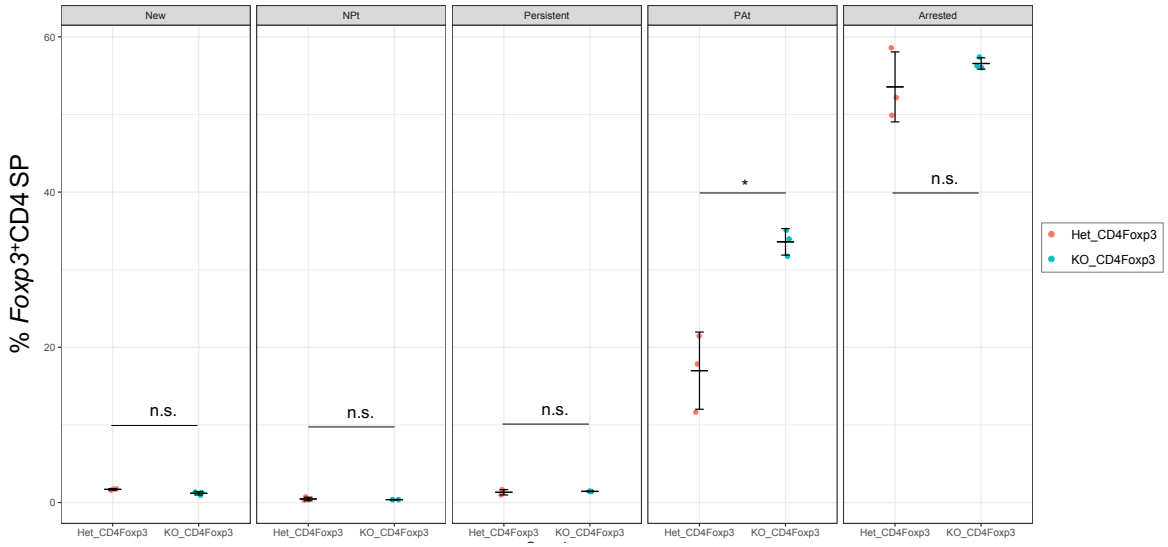

Figure 6.10: **Frequency of Bim-deficient *Foxp3*$^{+}$SP cells in each *Nr4a3*-Timer locus.**. *Foxp3*$^{+}$CD4 SP cells from 6 weeks old Bim$^{WT/KO}$ (Het_CD4Foxp3) and Bim$^{KO/KO}$ mice (KO_CD4Foxp3) were analysed by flow cytometry on a Fortessa III instrument. The percentage of cells in each Timer locus among their parent population is shown by scatter plot. Statistically significant differences from unpaired Student's t-test analysis are shown as * for $p<0.05$. Error bars are representative of mean ± s.d, where n = 3 biological replicates for each genotype. Data shown are representative of at least 4 independent experiments that used 2-4 mice per group. All mice used were *Foxp3*-GFP.

To investigate the impact of Bim deficiency on CD4 SP cells that recently upregulated *Foxp3*$^+$ following persistent TCR signals, CD69$^+$*Foxp3*$^+$CD4 SP cells were sorted from KO and Het mice according to Timer protein expression as follows: Blue$^+$Red$^+$Bim$^{WT/KO}$ (Het_FoxBR), Blue$^+$Red$^+$Bim$^{KO/KO}$ (KO_FoxBR), Blue$^-$Red$^+$Bim$^{WT/KO}$ (Het_FoxR) and Blue$^-$Red$^+$Bim$^{KO/KO}$ (KO_FoxR). On a PCA plot of gene expression data, the difference between cells with or without active *Nr4a3* transcription (shown by the PC2 axis) was much larger than the difference between genotypes (shown by the PC1 axis, Fig.6.11). This indicates that between-genotype variations are largely dominated by between-population variations.

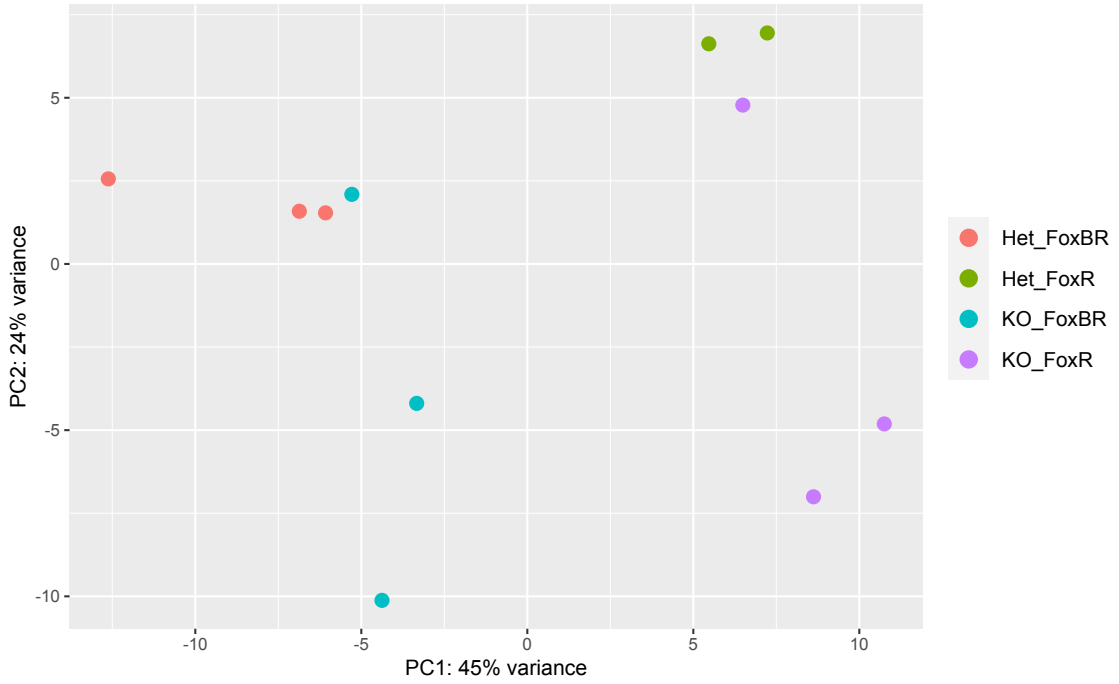

Figure 6.11: **PCA of gene expression data from Bim-sufficient and Bim-deficient *Foxp3*$^+$CD4 SP cells.** CD69$^+$*Foxp3*$^+$CD4 SP cell populations were sorted from 6-7 weeks old Bim$^{WT/KO}$ and Bim$^{KO/KO}$ *Nr4a3*-Tocky mice according to Timer protein expression as follows: Blue$^+$Red$^+$Bim$^{WT/KO}$ (Het_FoxBR), Blue$^+$Red$^+$Bim$^{KO/KO}$ (KO_FoxBR), Blue$^-$Red$^+$Bim$^{WT/KO}$ (Het_FoxR) and Blue$^-$Red$^+$Bim$^{KO/KO}$ (KO_FoxR). 2000 cells were sorted for each population and subjected to RNAseq. Normalised counts of expressed genes were obtained using the algorithm DESeq2 and a PCA plot of their transcriptomes is shown.

There was a significant increase in Bim transcript levels in KO cells (Fig.6.12). This

indicates a negative feedback effect of Bim protein on its transcription.

According to the heatmap in Fig.6.13, there was no genotype effect on the overall TNFRSF gene expression. The only exception was the transcript of CD30, a co-stimulatory molecule which might be involved in caspase-1 and caspase-3-dependent thymic programmed cell death (Chiarle et al., 1999). CD30 transcript appeared to be preferentially expressed by KO_FoxBR cells. However, no significant differences in its expression were found between genotypes according to p-adjusted value (Fig.6.14).

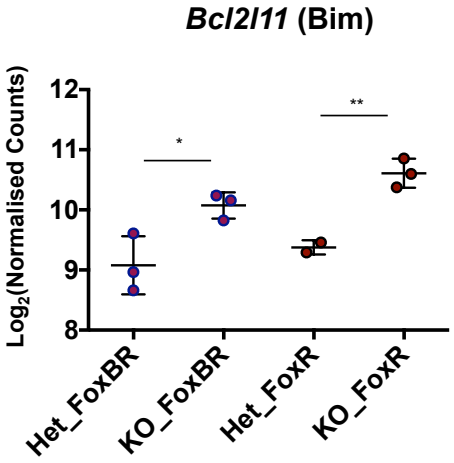

Figure 6.12: **Summary data of *Bcl211* transcription in Bim-sufficient and Bim-deficient *Foxp3*$^+$CD4 SP cells.** CD69$^+$*Foxp3*$^+$CD4 SP cells were sorted for RNAseq analysis from 6-7 weeks old Bim$^{WT/KO}$ and Bim$^{KO/KO}$ mice according to *Nr4a3*-Timer expression as described in Fig.6.11. 2000 cells were sorted for each population and subjected to RNAseq. Normalised counts of expressed genes were obtained using the algorithm DESeq2. Normalised counts of the gene *Bcl2l11* were obtained using the algorithm DESeq2. Data are shown as $\log_2$ of normalised counts. Error bars are representative of mean $\pm$ s.d, where n = 3 biological replicates. Individual comparisons between the two genotypes by Tukey's post-hoc analysis are shown as * for $p<0.05$ and ** for $p<0.01$.

Very few genes were in fact differentially expressed between Bim-sufficient and Bim-deficient cells when a threshold of adjusted p value of <0.05 was applied (Fig.6.14 and Fig.6.15). Apart from the gene encoding for Bim, the only one which was found to be of particular biological significance in the context of this study was *Il2ra*, encoding the CD25 molecule. KO cells which have terminated transcription showed significantly lower levels of CD25 transcript Fig.6.16. Bim deficiency, therefore, may lead to an accumulation of

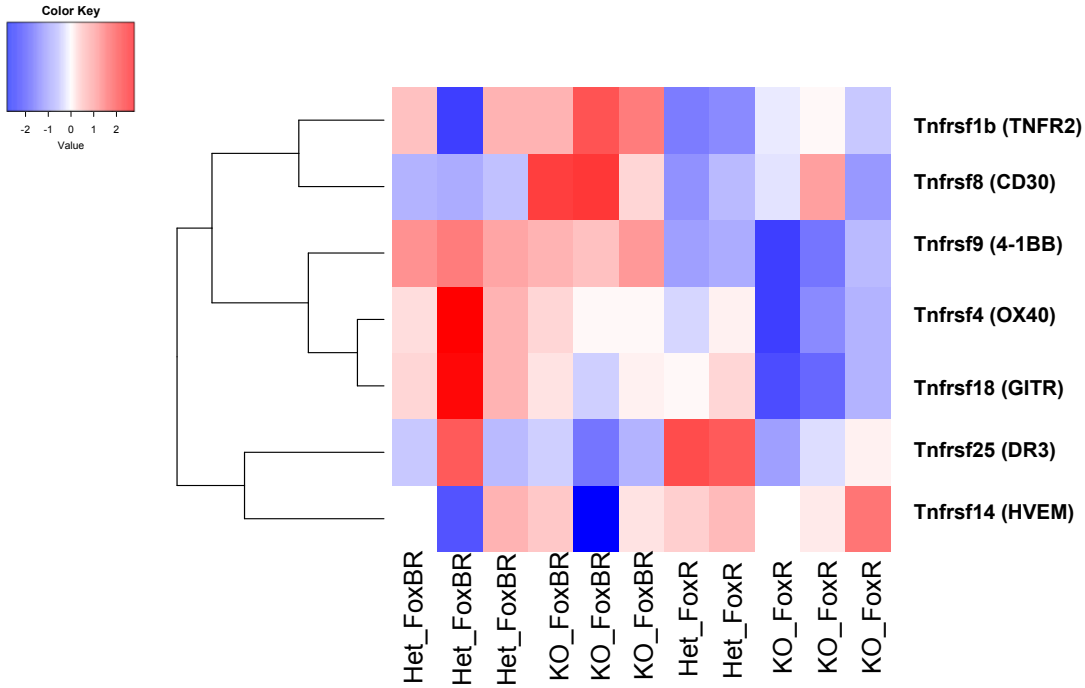

Figure 6.13: **Differentially expressed TNFRSF members by Bim-sufficient and Bim-deficient *Foxp3*$^+$CD4 SP cells.** CD69$^+$*Foxp3*$^+$CD4 SP cells were sorted for RNAseq analysis from 6-7 weeks old Bim$^{WT/KO}$ and Bim$^{KO/KO}$ mice according to *Nr4a3*-Timer expression as described in Fig.6.11. 2000 cells were sorted for each population and subjected to RNAseq. Normalised counts of expressed genes were obtained using the algorithm DESeq2. Heatmap analysis of differential gene expression of several members of the TNFRSF is shown. The heatmap was scaled across genes.

CD25$^-$*Foxp3*$^+$ cells. To further address this, this study first sought to investigate the relationship between CD25 levels of expression and the dynamics of TCR signalling and *Foxp3* transcription of developing *Foxp3*$^+$CD4 SP.

EntrezID	ENSEMBL	GeneSymbol	baseMean	log2FoldChange	lfcSE	stat	pvalue	padj
14584	ENSMUSG00000020363	Gfpt2	16.12	-7.48	1.69	-4.43	9.52E-06	0.0076
12876	ENSMUSG00000037852	Cpe	14.74	-6.78	1.64	-4.14	3.44E-05	0.0181
70729	ENSMUSG00000038473	Nos1ap	21.64	-6.58	1.73	-3.81	0.00014	0.0485
16562	ENSMUSG00000020821	Kif1c	42.07	-6.05	1.27	-4.76	1.97E-06	0.0024
223739	ENSMUSG00000036046	5031439G07Rik	28.38	-5.26	1.08	-4.87	1.11E-06	0.0017
208440	ENSMUSG00000048264	Dip2c	42.06	-3.28	0.72	-4.54	5.75E-06	0.0055
65967	ENSMUSG00000033216	Eefsec	511.87	-1.22	0.31	-3.98	6.87E-05	0.0301
227298	ENSMUSG00000049339	Retreg2	404.53	-1.15	0.27	-4.28	1.89E-05	0.0121
68539	ENSMUSG00000034659	Tmem109	488.92	-1.13	0.25	-4.48	7.41E-06	0.0063
22695	ENSMUSG00000044786	Zfp36	538.41	0.76	0.20	3.82	0.00013	0.0478
67287	ENSMUSG00000025237	Parp6	416.84	0.93	0.23	4.12	3.75E-05	0.0181
76793	ENSMUSG00000050213	Snip1	364.23	0.96	0.23	4.15	3.37E-05	0.0181
12125	ENSMUSG00000027381	Bcl2l11	1066.61	1.28	0.33	3.95	7.92E-05	0.0336
79233	ENSMUSG00000046556	Zfp319	311.48	1.49	0.36	4.14	3.48E-05	0.0181
73182	ENSMUSG00000028073	Pear1	323.51	1.85	0.48	3.85	0.00012	0.0444
12121	ENSMUSG00000003452	Bicd1	184.92	2.46	0.53	4.60	4.21E-06	0.0044
11816	ENSMUSG00000002985	Apoe	293.00	2.51	0.53	4.78	1.78E-06	0.0024
76788	ENSMUSG00000029775	Klhdc10	67.57	2.76	0.70	3.93	8.43E-05	0.0346
258963	ENSMUSG00000059136	Olfr539	217.84	3.46	0.70	4.96	6.95E-07	0.0015
20355	ENSMUSG00000000627	Sema4f	53.79	3.61	0.84	4.27	1.96E-05	0.0121
71709	ENSMUSG00000032714	Syde1	39.46	4.36	1.05	4.16	3.13E-05	0.0181
19271	ENSMUSG00000025314	Ptprj	48.63	4.45	1.14	3.89	9.92E-05	0.0385
71361	ENSMUSG00000020085	Aifm2	22.07	4.55	1.11	4.11	4.00E-05	0.0187
14049	ENSMUSG00000017897	Eya2	29.37	5.80	1.33	4.38	1.19E-05	0.0090
268301	ENSMUSG00000098188	Sowahc	19.21	6.83	1.80	3.80	0.00014	0.0485
14961	ENSMUSG00000073421	H2-Ab1	153.09	6.97	1.69	4.12	3.72E-05	0.0181
231147	ENSMUSG00000036553	Sh3tc1	31.49	7.23	1.67	4.32	1.54E-05	0.0110
58809	ENSMUSG00000021876	Rnase4	25.36	7.25	1.45	5.01	5.52E-07	0.0015
14127	ENSMUSG00000058715	Fcer1g	24.09	7.59	1.63	4.65	3.38E-06	0.0038
110784	ENSMUSG00000031618	Nr3c2	14.06	7.62	1.98	3.84	0.00012	0.0453
15122	ENSMUSG00000069919	Hba-a1	1205.05	7.78	1.93	4.02	5.71E-05	0.0258
11498	ENSMUSG00000072972	Adam4	23.04	7.79	1.60	4.89	1.03E-06	0.0017
208117	ENSMUSG00000032375	Aph1b	16.51	8.25	1.92	4.29	1.81E-05	0.0121
12260	ENSMUSG00000036905	C1qb	32.89	8.48	1.87	4.52	6.11E-06	0.0055
110257	ENSMUSG00000069917	Hba-a2	3536.87	8.51	1.58	5.40	6.85E-08	0.0005
20617	ENSMUSG00000025889	Snca	26.01	21.24	4.08	5.20	1.96E-07	0.0007

Figure 6.14: **Diferentially expressed genes between the KO_BR and Het_BR populations.** CD69^{+}*Foxp3*$^{+}$CD4 SP cells were sorted for RNAseq analysis from 6-7 weeks old Bim$^{WT/KO}$ and Bim$^{KO/KO}$ mice according to *Nr4a3*-Timer expression as described in Fig.6.11. 2000 cells were sorted for each population and subjected to RNAseq. Normalised counts of expressed genes were obtained using the algorithm DESeq2 and differential gene expression between KO_BR and Het_BR populations for adjusted p value of <0.05 was determined using the DESeq2 function results. In order from left to right, columns represent the gene ID (EntezID), the Ensembl ID (ENSEMBL), the corresponding gene symbol (GeneSymbol), the average of the normalised count values (baseMean), the effect size estimate reported on a logarithmic scale to base 2 (log2FoldChange), the standard error estimate for the log2FoldChange estimate (lfcSE), the Wald statistic (stat), the Wald test p-value (pvalue) and the Benjamin-Hochberg correction adjusted p-value (padj).

EntrezID	ENSEMBL	GeneSymbol	baseMean	log2FoldChange	lfcSE	stat	pvalue	padj
16516	ENSMUSG00000062609	Kcnj15	39.84	-4.65	1.14	-4.08	4.59E-05	0.020549
268880	ENSMUSG00000047434	Xxylt1	258.90	-1.45	0.37	-3.92	8.77E-05	0.029453
22415	ENSMUSG00000000125	Wnt3	169.43	-1.43	0.31	-4.55	5.39E-06	0.004477
171170	ENSMUSG00000036109	Mbnl3	665.02	-1.22	0.20	-6.23	4.54E-10	0.000004
13601	ENSMUSG00000028108	Ecm1	2448.30	-1.15	0.25	-4.64	3.49E-06	0.003515
16184	ENSMUSG00000026770	Il2ra	2284.23	-0.74	0.18	-4.08	4.45E-05	0.020549
19414	ENSMUSG00000031453	Rasa3	2796.43	-0.71	0.18	-3.94	8.17E-05	0.029049
230737	ENSMUSG00000028869	Gnl2	656.43	0.81	0.19	4.28	1.88E-05	0.010340
21414	ENSMUSG00000000782	Tcf7	3451.21	0.88	0.22	3.93	8.55E-05	0.029453
17357	ENSMUSG00000047945	Marcksl1	816.90	1.15	0.28	4.14	3.52E-05	0.017017
16768	ENSMUSG00000030124	Lag3	510.19	1.64	0.37	4.36	1.29E-05	0.007806
12125	ENSMUSG00000027381	Bcl2l11	1066.61	1.66	0.36	4.57	4.88E-06	0.004477
67393	ENSMUSG00000046668	Cxxc5	74.89	2.21	0.53	4.17	3.05E-05	0.016031
11816	ENSMUSG00000002985	Apoe	293.00	2.35	0.59	3.97	7.17E-05	0.027119
13195	ENSMUSG00000020182	Ddc	106.19	2.35	0.55	4.29	1.81E-05	0.010340
70556	ENSMUSG00000028982	Slc25a33	59.60	3.56	0.88	4.03	5.48E-05	0.022089
217734	ENSMUSG00000034126	Pomt2	61.09	3.86	0.93	4.15	3.38E-05	0.017017
13498	ENSMUSG00000004263	Atn1	51.59	4.08	0.90	4.54	5.55E-06	0.004477
14960	ENSMUSG00000036594	H2-Aa	161.79	4.53	1.03	4.42	9.99E-06	0.006711
320664	ENSMUSG00000074570	Cass4	48.86	4.58	0.88	5.20	1.99E-07	0.000401
70458	ENSMUSG00000049916	2610318N02Rik	37.34	4.82	1.28	3.77	0.00016	0.048571
14087	ENSMUSG00000032815	Fanca	37.79	5.05	1.05	4.81	1.49E-06	0.001640
14049	ENSMUSG00000017897	Eya2	29.37	5.09	1.26	4.04	5.24E-05	0.021860
241576	ENSMUSG00000048058	Ldlrad3	48.41	5.31	1.19	4.46	8.14E-06	0.005792
171543	ENSMUSG00000040093	Bmf	112.49	6.01	1.13	5.33	9.92E-08	0.000246
16069	ENSMUSG00000067149	Jchain	79.18	6.08	1.21	5.02	5.23E-07	0.000703
72544	ENSMUSG00000109941	Exosc6	40.73	6.86	1.72	3.99	6.49E-05	0.025342
71361	ENSMUSG00000020085	Aifm2	22.07	6.99	1.83	3.82	0.00013	0.041833
19731	ENSMUSG00000026482	Rgl1	17.95	7.08	1.80	3.94	8.04E-05	0.029049
57875	ENSMUSG00000002289	Angptl4	39.09	7.19	1.64	4.38	1.18E-05	0.007483
66569	ENSMUSG00000061666	Gdpd1	23.68	7.29	1.88	3.88	0.00010	0.034292
20341	ENSMUSG00000068874	Selenbp1	41.74	8.26	1.65	5.02	5.21E-07	0.000703
12260	ENSMUSG00000036905	C1qb	32.89	8.31	2.18	3.82	0.00013	0.041833
54698	ENSMUSG00000032021	Crtam	50.87	8.34	1.84	4.52	6.22E-06	0.004705
15122	ENSMUSG00000069919	Hba-a1	1205.05	8.87	2.19	4.05	5.11E-05	0.021860
110257	ENSMUSG00000069917	Hba-a2	3536.87	9.74	1.79	5.44	5.23E-08	0.000211
20617	ENSMUSG00000025889	Snca	26.01	28.34	4.60	6.16	7.40E-10	0.000004

Figure 6.15: **Diferentially expressed genes between the KO_R and Het_R populations.** CD69^{+}*Foxp3*$^{+}$CD4 SP cells were sorted for RNAseq analysis from 6-7 weeks old Bim$^{\mathrm{WT/KO}}$ and Bim$^{\mathrm{KO/KO}}$ mice according to *Nr4a3*-Timer expression as described in Fig.6.11. 2000 cells were sorted for each population and subjected to RNAseq. Normalised counts of expressed genes were obtained using the algorithm DESeq2 and differential gene expression between KO_R and Het_R populations for adjusted p value of <0.05 was determined using the DESeq2 function results. In order from left to right, columns represent the gene ID (EntezID), the Ensembl ID (ENSEMBL), the corresponding gene symbol (GeneSymbol), the average of the normalised count values (baseMean), the effect size estimate reported on a logarithmic scale to base 2 (log2FoldChange), the standard error estimate for the log2FoldChange estimate (lfcSE), the Wald statistic (stat), the Wald test p-value (pvalue) and the Benjamin-Hochberg correction adjusted p-value (padj).

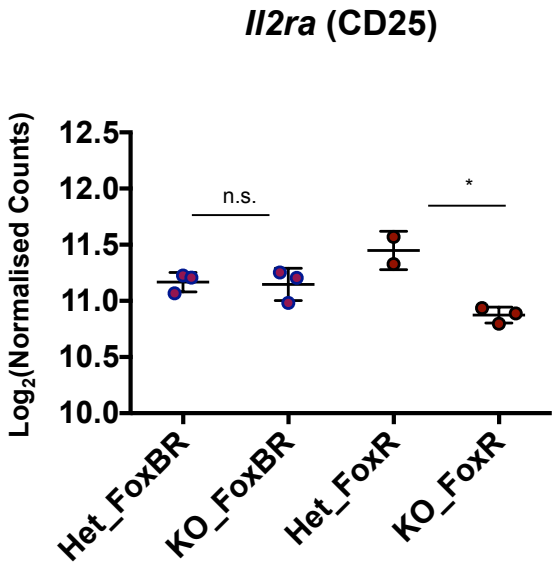

Figure 6.16: **Summary data of *Il2ra* transcription in Bim-sufficient and Bim-deficient *Foxp3*$^+$CD4 SP cells.** CD69$^+$*Foxp3*$^+$CD4 SP cells were sorted for RNAseq analysis from 6-7 weeks old Bim$^{WT/KO}$ and Bim$^{KO/KO}$ mice according to *Nr4a3*-Timer expression as described in Fig.6.11. 2000 cells were sorted for each population and subjected to RNAseq. Normalised counts of the gene *Il2ra* encoding the molecule CD25 were obtained using the algorithm DESeq2. Data are shown as $\log_2$ of normalised counts. Error bars are representative of mean ± s.d, where n = 3 biological replicates. Individual comparisons between the two genotypes by Tukey's post-hoc analysis are shown as * for $p<0.05$.

6.2.3 The temporally dynamic changes in *Nr4a3* transcription according to CD25 expression

To explore the implication of CD25 expression on TCR signalling, *Nr4a3*-Tocky mice were used. Three *Foxp3*$^{+}$CD4 SP populations were defined according to expression of this marker, as described in Fig.6.17A and B: CD25^{-} *Foxp3*$^{+}$CD4 SP (CD25^{-}), CD25^{lo} *Foxp3*$^{+}$CD4 SP (CD25^{lo}) and CD25^{+} *Foxp3*^{hi}CD4 SP (CD25^{hi}).

Nr4a3-Timer dynamics appeared quite similar between populations on flow cytometry plots (Fig.6.17C) and this was confirmed by Timer locus analysis, where no significant differences were detected between Timer^{+} cell distribution in each Timer locus (Fig.6.18), as well as by the mean Timer angle value, which was comparable between the three populations (Fig.6.19A). Therefore, CD25 expression does not affect the TCR signalling requirements for *Foxp3*^{hi}CD4 SP development.

The percentage of Timer^{-} cells was reduced as CD25 expression increased (Fig.6.17C). Furthermore, the higher CD25 expression was, the higher Timer intensity was (Fig.6.19B). This suggests that the level of CD25 accumulation is proportional to TCR signal strength. According to this, CD25^{-} cells received the lowest intensity signals, CD25^{lo} may be in the process of accumulating both Timer and CD25 proteins and the CD25^{hi} phenotype arose in respose to high-intensity, sustained TCR signalling.

GITR and OX40 also accumulated with increasing CD25 expression (Fig.6.20). While GITR levels were maintained throughout Timer protein maturation, OX40 expression peaked in the New locus and became gradually decreased as Blue protein matured to Red. This raises the possibility that Blue^{+}Red^{-}OX^{hi} cells are deleted by negative selection. The significant differences in GITR and OX40 expression between CD25^{-} and CD25^{+} cells further supports the fact that the former population receives weaker signals.

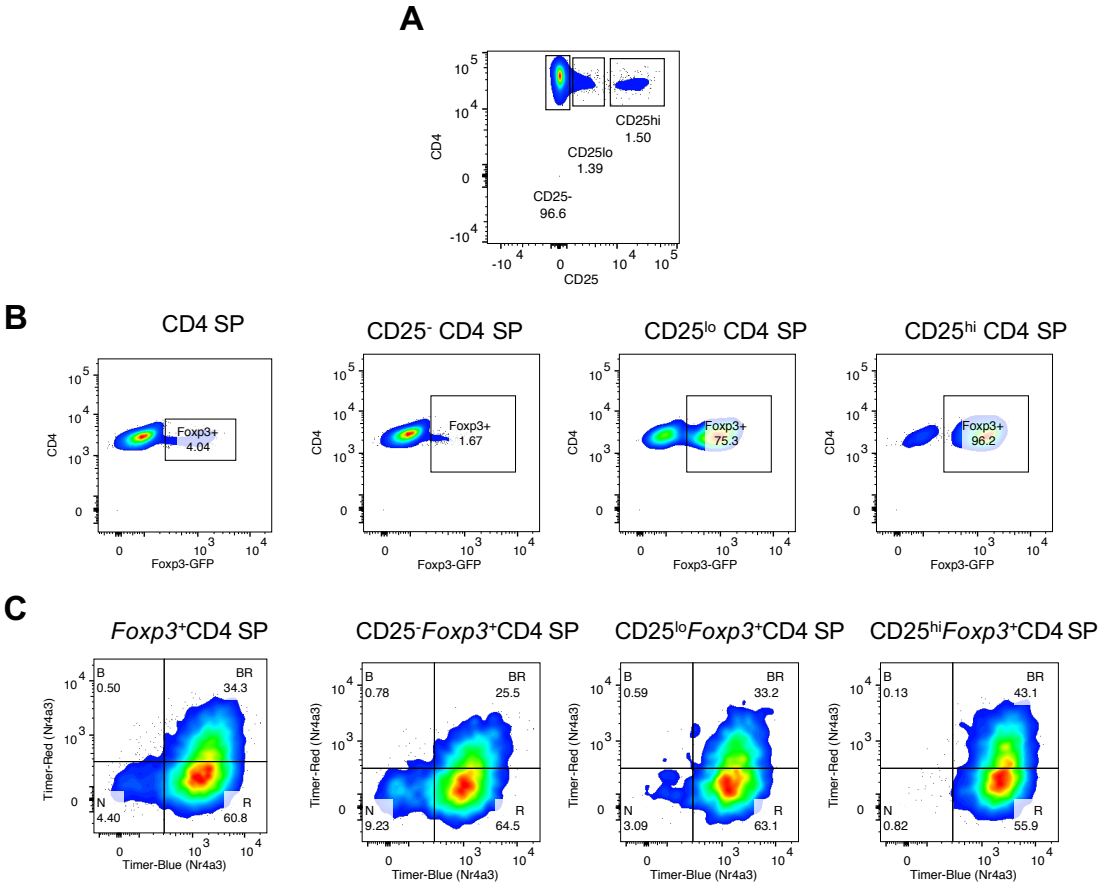

Figure 6.17: **The effect of CD25 expression on *Nr4a3*-Timer protein expression patterns.** Thymocytes from 4 weeks old *Nr4a3*-Tocky mice were analysed by flow cytometry on on a Cytek Aurora spectral analyser and the resulting 2-D plots are shown. (A) Gating strategy for three levels of CD25 expression. (B) Gating strategy for *Foxp3*$^+$ cells. (C) *Nr4a3*-Timer protein expression patterns of *Foxp3*$^+$ populations gated according to CD25 expression. Data are representative of at least 2 independent experiments that used 4 mice per group. All mice used were *Foxp3*-GFP.

CD25^{lo} cells may be in the process of becoming CD25^{hi} if they sustain TCR signals for long enough to accumulate it. Alternatively, they might bear a different TCR repertoire with sufficient affinity to self-antigen to upregulate *Foxp3*, but not fit to sustain TCR signals enough to accumulate as many CD25 and, consequently, GITR and OX40 molecules, as CD25^{hi} cells.

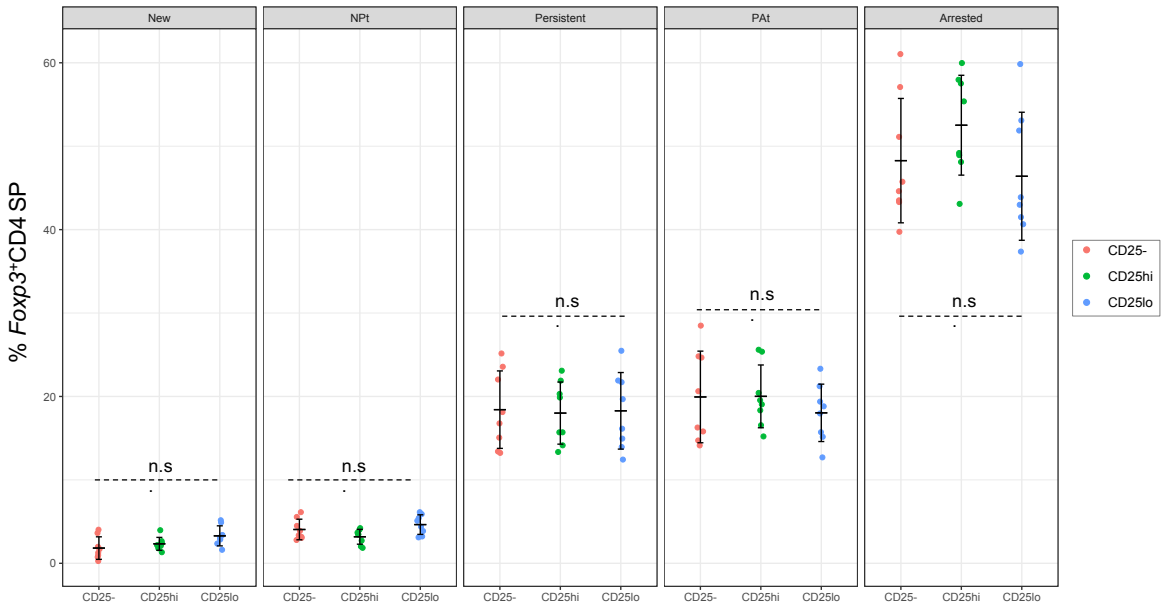

Figure 6.18: **Frequency of CD25-expressing cells in each *Nr4a3*-Timer locus.** Thymocytes from 4 weeks old *Nr4a3*-Tocky mice were analysed by a Cytek Aurora spectral analyser in two independent experiments and data was combined. The percentage of cells in each Timer locus among their parent population is shown by scatter plot for three populations: CD25^{-} *Foxp3*$^{+}$CD4 SP (CD25^{-}), CD25^{lo} *Foxp3*$^{+}$CD4 SP (CD25^{lo}) and CD25^{hi} *Foxp3*$^{+}$CD4 SP (CD25^{hi}). No statistically significant differences were detected by one-way ANOVA analysis. Error bars are representative of mean ± s.d, where n = 8 biological replicates. All mice used were *Foxp3*-GFP.

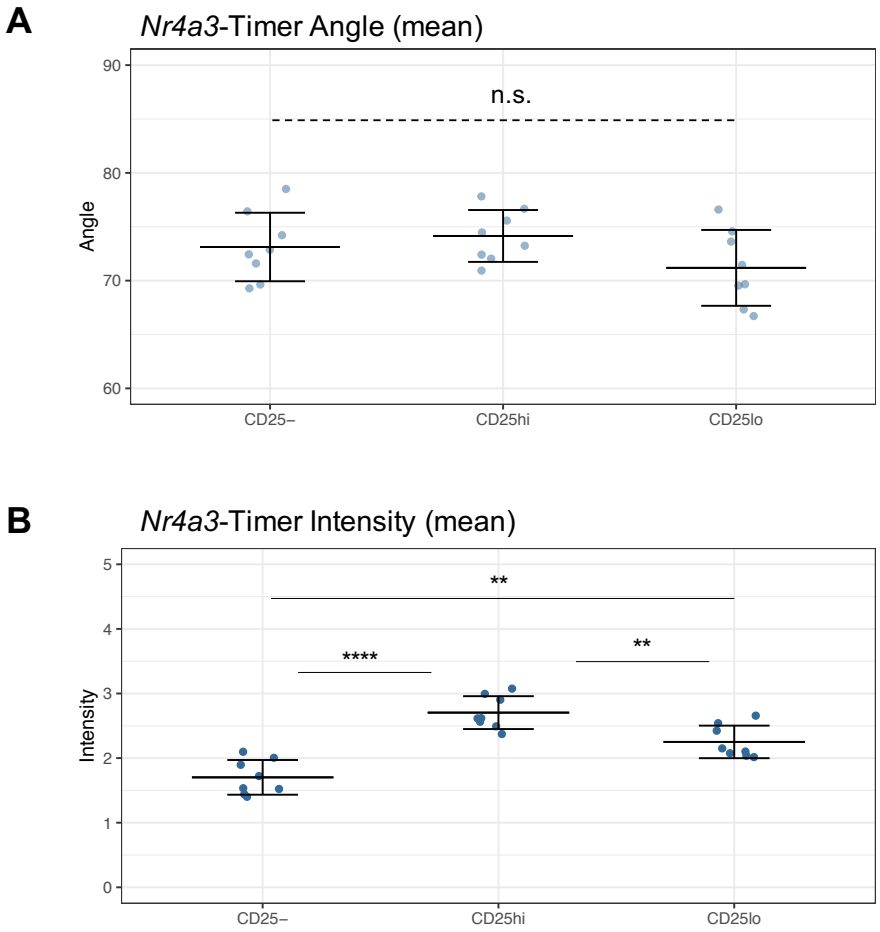

Figure 6.19: **Mean Timer angle and intensity of *Nr4a3*-Timer in CD25-expressing populations.** Thymocytes from 4 weeks old *Nr4a3*-Tocky mice were analysed by a Cytek Aurora spectral analyser in two independent experiments and data was combined. Mean *Nr4a3*-Timer angle (A) and intensity (B) are shown for three populations:CD25^{-}*Foxp3*$^{+}$CD4 SP (CD25^{-}), CD25^{lo}*Foxp3*$^{+}$CD4 SP (CD25^{lo}) and CD25^{hi}*Foxp3*$^{+}$ CD4 SP (CD25^{hi}). Dashed line shows no statistically significant differences by one-way ANOVA analysis. Solid lines show statistically significant differences from Tukey's post-hoc analysis as ** for p<0.01 and **** for p<0.0001. Error bars are representative of mean ± s.d, where n = 8 biological replicates. All mice used were *Foxp3*-GFP.

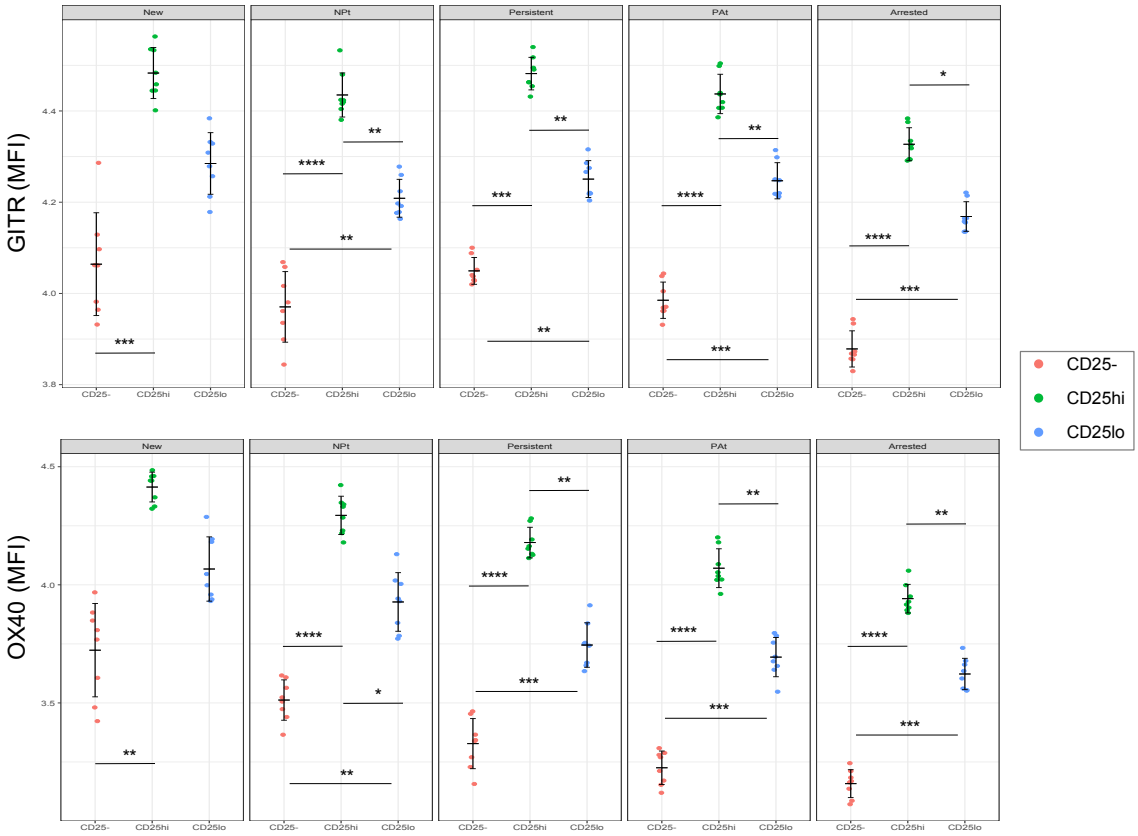

Figure 6.20: **GITR and OX40 MFI of CD25-expressing cells in each *Nr4a3*-Timer locus.** Thymocytes from 4 weeks old *Nr4a3*-Tocky mice were analysed by a Cytek Aurora spectral analyser in two independent experiments and data was combined. Plots show mean fluorescence intensity of the markers GITR (top) and OX40 (bottom) expressed in each Timer locus by three populations:CD25^{-}*Foxp3*$^{+}$CD4 SP (CD25^{-}), CD25^{lo}*Foxp3*$^{+}$CD4 SP (CD25^{lo}) and CD25^{hi}*Foxp3*$^{+}$ CD4 SP (CD25^{hi}). Any statistically significant differences from Tukey's post-hoc analysis as * for p<0.05, ** for p<0.01, *** for p<0.001 and ****for p<0.0001. Error bars are representative of mean ± s.d, where n = 8 biological replicates. All mice used were *Foxp3*-GFP.

6.2.4 The effect of CD25 expression on *Foxp3* transcription dynamics

Foxp3-Tocky mice were used in order to determine the effect of CD25 expression on *Foxp3* transcriptional dynamics in developing CD4 SP. Three CD4 SP populations were defined according to CD25 expression using the gating strategy shown in Fig.6.17: $CD25^{-}$CD4 SP ($CD25^{-}$), $CD25^{lo}$CD4 SP ($CD25^{lo}$) and $CD25^{hi}$CD4 SP ($CD25^{hi}$) and their *Foxp3*-$Timer^{+}$ cell populations were investigated.

In CD4 SP, most *Foxp3* transcription occurred in the $B^{+}R^{+}$ fraction (Fig.6.21). Therefore, once cells upregulated *Foxp3*, its transcription is constantly maintained. Barely any $Timer^{+}$ cells were detected in the $CD25^{-}$ fraction, while $CD25^{hi}$ cells showed the most events on a flow cytometry plot. As a result, $CD25^{hi}$ had the highest Timer intensity, followed by $CD25^{lo}$ and finally by $CD25^{-}$ (Fig.6.22).

Timer locus analysis supports the scenario in which at least some $CD25^{lo}$ cells become $CD25^{hi}$, as most of their *Foxp3* transcription was captured in the New locus, while the majority of $CD25^{hi}$ cells showed more mature transcription as they preferentially resided in the NPt and Persistent loci (Fig.6.23). It is also possible that some $CD25^{lo}$ cells fail to maintain persistent *Foxp3* transcription and, as a result, downregulate CD25 and eventually join the $CD25^{-}$ pool.

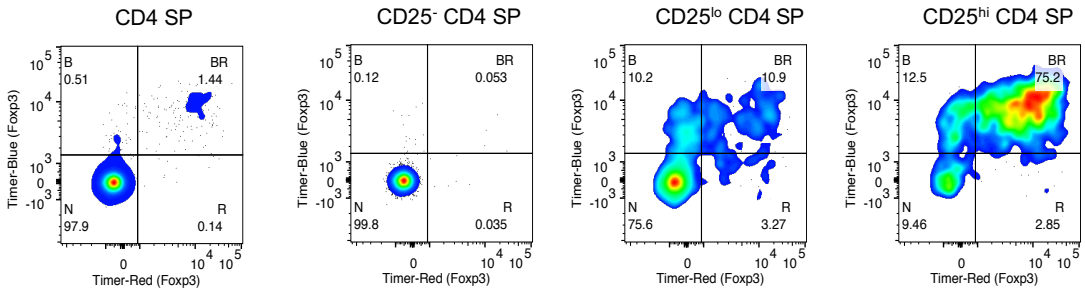

Figure 6.21: **Effect of CD25 expression on *Foxp3*-Timer protein expression patterns.** Thymocytes from 4 weeks old *Nr4a3*-Tocky mice were analysed by a Cytek Aurora spectral analyser and the resulting 2-D plots show *Foxp3*-Timer protein expression patterns for population defined according to CD25 expression, as described in Fig.6.17. Data shown are representative of 2 independent experiments that used 2 and 5 mice per experiment.

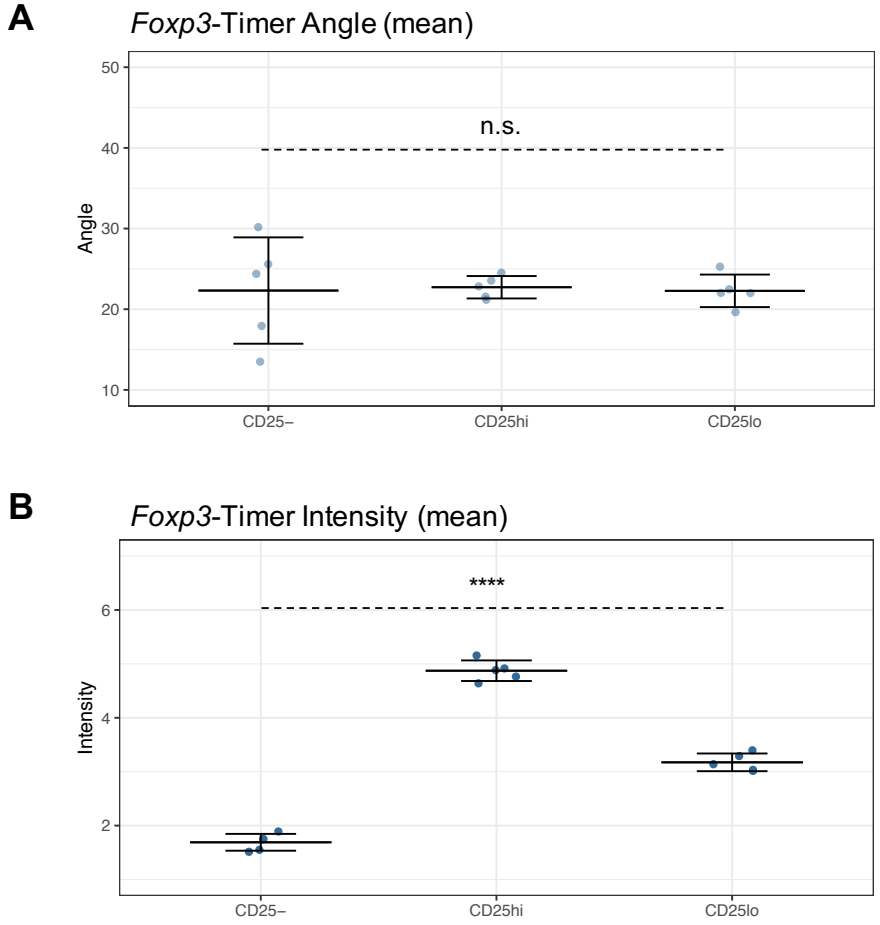

Figure 6.22: **Mean Timer angle and intensity of *Foxp3*-Timer in CD25-expressing populations.** Thymocytes from 4 weeks old *Foxp3*-Tocky mice were analysed by a Cytek Aurora spectral analyser. Mean *Foxp3*-Timer angle (A) and intensity (B) are shown for three populations:CD25^{-}CD4 SP (CD25^{-}), CD25^{lo}CD4 SP (CD25^{lo}) and CD25^{hi}CD4 SP (CD25^{hi}). Dashed line shows statistically significant differences by one-way ANOVA analysis as **** for $p<0.0001$. Error bars are representative of mean $\pm$ s.d, where $n = 5$ biological replicates. Data shown are representative of 2 independent experiments that used 2 and 5 mice per experiment.

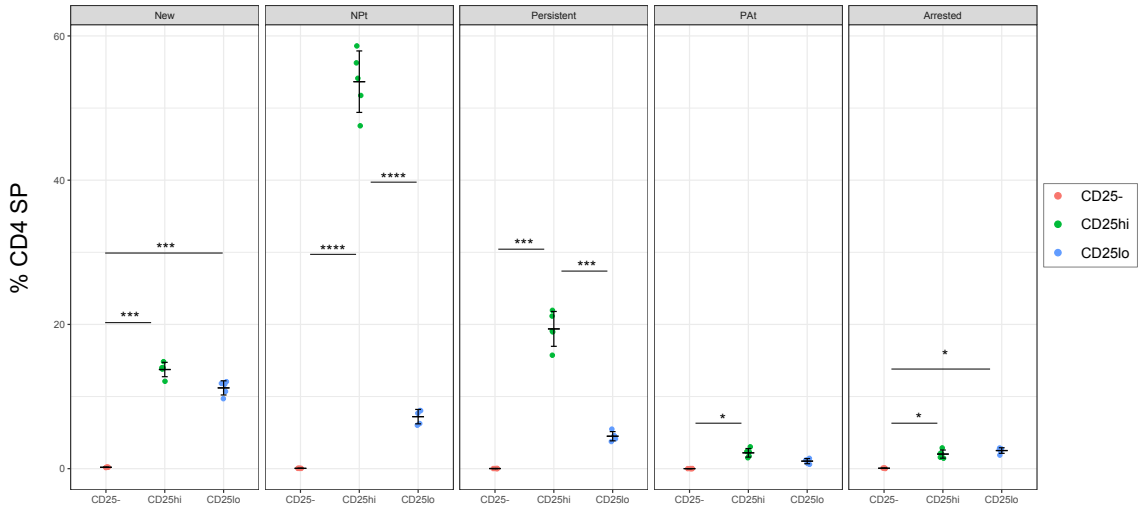

Figure 6.23: **Frequency of CD25-expressing cells in each *Foxp3*-Timer locus.** Thymocytes from 4 weeks old *Foxp3*-Tocky mice were analysed by a Cytek Aurora spectral analyser. The percentage of cells in each Timer locus among their parent population is shown by scatter plot for three populations:CD25^{-} CD4 SP (CD25^{-}), CD25^{lo}CD4 SP (CD25^{lo}) and CD25^{hi}CD4 SP (CD25^{hi}). Any statistically significant differences from Tukey's post-hoc analysis as * for $p<0.05$, ** for $p<0.01$, *** for $p<0.001$ and ****for $p<0.0001$. Error bars are representative of mean ± s.d, where n = 5 biological replicates. Data shown are representative of 2 independent experiments that used 2 and 5 mice per experiment.

The MFI of PD-1 peaked in the Persistent *Nr4a3*-Timer locus, irrespective of CD25 levels (Fig.6.24). As Timer protein matured and cells stopped transcribing *Nr4a3*, PD-1 became downregulated. According to the data illustrated in Fig.6.24, $CD25^{-}$ and $CD25^{lo}$ cells require PD-1 both during persistent TCR signalling and for sustained *Foxp3* transcription. $CD25^{hi}$ cells, on the other hand, did not induce PD-1 during *Foxp3* transcription. This raises the possibility that CD25 expression may facilitate the survival of PD-1^{lo} cells and, in its absence, cells may require PD-1 for maintaining their *Foxp3*$^{+}$ phenotype.

In *Foxp3*-Tocky mice, $CD25^{hi}$ cells only upregulated PD-1 in the Arrested locus, when *Foxp3* is no longer transcribed. This suggests that when *Foxp3* transcription is persistent and CD25 expression is sufficiently high for enough IL-2 signals to be conveyed, PD-1 is repressed. Alternatively and not exclusively, PD-$1^{hi}CD25^{hi}$ cells may be deleted before becoming $B^{-}R^{+}$. Further, it is also possible that PD-1 expression is downregulated by PD-1 ligation through PD-1 ligands, which are expressed by TECs (Brown et al., 2003).

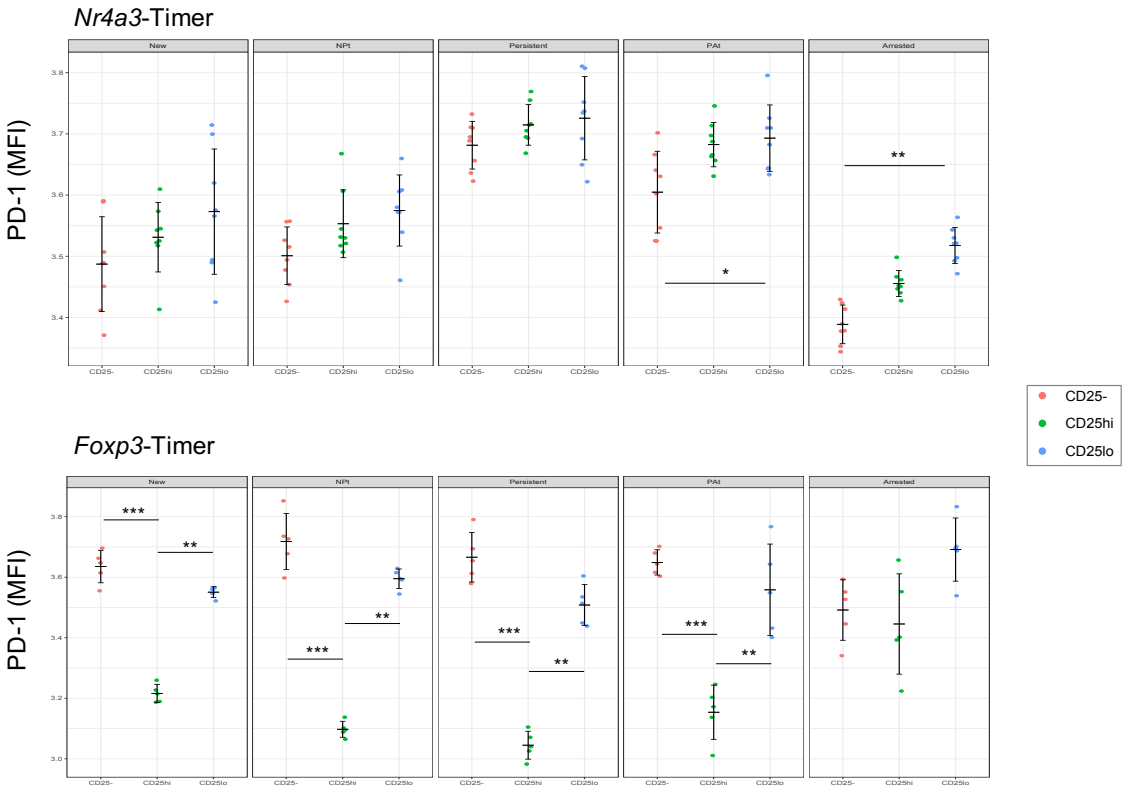

Figure 6.24: **PD-1 MFI of CD25-expressing cells in each *Nr4a3*-Timer and *Foxp3*-Timer locus**. Plots show mean fluorescence intensity of the marker PD-1 across *Nr4a3*-Timer loci (top figure) or *Foxp3*-Timer loci (bottom figure). Any statistically significant differences from Tukey's post-hoc analysis as * for $p<0.05$, ** for $p<0.01$, *** for $p<0.001$ and **** for $p<0.0001$. Error bars are representative of mean ± s.d, where n = 8 biological replicates (top figure, two independent experiments from which data was combined) or 5 biological replicates (bottom figure, data are representative of two independent experiments that used 2 and 5 mice each).

6.2.5 Consequences of Bim deficiency on CD25 expression by developing *Foxp3*$^+$CD4 SP cells

The CD25$^-$, CD25^{lo} and CD25^{hi} populations defined as shown in Fig.6.17 were next analysed in KO and Het mice in order to address the reduction in CD25 transcript level in KO mice (Fig.6.16). For each genotype, *Nr4a3*-Timer protein expression patterns of the three populations are shown in Fig.6.25. The patterns of *Nr4a3*-Timer transcription appeared quite similar between the two genotypes, where most cells resided in the Arrested locus and the proportion of Persistent cells was the largest in CD25^{hi}, followed by CD25^{lo} and then by CD25$^-$ cells (Fig.6.25). The proportions of CD25$^-$, CD25^{lo} and CD25^{hi} cells in the *Foxp3*$^+$CD4 SP parent population, however, were different in KO mice compared to the control (Fig.6.26A). Specifically, KO *Foxp3*$^+$CD4 SP had significantly lower proportions of CD25^{hi} cells and were highly enriched with CD25$^-$ cells. Because KO mice have higher absolute numbers and proportions of *Foxp3*$^+$CD4 SP compared to Het (Fig.6.8), these three populations were also measured as a percentage of the total live cell pool (Fig.6.26B). According to absolute cell number and percentage data, KO mice accumulated both CD25$^-$ and CD25^{lo} cells, while the CD25^{hi} fraction was not much altered. However, both CD25$^-$ and CD25^{hi} KO populations expressed significantly higher levels of PD-1 compared to Het (Fig.6.26C). This suggests that although the proportion of CD25^{hi} cells remains constant in the absence of Bim, the TCR repertoire is shifted. These findings suggests that unlike in the case of CD25$^-$, the antigen niche associated with CD25^{hi} development is saturated.

In Het mice, the *Nr4a3* transcription dynamics appeared unchanged by CD25 expression, as no significant differences were detected between the three populations in each Timer locus (Fig.6.27A). They mostly distributed in the Arrested locus, with under 20% of them residing in the PAt. In the absence of Bim, however, CD25^{hi} cells distributed

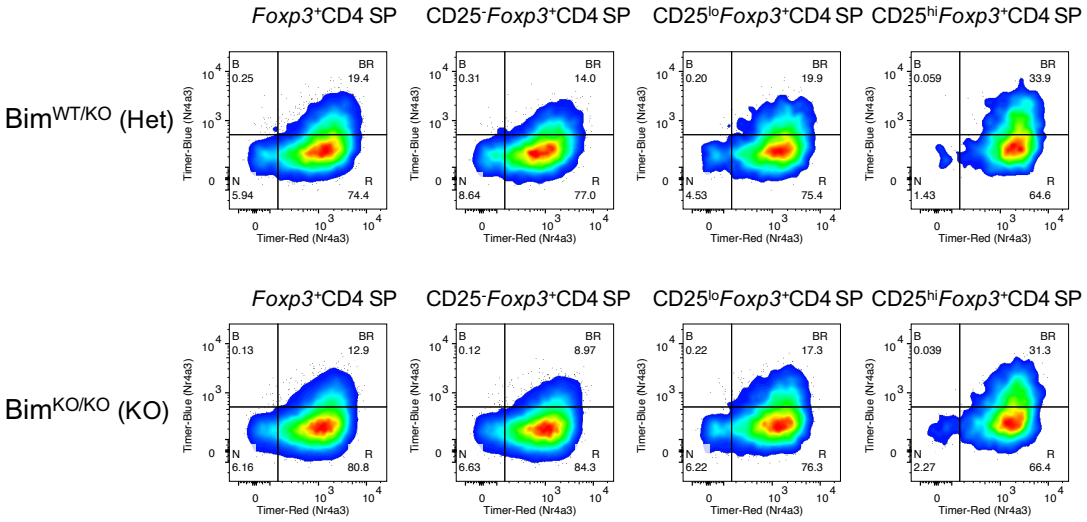

Figure 6.25: ***Nr4a3*-Timer protein expression in Bim-sufficient and Bim-defficient cells according to CD25 surface levels.** Thymocytes were harvested from 6 weeks old *Nr4a3*-Tocky:Bim$^{WT/KO}$ or *Nr4a3*-Tocky:Bim$^{KO/KO}$ mice and were analysed by flow cytometry on a Fortessa III instrument. For each genotype, *Nr4a3*-Timer expression is shown in several populations defined according to CD25 expression as described in Fig.6.17. Data shown are representative of at least 4 independent experiments that used 2-4 mice per group. All mice used were *Foxp3*-GFP.

almost evently between the PAt and Arrested loci (Fig.6.27B). This further supports that in KO mice the TCR repertoire of the CD25^{hi} population is altered.

The dominant population in the Arrested locus in KO mice was CD25^{-} and their Timer angle was significantly higher than the control (Fig.6.27B and6.28A). Both KO CD25^{-} and CD25^{hi} cells had significantly higher Timer Intensities than the control (Fig.6.28B). Collectively, these findings suggests that Bim deletes self-reactive precursors of CD25^{-} and CD25^{+} populations, which in its absence survive and upregulate PD-1.

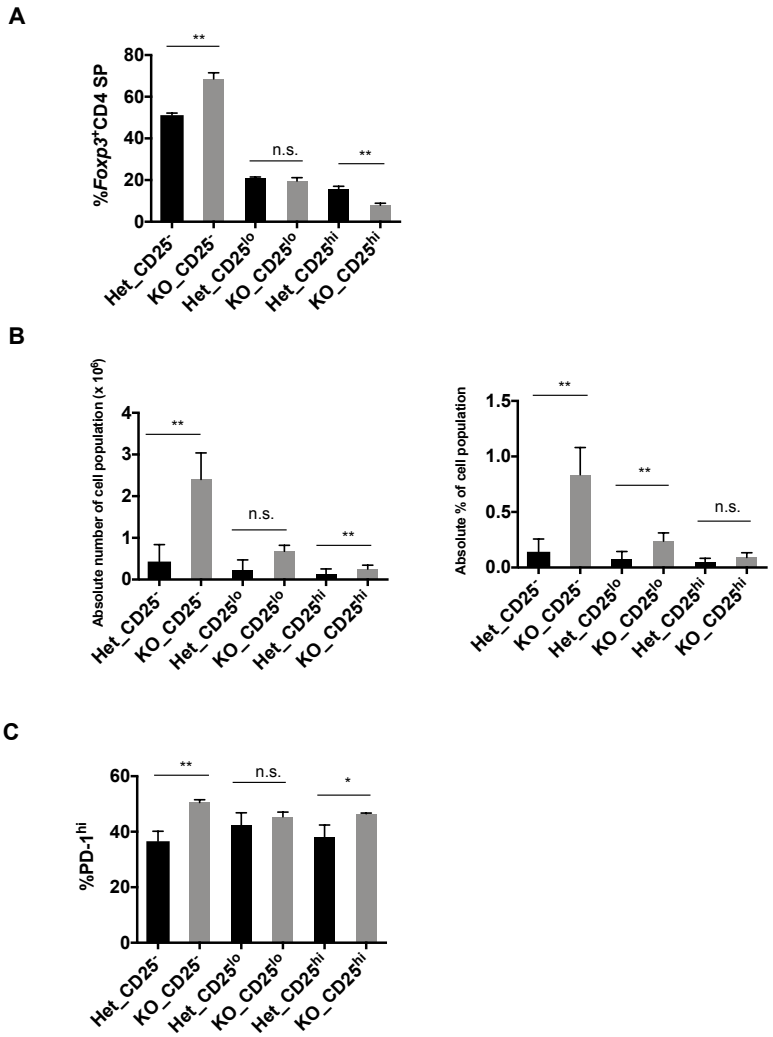

Figure 6.26: **Effect of Bim deficiency on the proportions of CD25-expressing *Foxp3*$^+$CD4 SP populations.** Thymocytes were harvested from 5-7 weeks old *Nr4a3*-Tocky:Bim$^{WT/KO}$ or *Nr4a3*-Tocky:Bim$^{KO/KO}$ mice and were analysed by flow cytometry on a Fortessa III instrument.

(A) Bar chart shows what percentage of the total *Foxp3*$^+$CD4 SP pool each *Foxp3*$^+$CD4 SP CD25-expressing population represents in either genotype.
(B) The first bar chart shows the absolute cell number of each CD25-expressing *Foxp3*$^+$CD4 SP population in either genotype. The second bar chart shows what percentage each CD25-expressing *Foxp3*$^+$CD4 SP population represents out of the total live cell pool in either genotype.
(C) Bar chart shows the percentage of PD-1^{hi} cells in each *Foxp3*$^+$CD4 SP CD25-expressing fraction for either genotype.

Each population was individually compared between the two genotypes and any statistically significant differences from Mann-Whitney U test (performed on all percentage data) or from unpaired Student's t-test (performed on cell number data) are shown as * for $p<0.05$, ** for $p<0.01$, *** for $p<0.001$ and ****for $p<0.0001$. Error bars are representative of mean ± s.d, where n = 6 biological replicates for each genotype. Data from three independent experiments was combined.

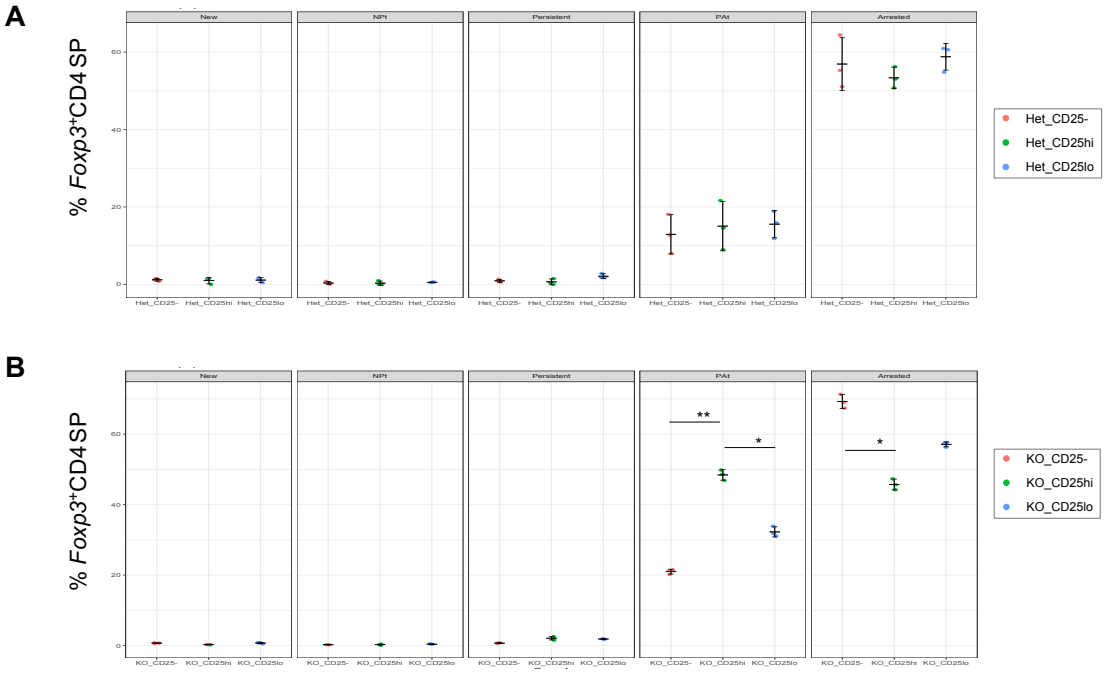

Figure 6.27: **Frequency of CD25-expressing cells in each *Nr4a3*-Timer locus in Bim-sufficient and Bim-deficient mice.** Thymocytes were harvested from 6 weeks old *Nr4a3*-Tocky:Bim$^{WT/KO}$ or *Nr4a3*-Tocky:Bim$^{KO/KO}$ mice and were analysed by flow cytometry on a on a Fortessa III instrument. The percentage of cells in each Timer locus among their parent population is shown by scatter plot for three populations:CD25^{-} *Foxp3*$^{+}$CD4 SP (CD25^{-}), CD25^{lo} *Foxp3*$^{+}$CD4 SP (CD25^{lo}) and CD25^{hi} *Foxp3*$^{+}$ CD4 SP (CD25^{hi}). (A) Timer locus analysis of Bim$^{WT/KO}$ cells. (B) Timer locus analysis of Bim$^{KO/KO}$ cells. Any statistically significant differences from Tukey's post-hoc analysis are shown as * for $p<0.05$, ** for $p<0.01$, *** for $p<0.001$ and ****for $p<0.0001$. Error bars are representative of mean ± s.d, where n = 3 biological replicates for each genotype. Data shown are representative of at least 4 independent experiments that used 2-4 mice per group. All mice used were *Foxp3*-GFP.

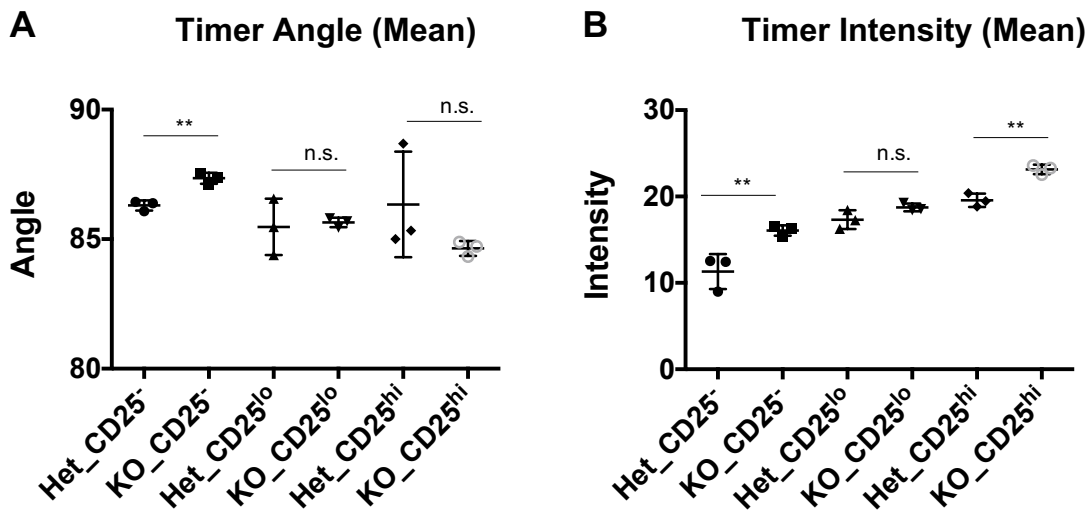

Figure 6.28: **Mean Timer angle and intensity of CD25-expressing cells in Bim-sufficient and Bim-deficient mice.** Thymocytes were harvested from 6 weeks old *Nr4a3*-Tocky:Bim$^{WT/KO}$ or *Nr4a3*-Tocky:Bim$^{KO/KO}$ mice and were analysed by flow cytometry on a on a Fortessa III instrument. Mean Timer angle (A) and intensity (B) are shown for three populations:CD25^{-}*Foxp3*$^{+}$CD4 SP (CD25^{-}), CD25^{lo}*Foxp3*$^{+}$CD4 SP (CD25^{lo}) and CD25^{hi}*Foxp3*$^{+}$ CD4 SP (CD25^{hi}). Each population was individually compared between the two genotypes and statistically significant differences from unpaired Student's t-test are shown as ** for $p<0.01$. Error bars are representative of mean $\pm$ s.d, where n = 3 biological replicates for each genotype. Data shown are representative of at least 4 independent experiments that used 2-4 mice per group. All mice used were *Foxp3*-GFP.

6.2.6 CD4/CD8 lineage effect on *Foxp3*$^+$SP development

Although they represent a rare population, *Foxp3*$^+$CD8 SP do develop in the thymus. Compared to CD4 T cells, a much lower fraction of CD8 SP cells expressed *Foxp3* (Fig.6.29). *Nr4a3*-Tocky mice were used in order to determine whether the TCR signalling requirements for *Foxp3* upregulation were distinct between T cell lineages. CD25$^+$*Foxp3*$^+$CD8 SP cells were previously found to share several biological and functional characteristics with cells of a similar phenotype from the CD4 lineage (Cosmi et al., 2003). However, this population was very small in *Nr4a3*-Tocky mice (Fig.6.30). For this reason, CD4 and CD8 SP cells were compared in bulk.

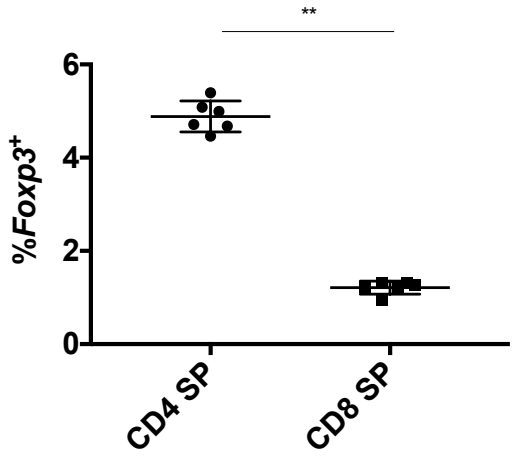

Figure 6.29: ***Foxp3* expression by CD4 and CD8 SP cells.** Thymocytes from 4 weeks old *Nr4a3*-Tocky mice were analysed by flow cytometry on a Fortessa III instrument in three independent experiments and data was combined. The total fraction of *Foxp3*$^+$ cells is compared between CD4 SP and CD8 SP cells and statistically significant differences by Mann-Whitney U test are shown as ** for $p<0.01$. Error bars are representative of mean ± s.d, where n = 6 biological replicates. All mice used were *Foxp3*-GFP.

For the most part, *Foxp3*$^+$CD4 SP and *Foxp3*$^+$CD8 SP cells shared very similar *Nr4a3*-Timer dynamics (Fig.6.31). *Foxp3*$^+$CD8 SP, however, accumulated slightly more cells in the Arrested locus, resulting in a significantly higher Timer angle value (Fig.6.32A). Their Timer intensity, however, was lower than that of *Foxp3*$^+$CD4 SP cells (Fig.6.32B). Ac-

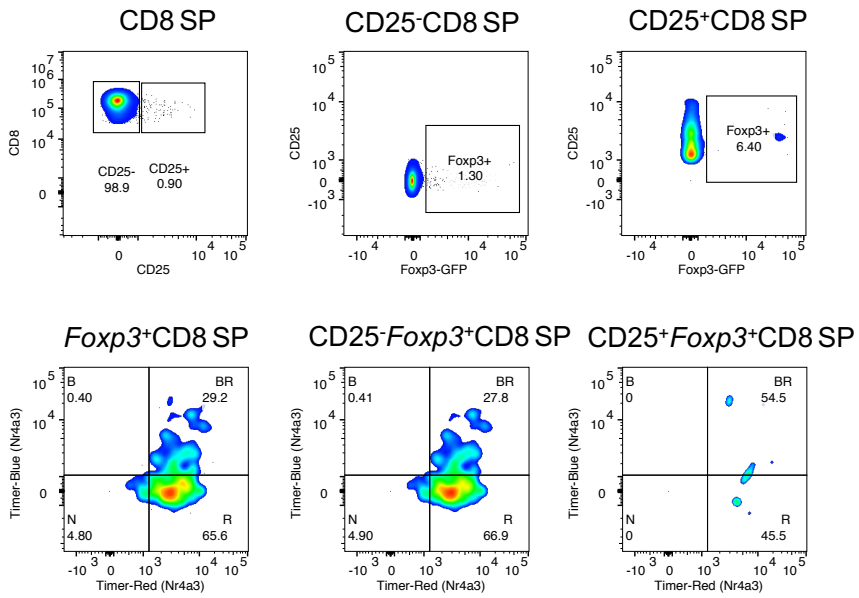

Figure 6.30: ***Nr4a3*-Timer protein expression patterns in *Foxp3*$^+$ CD8 SP cells.** Thymocytes from 4 weeks old *Nr4a3*-Tocky mice were analysed by flow cytometry on on a Cytek Aurora spectral analyser and the resulting 2-D plots are shown. Top figure shows the gating strategy for CD25$^-$ and CD25$^+$CD8 SP cells. Bottom figure shows *Nr4a3*-Timer protein expression patterns of *Foxp3*-GFP$^+$CD8 SP populations gated according to CD25 expression. Data shown are representative of at least 2 independent experiments that used 4 mice per group. All mice used were *Foxp3*-GFP.

cording to these findings, *Foxp3*$^+$CD8 SP have weaker, less sustained TCR signalling, resulting in a larger fraction of cells with arrested *Nr4a3* transcription. Therefore, *Foxp3*$^+$CD8 SP TCR repertoires may have weaker affinities to MHC-I molecules compared to the affinities of *Foxp3*$^+$CD4 SP TCR repertoires to MHC-II.

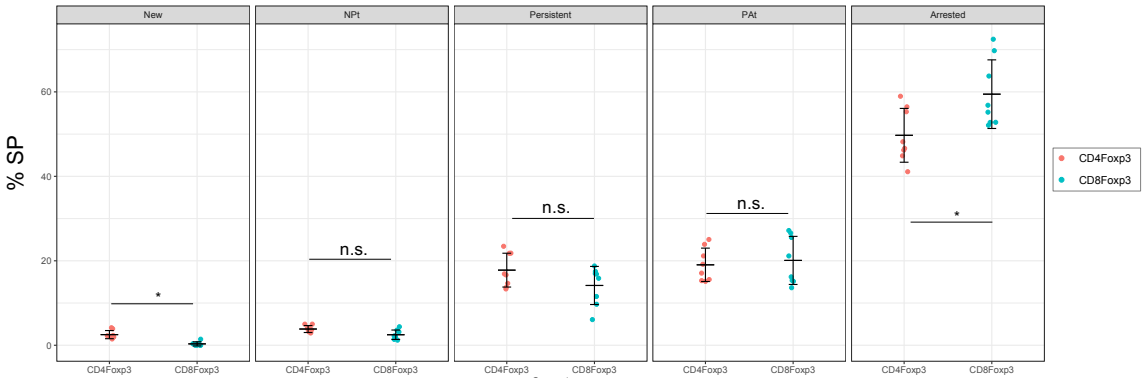

Figure 6.31: **Frequency of CD4 and CD8 *Foxp3*$^+$ cells in each *Nr4a3*-Timer locus.** Thymocytes from 4 weeks old *Nr4a3*-Tocky mice were analysed by a Cytek Aurora spectral analyser in two independent experiments and data was combined. The percentage of cells in each Timer locus among their parent population is shown by scatter plot for two populations: *Foxp3*$^+$CD4 SP (CD4Foxp3) and *Foxp3*$^+$CD8 SP (CD8Foxp3). Statistically significant differences by unpaired Student's t-test are shown as * for $p<0.05$. Error bars are representative of mean ± s.d, where n = 8 biological replicates. All mice used were *Foxp3*-GFP.

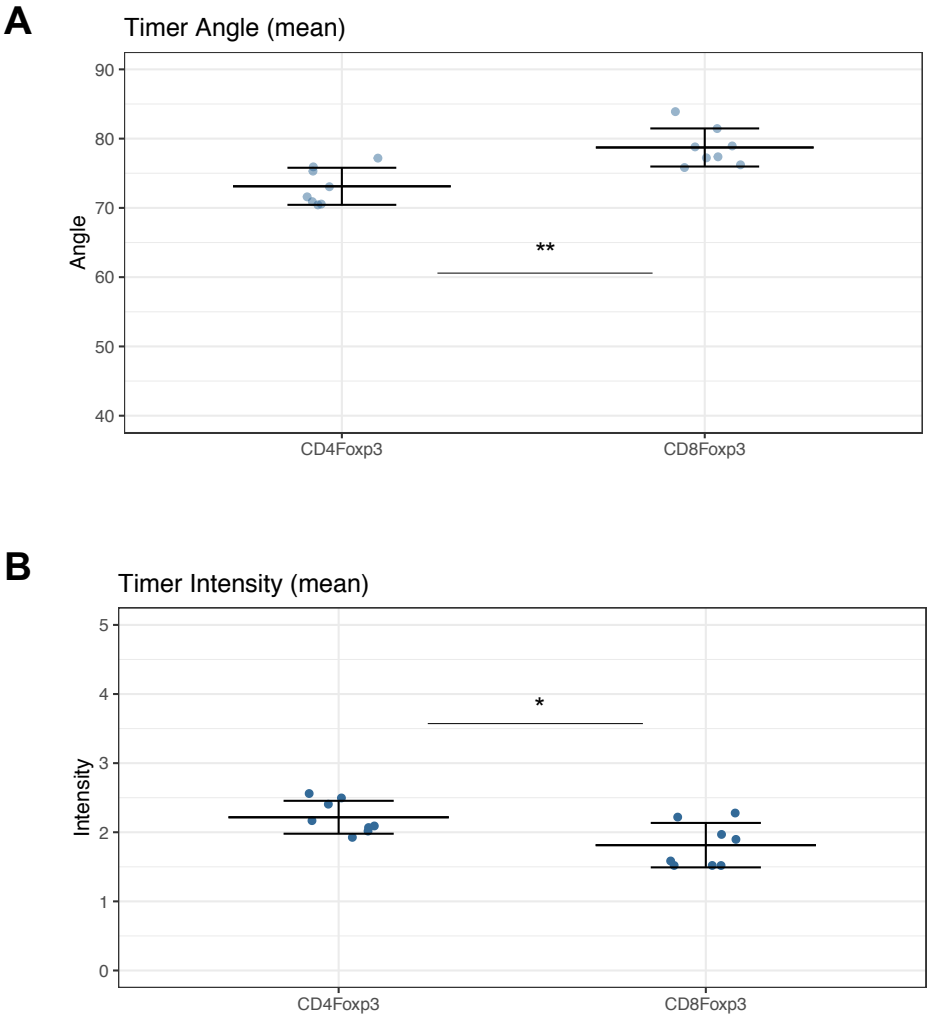

Figure 6.32: **Mean *Nr4a3*-Timer angle and intensity of *Foxp3*$^+$ CD4 and CD8 SP cells.** Thymocytes from 4 weeks old *Nr4a3*-Tocky mice were analysed by a Cytek Aurora spectral analyser in two independent experiments and data was combined. Mean *Nr4a3*-Timer angle (A) and intensity (B) are shown for two populations: *Foxp3*$^+$CD4 SP (CD4Foxp3) and *Foxp3*$^+$CD8 SP (CD8Foxp3). Dashed line shows no statistically significant differences by one-way ANOVA analysis. Statistically significant differences by unpaired Student's t-test are shown as * for $p<0.05$ and ** for $p<0.01$. Error bars are representative of mean ± s.d, where n = 8 biological replicates. All mice used were *Foxp3*-GFP.

Foxp3-Tocky mice were used in order to determine whether the dynamics of *Foxp3* transcription are affected by T cell lineage. Very few CD8 SP were Timer$^+$ according to flow cytometry plots (Fig.6.33). Using *Foxp3*-Tocky:*Nr4a3*-GFP mice, it was shown that, irrespective of T cell lineage, *Foxp3* transcription is only induced and sustained following strong TCR signals. Considering that Blue$^+$Red$^+$ cells from *Nr4a3*-Tocky mice have high Timer intensities (Chapter III, Fig.5.3), *Nr4a3*-GFP^{hi} cells may have received frequent TCR signals (Fig.6.34).

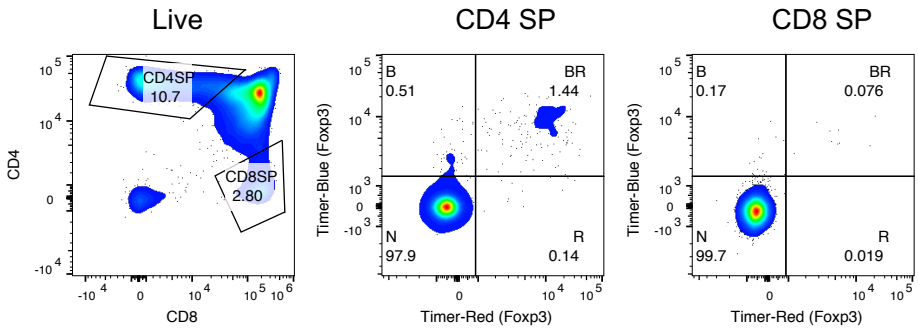

Figure 6.33: ***Foxp3*-Timer protein expression in CD4 and CD8 SP cells.** Thymocytes from 4 weeks old *Nr4a3*-Tocky mice were analysed by flow cytometry on on a Cytek Aurora spectral analyser and the *Foxp3*-Timer expression patterns are shown for CD4 SP and CD8 SP cells. Data shown are representative of 2 independent experiments that used 2 and 5 mice per experiment.

Given the much lower Timer angle and intensity values of CD8 SP cells compared to CD4 SP cells, it is possible that cells which express *Foxp3* do not survive very well in this population (Fig.6.35). While most Timer$^+$ cells of the CD4 SP pool were found in the Persistent locus, in CD8 SP they were found in the New locus (Fig.6.36). This suggests that while CD8 SP cells are able to induce *Foxp3*, they are less capable of sustaining it.

Although CD25 MFI was significantly lower in Timer$^+$CD8 SP cells compared to CD4, its pattern of expression was equivalent between the two populations. This indicates a universal effect of CD25 expression on *Foxp3* transcription dynamics. Continuous *Foxp3* transcription accumulates CD25 and when it is no longer sustained, CD25 becomes down-

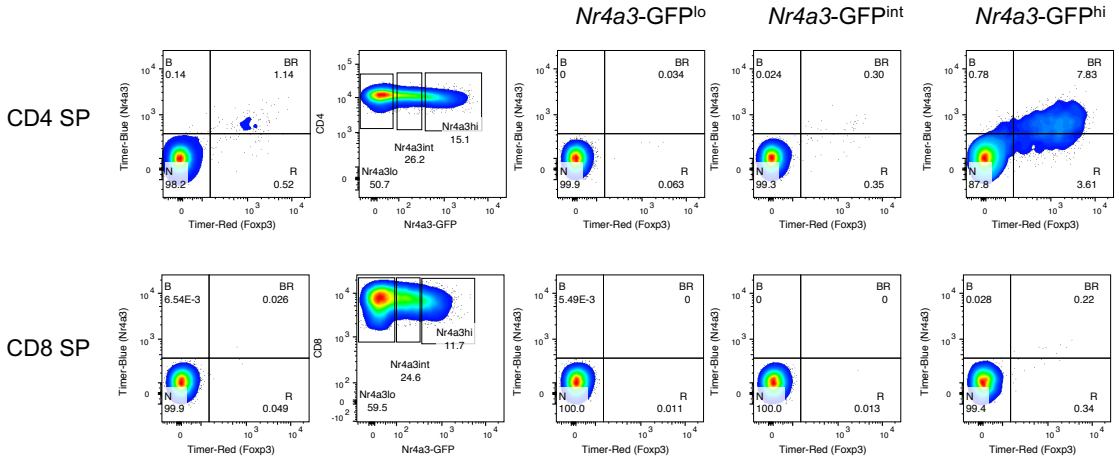

Figure 6.34: ***Foxp3*-Timer protein expression in *Nr4a3*$^+$ CD4 and CD8 SP cells.** Thymocytes from 5 weeks old *Foxp3*-Tocky:*Nr4a3*-GFP mice were analysed by flow cytometry on on a Fortessa III instrument and the *Foxp3*-Timer expression patterns are shown for CD4 SP and CD8 SP cells according to their expression levels of *Nr4a3*-GFP. Data are representative of three independent experiments that used 3 mice per experiment.

regulated (Fig.6.37). Since CD8 SP were mostly in the New locus, it is possible that they are immediately deleted (Fig.6.36) and their poor survival outcome is likely due to the fact that they cannot upregulate CD25 much to receive IL-2 signalling (Fig.6.37).

As shown by the RNAseq data (Fig.6.6), *Foxp3* accumulation was associated with an increase in TNFRSF members. Here, consistent levels of GITR and OX40 were expressed in each Timer locus by CD4 SP cells (Fig.6.38). CD8 SP showed significantly lower levels of both markers. While GITR became upregulated with sustained *Foxp3* transcription, OX40 levels remained at a base line. Developing *Foxp3*$^+$ cells may be less reliant on OX40 in the CD8 lineage compared to CD4. Alternatively, reduced OX40 levels past the New locus could account for the poor survival rate of *Foxp3*-expressing CD8 SP.

Both *Foxp3*$^+$CD4 and CD8 SP cells accumulated PD-1 upon sustained TCR signals, with the latter showing significantly higher levels (Fig.6.39A). PD-1 expression was high in both CD4 and CD8 SP cells in the New *Foxp3*-Timer locus, which is consistent with the

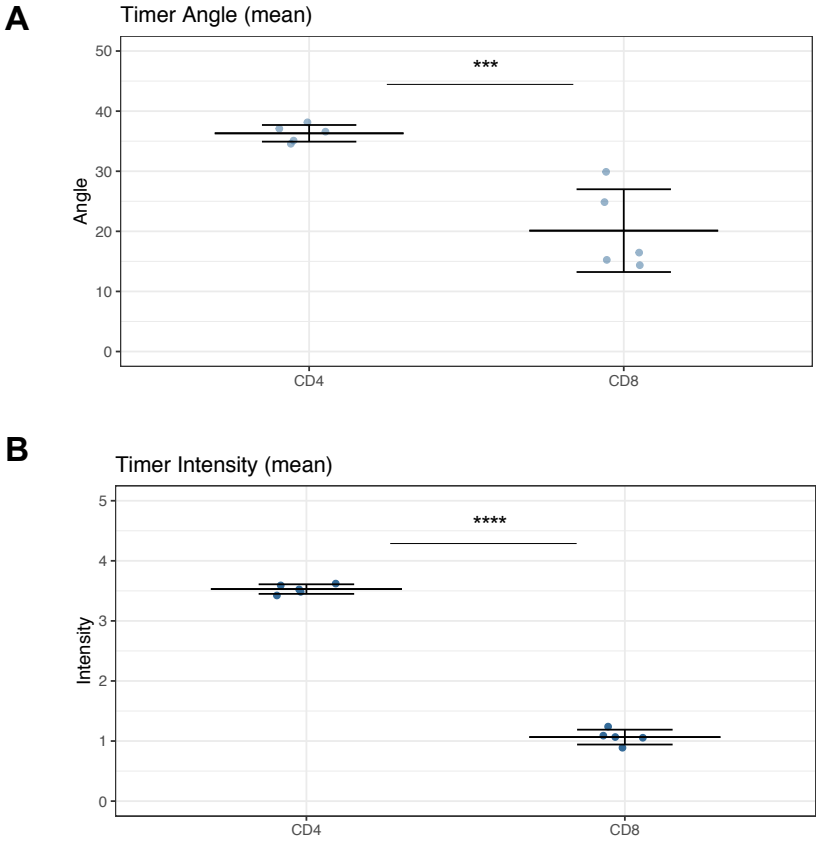

Figure 6.35: ***Foxp3*-Timer angle and intensity of CD4 and CD8 SP cells.** Thymocytes from 4 weeks old *Foxp3*-Tocky mice were analysed by a Cytek Aurora spectral analyser. Mean *Foxp3*-Timer angle (A) and intensity (B) are shown for CD4 SP and CD8 SP cells. Statistically significant differences by unpaired Student's t-test are shown as *** for $p<0.001$ and **** for $p<0.0001$. Error bars are representative of mean ± s.d, where $n = 5$ biological replicates. Data shown are representative of 2 independent experiments that used 2 and 5 mice per experiment.

fact that *de novo Foxp3* transcription requires persistent TCR signals. As *Foxp3*-Timer protein matured, however, there was a large discrepancy in PD-1 expression between CD4 and CD8 SP cells. While PD-1 appeared to be mostly dispensable for sustained *Foxp3* transcription by CD4 SP, CD8 SP cells seemed heavily reliant on it for this purpose. Alternatively, some PD-1^{hi}CD4 SP may be deleted, while the ones that survive are interacting with PD-1 ligands on TECs. It was shown earlier in *Foxp3*$^+$CD4 SP populations that $CD25^-$ cells are enriched with PD-1 (Fig.6.24). The fact that most *Foxp3*$^+$CD8 SP cells were $CD25^-$ justifies the overall PD-1^{hi} phenotype (Fig.6.39).

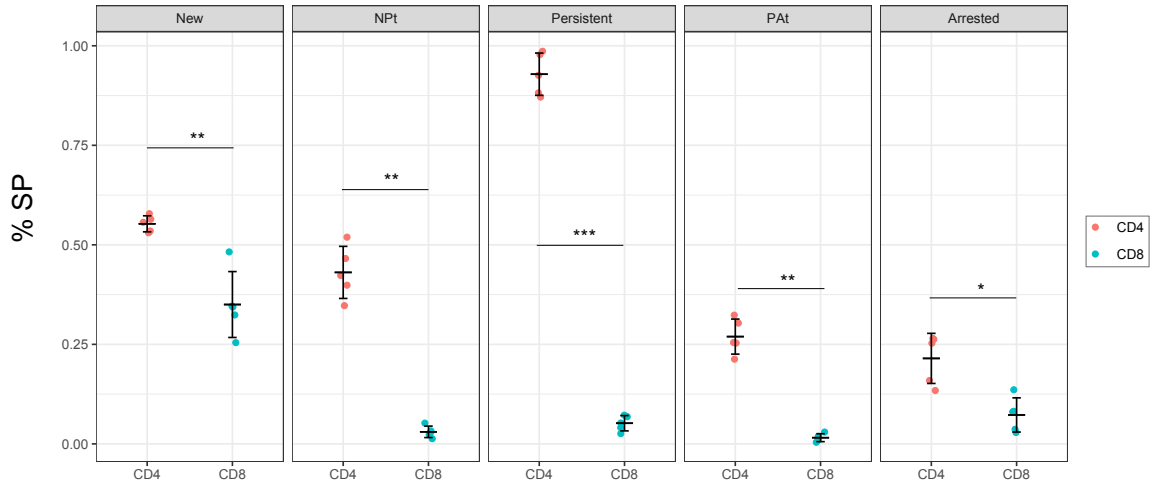

Figure 6.36: **Frequency of *Foxp3*$^+$ CD4 and CD8 SP cells in each *Foxp3*-Timer locus.** Thymocytes from 4 weeks old *Foxp3*-Tocky mice were analysed by a Cytek Aurora spectral analyser. The percentage of cells in each Timer locus among their parent population is shown by scatter plot for CD4 SP and CD8 SP cells. Any statistically significant differences from unpaired Student's t test are shown as * for p<0.05, ** for p<0.01, *** for p<0.001 and ****for p<0.0001. Error bars are representative of mean ± s.d, where n = 5 biological replicates. Data shown are representative of 2 independent experiments that used 2 and 5 mice per experiment.

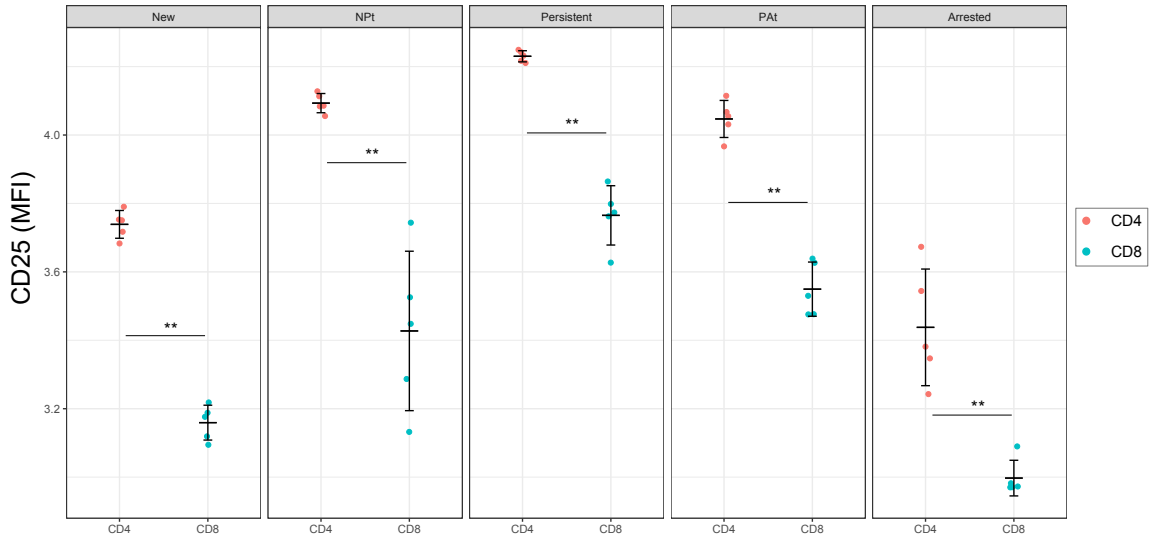

Figure 6.37: **CD25 MFI of CD4 and CD8 SP cells in each *Foxp3*-Timer locus.** Thymocytes from 4 weeks old *Foxp3*-Tocky mice were analysed by a Cytek Aurora spectral analyser. Plots show mean fluorescence intensity of the marker CD25 expressed in each Timer locus by CD4 SP and CD8 SP cells. Any statistically significant differences from unpaired Student's t test are shown as * for p<0.05, ** for p<0.01, *** for p<0.001 and ****for p<0.0001. Error bars are representative of mean ± s.d, where n = 5 biological replicates. Data shown are representative of 2 independent experiments that used 2 and 5 mice per experiment.

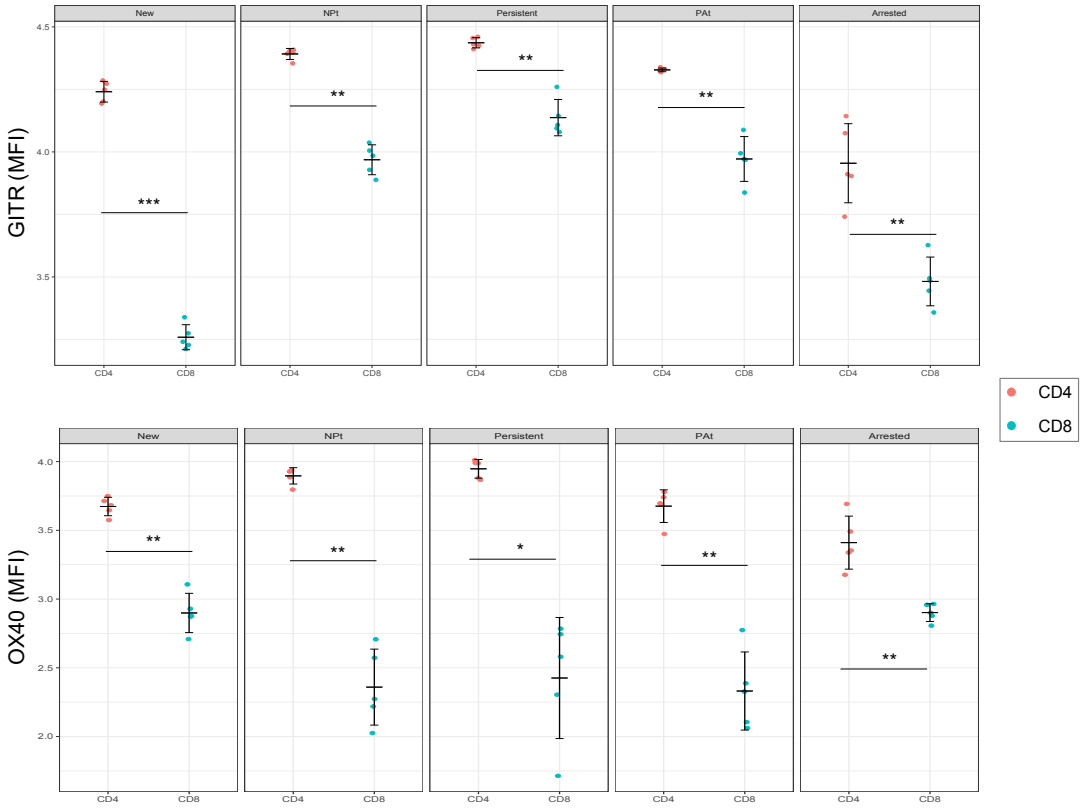

Figure 6.38: **GITR and OX40 MFI of CD4 and CD8 SP cells in each *Nr4a3*-Timer locus.** Thymocytes from 4 weeks old *Foxp3*-Tocky mice were analysed by a Cytek Aurora spectral analyser. Plots show mean fluorescence intensity of the markers GITR (top) and OX40 (bottom) expressed in each Timer locus by CD4 SP and CD8 SP cells. Any statistically significant differences from unpaired Student's t test are shown as * for $p<0.05$, ** for $p<0.01$, *** for $p<0.001$ and ****for $p<0.0001$. Error bars are representative of mean ± s.d, where n = 5 biological replicates. Data shown are representative of 2 independent experiments that used 2 and 5 mice per experiment.

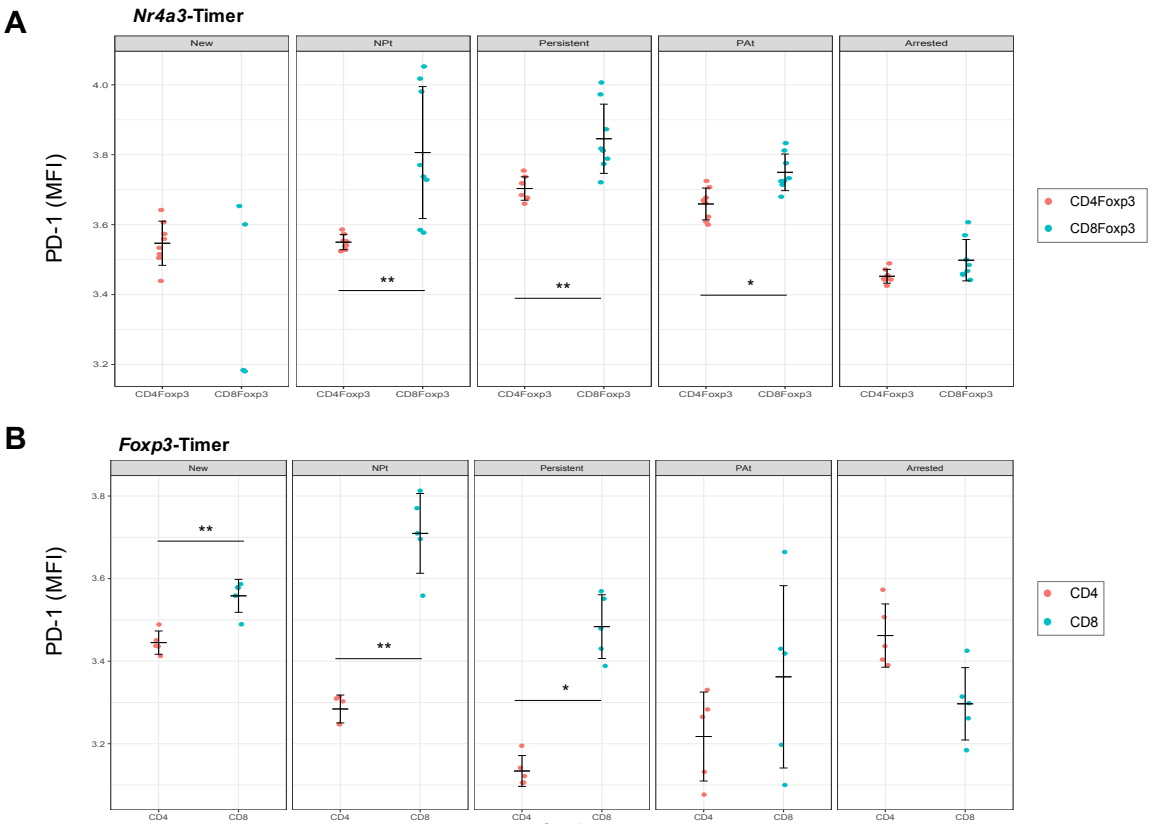

Figure 6.39: **PD-1 MFI of CD4 and CD8 SP cells in each *Nr4a3*-Timer and *Foxp3*-Timer locus.** Plots show mean fluorescence intensity of the marker PD-1 across *Nr4a3*-Timer loci by *Foxp3*$^+$CD4 SP (CD4Foxp3) and *Foxp3*$^+$CD8 SP (CD8Foxp3) cells (top figure) or *Foxp3*-Timer loci by CD4 SP and CD8 SP cells (bottom figure). Any statistically significant differences from unpaired Student's t-test are shown as * for $p<0.05$, ** for $p<0.01$, *** for $p<0.001$ and ****for $p<0.0001$. Error bars are representative of mean $\pm$ s.d, where n = 8 biological replicates (top figure, two independent experiments from which data was combined) or 5 biological replicates (bottom figure, data are representative of two independent experiments that used 2 and 5 mice each).

6.2.7 The impact of Bim deficiency on *Foxp3*$^+$CD8 SP development

Foxp3$^+$CD8 SP cells were analysed in KO mice in order to determine whether Bim-mediated deletion also occurs in this population. *Foxp3*$^+$CD8 SP cells were gated according to CD25 expression into CD25$^-$ and CD25$^+$ subpopulations (Fig.6.41).

KO CD8 SP cells expressed significantly higher proportions of *Foxp3* than Het (Fig.6.40A), as well as absolute cell numbers of *Foxp3*$^+$CD8 SP (Fig.6.40B). The proportions between CD25$^-$ and CD25$^+$ cells were similar between the two genotypes within the *Foxp3*$^+$CD8 SP parent population (Fig.6.40C) because KO mice accumulated both CD25$^-$ and CD25$^+$ *Foxp3*$^+$CD8 SP cells (Fig.6.40D-E). This suggests that in the case of *Foxp3*CD8 SP cells, the antigen niches associated with CD25$^-$ and CD25$^+$ population development are not normally saturated. These two populations were not particularly enriched with PD-1^{hi} cells (Fig.6.40F), as it was observed in the CD4 lineage (Fig.6.26D). Unlike *Foxp3*$^+$CD4 SP, they were also not significantly different between genotypes in terms of Timer angle, intensity and Timer locus distribution of Timer$^+$ cells (Fig.6.42, Fig.6.43). This suggests that the *Foxp3*$^+$CD8 SP populations that accumulate in the absence of Bim do not have particularly more self-reactive TCRs than the ones which develop normally.

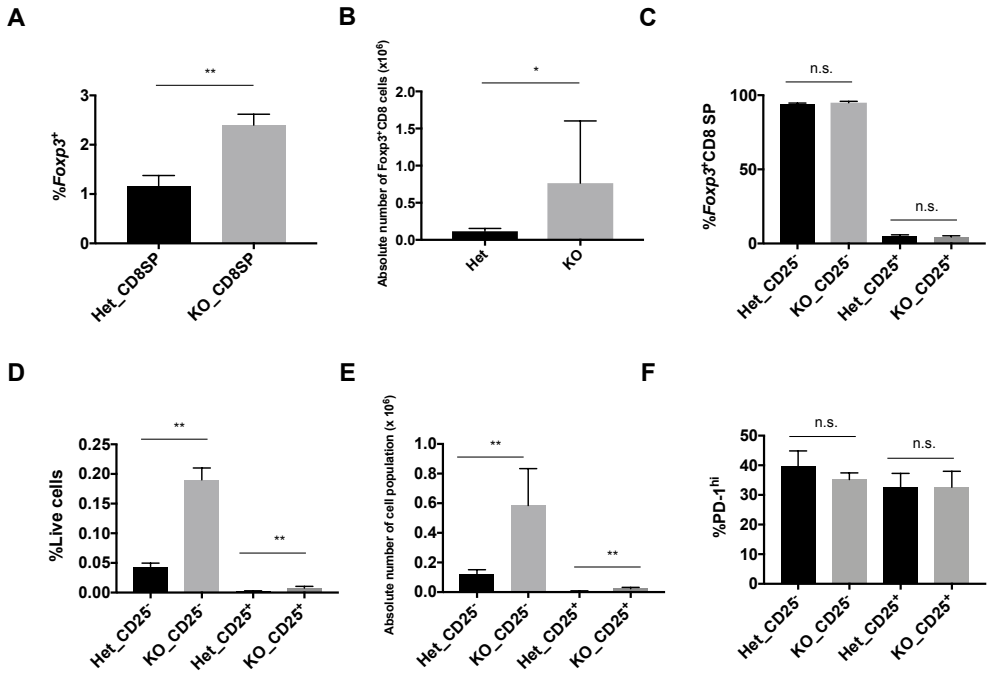

Figure 6.40: **Effect of Bim deficiency on the proportions of CD25$^-$ and CD25$^+$*Foxp3*$^+$CD8 SP populations.** Thymocytes were harvested from 5-7 weeks old *Nr4a3*-Tocky:Bim$^{WT/KO}$ or *Nr4a3*-Tocky:Bim$^{KO/KO}$ mice and were analysed by flow cytometry on a Fortessa III instrument.

(A) Bar chart shows the percentage of *Foxp3*$^+$ cells in the CD8 SP fraction for either genotype.
(B) Bar chart shows the absolute cell number of *Foxp3*$^+$CD8 SP in the thymus in either genotype.
(C) Bar chart shows what percentage of the total *Foxp3*$^+$CD8 SP pool the CD25$^-$*Foxp3*$^+$CD8 SP and CD25$^+$*Foxp3*$^+$CD8 SP subpopulations represent in either genotype.
(D) Bar chart shows the absolute percentage of the CD25$^-$*Foxp3*$^+$CD8 SP and CD25$^+$*Foxp3*$^+$CD8 SP subpopulations in the thymus in either genotype.
(E) Bar chart shows the absolute cell number of the CD25$^-$*Foxp3*$^+$CD8 SP and CD25$^+$*Foxp3*$^+$CD8 SP subpopulations in the thymus in either genotype.
(F) Bar chart shows the percentage of PD-1^{hi} cells in the CD25$^-$*Foxp3*$^+$CD8 SP and CD25$^+$*Foxp3*$^+$CD8 SP subpopulations for either genotype.

Each population was individually compared between the two genotypes and any statistically significant differences from Mann-Whitney U test (performed on percentage data) or unpaired Student's t-test (performed on absolute count data) are shown as * for $p<0.05$, ** for $p<0.01$, *** for $p<0.001$ and ****for $p<0.0001$. Error bars are representative of mean ± s.d, where n = 6 biological replicates for each genotype. Data from three independent experiments was combined. All mice used were *Foxp3*-GFP.

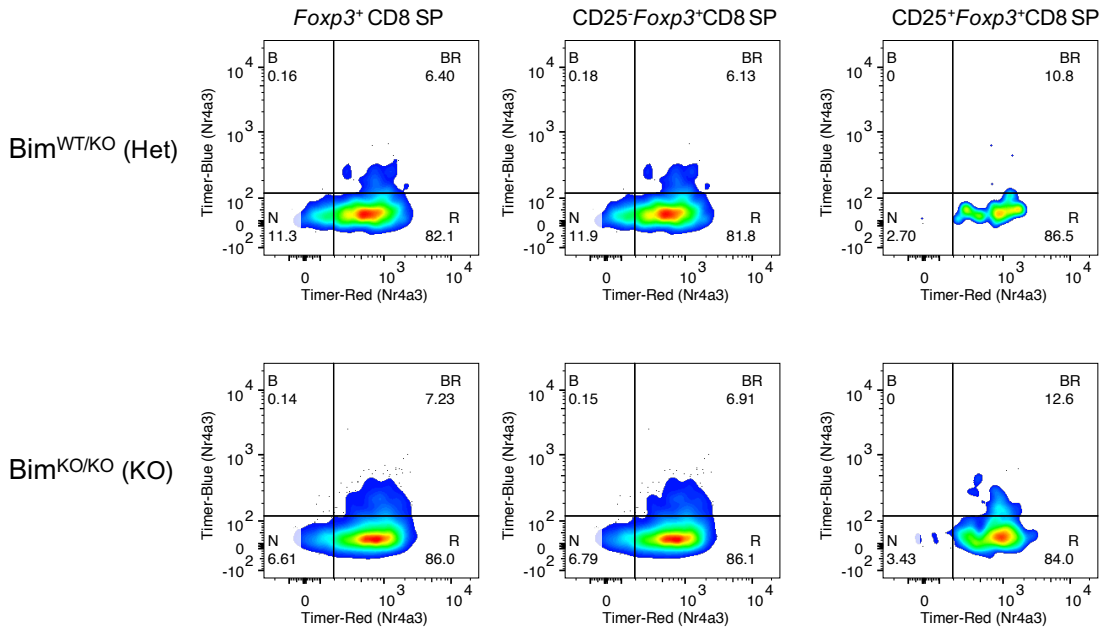

Figure 6.41: **Effect of CD25 expression on *Nr4a3*-Timer protein expression in Bim-sufficient and Bim-defficient *Foxp3*$^+$CD8SP cells.** Thymocytes were harvested from 6 weeks old *Nr4a3*-Tocky:Bim$^{WT/KO}$ or *Nr4a3*-Tocky:Bim$^{KO/KO}$ mice and were analysed by flow cytometry on a Fortessa III instrument. The resulting 2-D flow cytometry plots show the *Nr4a3*-Timer protein expression patterns by CD25$^-$ or CD25$^+$ *Foxp3*$^+$CD8 SP cells. Data shown are representative of at least 4 independent experiments that used 2-4 mice per group. All mice used were *Foxp3*-GFP.

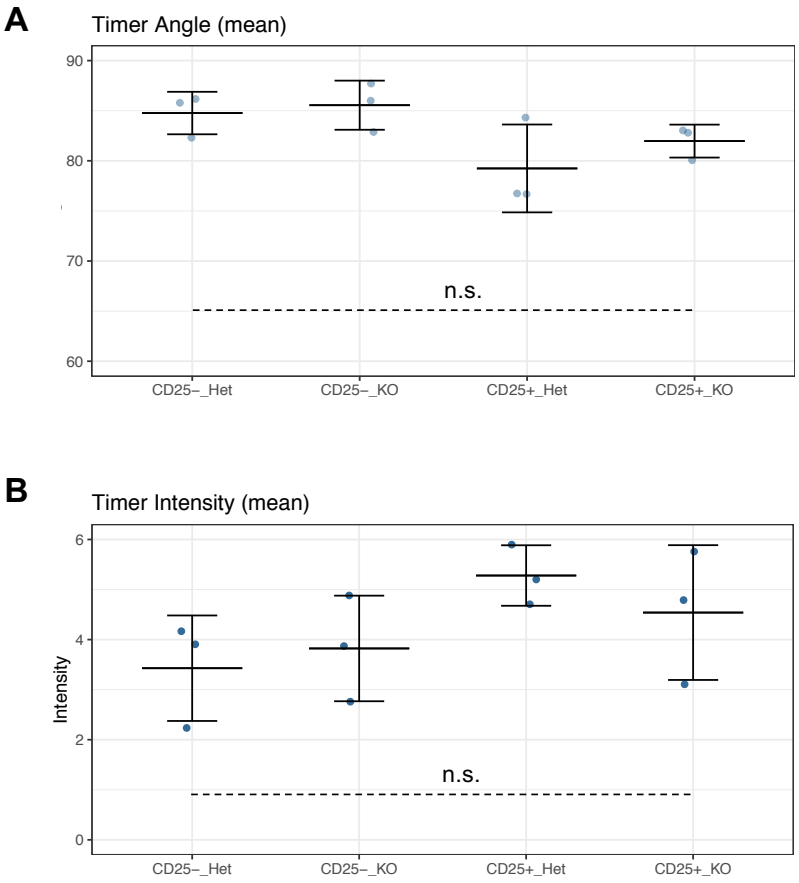

Figure 6.42: **Mean Timer angle and intensity of Bim-sufficient and Bim-defficient *Foxp3*$^{+}$CD8SP cells.** Thymocytes were harvested from 6 weeks old *Nr4a3*-Tocky:Bim$^{WT/KO}$ or *Nr4a3*-Tocky:Bim$^{KO/KO}$ mice and were analysed by flow cytometry on a on a Fortessa III instrument. Mean Timer angle (A) and intensity (B) are shown for two populations: CD25^{-}*Foxp3*$^{+}$CD8 SP (CD25^{-}) and CD25^{+}*Foxp3*$^{+}$CD8 SP (CD25^{+}). No statistically significant differences were found by one-way ANOVA analysis (dashed line). Error bars are representative of mean ± s.d, where n = 3 biological replicates for each genotype. Data shown are representative of at least 4 independent experiments that used 2-4 mice per group. All mice used were *Foxp3*-GFP.

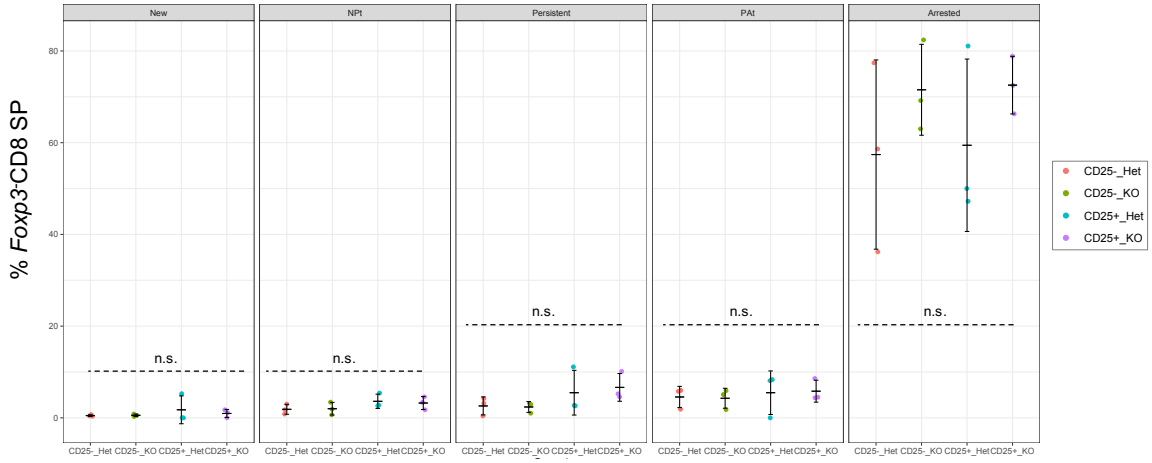

Figure 6.43: **Frequency of *Foxp3*$^{+}$CD8SP cells cells in each *Nr4a3*-Timer locus in Bim-sufficient and Bim-deficient mice.** Thymocytes were harvested from 6 weeks old *Nr4a3*-Tocky:Bim$^{WT/KO}$ or *Nr4a3*-Tocky:Bim$^{KO/KO}$ mice and were analysed by flow cytometry on a on a Fortessa III instrument. The percentage of cells in each Timer locus among their parent population is shown by scatter plot for two populations: CD25^{-}*Foxp3*$^{+}$CD8 SP (CD25^{-}) and CD25^{+}*Foxp3*$^{+}$CD8 SP (CD25^{+}). No statistically significant differences were found by one-way ANOVA analysis (dashed line). Error bars are representative of mean ± s.d, where n = 3 biological replicates for each genotype. Data shown are representative of at least 4 independent experiments that used 2-4 mice per group. All mice used were *Foxp3*-GFP.

6.3 Discussion

Based on the findings presented in this chapter, the model for CD4 SP thymic development in *Nr4a3*-Tocky mice previously proposed in Chapter III was further expanded to include *Foxp3*$^+$ cells (Fig.6.44). Since *Foxp3* was only upregulated following persistent TCR signals, the immediate precursors of Fox_BR cells must be CD4_BR cells. In this model, CD4_BR cells represent a heterogeneous population comprised of cells that encountered their cognate antigen either at the DP or SP stage and survived negative selection. If a cell has moderate affinity to self-antigen, it upregulates Blue protein. However, there are upper and lower ends of the spectrum in terms of what moderate affinity represents. Cells with moderately-low affinity will become CD4_BR and then terminate signalling as they mature to CD4_R. Cells with moderately-high affinity to self-antigen will also become CD4_BR at first and sustain TCR signals of higher intensity, perhaps for a slightly longer duration than CD4_R precursors, leading to *Foxp3* transcription and subsequent maturation to Fox_R.

According to this model, early Fox_R progenitors can be either positively selected CD4_N or DP_N cells, which will encounter their cognate antigen to become CD4_B or DP_B, respectively. In WT mice, T cells do not maintain their DP phenotype for long enough to become B$^+$R$^+$ (Chapter II), the phenotype preceding *Foxp3* upregulation. This provides an explanation for why Treg are not naturally encountered in the cortex, although many can undergo selection there without the involvement of the medulla (Bensinger et al., 2001; Liston et al., 2008; Owen et al., 2019).

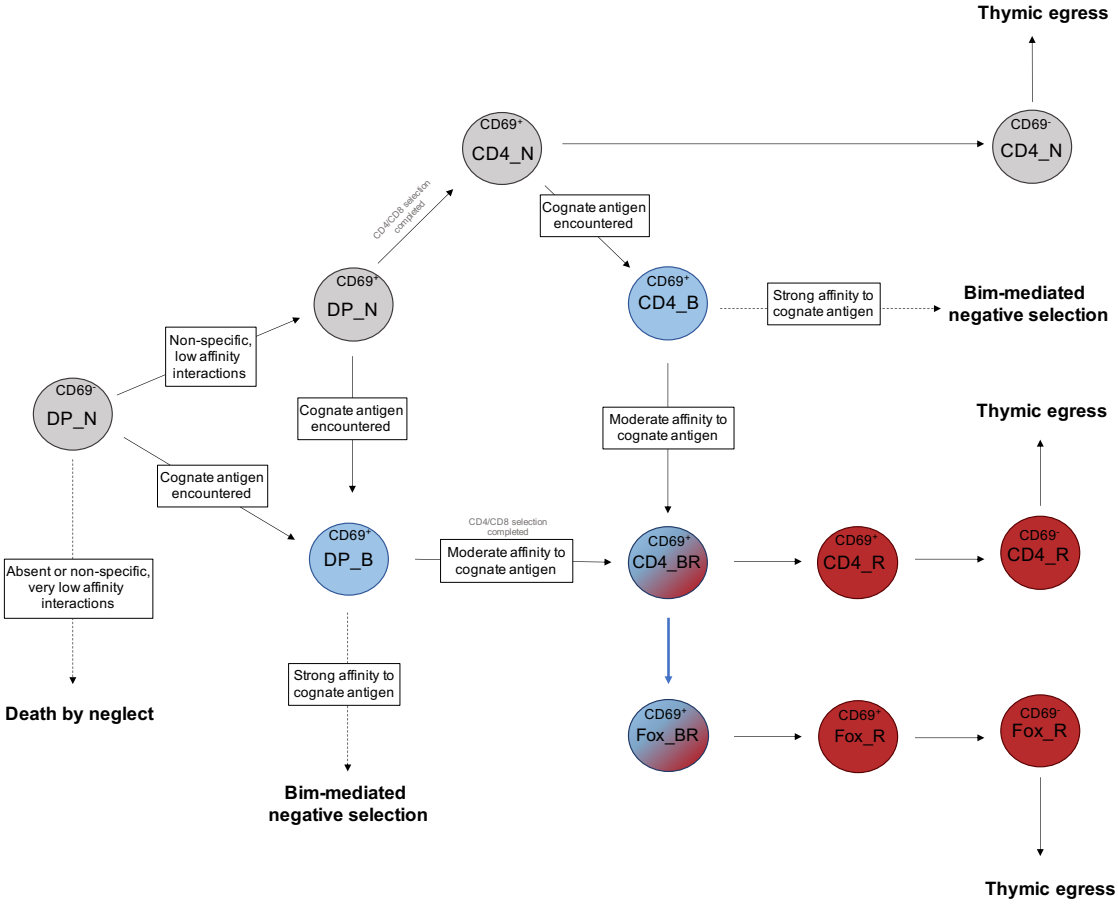

Figure 6.44: **Proposed model for thymic CD4 SP cell development.** Figure shows a new model of Foxp3^{-}CD4 SP and Foxp3^{+}CD4 SP cell differentiation from the DP stage, where CD69 expression and *Nr4a3*-Timer maturation are used to identify key thymic developmental stages.

In the absence of Bim, DP_B cells that escape negative selection become either DP_BR or DP_R. Some of these cells are $CD4^{hi}$ and express *Foxp3* (Chapter II). They likely join the the mature *Foxp3*$^+$ pool which accumulates in the absence of Bim (Zhan et al., 2011; Krishnamurthy et al., 2015). Based on these observations, together with the data presented in this chapter, a model for Bim-deficient *Foxp3*$^+$CD4 SP cell development in *Nr4a3*-Tocky mice is illustrated in Fig.6.45.

The transcriptional profiles of Bim-sufficient and Bim-deficient *Foxp3*$^+$ cells were very similar. Bim deficiency changes the dynamics of cellular development, while the transcriptome of each cell at each developmental stage may not be different when the Tocky system is used and the time domain is closely analysed. One key transcriptional difference observed was in the level of CD25 transcript accumulated by Fox_R cells, which was much lower in the absence of Bim. This was because Bim-deficient mice accumulated a large population of CD25$^-$*Foxp3*$^+$CD4 SP cells. While the proportion of CD25$^+$*Foxp3*$^+$CD4 SP cells was not affected in these mice, they were enriched with more self-reactive T cells. Therefore, CD25$^+$*Foxp3*$^+$CD4 SP precursors compete for very limited antigen availability compared to CD25$^-$*Foxp3*$^+$CD4 SP. Bim therefore, deletes self-reactive precursors of both of these populations. CD25 ligation is dispensable for Treg lineage stability, but essential for their suppressive function in the periphery (Toomer et al., 2019). Preferential accumulation of CD25$^-$ Treg in the $Bim^{KO/KO}$ model likely contributes to the fact that mice still develop disease, despite the increase in *Foxp3*$^+$ cells.

While the temporally dynamic changes in *Nr4a3* transcription were not influenced by the levels of CD25, *Foxp3* transcription was highly affected. According to *Nr4a3* and *Foxp3*-Timer data, persistent signals are required for initial upregulation of *Foxp3*. CD25 also becomes progressively upregulated with sustained TCR signals of high intensity. CD25$^-$*Foxp3*$^+$CD4 SP cells therefore, receive persistent, low-intensity TCR signals. As a result, they show much lower levels of GITR and OX40 compared to CD25$^+$ cells and

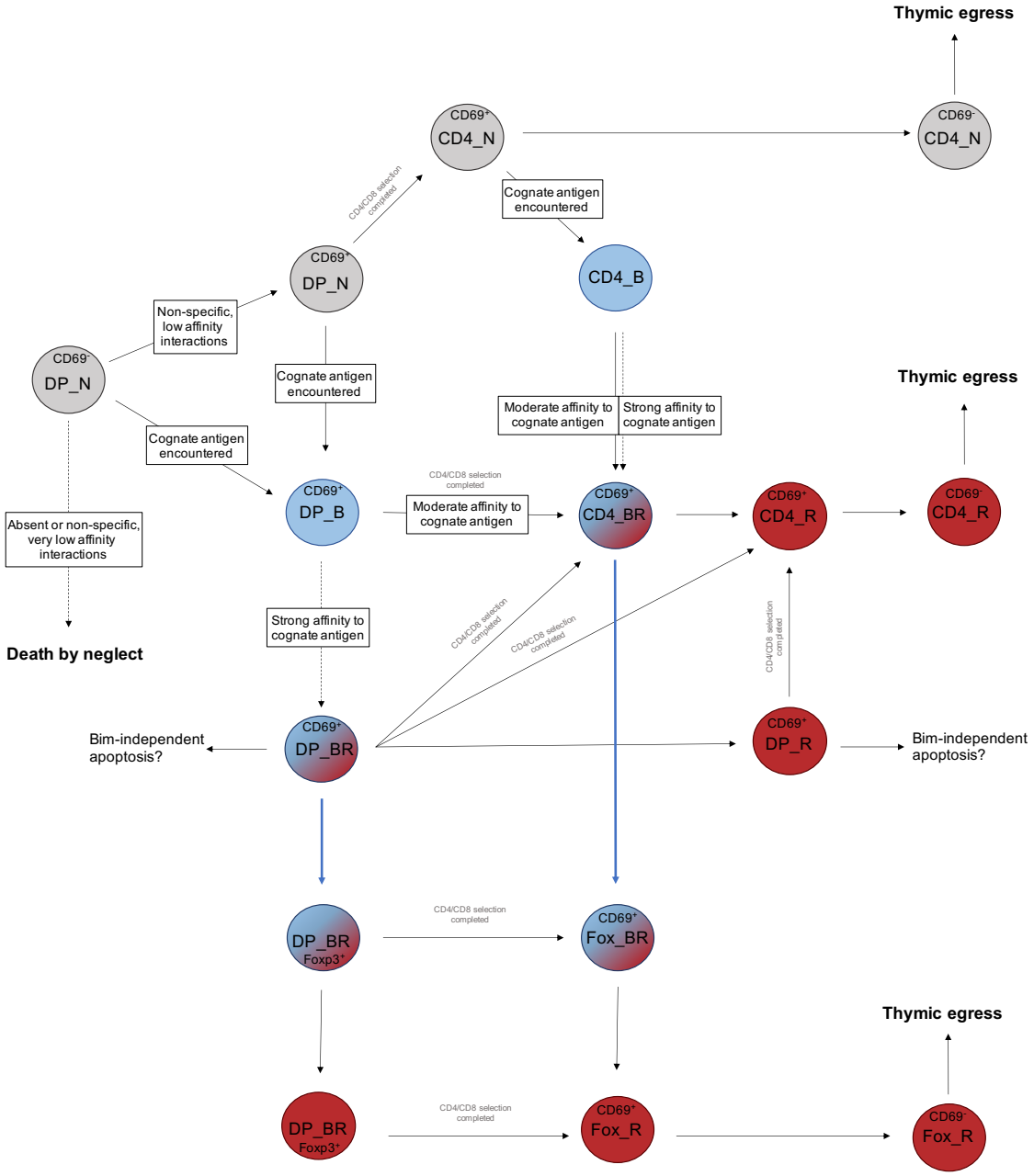

Figure 6.45: **Proposed model for Bim-deficient thymic CD4 SP cell development.** Figure shows a new model of Foxp3$^-$CD4 SP and Foxp3$^+$CD4 SP cell differentiation from the DP stage in Bim-deficient mice, where CD69 expression and *Nr4a3*-Timer maturation are used to identify key thymic developmental stages.

transcribe very little *Foxp3*. CD25^{lo}*Foxp3*$^+$CD4 SP may be a heterogenous population, comprised of CD25^{hi}*Foxp3*$^+$CD4 SP precursors and cells with a different TCR repertoire, which receive weaker signals but sufficient to maintain a *Foxp3*$^+$ phenotype.

Sustained *Foxp3*-Timer transcription by CD25^{hi}*Foxp3*$^{+}$CD4 SP cells resulted in down-regulation of PD-1. This could be due to PD-1 ligation-mediated suppression of TCR signalling downstream, as wells as to negative selection of cells that would differentiate into CD25^{hi}PD-1^{hi}*Foxp3*$^{+}$CD4 SP, which is supported by the fact that this population was accumulated in Bim-deficient mice. Both CD25^{-} and CD25^{lo} cells, however, maintained high levels of PD-1 throughout *Foxp3*-Timer protein maturation. Since both of these populations accumulate less *Foxp3* transcript than CD25^{hi} cells, yet bear TCR repertoires that are much more self-reactive than *Foxp3*$^{-}$ T cells, it is possible that high PD-1 expression acts a compensatory mechanism to prevent their possible pathogenicity. This is supported by the fact that mice with partial insufficiency of *Foxp3* only develop autoimmunity in the absence of PD-1 (Zhang et al., 2016).

The temporally dynamic changes in *Nr4a3* transcription associated with *Foxp3* upregulation were not influenced by CD4/CD8 lineage selection. Although a much smaller proportion of CD8 SP cells expressed *Foxp3*, they still required persistent TCR signals of high intensity. In CD8 SP cells, however, the ratio between CD25^{+} and CD25^{-}*Foxp3*$^{+}$ cells was much smaller than that of CD4 SP. This was consistent with the observation that, on average, *Foxp3*$^{+}$CD8 SP cells received signals of lower intensity than CD4SP. As a result, most CD8 SP cells showed new *Foxp3* transcription that failed to be sustained.

As *Foxp3*-Timer protein matured in CD4 SP cells, levels of GITR and OX40 peaked upon persistent transcription. The very few CD8 SP cells that persistently transcribed *Foxp3* also had high GITR expression levels, but diminished OX40 compared to cells that newly upregulated it. An inability to maintain consistent levels of OX40 might justify why CD8 SP cells are not as efficient at sustaining *Foxp3* transcription as CD4 SP. This is supported by the finding that OX40-deficient mice have significantly lower numbers of mature thymic CD25^{+}*Foxp3*$^{+}$ T cells (Kumar et al., 2018). Furthermore, OX40 activates NF-κB to promote survival and proliferation, indirectly causes Bcl-2 anti-apoptotic

family activation and OX40 deficient cells have poor survival rates (Rogers et al., 2001; Song, So and Croft, 2008). Therefore, it is likely that diminished OX40 expression by *Foxp3*$^+$CD8 SP cells contributes to their poor survival outcome.

Bim-deficient mice accumulated both CD25$^-$ and CD25$^+$*Foxp3*$^+$CD8 SP cells. This shows that while CD4 SP cells compete for antigen availability to become CD25$^+$*Foxp3*$^+$, in the CD8 lineage the antigen niches associated with CD25$^+$*Foxp3*$^+$ cell development are not saturated. Interestingly, the *Foxp3*$^+$CD8 SP cells accumulated in Bim-deficient mice did not appear more self-reactive than the control based on *Nr4a3*-Timer intensity and transcriptional dynamics. If CD8 SP differentiation from DP cells requires shorter TCR signals, as discussed in Chapter III, it is possible that highly self-reactive, MHC-I-restricted T cells that could upregulate *Foxp3* were diverted towards the CD4 lineage following prolonged TCR signalling in the absence of Bim. Collectively, the findings in this chapter indicate that some *Foxp3*$^+$ cells are deleted in a Bim-mediated manner in CD4 SP after receiving strong TCR signals, while the survival of *Foxp3*$^+$CD8 SP is mainly impaired by the absence of sustained survival signals.

Conclusions

Thymic T cell development is a dynamic, highly complex process that is essential for protection against recurring infections. Several mechanisms are in place to ensure thymic output of mature T cells capable of reacting to foreign antigen, while remaining tolerant to self. Any malfunction in this process can have detrimental consequences, such as in the case of autoimmune disease. The complexity of thymic T cell development poses a great challenge for scientists to understand how all the different components involved act and interact in order to prevent such undesirable outcomes. All major developmental steps are triggered by TCR interactions with self-antigen and cellular fate is ultimately dictated by the nature of TCR signals. Therefore, the development of transgenic models in which TCR signalling activity is reported represents a major step forward in "deciphering" thymic T cell development.

This study developed and used the novel Tocky system in order to investigate how thymic T cells progress from immature DP to mature SP. The advantage of this technology is that it helps capture the dynamic changes occurring during T cell differentiation and maturation. This enables us to piece together the temporal order of events involved in thymic T cell development.

Using the *Nr4a3*-Tocky model, it was shown that while most DPs that passed positive selection and upregulated CD69^{+} received weak TCR signals, over 5% received strong TCR signals and expressed Blue protein. This work supports several fates for Blue^{+}Red^{-} DPs. They are either rapidly deleted in a Bim-mediated manner, before Blue protein matures to Red, or they completely downregulate one of their co-receptors and become SP. Some of the Blue^{+}Red^{-} DPs that mature to the SP stage may upregulate *Foxp3* following persistent signals and mature as Treg. While lineage selection precedes Treg

differentiation, it is possible that cognate antigen recognition at the DP stage primes cells to differentiate into Treg if TCR signalling is sustained.

The *Nr4a3*-Tocky:Bim$^{KO/KO}$ model proved very useful in identifying self-reactive DP cells that erroneously survive Bim-mediated negative selection. These DPs were either Blue^{+}Red^{+} or Blue^{-}Red^{+}. The largest proportion expressed a PD-1^{hi}CD4^{lo}CD8^{lo} phenotype, suggesting that this is the subpopulation most susceptible to negative selection. This study also showed that some self-reactive DPs that escape negative selection have a GITR^{hi}*Foxp3*$^{+}$CD4^{hi} CD8^{lo} phenotype, rendering them the most likely precursor of self-reactive *Foxp3*$^{+}$ SP that accumulate in the absence of Bim.

Regardless of surface marker expression, all SP cells required persistent TCR signals for *Foxp3* upregulation. Using the *Foxp3*-Tocky system, it was shown that *Foxp3* transcriptional dynamics differed according to CD4/CD8 lineage, as well as to CD25 levels. Although *Foxp3* was upregulated regardless of surface marker expression, its transcription was better sustained by cells from the CD4 lineage compared to CD8. On average, *Foxp3*$^{+}$CD4 SP received signals of higher intensity than *Foxp3*$^{+}$CD8 SP. They were also composed of a larger proportion of cells that showed high CD25 expression. CD25^{hi}CD4 SP received signals of higher intensity than CD25^{lo}CD4 SP or CD25^{-}CD4 SP and were much better at sustaining *Foxp3* transcription. Additionally, *Nr4a3*-Tocky:Bim$^{KO/KO}$ data showed that in CD4 SP, all antigen niches for CD25^{+}*Foxp3*$^{+}$CD4 SP development become saturated during thymic development, while the ones for CD25^{+}*Foxp3*$^{+}$CD8 SP do not. Furthermore, while Bim-deficient *Foxp3*$^{+}$CD4 SP received signals of higher intensity than Bim-sufficient ones, this genotype effect was not observed in *Foxp3*$^{+}$CD8 SP. Therefore, most CD8 SP do not receive signals of high enough intensity to express CD25 and sustain *Foxp3* transcription. In the absence of IL-2 signals they may not survive very well, which would explain the large difference in *Foxp3*-expressing cells between the CD4/CD8 lineages. In light of these findings, it is tempting to speculate that there is

a signalling threshold imposed on MHC-I-restricted TCRs. It would be interesting to sort CD8 SP populations according to *Foxp3* and *Nr4a3*-Timer protein expression for RNAseq analysis, in order to further explore the differences between the CD4/CD8 lineages at transcript level.

Overall, this study provides a framework for a more sensitive approach to studying developing T cells in the thymus. Because only a small proportion of all thymic T cells are actively engaged in one of the selection processes at any given time, bulk analysis makes it challenging to successfully capture and closely investigate such events. This work therefore proposes a novel approach to understanding thymic T cell selection and maturation, by which developing cell populations are defined according to the temporal order of the dynamic changes in their gene transcription.

Bibliography

Ahn, S., Lee, G., Yang, S.J., Lee, D., Lee, S., Shin, H.S., Kim, M.C., Lee, K.N., Palmer, D.C., Theoret, M.R., Jenkinson, E.J., Anderson, G., Restifo, N.P. and Kim, M.G. (2008). TSCOT+ Thymic Epithelial Cell-Mediated Sensitive CD4 Tolerance by Direct Presentation. PLoS Biology, 6(8), p.e191.

Alberts, B. (2015). Molecular biology of the cell. New York, Ny: Garland Science.

Alyanakian, M.A., You, S., Damotte, D., Gouarin, C., Esling, A., Garcia, C., Havouis, S., Chatenoud, L. and Bach, J.F. (2003). Diversity of regulatory CD4+T cells controlling distinct organ-specific autoimmune diseases. Proceedings of the National Academy of Sciences, 100(26), pp.15806–15811.

Annacker, O., Pimenta-Araujo, R., Burlen-Defranoux, O., Barbosa, T.C., Cumano, A. and Bandeira, A. (2001). CD25+CD4+ T Cells Regulate the Expansion of Peripheral CD4 T Cells Through the Production of IL-10. The Journal of Immunology, 166(5), pp.3008–3018.

Baldwin, T.A. and Hogquist, K.A. (2007). Transcriptional Analysis of Clonal Deletion In Vivo. The Journal of Immunology, 179(2), pp.837–844.

Barthlott, T., Kohler, H. and Eichmann, K. (1997). Asynchronous Coreceptor Downregulation after Positive Thymic Selection: Prolonged Maintenance of the Double Positive State in CD8 Lineage Differentiation Due to Sustained Biosynthesis of the CD4 Coreceptor. The Journal of Experimental Medicine, 185(2), pp.357–362.

Bending, D., Martín, P.P., Paduraru, A., Ducker, C., Marzaganov, E., Laviron, M., Kitano, S., Miyachi, H., Crompton, T. and Ono, M. (2018). A timer for analyzing temporally dynamic changes in transcription during differentiation in vivo. The Journal of Cell Biology, 217(8), pp.2931–2950.

Bensinger, S.J., Bandeira, A., Jordan, M.S., Caton, A.J. and Laufer, T.M. (2001). Major Histocompatibility Complex Class II–Positive Cortical Epithelium Mediates the Selection of Cd4+25+ Immunoregulatory T Cells. Journal of Experimental Medicine, 194(4), pp.427–438.

Blank, C., Brown, I., Marks, R., Nishimura, H., Honjo, T. and Gajewski, T.F. (2003). Absence of Programmed Death Receptor 1 Alters Thymic Development and Enhances Generation of CD4/CD8 Double-Negative TCR-Transgenic T Cells. The Journal of Immunology, 171(9), pp.4574–4581.

Bonasio, R., Scimone, M.L., Schaerli, P., Grabie, N., Lichtman, A.H. and von Andrian, U.H. (2006). Clonal deletion of thymocytes by circulating dendritic cells homing to the thymus. Nature Immunology, 7(10), pp.1092–1100.

Bosselut, R., Guinter, T.I., Sharrow, S.O. and Singer, A. (2003). Unraveling a Revealing Paradox: Why major histocompatibility complex I-signaled thymocytes “paradoxically” appear as CD4+8lo transitional cells during positive selection of CD8+ T cells. The Journal of Experimental Medicine, 197(12), pp.1709–1719.

Bouillet, P., Metcalf, D., Huang, D.C., Kay, T.W., Adams, J.M. and Strasser, A. (1999). Proapoptotic Bcl-2 Relative Bim Required for Certain Apoptotic Responses, Leukocyte Homeostasis, and to Preclude Autoimmunity. Science, 286(5445), pp.1735–1738.

Brown, J.A., Dorfman, D.M., Ma, F .R., Sullivan, E.L., Munoz, O., Wood, C.R., Greenfield, E.A. and Freeman, G.J. (2003). Blockade of Programmed Death-1 Ligands on Dendritic Cells Enhances T Cell Activation and Cytokine Production. The Journal of Immunology, 170(3), pp.1257–1266.

Brugnera, E., Bhandoola, A., Cibotti, R., Yu, Q., Guinter, T.I., Yamashita, Y., Sharrow, S.O. and Singer, A. (2000). Coreceptor Reversal in the Thymus. Immunity, 13(1), pp.59–71.

Cainan, B.J., Szychowski, S., Ka-Ming Chan, F., Cado, D. and Winoto, A. (1995). A role for the orphan steroid receptor Nur77 in apoptosis accompanying antigen-induced negative selection. Immunity, 3(3), pp.273–282.

Campbell, R.E., Tour, O., Palmer, A.E., Steinbach, P.A., Baird, G.S., Zacharias, D.A. and Tsien, R.Y. (2002). A monomeric red fluorescent protein. Proceedings of the National Academy of Sciences, 99(12), pp.7877–7882.

Canté-Barrett, K., Gallo, E.M., Winslow, M.M. and Crabtree, G.R. (2006). Thymocyte Negative Selection Is Mediated by Protein Kinase C- and Ca2+-Dependent Transcriptional Induction of Bim. The Journal of Immunology, 176(4), pp.2299–2306.

Carpenter, A.C. and Bosselut, R. (2010). Decision checkpoints in the thymus. Nature Immunology, 11(8), pp.666–673.

Carson-Jurica, M.A., Schrader, W.T. and O'Malley, B.W. (1990). Steroid Receptor Family: Structure and Functions. Endocrine Reviews, 11(2), pp.201–220.

Chan, S.H., Cosgrove, D., Waltzinger, C., Benoist, C. and Mathis, D. (1993). Another

view of the selective model of thymocyte selection. Cell, 73(2), pp.225–236.

Cheng, L.E .C., Chan, F.K .M., Cado, D. and Winoto, A. (1997). Functional redundancy of the Nur77 and Nor-1 orphan steroid receptors in T-cell apoptosis. The EMBO Journal, 16(8), pp.1865–1875.

Cheng, A.M., Saxton, T.M., Sakai, R., Kulkarni, S., Mbamalu, G., Vogel, W., Tortorice, C.G., Cardiff, R.D., Cross, J.C., Muller, W.J. and Pawson, T. (1998). Mammalian Grb2 Regulates Multiple Steps in Embryonic Development and Malignant Transformation. Cell, 95(6), pp.793–803.

Chiarle, R., Podda, A., Prolla, G., Podack, E.R., Thorbeke, G.J. and Inghirami, G. (1999). CD30 Overexpression Enhances Negative Selection in the Thymus and Mediates Programmed Cell Death Via a Bcl-2-Sensitive Pathway. The Journal of Immunology, 163(1), pp.194–205.

Chinen, T., Kannan, A.K., Levine, A.G., Fan, X., Klein, U., Zheng, Y., Gasteiger, G., Feng, Y., Fontenot, J.D. and Rudensky, A.Y. (2016). An essential role for the IL-2 receptor in Treg cell function. Nature Immunology, 17(11), pp.1322–1333.

Chow, C.-W., Rincón, M., Cavanagh, J., Dickens, M. and Davis, R.J. (1997). Nuclear Accumulation of NFAT4 Opposed by the JNK Signal Transduction Pathway. Science, 278(5343), pp.1638–1641.

Churlaud, G., Pitoiset, F., Jebbawi, F., Lorenzon, R., Bellier, B., Rosenzwajg, M. and Klatzmann, D. (2015). Human and Mouse CD8+CD25+FOXP3+ Regulatory T Cells at Steady State and during Interleukin-2 Therapy. Frontiers in Immunology, 6.

Cibotti, R., Bhandoola, A., Guinter, T.I., Sharrow, S.O. and Singer, A. (2000). CD8 Coreceptor Extinction in Signaled CD4+CD8+ Thymocytes: Coordinate Roles for Both Transcriptional and Posttranscriptional Regulatory Mechanisms in Developing Thymocytes. Molecular and Cellular Biology, 20(11), pp.3852–3859.

Cormack, B.P., Valdivia, R.H. and Falkow, S. (1996). FACS-optimized mutants of the green fluorescent protein (GFP). Gene, 173(1), pp.33–38.

Cosmi, L., Liotta, F., Lazzeri, E., Francalanci, M. and Annunziato, F. (2003). Human CD8+CD25+ thymocytes share phenotypic and functional features with CD4+CD25+ regulatory thymocytes. Blood, 102(12), pp.4107–4114.

Craggs, T.D. (2009). Green fluorescent protein: structure, folding and chromophore maturation. Chemical Society Reviews, 38(10), p.2865.

Crispe, I.N. and Benvan, M.J. (1987). Expression and functional significance of the J11d marker on mouse thymocytes. J. Immunol, 138(7), pp.2013–2018.

Cunningham, N.R., Artim, S.C., Fornadel, C.M., Sellars, M.C., Edmonson, S.G., Scott, G., Albino, F., Mathur, A. and Punt, J.A. (2006). Immature CD4+CD8+ Thymocytes and Mature T Cells Regulate Nur77 Distinctly in Response to TCR Stimulation. The Journal of Immunology, 177(10), pp.6660–6666.

Davis, C.B., Killeen, N., Crooks, M.E.C., Raulet, D. and Littman, D.R. (1993). Evidence for a stochastic mechanism in the differentiation of mature subsets of T lymphocytes. Cell, 73(2), pp.237–247.

Derbinski, J., Pinto, S., Rosch, S., Hexel, K. and Kyewski, B. (2008). Promiscuous gene

expression patterns in single medullary thymic epithelial cells argue for a stochastic mechanism. Proceedings of the National Academy of Sciences, 105(2), pp.657–662.

Engel, M., Sidwell, T., Vasanthakumar, A., Grigoriadis, G. and Banerjee, A. (2013). Thymic Regulatory T Cell Development: Role of Signalling Pathways and Transcription Factors. Clinical and Developmental Immunology, 2013, pp.1–8.

Fassett, M.S., Jiang, W., D'Alise, A.M., Mathis, D. and Benoist, C. (2012). Nuclear receptor Nr4a1 modulates both regulatory T-cell (Treg) differentiation and clonal deletion. Proceedings of the National Academy of Sciences, 109(10), pp.3891–3896.

Faustman, D.L. and Davis, M. (2013). TNF Receptor 2 and Disease: Autoimmunity and Regenerative Medicine. Frontiers in Immunology, 4.

Fontenot, J.D., Rasmussen, J.P., Williams, L.M., Dooley, J.L., Farr, A.G. and Rudensky, A.Y. (2005). Regulatory T Cell Lineage Specification by the Forkhead Transcription Factor Foxp3. Immunity, 22(3), pp.329–341.

Frommer, F. and Waisman, A. (2010). B Cells Participate in Thymic Negative Selection of Murine Auto-reactive CD4+ T Cells. PLoS ONE, 5(10), p.e15372.

Fujii, H., Josse, J., Tanioka, M., Miyachi, Y., Husson, F. and Ono, M. (2016). Regulatory T Cells in Melanoma Revisited by a Computational Clustering of FOXP3+T Cell Subpopulations. The Journal of Immunology, 196(6), pp.2885–2892.

Gallegos, A.M. and Bevan, M.J. (2004). Central Tolerance to Tissue-specific Antigens Mediated by Direct and Indirect Antigen Presentation. Journal of Experimental Medicine, 200(8), pp.1039–1049.

Gaud, G., Lesourne, R. and Love, P.E. (2018). Regulatory mechanisms in T cell receptor signalling. Nature Reviews Immunology, 18(8), pp.485–497.

Gershon, R.K. and Kondo, K. (1970). Cell interactions in the induction of tolerance: the role of thymic lymphocytes. pp.18:723–737.

Gray, D., Abramson, J., Benoist, C. and Mathis, D. (2007). Proliferative arrest and rapid turnover of thymic epithelial cells expressing Aire. Journal of Experimental Medicine, 204(11), pp.2521–2528.

He, X., He, X., Dave, V.P., Zhang, Y., Hua, X., Nicolas, E., Xu, W., Roe, B.A. and Kappes, D.J. (2005). The zinc finger transcription factor Th-POK regulates CD4 versus CD8 T-cell lineage commitment. Nature, 433(7028), pp.826–833.

He, X., Park, K. and Kappes, D.J. (2010). The Role of ThPOK in Control of CD4/CD8 Lineage Commitment. Annual Review of Immunology, 28(1), pp.295–320.

d'Hennezel, E., Ben-Shoshan, M., Ochs, H.D., Torgerson, T.R., Russell, L.J., Lejtenyi, C., Noya, F.J., Jabado, N., Mazer, B. and Piccirillo, C.A. (2009). FOXP3 Forkhead Domain Mutation and Regulatory T Cells in the IPEX Syndrome. New England Journal of Medicine, 361(17), pp.1710–1713.

Hernández-Hoyos, G., Sohn, S.J., Rothenberg, E.V. and Alberola-Ila, J. (2000). Lck Activity Controls CD4/CD8 T Cell Lineage Commitment. Immunity, 12(3), pp.313–322.

Hogquist, K.A., Baldwin, T.A. and Jameson, S.C. (2005). Central tolerance: learning self-control in the thymus. Nature Reviews Immunology, 5(10), pp.772–782.

Hsieh, C .S., Lee, H .M. and Lio, C.W.J. (2012). Selection of regulatory T cells in the thymus. Nature Reviews Immunology, 12(3), pp.157–167.

Hsieh, C.S., Liang, Y., Tyznik, A.J., Self, S.G., Liggitt, D. and Rudensky, A.Y. (2004). Recognition of the Peripheral Self by Naturally Arising CD25+ CD4+ T Cell Receptors. Immunity, 21(2), pp.267–277.

Hu, Q., Sader, A., Parkman, J.C. and Baldwin, T.A. (2009). Bim-Mediated Apoptosis Is Not Necessary for Thymic Negative Selection to Ubiquitous Self-Antigens. The Journal of Immunology, 183(12), pp.7761–7767.

Hu, Q.N. and Baldwin, T.A. (2015). Differential Roles for Bim and Nur77 in Thymocyte Clonal Deletion Induced by Ubiquitous Self-Antigen. The Journal of Immunology, 194(6), pp.2643–2653.

Irving, B.A. (1998). Thymocyte Development in the Absence of Pre-T Cell Receptor Extracellular Immunoglobulin Domains. Science, 280(5365), pp.905–908.

Jennings, E., Elliot, T.A.E., Thawait, N., Kanabar, S., Yam-Puc, J.C., Ono, M., Toellner, K.-M., Wraith, D.C., Anderson, G. and Bending, D. (2019). Differential Nr4a1 and Nr4a3 expression discriminates tonic from activated TCR signalling events in vivo. bioRXV.

Jin, R., Wang, W., Yao, J.Y., Zhou, Y.B., Qian, X.P., Zhang, J., Zhang, Y. and Chen, W.F. (2008). Characterization of the In Vivo Dynamics of Medullary $CD4^{+}CD8^{-}$ Thymocyte Development. The Journal of Immunology, 180(4), pp.2256–2263.

Jorgensen, T.N., McKee, A., Wang, M., Kushnir, E., White, J., Refaeli, Y., Kappler,

J.W. and Marrack, P. (2007). Bim and Bcl-2 Mutually Affect the Expression of the Other in T Cells. The Journal of Immunology, 179(6), pp.3417–3424.

Kanamaru, F., Youngnak, P., Hashiguchi, M., Nishioka, T., Takahashi, T., Sakaguchi, S., Ishikawa, I. and Azuma, M. (2004). Costimulation via Glucocorticoid-Induced TNF Receptor in Both Conventional and CD25+ Regulatory CD4+ T Cells. The Journal of Immunology, 172(12), pp.7306–7314.

Kappes, D.J. and Soboloff, J. (2018). Signaling Mechanisms Regulating T Cell Diversity and Function. Crc Press.

Kimura, M.Y., Thomas, J., Tai, X., Guinter, T.I., Shinzawa, M., Etzensperger, R., Li, Z., Love, P., Nakayama, T. and Singer, A. (2016). Timing and duration of MHC I positive selection signals are adjusted in the thymus to prevent lineage errors. Nature Immunology, 17(12), pp.1415–1423.

Klein, L., Hinterberger, M., Wirnsberger, G. and Kyewski, B. (2009). Antigen presentation in the thymus for positive selection and central tolerance induction. Nature Reviews Immunology, 9(12), pp.833–844.

Klein, L., Kyewski, B., Allen, P.M. and Hogquist, K.A. (2014). Positive and negative selection of the T cell repertoire: what thymocytes see (and don't see). Nature Reviews Immunology, 14(6), pp.377–391.

Koble, C. and Kyewski, B. (2009). The thymic medulla: a unique microenvironment for intercellular self-antigen transfer. The Journal of Experimental Medicine, 206(7), pp.1505–1513.

Kovalovsky, D., Pezzano, M., Ortiz, B.D. and Sant'Angelo, D.B. (2010). A Novel TCR Transgenic Model Reveals That Negative Selection Involves an Immediate, Bim-Dependent Pathway and a Delayed, Bim-Independent Pathway. PLoS ONE, 5(1), p.e8675.

Krishnamurthy, B., Chee, J., Jhala, G., Trivedi, P., Catterall, T., Selck, C., Gurzov, E.N., Brodnicki, T.C., Graham, K.L., Wali, J.A., Zhan, Y., Gray, D., Strasser, A., Allison, J., Thomas, H.E. and Kay, T.W.H. (2015). BIM Deficiency Protects NOD Mice From Diabetes by Diverting Thymocytes to Regulatory T Cells. Diabetes, 64(9), pp.3229–3238.

Kuang, A.A., Cado, D. and Winoto, A. (1999). Nur77 transcription activity correlates with its apoptotic functionin vivo. European Journal of Immunology, 29(11), pp.3722–3728.

Kumar, P., Marinelarena, A., Raghunathan, D., Ragothaman, V.K., Saini, S., Bhattacharya, P., Fan, J., Epstein, A.L., Maker, A.V. and Prabhakar, B.S. (2018). Critical role of OX40 signaling in the TCR-independent phase of human and murine thymic Treg generation. Cellular & Molecular Immunology, 16(2), pp.138–153.

Lee, S., Wesselschmidt, R., Linette, G., Kanagawa, O., Russell, J. and Milbrandt, J. (1995). Unimpaired thymic and peripheral T cell death in mice lacking the nuclear receptor NGFI-B (Nur77). Science, 269(5223), pp.532–535.

Lehmann, J., Huehn, J., Rosa, M. de la, Maszyna, F., Kretschmer, U., Krenn, V., Brunner, M., Scheffold, A. and Hamann, A. (2002). Expression of the integrin αEβ7 identifies unique subsets of $CD25^{+}$ as well as $CD25^{-}$ regulatory T cells. Proceedings of the National Academy of Sciences, 99(20), pp.13031–13036.

Li, J., Park, J., Foss, D. and Goldschneider, I. (2009). Thymus-homing peripheral den-

dritic cells constitute two of the three major subsets of dendritic cells in the steady-state thymus. The Journal of Experimental Medicine, 206(3), pp.607–622.

Li, M.O. and Rudensky, A.Y. (2016). T cell receptor signalling in the control of regulatory T cell differentiation and function. Nature Reviews Immunology, [online] 16(4), pp.220–233.

Lio, C.W.J. and Hsieh, C.S. (2008). A Two-Step Process for Thymic Regulatory T Cell Development. Immunity, 28(1), pp.100–111.

Liston, A., Nutsch, K.M., Farr, A.G., Lund, J.M., Rasmussen, J.P., Koni, P.A. and Rudensky, A.Y. (2008). Differentiation of regulatory Foxp3+ T cells in the thymic cortex. Proceedings of the National Academy of Sciences, 105(33), pp.11903–11908.

Liu, Z.G., Smith, S.W., McLaughlin, K.A., Schwartz, L.M. and Osborne, B.A. (1994). Apoptotic signals delivered through the T-cell receptor of a T-cell hybrid require the immediate–early gene nur77. Nature, 367(6460), pp.281–284.

Lucas, B. and Germain, R.N. (1996). Unexpectedly Complex Regulation of CD4/CD8 Coreceptor Expression Supports a Revised Model for CD4+CD8+ Thymocyte Differentiation. Immunity, 5(5), pp.461–477.

Lundberg, K., Heath, W., Köntgen, F., Carbone, F.R. and Shortman, K. (1995). Intermediate steps in positive selection: differentiation of CD4+8int TCRint thymocytes into CD4-8+TCRhi thymocytes. The Journal of Experimental Medicine, 181(5), pp.1643–1651.

Macian, F. (2005). NFAT proteins: key regulators of T-cell development and function. Nature Reviews Immunology, [online] 5(6), pp.472–484.

Maehr, R., Mintern, J.D., Herman, A.E., Mathis, D., Benoist, C. and Ploegh, H. (2005). Cathepsin L is essential for onset of autoimmune diabetes in NOD mice. Journal of Clinical Investigation, 115(10), pp.2934–2943.

Mahmud, S.A., Manlove, L.S., Schmitz, H.M., Xing, Y., Wang, Y., Owen, D.L., Schenkel, J.M., Boomer, J.S., Green, J.M., Yagita, H., Chi, H., Hogquist, K.A. and Farrar, M.A. (2014). Costimulation via the tumor-necrosis factor receptor superfamily couples TCR signal strength to the thymic differentiation of regulatory T cells. Nature Immunology, 15(5), pp.473–481.

Mallis, R.J., Bai, K., Arthanari, H., Hussey, R.E., Handley, M., Li, Z., Chingozha, L., Duke-Cohan, J.S., Lu, H., Wang, J.H., Zhu, C., Wagner, G. and Reinherz, E.L. (2015). Pre-TCR ligand binding impacts thymocyte development before αβTCR expression. Proceedings of the National Academy of Sciences, 112(27), pp.8373–8378.

Maloy, K.J. and Powrie, F. (2001). Regulatory T cells in the control of immune pathology. Nature Immunology, 2(9), pp.816–822.

Matechak, E.O., Killeen, N., Hedrick, S.M. and Fowlkes, B.. (1996). MHC Class II–Specific T Cells Can Develop in the CD8 Lineage When CD4 Is Absent. Immunity, 4(4), pp.337–347.

Matz, M.V., Fradkov, A.F., Labas, Y.A., Savitsky, A.P., Zaraisky, A.G., Markelov, M.L. and Lukyanov, S.A. (1999). Fluorescent proteins from nonbioluminescent Anthozoa species. Nature Biotechnology, 17(10), pp.969–973.

McCaughtry, T.M., Baldwin, T.A., Wilken, M.S. and Hogquist, K.A. (2008). Clonal deletion of thymocytes can occur in the cortex with no involvement of the medulla. The

Journal of Experimental Medicine, 205(11), pp.2575–2584.

McCaughtry, T.M. and Hogquist, K.A. (2008). Central tolerance: what have we learned from mice? Seminars in Immunopathology, 30(4), pp.399–409.

McCaughtry, T.M., Wilken, M.S. and Hogquist, K.A. (2007). Thymic emigration revisited. The Journal of Experimental Medicine, 204(11), pp.2513–2520.

Melichar, H.J., Ross, J.O., Herzmark, P., Hogquist, K.A. and Robey, E.A. (2013). Distinct Temporal Patterns of T Cell Receptor Signaling During Positive Versus Negative Selection in Situ. Science Signaling, 6(297), pp.ra92–ra92.

Millet, V., Naquet, P. and Guinamard, R.R. (2008). Intercellular MHC transfer between thymic epithelial and dendritic cells. European Journal of Immunology, 38(5), pp.1257–1263.

Moran, A.E., Holzapfel, K.L., Xing, Y., Cunningham, N.R., Maltzman, J.S., Punt, J. and Hogquist, K.A. (2011). T cell receptor signal strength in Treg and iNKT cell development demonstrated by a novel fluorescent reporter mouse. The Journal of Experimental Medicine, 208(6), pp.1279–1289.

Murata, S., Sasaki, K., Kishimoto, T., Niwa, S. -i., Hayashi, H., Takahama, Y. and Tanaka, K. (2007). Regulation of CD8+ T Cell Development by Thymus-Specific Proteasomes. Science, 316(5829), pp.1349–1353.

Murata, S., Takahama, Y. and Tanaka, K. (2008). Thymoproteasome: probable role in generating positively selecting peptides. Current Opinion in Immunology, 20(2), pp.192–196.

Murphy, K.M., Weaver, C., Mowat, A., Berg, L., Chaplin, D., Janeway, C.A., Travers, P. and Walport, M. (2017). Janeway's immunobiology. New York London Gs, Garland Science, Taylor & Francis Group.

Nakagawa, T., Roth, W., Wong, P., Nelson, A., Peters, H., Ploegh, C. and Rudensky, A.Y. (1998). Cathepsin L: Critical Role in Ii Degradation and CD4 T Cell Selection in the Thymus. Science, 280(5362), pp.450–453.

Nedjic, J., Aichinger, M., Mizushima, N. and Klein, L. (2009). Macroautophagy, endogenous MHC II loading and T cell selection: the benefits of breaking the rules. Current Opinion in Immunology, 21(1), pp.92–97.

Nishimura, E., Sakihama, T., Setoguchi, R., Tanaka, K. and Sakaguchi, S. (2004). Induction of antigen-specific immunologic tolerance by in vivo and in vitro antigen-specific expansion of naturally arising Foxp3+CD25+CD4+ regulatory T cells. International Immunology, 16(8), pp.1189–1201.

Nishimura, H., Honjo, T. and Minato, N. (2000). Facilitation of β Selection and Modification of Positive Selection in the Thymus of Pd-1–Deficient Mice. The Journal of Experimental Medicine, 191(5), pp.891–898.

Nishimura, H., Nose, M., Hiai, H., Minato, N. and Honjo, T. (1999). Development of Lupus-like Autoimmune Diseases by Disruption of the PD-1 Gene Encoding an ITIM Motif-Carrying Immunoreceptor. Immunity, 11(2), pp.141–151.

Nishimura, H., Okazaki, T., Tanaka, Y., Nakatani, K., Hara, M., Matsumori, A., Sasayama, S., Mizoguchi, A., Hiai, H., Minato, N. and Honjo, T. (2001). Autoimmune Dilated Car-

diomyopathy in PD-1 Receptor-Deficient Mice. Science, 291(5502), pp.319–322.

Nitta, T., Murata, S., Sasaki, K., Fujii, H., Ripen, A.M., Ishimaru, N., Koyasu, S., Tanaka, K. and Takahama, Y. (2010). Thymoproteasome Shapes Immunocompetent Repertoire of CD8+ T Cells. Immunity, 32(1), pp.29–40.

Nocentini, G., Giunchi, L., Ronchetti, S., Krausz, L.T., Bartoli, A., Moraca, R., Migliorati, G. and Riccardi, C. (1997). A new member of the tumor necrosis factor/nerve growth factor receptor family inhibits T cell receptor-induced apoptosis. Proceedings of the National Academy of Sciences, 94(12), pp.6216–6221.

Okazaki, T., Maeda, A., Nishimura, H., Kurosaki, T. and Honjo, T. (2001). PD-1 immunoreceptor inhibits B cell receptor-mediated signaling by recruiting src homology 2-domain-containing tyrosine phosphatase 2 to phosphotyrosine. Proceedings of the National Academy of Sciences, 98(24), pp.13866–13871.

Ono, M., Shimizu, J., Miyachi, Y. and Sakaguchi, S. (2006). Control of Autoimmune Myocarditis and Multiorgan Inflammation by Glucocorticoid-Induced TNF Receptor Family-Related Proteinhigh, Foxp3-Expressing CD25+ and CD25- Regulatory T Cells. The Journal of Immunology, 176(8), pp.4748–4756.

Ono, M., Tanaka, R.J. and Kano, M. (2014). Visualisation of the T cell differentiation programme by Canonical Correspondence Analysis of transcriptomes. BMC Genomics, 15(1), p.1028.

Orm, M., Cubitt, A.B., Kallio, K., Gross, L.A., Tsien, R.Y. and Remington, S.J. (1996). Crystal Structure of the Aequorea victoria Green Fluorescent Protein. Science, 273(5280), pp.1392–1395.

Oukka, M., Ho, I.-C., de la Brousse, F.C., Hoey, T., Grusby, M.J. and Glimcher, L.H. (1998). The Transcription Factor NFAT4 Is Involved in the Generation and Survival of T Cells. Immunity, 9(3), pp.295–304.

Owen, D.L., Mahmud, S.A., Sjaastad, L.E., Williams, J.B., Spanier, J.A., Simeonov, D.R., Ruscher, R., Huang, W., Proekt, I., Miller, C.N., Hekim, C., Jeschke, J.C., Aggarwal, P., Broeckel, U., LaRue, R.S., Henzler, C.M., Alegre, M.L., Anderson, M.S., August, A., Marson, A., Zheng, Y., Williams, C.B. and Farrar, M.A. (2019). Thymic regulatory T cells arise via two distinct developmental programs. Nature Immunology, 20(2), pp.195–205.

Pacholczyk, R., Ignatowicz, H., Kraj, P. and Ignatowicz, L. (2006). Origin and T Cell Receptor Diversity of Foxp3+CD4+CD25+ T Cells. Immunity, 25(2), pp.249–259.

Park, J.H., Adoro, S., Guinter, T., Erman, B., Alag, A.S., Catalfamo, M., Kimura, M.Y., Cui, Y., Lucas, P.J., Gress, R.E., Kubo, M., Hennighausen, L., Feigenbaum, L. and Singer, A. (2010). Signaling by intrathymic cytokines, not T cell antigen receptors, specifies CD8 lineage choice and promotes the differentiation of cytotoxic-lineage T cells. Nature Immunology, 11(3), pp.257–264.

Pereira, P., Boucontet, L. and Cumano, A. (2012). Temporal Predisposition to and T Cell Fates in the Thymus. The Journal of Immunology, 188(4), pp.1600–1608.

Peterson, P., Org, T. and Rebane, A. (2008). Transcriptional regulation by AIRE: molecular mechanisms of central tolerance. Nature Reviews Immunology, 8(12), pp.948–957.

Phillips, G. (2001). Green fluorescent protein – a bright idea for the study of bacterial

protein localization. FEMS Microbiology Letters, 204(1), pp.9–18.

Picelli, S., Faridani, O.R., Björklund, Å.K., Winberg, G., Sagasser, S. and Sandberg, R. (2014). Full-length RNA-seq from single cells using Smart-seq2. Nature Protocols, 9(1), pp.171–181.

Proietto, A.I., van Dommelen, S., Zhou, P., Rizzitelli, A., D'Amico, A., Steptoe, R.J., Naik, S.H., Lahoud, M.H., Liu, Y., Zheng, P., Shortman, K. and Wu, L. (2008). Dendritic cells in the thymus contribute to T-regulatory cell induction. Proceedings of the National Academy of Sciences, 105(50), pp.19869–19874.

Punt, J.A., Suzuki, H., Granger, L.G., Sharrow, S.O. and Singer, A. (1996). Lineage Commitment in the Thymus: Only the Most Differentiated (TCRhibcl-2hi) Subset of CD4+CD8+ Thymocytes Has Selectively Terminated CD4 or CD8 Synthesis. Journal of Experimental Medicine, 184(6), pp.2091–2100.

Rajpal, A., Cho, Y., Yelent, B., Koza-Taylor, P.K., Li, D., Chen, E., Whang, M., Kang, C., Turi, T. and Winoto, A. (2003). Transcriptional activation of known and novel apoptotic pathways by Nur77 orphan steroid receptor. The EMBO Journal, 22(24), pp.6526–6536.

Ramsdell, F. (2003). Foxp3 and Natural Regulatory T Cells. Immunity, 19(2), pp.165–168.

Rincón, M., Flavell, R.A. and Davis, R.A. (2000). The JNK and P38 MAP kinase signaling pathways in T cell–mediated immune responses44This team of investigators has contributed extensively to the field of MAP kinase signal transduction in thymocyte and T cell differentiation. Free Radical Biology and Medicine, 28(9), pp.1328–1337.

Robey, E.A., Fowlkes, B.J., Gordon, J.W., Kioussis, D., von Boehmer, H., Ramsdell, F. and Axel, R. (1991). Thymic selection in CD8 transgenic mice supports an instructive model for commitment to a CD4 or CD8 lineage. Cell, 64(1), pp.99–107.

Rogers, P.R., Song, J., Gramaglia, I., Killeen, N. and Croft, M. (2001). OX40 Promotes Bcl-xL and Bcl-2 Expression and Is Essential for Long-Term Survival of CD4 T Cells. Immunity, 15(3), pp.445–455.

Rooke, R., Waltzinger, C., Benoist, C. and Mathis, D. (1997). Targeted Complementation of MHC Class II Deficiency by Intrathymic Delivery of Recombinant Adenoviruses. Immunity, 7(1), pp.123–134.

Ross, J.O., Melichar, H.J., Au-Yeung, B.B., Herzmark, P., Weiss, A. and Robey, E.A. (2014). Distinct phases in the positive selection of CD8+ T cells distinguished by intrathymic migration and T-cell receptor signaling patterns. Proceedings of the National Academy of Sciences, 111(25), pp.E2550–E2558.

Sacchetti, A., El Sewedy, T., Nasr, A.F. and Alberti, S. (2001). Efficient GFP mutations profoundly affect mRNA transcription and translation rates. FEBS Letters, 492(1–2), pp.151–155.

Sancho, D., Gómez, M. and Sánchez-Madrid, F. (2005). CD69 is an immunoregulatory molecule induced following activation. Trends in Immunology, 26(3), pp.136–140.

Sarafova, S.D., Erman, B., Yu, Q., Van Laethem, F., Guinter, T., Sharrow, S.O., Feigenbaum, L., Wildt, K.F., Ellmeier, W. and Singer, A. (2005). Modulation of Coreceptor Transcription during Positive Selection Dictates Lineage Fate Independently of TCR/-Coreceptor Specificity. Immunity, 23(1), pp.75–87.

Sato, T., Ohno, S., Hayashi, T., Sato, C., Kohu, K., Satake, M. and Habu, S. (2005). Dual Functions of Runx Proteins for Reactivating CD8 and Silencing CD4 at the Commitment Process into CD8 Thymocytes. Immunity, 22(3), pp.317–328.

Sekiya, T., Kashiwagi, I., Yoshida, R., Fukaya, T., Morita, R., Kimura, A., Ichinose, H., Metzger, D., Chambon, P. and Yoshimura, A. (2013). Nr4a receptors are essential for thymic regulatory T cell development and immune homeostasis. Nature Immunology, 14(3), pp.230–237.

Shaner, N.C., Campbell, R.E., Steinbach, P.A., Giepmans, B.N.G., Palmer, A.E. and Tsien, R.Y. (2004). Improved monomeric red, orange and yellow fluorescent proteins derived from Discosoma sp. red fluorescent protein. Nature Biotechnology, 22(12), pp.1567–1572.

Sheppard, K.A., Fitz, L.J., Lee, J.M., Benander, C., George, J.A., Wooters, J., Qiu, Y., Jussif, J.M., Carter, L.L., Wood, C.R. and Chaudhary, D. (2004). PD-1 inhibits T-cell receptor induced phosphorylation of the ZAP70/CD3ζ signalosome and downstream signaling to PKCϑ. FEBS Letters, 574(1–3), pp.37–41.

Sinclair, C. and Seddon, B. (2014). Overlapping and Asymmetric Functions of TCR Signaling during Thymic Selection of CD4 and CD8 Lineages. The Journal of Immunology, 192(11), pp.5151–5159.

Singer, A., Adoro, S. and Park, J.-H. (2008). Lineage fate and intense debate: myths, models and mechanisms of CD4- versus CD8-lineage choice. Nature Reviews Immunology, 8(10), pp.788–801.

Song, J., So, T. and Croft, M. (2008). Activation of NF-κB1 by OX40 Contributes to Antigen-Driven T Cell Expansion and Survival. The Journal of Immunology, 180(11), pp.7240–7248.

Starr, T.K., Jameson, S.C. and Hogquist, K.A. (2003). Positive and Negative Selection of T cells. Annual Review of Immunology, 21(1), pp.139–176.

Strack, R.L., Strongin, D.E., Mets, L., Glick, B.S. and Keenan, R.J. (2010). Chromophore Formation in DsRed Occurs by a Branched Pathway. Journal of the American Chemical Society, 132(24), pp.8496–8505.

Subach, F.V., Subach, O.M., Gundorov, I.S., Morozova, K.S., Piatkevich, K.D., Cuervo, A.M. and Verkhusha, V.V. (2009). Monomeric fluorescent timers that change color from blue to red report on cellular trafficking. Nature Chemical Biology, 5(2), pp.118–126.

Suzuki, H., Punt, J.A., Granger, L.G. and Singer, A. (1995). Asymmetric signaling requirements for thymocyte commitment to the CD4+ versus CD8+ T cell lineages: A new perspective on thymic commitment and selection. Immunity, 2(4), pp.413–425.

Tai, X., Erman, B., Alag, A., Mu, J., Kimura, M., Katz, G., Guinter, T., McCaughtry, T., Etzensperger, R., Feigenbaum, L., Singer, D.S. and Singer, A. (2013). Foxp3 Transcription Factor Is Proapoptotic and Lethal to Developing Regulatory T Cells unless Counterbalanced by Cytokine Survival Signals. Immunity, 38(6), pp.1116–1128.

Takahashi, T., Tagami, T., Yamazaki, S., Uede, T., Shimizu, J., Sakaguchi, N., Mak, T.W. and Sakaguchi, S. (2000). Immunologic Self-Tolerance Maintained by Cd25+Cd4+Regulatory T Cells Constitutively Expressing Cytotoxic T Lymphocyte–Associated Antigen 4. The Journal of Experimental Medicine, 192(2), pp.303–310.

Terskikh, A., Fradkov, A., Ermakova, G., Zaraisky, A., Tan, P., Kajava, A., Zhao, X. and Siebert, P. (2000). "Fluorescent Timer": Protein That Changes Color with Time. Science, 290(5496), pp.1585–1588.

Thompson, J. and Winoto, A. (2008). During negative selection, Nur77 family proteins translocate to mitochondria where they associate with Bcl-2 and expose its proapoptotic BH3 domain. The Journal of Experimental Medicine, 205(5), pp.1029–1036.

Toomer, K.H., Lui, J.B., Altman, N.H., Ban, Y., Chen, X. and Malek, T.R. (2019). Essential and non-overlapping IL-2Rα-dependent processes for thymic development and peripheral homeostasis of regulatory T cells. Nature Communications, 10(1).

Viken, M.K., Blomhoff, A., Olsson, M., Akselsen, H.E., Pociot, F., Nerup, J., Kockum, I., Cambon-Thomsen, A., Thorsby, E., Undlien, D.E. and Lie, B.A. (2009). Reproducible association with type 1 diabetes in the extended class I region of the major histocompatibility complex. Genes & Immunity, 10(4), pp.323–333.

Vuddamalay, Y., Attia, M., Vicente, R., Pomié, C., Enault, G., Leobon, B., Joffre, O., Romagnoli, P. and van Meerwijk, J.P.M. (2016). Mouse and human CD8+CD28lowregulatory T lymphocytes differentiate in the thymus. Immunology, 148(2), pp.187–196.

Walters, S.N., Webster, K.E., Daley, S. and Grey, S.T. (2014). A Role for Intrathymic B Cells in the Generation of Natural Regulatory T Cells. The Journal of Immunology, 193(1), pp.170–176.

Wang, L., Wildt, K.F., Zhu, J., Zhang, X., Feigenbaum, L., Tessarollo, L., Paul, W.E., Fowlkes, B.J. and Bosselut, R. (2008a). Distinct functions for the transcription factors

GATA-3 and ThPOK during intrathymic differentiation of CD4+ T cells. Nature Immunology, 9(10), pp.1122–1130.

Wang, Y., Kissenpfennig, A., Mingueneau, M., Richelme, S., Perrin, P., Chevrier, S., Genton, C., Lucas, B., DiSanto, J.P., Acha-Orbea, H., Malissen, B. and Malissen, M. (2008b). Th2 Lymphoproliferative Disorder of LatY136F Mutant Mice Unfolds Independently of TCR-MHC Engagement and Is Insensitive to the Action of Foxp3+ Regulatory T Cells. The Journal of Immunology, 180(3), pp.1565–1575.

Ward-Kavanagh, L.K., Lin, W.W., Šedý, J.R. and Ware, C.F. (2016). The TNF Receptor Superfamily in Co-stimulating and Co-inhibitory Responses. Immunity, 44(5), pp.1005–1019.

Wiest, D.L. (1993). Regulation of T cell receptor expression in immature CD4+CD8+ thymocytes by p56lck tyrosine kinase: basis for differential signaling by CD4 and CD8 in immature thymocytes expressing both coreceptor molecules. Journal of Experimental Medicine, 178(5), pp.1701–1712.

Winoto, A. and Littman, D.R. (2002). Nuclear Hormone Receptors in T Lymphocytes. Cell, 109(2), pp.S57–S66.

Woronicz, J.D., Calnan, B., Ngo, V. and Winoto, A. (1994). Requirement for the orphan steroid receptor Nur77 in apoptosis of T-cell hybridomas. Nature, 367(6460), pp.277–281.

Wyss, L., Stadinski, B.D., King, C.G., Schallenberg, S., McCarthy, N.I., Lee, J.Y., Kretschmer, K., Terracciano, L.M., Anderson, G., Surh, C.D., Huseby, E.S. and Palmer, E. (2016). Affinity for self antigen selects Treg cells with distinct functional properties. Nature Immunology, 17(9), pp.1093–1101.

Xing, Y., Jameson, S.C. and Hogquist, K.A. (2013). Thymoproteasome subunit- 5T generates peptide-MHC complexes specialized for positive selection. Proceedings of the National Academy of Sciences, 110(17), pp.6979–6984.

Xing, Y., Wang, X., Jameson, S.C. and Hogquist, K.A. (2016). Late stages of T cell maturation in the thymus involve NF-κB and tonic type I interferon signaling. Nature Immunology, 17(5), pp.565–573.

Xiong, Y., Castro, E., Yagi, R., Zhu, J., Lesourne, R., Love, P.E., Feigenbaum, L. and Bosselut, R. (2013). Thpok-independent repression ofRunx3by Gata3 during CD4+T-cell differentiation in the thymus. European Journal of Immunology, 43(4), pp.918–928.

Yamano, T., Nedjic, J., Hinterberger, M., Steinert, M., Koser, S., Pinto, S., Gerdes, N., Lutgens, E., Ishimaru, N., Busslinger, M., Brors, B., Kyewski, B. and Klein, L. (2015). Thymic B Cells Are Licensed to Present Self Antigens for Central T Cell Tolerance Induction. Immunity, 42(6), pp.1048–1061.

Yamasaki, S., Ishikawa, E., Sakuma, M., Ogata, K., Sakata-Sogawa, K., Hiroshima, M., Wiest, D.L., Tokunaga, M. and Saito, T. (2005). Mechanistic basis of pre–T cell receptor–mediated autonomous signaling critical for thymocyte development. Nature Immunology, 7(1), pp.67–75.

Yang, X. and Mariuzza, R.A. (2015). Pre–T-cell receptor binds MHC: Implications for thymocyte signaling and selection. Proceedings of the National Academy of Sciences, 112(27), pp.8166–8167.

Yin, X., Ladi, E., Chan, S.W., Li, O., Killeen, N., Kappes, D.J. and Robey, E.A. (2007).

CCR7 Expression in Developing Thymocytes Is Linked to the CD4 versus CD8 Lineage Decision. The Journal of Immunology, 179(11), pp.7358–7364.

Yu, Q., Erman, B., Bhandoola, A., Sharrow, S.O. and Singer, A. (2003). In Vitro Evidence That Cytokine Receptor Signals Are Required for Differentiation of Double Positive Thymocytes into Functionally Mature CD8+ T Cells. Journal of Experimental Medicine, 197(4), pp.475–487.

Zelenay, S., Lopes-Carvalho, T., Caramalho, I., Moraes-Fontes, M.F., Rebelo, M. and Demengeot, J. (2005). Foxp3+ CD25- CD4 T cells constitute a reservoir of committed regulatory cells that regain CD25 expression upon homeostatic expansion. Proceedings of the National Academy of Sciences, 102(11), pp.4091–4096.

Zhang, B., Chikuma, S., Hori, S., Fagarasan, S. and Honjo, T. (2016). Nonoverlapping roles of PD-1 and FoxP3 in maintaining immune tolerance in a novel autoimmune pancreatitis mouse model. Proceedings of the National Academy of Sciences, 113(30), pp.8490–8495.

Zhou, T., Cheng, J., Yang, P., Wang, Z., Liu, C., Su, X., Bluethmann, H. and Mountz, J.D. (1996). Inhibition of Nur77/Nurr1 leads to inefficient clonal deletion of self- reactive T cells. Journal of Experimental Medicine, 183(4), pp.1879–1892.